Synthetic Strategies for High Dielectric Constant Silicone Elastomers

Madsen, Frederikke Bahrt

Publication date:
2014

Document Version
Publisher's PDF, also known as Version of record

Synthetic Strategies for High Dielectric Constant Silicone Elastomers

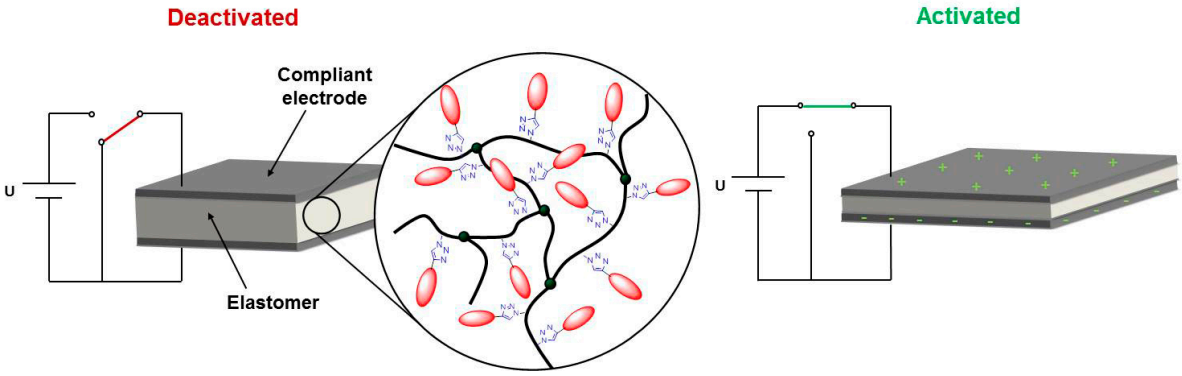

Frederikke Bahrt Madsen
Ph.D. Thesis
August 2014

DTU Chemical Engineering
Department of Chemical and Biochemical Engineering

Synthetic Strategies for High Dielectric Constant Silicone Elastomers

Frederikke Bahrt Madsen

Ph.D. Thesis

August 2014

DTU Chemical Engineering
Department of Chemical and Biochemical Enginee

Address: The Danish Polymer Centre
Department of Chemical and Biochemical Engineering
Technical University of Denmark
Building 227
DK-2800 Kgs. Lyngby
Denmark
Phone: +45 4525 6801
Web: www.dpc.kt.dtu.dk

Print: J&R Frydenberg A/S
København
Decenber 2014

ISBN: 978-87-93054-56-1

Preface

The work presented herein is the result of my PhD study carried out at the Danish Polymer Centre (DPC), Department of Chemical and Biochemical Engineering, Technical University of Denmark, DTU. The project was carried out as a part of the research project DEAP, a joint project with DTU, Aalborg University, AAU, University of Southern Denmark, SDU, Danfoss Polypower A/S, Bang & Olufsen A/S, ESS Technology A/S and Wavestar A/S. The project is funded by InnovationsFonden. All the work was carried out between August 15th, 2011 and August 14th, 2014.

First of all, thanks should be directed to my main supervisor Anne Ladegaard Skov for offering me this opportunity and for her continuous and excellent guidance and support during the project work. I have really appreciated your friendly approach towards me and through the different challenges that have occurred during the project. I would also like to thank you for the many amazing and fun experiences at conferences around the world.

I also owe many thanks to my two co-supervisors; Anders Egede Daugaard for his invaluable ideas and advice on synthesis and characterisation related issues and Søren Hvilsted for great advice and knowledge during the project, especially on how to present research results.

Special thanks are directed to my colleagues at DPC for creating a wonderful working environment and for many fun gatherings and occasions, Irakli Javakhishvili for guidance during experimental work and helpful and interesting discussions, Liyun Yu for exceptionally competent help with film preparation and testing, Kim Chi Szabo for help with TGA, DSC and the many other laboratory issues.

Finally I thank my family and friends for your encouragement and interest during these years.

Kgs. Lyngby, August 2014

Frederikke Bahrt Madsen

Til Anders

Abstract

Dielectric electroactive polymers (DEAPs) are a new and promising transducer technology and are often referred to as 'artificial muscles', due to their ability to undergo large deformations when stimulated by electric fields. DEAPs consist of a soft and thin elastomeric film (an elastomer) sandwiched between compliant electrodes and have many interesting properties such as a simple working principle, large achievable strains, high-energy densities and the fact that they are light weight and low in cost. Some issues, however, limit the current commercial viability of the technology, as high driving voltages (several kV's), for instance, are necessary to activate the material. Driving voltage can be lowered by increasing the energy density of the DEAP elastomer film, achieved by creating elastomers with high dielectric constants, which is a material's ability to store electrical energy.

Two synthetic strategies were developed in this Ph.D. thesis, in order to create silicone elastomers with high dielectric constants and thereby higher energy densities. The work focused on maintaining important properties such as dielectric loss, electrical breakdown strength and elastic modulus. The methodology therefore involved chemically grafting high dielectric constant chemical groups onto the elastomer network, as this would potentially provide a stable elastomer system upon continued activation of the material.

The first synthetic strategy involved the synthesis of a new type of cross-linker for silicone polymer networks. The silicone compatible cross-linker allowed for copper-catalysed azide-alkyne cycloadditions (CuAAC) and thereby the attachment of functional groups to the network cross-linking point. The functional groups were very well-distributed in the silicone elastomer matrix, and various functional groups provided a number of elastomers with diverse properties. High dielectric constant molecules, such as the dipolar 4-nitrobenzene and nitroazobenzene, resulted in elastomers with an approximately 20% increase in dielectric constant at low concentrations of dipolar species (~0.5 wt%). The second synthetic strategy was to create elastomers with high concentrations of functional groups and thereby even higher dielectric constants through the synthesis of novel copolymers. Two different routes were followed to accomplish this aim. One route involved the synthesis of a so-called 'chain extender' that allowed for chemical modifications such as CuAAC. This route was promising for one-pot elastomer preparation and as a high dielectric constant additive to commercial silicone systems. The second approach used the borane-catalysed Piers-Rubinsztajn reaction to form spatially well-distributed copolymers where functional groups could be attached along the polymer backbone. The functional copolymers contained vinyl or allyl end groups that allowed for elastomer synthesis. The dielectric properties of the formed elastomers were found to increase significantly and an optimum concentration of functional groups was identified. At a concentration of 5.6 wt% of a nitrobenzene functional group the dielectric permittivity increased 70% while at this loading important properties such as electrical breakdown strength, elastic modulus and dielectric loss were not significantly compromised.

The developed synthetic strategies facilitate new ways of functionalising elastomers in general and dielectric elastomers in particular.

Resumé

Dielektriske elektroaktive polymerer (DEAP) er en ny lovende transducerteknologi, der ofte bliver refereret til som 'kunstige muskler' pga. deres evne til at udvise store deformationer, når en elektrisk spænding sættes til materialet. En DEAP består sædvanligvis af en tynd elastisk polymerfilm (en elastomer), der er anbragt mellem to ultratynde og fleksible elektroder. DEAP har mange interessante egenskaber såsom et simplet funktionsprincip, store opnåelige udvidelser, høj energitæthed, lav vægt og lave fremstillingsomkostninger. Teknologien har dog enkelte nuværende problemer, der begrænser den kommercielle bæredygtighed, da f.eks. meget store spændinger (kilovolt) er nødvendige for at aktivere DEAP'en. Aktiveringsspændingen kan sænkes ved at fremstille elastomermaterialer med højere dielektriske konstanter, dvs. bedre evne til at lagre elektrisk energi.

I denne ph.d.-afhandling blev to forskellige syntesestrategier til at lave silikoneelastomerer med høje dielektriske konstanter, og dermed højere energitæthed, udviklet. Udviklingsarbejdet fokuserede samtidig på at bibeholde vigtige materialeegenskaber såsom det dielektriske tab, den elektriske sammenbrudstyrke og elasticitetsmodulet. Fremgangsmåden var derfor at koble molekyler med høje dielektriske konstanter kemisk på elastomernetværker, da dette potentielt vil give et stabilt elastomersystem ved langvarig brug af DEAP'en.

Den første syntesestrategi var baseret på udviklingen af en ny type tværbinder til silikoneelastomerer. Denne tværbinder muliggjorde kobber-katalyseret azid-alkyn cycloaddition (CuAAC) og dermed fastgørelse af funktionelle grupper i elastomerens tværbindingspunkt. De påsatte funktionelle grupper viste sig at være godt fordelt i elastomermatricen, og forskellige funktionelle grupper gav elastomerer med varierende egenskaber. Molekyler med høje dielektriske konstanter såsom 4-nitrobenzen og nitroazobenzen gav elastomerer med 20% forhøjet dielektrisk konstant ved lave koncentrationer af de dipolære molekyler (~0,5 vægtpct).

Den anden syntesestrategi blev udviklet for at lave elastomerer med endnu højere indhold af funktionelle grupper og dermed endnu højere dielektriske konstanter. Dette blev realiseret ved at syntetisere nye copolymerer via to forskellige synteseveje. Den første syntesevej var baseret på syntesen af en såkaldt kædeforlænger, der muliggjorde kemiske modifikationer såsom CuAAC. Denne syntesevej viste sig at være lovende til én-pot-syntese af elastomerer og som et additiv med højt dielektrisk konstant til kommercielle silikoneelastomersystemer. Den anden syntesevej brugte den bor-katalyserede Piers-Rubinsztajn reaktion til at danne copolymerer, hvor funktionelle grupper kunne påsættes på polymerkæden. De funktionelle copolymerer indeholdte vinyl eller allyl endegrupper, der muliggjorde videre elastomersyntese. De dielektriske egenskaber af de dannede elastomerer steg betydeligt og en optimal koncentration af funktionalitet blev identificeret. Ved en koncentration på 5,6 vægtpct. nitrobenzen steg den dielektriske konstant 70% mens vigtige egenskaber såsom den elektriske sammenbrudstyrke, elasticitetsmodulet og det dielektriske tab bevaredes.

De udviklede syntesestrategier muliggør nye måder at funktionalisere elastomerer generelt og dielektriske elastomerer i særdeleshed.

Contents

Abbreviations and symbols

CuAAC	copper(I)-catalysed azide-alkyne cycloaddition
d	thickness of elastomer
DEAP	dielectric electroactive polymer
DMF	*N,N*-dimethyl formamide
DMSO	dimethyl sulfoxide
DSC	differential scanning calorimetry
ε'	dielectric permittivity
ε''	dielectric loss
ε_r	relative dielectric permittivity
ε_0	vacuum permittivity
EAP	electroactive polymer
E_B	dielectric breakdown strength
f	functionality
F	frequency
F_c	critical frequency
FEP	fluorinated ethylene propylene
F_{om}	figure of merit
FTIR	Fourier transform infrared
G^*	complex shear modulus
G'	storage modulus
G''	loss modulus
J	coupling constant
NMP	*N*-methyl-2-pyrrolidone
NMR	nuclear magnetic resonance
ν	Poisson's ratio
$\bar{M}_n$	number average molecular weight
$\bar{M}_w$	weight average molecular weight
μ	dipole moment
PANI	polyaniline
PDI	polydispersity index
PDMS	polydimethylsiloxane
PDVB	polydivinyl benzene
P_{el}	electrostatic pressure
r	stoichiometric imbalance/ratio
r_c	stoichiometric imbalance/ratio for critical gelation
RI	refractive index
RT	room temperature
σ	conductivity
s	strain
SEC	size exclusion chromatography
Tan δ	loss tangent
T_c	crystallisation temperature
TEA	triethyl amine
T_g	glass transition temperature
TGA	thermogravimetric analysis
THF	tetrahydrofuran
T_m	melting temperature
U	voltage
wt%	weight percent
Y	Young's modulus

Introduction

Objectives

The aim of this Ph.D. thesis is to chemically modify silicone polymers and elastomers, in order to increase the dielectric permittivity, also called the dielectric constant, of dielectric electroactive polymers (DEAPs). DEAPs are a new and promising transducer technology with many interesting and favourable properties such as large, achievable strains and high-energy densities as well as being light-weight and low in cost. There are, however, several issues that currently limit the commercial potential of the technology, including high driving voltages and short lifetime. There is consequently a need to optimise DEAP materials, in order to overcome the current shortcomings of the technology. One of the most important components of a DEAP is the elastomer. This work focuses on creating new and improved silicone elastomer systems with high dielectric permittivity, as this can potentially decrease necessary driving voltages by increasing energy density. Furthermore, the development of these new elastomers focuses on maintaining other important parameters that govern the lifetime of DEAPs, such as the elastic modulus, dielectric loss and electrical breakdown strength. Overall, two synthetic strategies were followed, in order to create elastomers with higher dielectric permittivity:

- Development of a new type of silicone-compatible cross-linker that allows for controlled and selective functionalisation of silicone elastomers at the cross-linking point.
- Synthesis of copolymers suitable for both elastomer formation and functionalisation with, for example, high dielectric permittivity molecules.

Outline

The thesis is divided into two main parts. Part 1 presents the first synthetic strategy for increasing the dielectric permittivity of silicone elastomers. A new type of silicone-compatible cross-linker that allows for orthogonal reactions – and thus functionalisation at the polymer network cross-linking point – is developed. This means a molecule that allows for the incorporation of dipolar species in a way that does not interfere with the network-forming hydrosilylation reaction. This part of the thesis is divided into three chapters. Chapter 2 involves the synthesis, development and testing of such orthogonal cross-linkers, Chapter 3 deals with the use and obtained properties of dipolar cross-linkers used in dielectric elastomers and Chapter 4 illustrates the specific use of a fluorescent cross-linker utilised as a labeller in so-called heterogeneous bimodal networks.

Part 2 comprises Chapters 5, 6 and 7 and relates to synthetic strategies for high dielectric permittivity siloxane copolymers and elastomers. Based on the results from Part 1, where good results are obtained from the use of a novel dipolar cross-linker, this part aims at developing polymers and elastomers with even higher concentrations of dipolar species. Due to natural limitations in the amount of cross-linkers one can add to an elastomer system without deteriorating the network properties, it is only possible to create elastomers with higher concentrations of dipolar groups if the dipolar species are attached along the backbone of the polymers. Two different approaches

were developed, in order to create polymers with functionality distributed along the chain – siloxane chain extenders and siloxane copolymers. Chapter 5 involves the synthesis and characterisation of copolymers prepared by applying the two different synthetic approaches and Chapter 6 and Chapter 7 examine the use and properties of functional copolymers as dielectric elastomers.

A conclusion and outlook for future work can be found in Chapter 8.

Unpublished experimental procedures can be found in Chapter 9, whereas the experimental procedures for the published work can be found in the respective appendices.

The thesis is based on the manuscripts listed below, which can be found in the following appendices:

Appendix A:

F. B. Madsen, I. Dimitrov, A. E. Daugaard, S. Hvilsted, A. L. Skov, 2013 Novel cross-linkers for PDMS networks for controlled and well distributed grafting of functionalities by click chemistry, *Polymer Chemistry*, **4**, 1700-1707.

Appendix B:

F. B. Madsen, A. E. Daugaard, S. Hvilsted, M. Y. Benslimane, A.L. Skov, 2013 Dipolar cross-linkers for PDMS networks with enhanced dielectric permittivity and low dielectric loss, *Smart Materials and Structures,* **22**, 104002.

Appendix C:

F. B. Madsen, A. E. Daugaard, C. Fleury, S. Hvilsted, A. L. Skov, 2014 Visualisation and characterisation of heterogeneous bimodal PDMS networks, *RSC Advances*, **4**, 6939-6945.

Appendix D:

F. B. Madsen, I. Javakhishvili, R. E. Jensen, A. E. Daugaard, S. Hvilsted, A. L. Skov, 2014 Synthesis of telechelic vinyl/allyl functional siloxane copolymers with structural control, *Polymer Chemistry*, **5**, 7054-7061.

Appendix E:

F. B. Madsen, L. Yu, A. E. Daugaard, S. Hvilsted, A. L. Skov, 2014 Silicone elastomers with high dielectric permittivity and high dielectric breakdown strength based on dipolar copolymers, *Polymer*, **55**, 6212-6219.

Other publications (not included in the thesis):

F. B. Madsen, A. E. Daugaard, S. Hvilsted, A. L. Skov, 2012 Udvikling af materialer til kunstige muskler, *Dansk Kemi*, **93** (9), 48-51.

F. B. Madsen, A. E. Daugaard, S. Hvilsted, A. L. Skov, 2013 Novel silicone compatible cross-linkers for controlled functionalization of PDMS networks, *Proceedings of SPIE*, **8687**, 86871H-1-86871H-13.

K. Goswami, F. B. Madsen, A. E. Daugaard, A. L. Skov, 2013 Silicone resembling poly(propylene glycol) interpenetrating networks based on no pre-stretch as basis for electrical actuators, *Proceedings of SPIE*, **8687**, 86871H-1-86871H-13.

F. B. Madsen, A. E. Daugaard, S. Hvilsted, A. L. Skov, 2013 Intelligente materialer som kunstige muskler og energi-høstere, *Aktuel Naturvidenskab*, **3**, 26-29.

Patents:

F. B. Madsen, A. E. Daugaard, S. Hvilsted, A. L. Skov, filed September 30 2013, “Silicone Chain Extender”, European patent application No. 13186588.3

1 Background

1.1 Dielectric electroactive polymers (DEAPs)

The search for materials that exhibit properties similar to the human muscle has been the focus of engineers and researchers for several decades. The challenge lies in the many excellent properties of human muscles, such as high energy densities and large, obtainable strains. Furthermore, human muscles generate linear motion, whereas the currently used electrical motors generate rotational motion[1–3]. Different “smart materials” have been suggested as materials for artificial muscles, such as piezoelectrics and shape memory alloys. These materials, however, have several limitations; piezoelectrics, for example, can only handle very small strains and suffer from high stiffness, while shape memory alloys show high instances of displacement when using resistive heating, but they must be actively cooled to obtain good operating frequencies. These issues increase the complexity and cost of the system[4,5].

Polymers offer an interesting alternative to the above mentioned materials, as they are lightweight and low in cost. Electroactive polymers (EAPs) consist of soft polymeric materials with large energy densities, relatively fast response times and the ability to undergo large deformations when stimulated by electric fields[5]. Although the concept of electroactive polymers dates back to an article from 1880 by Wilhelm Röntgen[6], who observed how a natural rubber film showed displacement upon sprayed-on electrical charges, the potential of EAPs as artificial muscles has only attracted extensive attention in the last two decades.

EAPs can be divided into two main groups: ionic and electronic. Ionic EAPs respond to an electric field through the diffusion of ions in a material. In addition, they generally require low driving voltages (as low as 1-2 V) but require an electrolyte, which means that encapsulating the aqueous environment is necessary. Furthermore, there is a need to maintain wetness, and it is difficult to maintain DC-induced displacements. The advantages of electronic EAPs over their ionic counterparts include higher energy density, they can be operated in air without major constraints, large actuation forces, rapid response times and long lifetimes. The major disadvantage of electronic EAPs is that they require high driving voltages to actuate (typically 500 V to 10 kV)[5,7], and so a great deal of research is therefore focused on reducing the driving voltage of electronic EAPs. Electronic EAPs can be divided further into subclasses, such as polymer electrets[8–10], electrostrictive graft elastomers[11] and dielectric electroactive polymers (DEAPs). In the field of electronic EAPs the dielectric electroactive polymers are a very interesting class of materials, due to high obtainable actuation speeds, strains and high work densities, a high degree of electromechanical coupling and good overall performance[12,13]. The work in this thesis therefore concerns the optimisation of dielectric EAPs.

DEAPs are promising materials for advanced electromechanical applications such as actuators, generators and sensors, due to their simple and flexible working principles. Furthermore, they consist of an elastomer film sandwiched between two thin and compliant electrodes, thereby forming a capacitor. The electrodes can be made from a variety of conducting materials such as gold[14], silver and carbon grease[13]. When an external voltage is applied to the electrodes,

electrostatic forces, which are negative on one electrode and positive on the other, are created. The electrostatic pressure acting on the film will squeeze the elastomer in thickness and as the elastomer is incompressible it is consequently expanded in planar directions. Electrical energy, in this case, is thus converted into mechanical energy. The driving force for the actuation process is the resulting reduction in charge density when the electrode area is enlarged[15]. When the external voltage is switched off, the elastomer film returns to its original shape. The actuation working principle can be seen in Figure 1.

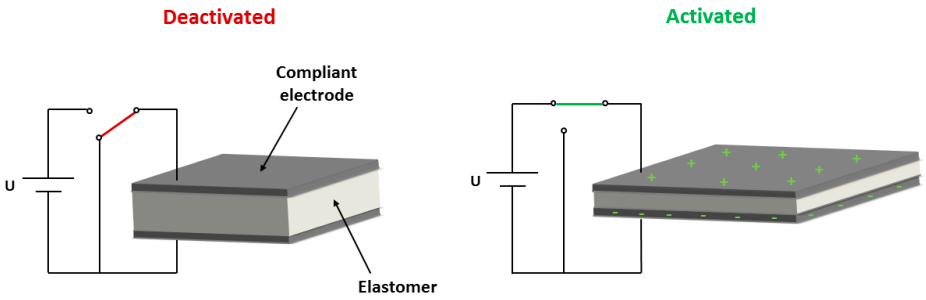

Figure 1 Schematic illustration of the actuation working principle of DEAPs.

DEAPs can also be used as generators to create electrical energy if the DEAP is stretched by an external force and electrical charges are placed on the film. When the DEAP is allowed to relax, elastic stresses work against the electric field pressure, thereby increasing the electrical energy. In this process opposite charges on the two electrodes are pushed further apart as the film contracts and increases in thickness, while similar charges are brought closer together with the decreasing area of the elastomer thus increasing energy density. These changes increase the voltage of the charge and the created energy can be extracted[16].

DEAPs have the potential to be used in novel applications which have not been possible previously or feasible through the use of other technologies. Especially within the actuator application area, DEAPs could provide novel solutions such as flat screen loud speakers[17], light-weight morphing structures and prosthetic-like actuation, especially due to the flexibility of the material, which offers the ability to be formed into complex shapes and still provide actuation[18]. Other DEAP applications range from valves and pumps[19] to robotics[20], Braille displays[21], wave energy harvesting[22] and active vibration control[23].

1.2 Materials and parameters for DEAPs

One of the most important components of a DEAP is the elastomer, as it governs dielectric permittivity and the breakdown strength.

Polydimethylsiloxane (PDMS) elastomers are one of the most used materials for DEAPs due to their high efficiency and fast response times[5,24]. Other materials commonly used for DEAPs include acrylics and polyurethanes. One advantage of silicone elastomers over other materials is

lower viscous loss, which means that it can be operated at higher frequencies with lower losses. Furthermore, silicones can be operated at a broader temperature range[5]. The disadvantage of silicone elastomers is that they possess a relatively low dielectric constant, which means that a higher electrical field is necessary to actuate the DEAP.

1.2.1 Dielectric permittivity

A very important property of dielectric elastomers is dielectric permittivity also called the dielectric constant, which is a material's ability to store electrical energy. When an electric field is induced, all materials become polarised. If the material is conducting, the electric field will induce charge transport. In an insulating material, such as a silicone elastomer, the material can be considered as consisting of small dipoles with separate internal charges but which are overall electrically neutral. The dipolar species consists of molecules that carry dipole moments or negatively charged species, such as electrons, anions and other chemical groups with negative partial charges, and positive species such as atomic nuclei, cations and groups with positive partial charges. When subjected to an electrical field, the dipoles will align with the field so that the negative part of the dipole will orient towards the higher potential and the positive part of the dipole will orient towards the lower potential. The principle behind such dielectric materials can be seen in Figure 2. Electrostatic energy created in the material is then converted to mechanical energy through different mechanisms, the simplest of which is Maxwell stress, whereby stress is proportional to the dielectric constant[15]. Dielectric constants of dielectric elastomers range from 2 to 8, and pristine silicone elastomers typically have dielectric constants at around 2-3.

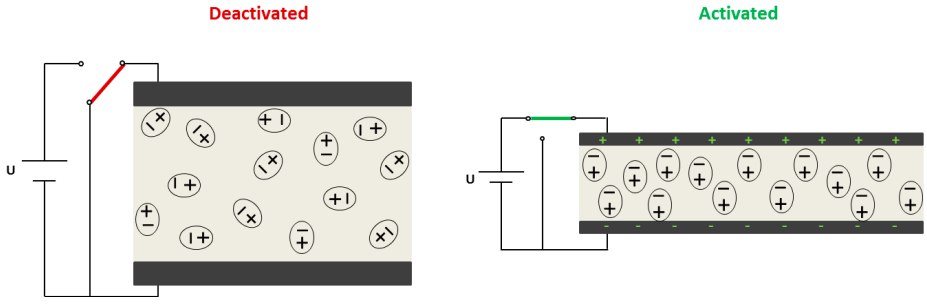

Figure 2 Schematic illustration of the alignment of dipoles in a dielectric material when not subjected (left) and subjected to an electrical field (right).

1.2.2 Other material parameters

The driving voltage that can be applied to a dielectric elastomer is limited upwards by the dielectric breakdown strength, E_B, which ideally is a material-specific constant. Breakdown strength is usually measured in units of V/µm and depends on the material's structure, its temperature and the presence of impurities[25]. High dielectric breakdown strength is desired so that the DEAP does not experience premature failure. This means that it is important for the elastomer to be free

from impurities or voids that cause locally reduced dielectric strength. Furthermore, it is important that the material exhibits low dielectric losses which continuously contribute to the generation of heat in the material. If heat generated by the dielectric losses exceeds heat lost to the surroundings, the temperature in the elastomer will rise, which in turn can lead to thermal breakdown.

Dielectric loss is usually given as the loss tangent, tan δ, as tan δ = $\varepsilon''/\varepsilon'$, where ε'' is the imaginary part of the dielectric permittivity attributed to, among other things, dipole relaxation phenomena, which gives rise to energy loss. ε' is the real part of the dielectric permittivity of the material, defined as $\varepsilon' = \varepsilon_0\varepsilon_r$, where ε_0 is vacuum permittivity and ε_r is relative permittivity. Relative permittivity is often called the dielectric constant; however, in this thesis, the frequency-dependent real part of relative permittivity, ε', will be referred to as the dielectric constant, as this is the current standard in the DEAP field[26–28].

Another important property is the conductivity of the elastomer. Silicone elastomers are in general electrically insulating materials, though no material can be considered as ideally insulating. Upon changing of the molecular structure of the elastomer or adding high dielectric constant fillers, unwanted conductive paths – and thereby charge transport – can occur in the elastomer. Increased conductivity, which can lead to large dielectric losses, is referred to as σ, where conductivity for insulating dielectric materials is dependent on dielectric loss and frequency (F) as: $\sigma = 2\pi F\varepsilon''\varepsilon_0$. When conducting paths are created, σ becomes independent of frequency below a critical frequency F_c[29].

Other important material parameters include the Young's modulus, Y, which, together with the electrodes, governs the obtainable strain of the DEAP. In the linear regime, which for silicone elastomers is up to approximately 15% strain[30], elastic and viscous properties are well described by the shear storage modulus, G', and the shear loss modulus, G''. Both are defined from the complex shear modulus $G^* = G'(\omega) + iG''(\omega)$. Due to the incompressibility of silicones (Poisson's ratio (ν) close to 0.5), the Young's modulus can be determined as $Y = 2(1 + \nu)G$, where $G = G'(\omega \rightarrow 0)$. When there is an insignificant dependence of G' on the applied frequency, the Young's modulus can be obtained as $Y = 3G'$, which describes frequency-independent elastic moduli up to a strain of approximately 15%. Furthermore, highly frequency-dependent viscous loss, which governs the viscous part of a viscoelastic material, i.e. the energy lost as heat to the surroundings, can be determined from G''. Viscous loss is usually referred to via the loss tangent, tan δ = G''/G'.

Sommer-Larsen and Larsen[31] defined a universal expression which, through a single parameter, the *figure of merit*, F_{om}, can be used to evaluate the performance of a DEAP at a constant potential. The figure of merit depends on the dielectric constant, the dielectric breakdown strength and the elastic modulus (Young's modulus) of the elastomer material, and it is defined as: $F_{om} = \frac{3\varepsilon' {E_B}^2}{Y}$. The figure of merit can be used, for example, as a guide when optimising the properties of elastomers for DEAPs.

1.3 Optimisation of DEAP materials

The silicone materials currently used for DEAP elastomers are off-the-shelf materials and as such have not been developed for use in this specific application and are not the result of targeted development. Therefore, recent years have seen a large increase in research on and the development of silicone materials for DEAPs. The development and optimisation of elastomers for DEAPs can be done on the basis of the equation for the actuation strain developed by Pelrine et al.[32], which correlates electrostatic pressure, P_{el}, to the strain, s, and the elastic modulus, Y, according to:

$$s = \frac{p_{el}}{Y} = \frac{\varepsilon_r \varepsilon_0}{Y}\left(\frac{U}{d}\right)^2 \quad (1)$$

where ε_0 = 8.854x10^{-12} F/m is vacuum permittivity, d is the thickness of the material, U is the voltage and ε_r is the relative dielectric permittivity of the elastomer film. Material optimisation is often done with the purpose of reducing the operating voltage of the DEAP, in order to remove the risks associated with high voltage and to increase commercial viability[5]. Equation 1 states that the voltage, U, can be lowered by reducing the thickness of the elastomer film, decreasing the elastic modulus of the elastomer and/or increasing the dielectric constant of the elastomer material. A reduction in elastomer film thickness will have the greatest impact on reducing the operating voltage and has the advantage of upholding dielectric loss and breakdown strength. A threshold value of 30-40 µm has been identified in current large-scale processing[33], and any further reduction will cause an increased importance of inhomogeneities, which will result in localised areas of high electrical fields and stresses and ultimately result in premature electrical breakdown[5]. The reduction in thickness also causes a reduction in output force, which can be increased by the use of elastomer film layers[34]. This, however, increases fabrication complexity significantly.

The elastic modulus and overall mechanical properties of silicone elastomers are generally favourable for DEAP purposes. Tear strength, however, is low and needs to be improved when the handling of thin films (such as DEAP elastomer films) is required. Nevertheless, tear strength is acceptable for micro-applications where the elastomer films are spin-coated in layers[35]. The tear strength of silicone elastomers is commonly improved by the addition of reinforcing silica particles in high concentrations (10-60 wt%). Reinforcing particles, on the other hand, do increase the elastic modulus of the elastomer and thereby decrease obtainable strain. A number of techniques have been employed to decrease the elastic modulus, such as solvent techniques[36] and bimodal networks[37], but silica particles are still the most used method to reinforce silicone elastomers. In doing so, elastic moduli around 0.1-1 MPa are commonly obtained. Decreasing operating voltage by altering the Young's modulus will introduce significant changes in several important properties, such as viscous dissipation, hysteresis, long-term stability and tear strength[26,38]. The large-scale processing of DEAPs is also heavily affected by both the Young's modulus and tear strength[33], so it is therefore most practical and feasible to optimise elastomers for DEAPs and lower the operating voltage by developing elastomers with higher dielectric permittivity.

1.3.1 Increasing dielectric permittivity

1.3.1.1 Fillers and blends

Dielectric permittivity has been improved by various techniques, most commonly through the use of filler materials with high dielectric constants. Examples include metal oxide fillers, such as TiO_2[28,39–49], $BaTiO_3$[28,48–52], Al_2O_3[48], and various other fillers, such as expanded graphite[53], carbon nanotubes[54–57], organically modified montmorillonite[58–60], lead magnesium niobate-lead titanate[28,49], lead-zirconate titanate[61], a copper-phthalocyanine oligomer[49,62], calcium copper titanate ($CaCuTi_4O_{12}$)[63], polydivinylbenzene (PDVB) particles[64] and poly(3,4-ethylenedioxythiophene)/polystyrene sulfonate/ethylene glycol particles[65]. These composite-type systems, however, do have certain drawbacks, such as large dielectric losses and reduced breakdown strengths as increases in dielectric permittivity are achieved at loadings near the percolation threshold, which means that the systems are prone to filler agglomeration and consequent significant changes in mechanical properties. Furthermore, the Young's modulus usually also rises significantly.

Various techniques have been developed, in order to avoid agglomeration and increasing stiffness when raising dielectric permittivity. These include the preparation of encapsulated polyaniline (PANI) particles with insulating PDVB shells that prevent agglomeration of the PANI particles[26,66]. Furthermore, blends of PDMS/poly(hexylthiophene)[67], PDMS/polythiophene[68] and PDMS/polyethylene glycol[69] have been developed to increase homogeneity between the matrix (PDMS) and filler (high dielectric permittivity polymer) and to maintain suitable elastic moduli.

1.3.1.2 Covalent grafting of organic dipoles to the silicone network

Another approach is to chemically graft organic dipoles to the PDMS elastomer network. This approach potentially leads to a more controlled network structure, as it does not rely on the efficient and perfect mixing of particles or blends. Furthermore, such covalently grafted systems should provide a more stable elastomer system upon continued activation of the material[47]. Several interesting systems have been developed in this respect.

Kussmaul et al.[70,71] and Risse et al.[72] added the synthesised dipolar molecule *N*-allyl-*N*-methyl-*p*-nitroaniline, together with compensating amounts of a hydride-functional cross-linker, to a PDMS matrix and a commercial silicone elastomer system, respectively, in one-step processes. Two-fold increases in dielectric permittivity were obtained. Dipolar molecules, however, were added in a competitive reaction with the network formation reaction, so there is a high risk of network imperfections such as dangling substructures and large sol-fractions, which can be washed out of the network[73]. Therefore, at high dipole concentrations, significantly softer networks were obtained and the electrical breakdown strengths were reduced.

Risse et al.[74] prepared a blend of a ~2300 g mol^{-1} cyanopropyl-functional PDMS and a PDMS matrix, where the cyano-functional PDMS acted both as a filler and as a plasticiser. Dielectric permittivity increased significantly (~two-fold), but the increase was accompanied by a 75% decrease in electrical breakdown strength (from 80 V/µm to 20 V/µm).

Racles et al.[75] developed another approach, where cyanopropyl-groups were distributed along the back-bone of PDMS chains. The cyanopropyl-functional hydroxyl-terminated PDMS was prepared by ring-opening polymerisation of different cyclotetrasiloxanes. Silicone elastomers were then prepared by cross-linking reactions with ethyltriacetoxysilane and a titanium tetra(2-ethylhexoxide) catalyst. Dielectric permittivity was found to increase two-fold, but the increase in permittivity was followed by an increase in conductivity and poorer mechanical properties. Good results were obtained when blends of the cyanopropyl-functional PDMS and a PDMS matrix were made.

1.4 Silicones

Polysiloxanes are an interesting and important class of polymers in which PDMS is the most widely used[76]. Polysiloxanes are based on the repeating unit RR'SiO, where R groups can be different organic groups such as vinyl, phenyl, hydride and alkanes, with the most common group being the methyl groups, such as those found in PDMS[77].

Polysiloxanes have many interesting properties, such as high thermal stability, chemical and biological stability and inertness, ozone and UV resistance, hydrophobicity, transparency, high gas permeability, low glass transition temperature, and low surface tension[78]. Polysiloxanes do not, however, possess good mechanical properties, and they are therefore often used as components in other systems or cross-linked and solidified into three-dimensional polymer networks, namely elastomers, which are usually formed by end-linking telechelic polymer chains in cross-linking reactions. When the siloxane polymer chains are linked together in networks, they cannot flow past each other and the network has the ability to return to its original shape after stress is applied. Silicone elastomers are viscoelastic materials and therefore exhibit properties as both elastic solids and viscous fluids. They furthermore have low mechanical losses and the ability to sustain high stresses.

Polysiloxanes, and in particular PDMS elastomers, have found widespread use as, for example, adhesives[79], membranes[80], sealants[81] and surface treatments[82,83] for soft lithography[84] and as dielectric elastomers. The PDMS elastomers utilised in these diverse applications are usually prepared by hydrosilylation, radical or condensation reactions forming a PDMS network. The most commonly applied preparation technique is the hydrosilylation reaction, where –Si-H groups react with $-CH=CH_2$ groups, as seen in Scheme 1. Hydrosilylation reactions are usually catalysed by a platinum catalyst, but they can also be catalysed by, for example, rhodium, ruthenium, palladium[85] and tris(pentafluorophenyl)borane[86,87]. The hydrosilylation reaction has the advantage over, say, a condensation reaction, in that it is very efficient and does not form by-products, which means that voids – in principle at least – can be avoided during elastomer synthesis.

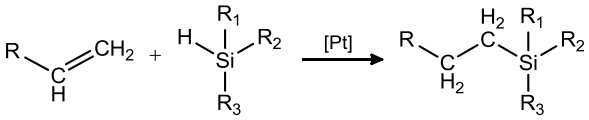

Scheme 1 Hydrosilylation reaction.

The most commonly employed cross-linking system uses *f*-functional hydride-functional cross-linker molecules and vinyl-terminated PDMS, as seen in Scheme 2. The functionality, *f*, of the cross-linker should be ≥3, in order to form a polymer network. The mechanical properties of a silicone network are governed primarily by the molecular weight of the PDMS chains, whereas the functionality of the cross-linker is less significant for cross-linkers with *f*>4 and no steric hindrance[88].

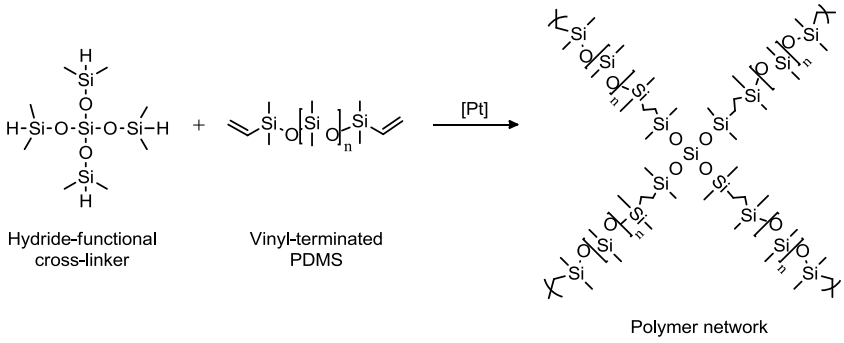

Scheme 2 PDMS hydrosilylation addition reaction with a tetra-functional hydride cross-linker and vinyl-terminated PDMS to form a PDMS network.

Despite many other excellent properties, PDMS elastomers suffer from low tear and tensile strength and are therefore considered as intrinsically weak. This is due to the low melting point of PDMS (−40°C) which means that above approximately −30°C the elastomer cannot reinforce itself through strain-induced crystallisation[89,90]. As a result, almost all applications require reinforced PDMS elastomers. The most common and efficient reinforcing filler for silicone elastomers is silica (SiO_2), which is added to elastomer systems in concentrations of 10-60 wt%. Other commonly used fillers for silicone elastomers include titania (TiO_2), zirconia (ZrO_2) and calcium carbonate ($CaCO_3$). The effectiveness of the reinforcement depends on the available surface area and the interaction between the filler and the base polymer such as van der Waals forces and hydrogen bonding. The fillers furthermore lead to a higher degree of orientation and immobilisation of the polymer chains in the strained elastomer.

1.5 Functional silicones

Functional silicones, i.e. silicones with chemical groups that alter the properties of the base polymer/elastomer, are in high demand for many advanced applications such as coatings[91], adhesives[92] and contact lenses[93]. Functionalisation reactions are very important in expanding the

application area of siloxanes. Although most commonly used to form silicone elastomers, the hydrosilylation reaction is also widely used to functionalise siloxane polymers[94,95] and elastomers[96] or smaller silanes/siloxanes[97–99]. This reaction is very efficient and robust, but it does use the expensive platinum catalyst.

1.5.1 Click chemistry

"Click reactions" are efficient and well-established reactions in the functionalisation of polymers and coupling of molecules, and they are known for being mild, selective and high-yielding reactions that bind two molecules together without the formation of by-products[100]. The most well-known is the 1,3-dipolar cycloaddition between an azide and an alkyne, first described by Huisgen[101]. The selective copper-catalysed variant known as the copper(I)-catalysed azide-alkyne cycloaddition (CuAAC), which yields 1,4-regioisomers of 1,2,3-triazoles, as seen in Scheme 3, was developed concomitantly by Meldal[102] and Sharpless[103].

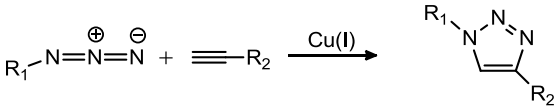

Scheme 3 Copper(I)-catalysed azide-alkyne cycloaddtion (CuAAC) reaction.

CuAAC reactions have been used widely to create functional polymers[104,105] in, for example, end-group functionalisations and block copolymer formations[106], surface functionalisations[107], dendrimer synthesis[108,109] and graft copolymers[110,111], thereby making it a highly versatile and robust reaction. CuAAC reactions have also been employed previously in the functionalisation of polysiloxanes[112–114] and in the formation of thermoplastic silicone elastomers[115]. Functional silicones that have been prepared through a copper-free variant of the click reaction between azides and alkynes should also be mentioned in this respect, including peptide- and carbohydrate-based silicone polymers[116], silicone surfactants[117], amphiphilic siloxane graft copolymers[118] and functionalised silicone elastomers[98].

1.5.2 Piers-Rubinsztajn reaction

Another approach for structured siloxanes and the controlled functionalisation of silicones is the dehydrocarbonative condensation of hydrosilanes and alkoxysilanes catalysed by tris(pentafluorophenyl)borane, as seen in Scheme 4. Piers reported its use as a catalyst for reactions involving organohydrosilanes[119–121], while Rubinsztajn and Cella used it thereafter as a catalyst for siloxane homo- and copolymers[122–124]. The Piers-Rubinsztajn reaction therefore refers to a tris(pentafluorophenyl)borane-catalysed reaction between a hydrosilane and an alkoxysilane forming siloxanes with the concomitant loss of an alkane[125]. The reaction is characterised by being mild and efficient since the reaction can be carried out rapidly at ambient temperatures and uses low amounts of borane catalyst.

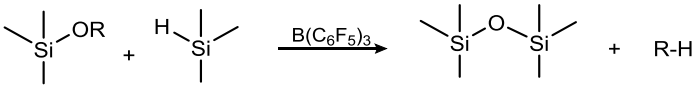

Scheme 4 Condensation reaction between hydrosilanes and alkoxysilanes forming an inert alkane by-product.

The Piers-Rubinsztajn reaction has been used to create alternating copolymers[87,122,123,126,127], small and functional siloxane molecules[117] and functional silicone polymers[128]. The reaction is tolerant towards many chemical groups such as the halides, phenyl and allyl groups[129].

A disadvantage of the Piers-Rubinsztajn reaction is that metathesis can occur. During metathesis the hydride and alkoxy groups switch places and the hydrosilane is consequently converted to alkoxysilane and vice versa. This can lead to less synthetic control and more disordered structures, especially when dealing with polycondensation reactions. Metathesis, however, is not always observed, a phenomenon which Brook et al.[125] suggest could be due to the sequence in which reagents are added to the reaction mixture. When the tris(pentafluorophenyl)borane is added to a mixture of the hydrosilane and alkoxysilane, metathesis is typically not observed. This is an important point to keep in mind when using the Piers-Rubinsztajn reaction.

Furthermore, flammable gas develops rapidly during the reaction and precautions, such as large reaction vessels, must be taken.

2 Synthesis of a novel cross-linker

The work in this chapter is based on the publication *Novel cross-linkers for PDMS networks for controlled and well distributed grafting of functionalities by click chemistry*, published in Polymer Chemistry, 2013, 4, 1700-1707 and reprinted with the kind permission of RSC publications. The manuscript can be found in Appendix A along with all experimental procedures and associated supporting information. Experimental procedures for unpublished reactions can be found in Chapter 9.

2.1 Introduction

The aim of the work in this chapter is to develop a method for incorporating evenly distributed functionality into silicone networks. This incorporation is envisioned to be performed through the covalent attachment of functional molecules with, for example, high dielectric constants to the network. Covalent attachment will provide a matrix with well-distributed modifications that prevent leakage of the functional moieties during use. A novel silicone-compatible cross-linker, containing an azido-group that opens up for CuAAC reactions, will provide networks with controlled and selective functionalisation, without compromising network formation and properties, as shown in Figure 3.

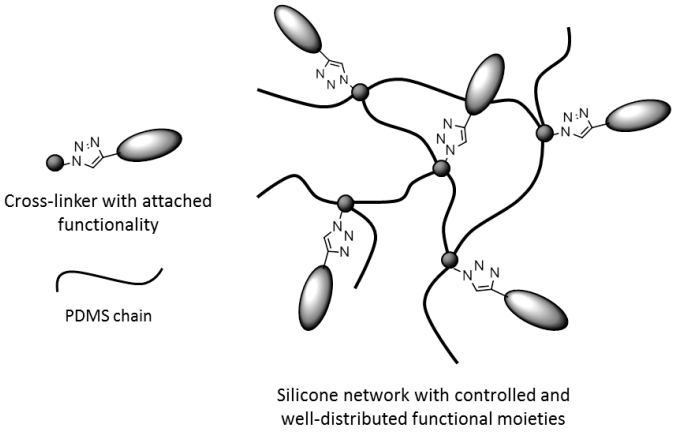

Figure 3 Schematic illustration of new functional cross-linkers used in a PDMS network forming reaction.

2.2 Results and discussion

2.2.1 Hydride-functional cross-linker

A hydride-functional cross-linker was first targeted, in order to create a system corresponding to the most commonly applied cross-linking systems, where hydride-functional cross-linkers react

with vinyl-terminated PDMS. In order to test the synthesis procedures and reaction conditions, a di-functional model compound was synthesised.

The hydride-functional model compound was prepared from 3-bromo-1,2-propanediol by first converting the hydroxyl groups into dimethylsilane groups using 1,1,3,3-tetramethyldisilazane and chlorodimethylsilane as a catalyst through a procedure adapted from Amela-Cortés et al.[130] and according to Scheme 5. It was not considered safe to first convert the bromine into an azido group, as small azido compounds are not chemically stable.

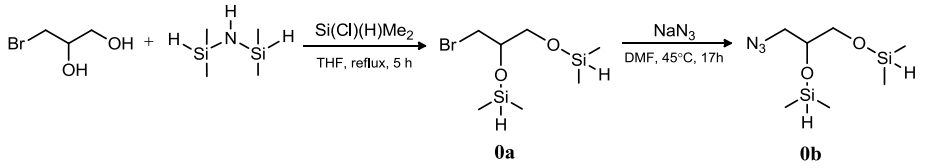

Scheme 5 Reaction procedures used to form the hydride-functional model compounds **0a** and **0b**.

Compound **0a** was characterised by FTIR, ^{1}H- and ^{13}C-NMR. FTIR confirmed the disappearance of the broad -OH band at approximately 3325 cm^{-1} and the presence of Si-H and Si-CH$_3$ groups as bands at approximately 2120 cm^{-1} and 1255 cm^{-1}, respectively. Through ^{1}H-NMR the Si-H groups (e) were detected as resonances at δ_H = 4.63 to 4.70 ppm (Figure 4). Compound **0a** was now reacted with sodium azide in a substitution reaction in *N,N*-dimethyl formamide (DMF) to form **0b**. FTIR confirmed the presence of the distinct azido band at approximately 2100 cm^{-1}. The Si-H band was not present from FTIR; however, a broad band at 3330 cm^{-1} was noticed. Upon examination of the ^{1}H-NMR spectrum it is clear that the Si-H protons have vanished, as seen in Figure 4.

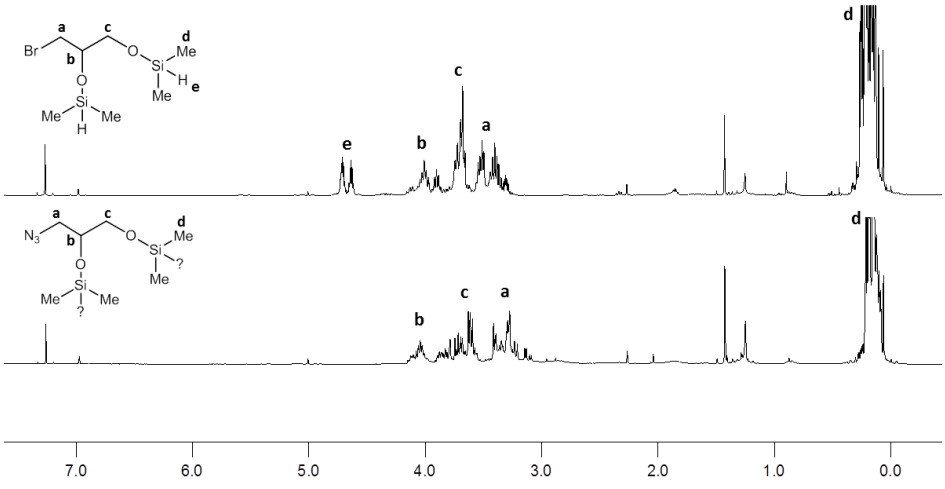

Figure 4 ^{1}H-NMR spectra of **0a** (top) and **0b** (bottom) showing the disappearance of the Si-H protons.

While it was possible to create a hydride-functional molecule (**0a**), it was not possible to create an azido-functional hydride molecule. The FTIR spectrum of **0b** might provide the answer to what made the Si-H groups disappear, as the broad band at 3330 cm^{-1} could be due to the presence of -OH groups. During the work-up and purification of **0b**, excess sodium azide and other salts were removed through extraction and washing with water. In the presence of water and an acidic or basic environment, Si-H groups can be converted into silanol groups[131], and it is therefore likely that a hydrolysation reaction took place. From these experiments it can be concluded that Si-H groups are too labile and unstable to be utilised for further functionalisation reactions, as CuAAC reactions also require basic reaction conditions and aqueous work-up. There is also the possibility, even upon successful synthesis, that the prepared molecules could have too poor a shelf-life.

2.2.2 Allyl-functional cross-linker

The development of a novel silicone-compatible cross-linker shifted toward the synthesis of an allyl-functional cross-linker molecule. This means that the hydrosilylation reaction seen in Scheme 2 is reversed, to $-CH_2=CH_2$ groups on the cross-linker and hydride groups on the PDMS polymer. Such hydride-terminated PDMS polymers are readily commercially available, and the polymer networks prepared from the reversed reaction should have identical final properties independent of the chemical groups of the starting materials.

The requirements for a new cross-linker with $-CH=CH_2$ groups are that it should be an easy to synthesise molecule that is silicone-compatible and bears ≥3 $-CH=CH_2$ groups. Thus, an azido-functional, silicone-compatible tri-functional cross-linker (**2**) was synthesised in two steps via the silyl ether reaction between (3-bromopropyl)trichlorosilane and allyl alcohol and the subsequent substitution of bromine with the azide anion, as illustrated in Scheme 6. The reaction to form **1** was selected, as it is a simple procedure with readily available starting materials. The reaction can furthermore be carried out at ambient temperatures and does not require extensive purification procedures other than filtration and the evaporation of by-products and excess reagents.

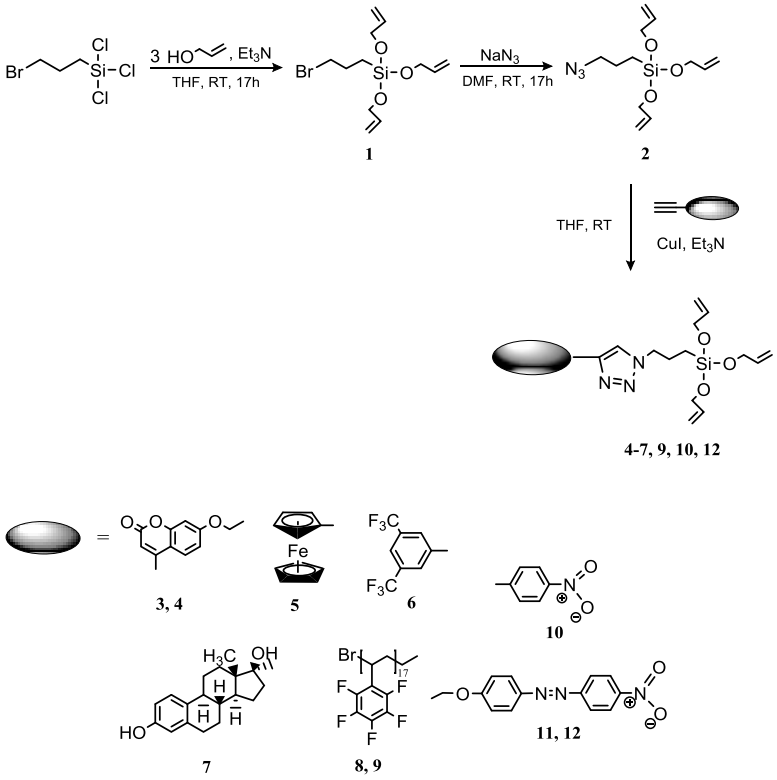

Scheme 6 Preparation of the azido-functional cross-linker **2** and functional cross-linkers via Cu-AAC reactions.

The azido cross-linker was isolated as an orange-yellowish oil in a high yield and high in purity. The cross-linker (**2**) proved to be hydrolytically stable under the utilised synthesis conditions, which included several extraction procedures with water. The stability of the formed silyl ether bond was evaluated using ^{1}H-NMR in D_2O. Spectra were recorded over time, and integration of the O-CH_2 resonances at δ_H = 4.30 ppm compared to the integration of other peaks indicated that no detectable cleavage of the Si-O-C bond had taken place in the stability test over the 72 hours.

A general reaction scheme, along with a variety of alkyne-functional molecules used in the Cu-AAC reactions with **2**, are shown in Scheme 6. Several types of alkyne-functional molecules were chosen, in order to illustrate the versatility of the novel cross-linker and the CuAAC reaction and also to detect any possible limitations in which groups that could be attached to the cross-linker. Furthermore, the different functional groups could provide PDMS elastomers with different final properties, which could consequently extend the application area of PDMS networks greatly, not only in the area of dielectric elastomers. Therefore, the properties of elastomers with different types of functional groups were investigated. Introducing 4-methylumbelliferone (**3** and **4**) will create a PDMS network with a fluorescent tag at the cross-linking site that can be used not only to visualise the distribution of incorporated functionality and networks densities (see Chapter 4) but

also create luminescent PDMS films. The incorporation of ferrocene (**5**) will provide PDMS films with potential applications within the optical, magnetic or electronic fields[132] and within cancer research, as certain ferricenium complexes are known to show anti-tumour activity[133]. Ferrocene has also been positioned recently on the surfaces of nanoparticles[134] or single-walled carbon nanotubes[135] through the application of click chemistry and ethynylferrocene. Different kinds of drugs or therapeutics for biomedical applications will also be possible through the introduction of an estradiol functionality (**7**)[136]. Recently, it has been shown that the introduction of trifluoromethyl groups improves the oil and solvent resistance of PDMS films[137]. With this in mind, bis(tri-fluoromethyl)phenyl (**6**) and a short poly(pentafluorostyrene) chain (**8** and **9**) are inserted into the PDMS network. Possible improvements to the release properties of such fluorine containing PDMS films during processing will also be investigated. And finally, push-pull dipolar molecules that potentially enhance dielectric permittivity of silicone elastomers can be inserted from a 1-ethynyl-4-nitrobenzene (**10**) and an alkyne-functional nitroazobenzene (**11** and **12**) and thus improve dielectric elastomer performance.

An important property of the system is that the alkyne-functional molecule – in principle – can be clicked onto the azido-functional cross-linker, before or after the cross-linking reaction that leads to the PDMS network. Presented herein, is the preparation and characterisation of novel PDMS networks containing elaborated functionalities using the pre-cross-linking approach with the series of new silicone-compatible cross-linkers. The pre-cross-linking procedure avoids the step of swelling the PDMS network for successful click reactions, and furthermore it allows for the comprehensive characterisation of the individual functional cross-linkers.

Three of the employed alkynes, **3**, **8** and **11,** were not commercially available but prepared for this study. Alkyne **8** was polymerised under controlled ATRP conditions using a previously published procedure[138] and yielding an alkyne-functional poly(pentafluorostyrene) of ~3300 g mol^{-1}, while **3** and **11** were prepared via a Williamson ether synthesis of the phenol-equivalents of **3** and **11** and propargylbromide with a K_2CO_3/18-crown-6 catalytic system, as shown in Scheme 7.

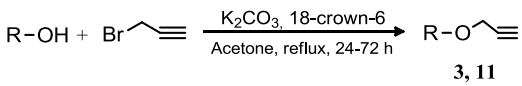

Scheme 7 General reaction procedure for the aromatic Williamson ether synthesis giving alkyne-functional **3** and **11**.

The functionalised cross-linkers were all prepared under similar CuAAC reaction conditions using a CuI/Et_3N catalytic system. The synthesised alkynes (**3**, **8** and **11**) and all novel functional cross-linkers, **4**-**7**, **9**, **10** and **12**, were characterised by FTIR, ^{1}H- and ^{13}C-NMR. FTIR was used to confirm the completion of the CuAAC reactions by the disappearances of the alkyne band at approximately 3300 cm^{-1} and the very distinct azido band at approximately 2100 cm^{-1}. The presence of the triazole proton in ^{1}H-NMR points to the successful formation of reaction products. The triazole proton appears from δ_H = 7.42 ppm to δ_H = 7.91 ppm, depending on the electron density of the triazole. A representative ^{1}H-NMR spectrum of **4** with assignments can be seen in Figure 5.

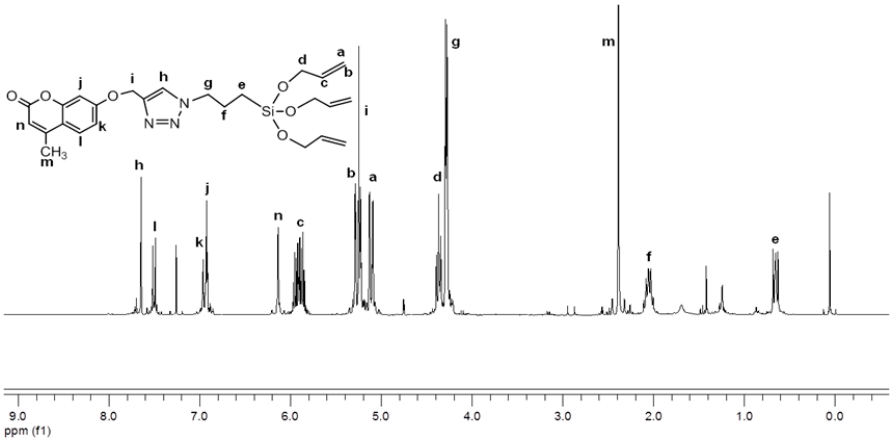

Figure 5 ^{1}H-NMR spectrum of **4** showing the formation of the triazole proton (h).

If small residues of azido/alkyne can be detected, they are easily removed through the use of resins, which facilitate a simple purification procedure, along with extraction and washing, to remove catalysts. For example, in connection with the synthesis of **6**, a small alkyne band was detected by FTIR, and a peak for the alkyne proton was also detected by ^{1}H-NMR at δ_H = 3.26 ppm. Cross-linker **6** was consequently treated with an azido-functional Merrifield resin, in order to remove residual alkyne reactant through an additional CuAAC reaction and the resulting attachment of the alkyne reactant to the resin. The azido resin with the excess alkyne attached could thereafter be removed from the reaction mixture by simple filtration.

The PDMS networks were prepared from cross-linkers **2**, **4**-**7**, **9**, **10** and **12**, hydride-terminated PDMS and a platinum catalyst, according to Scheme 8.

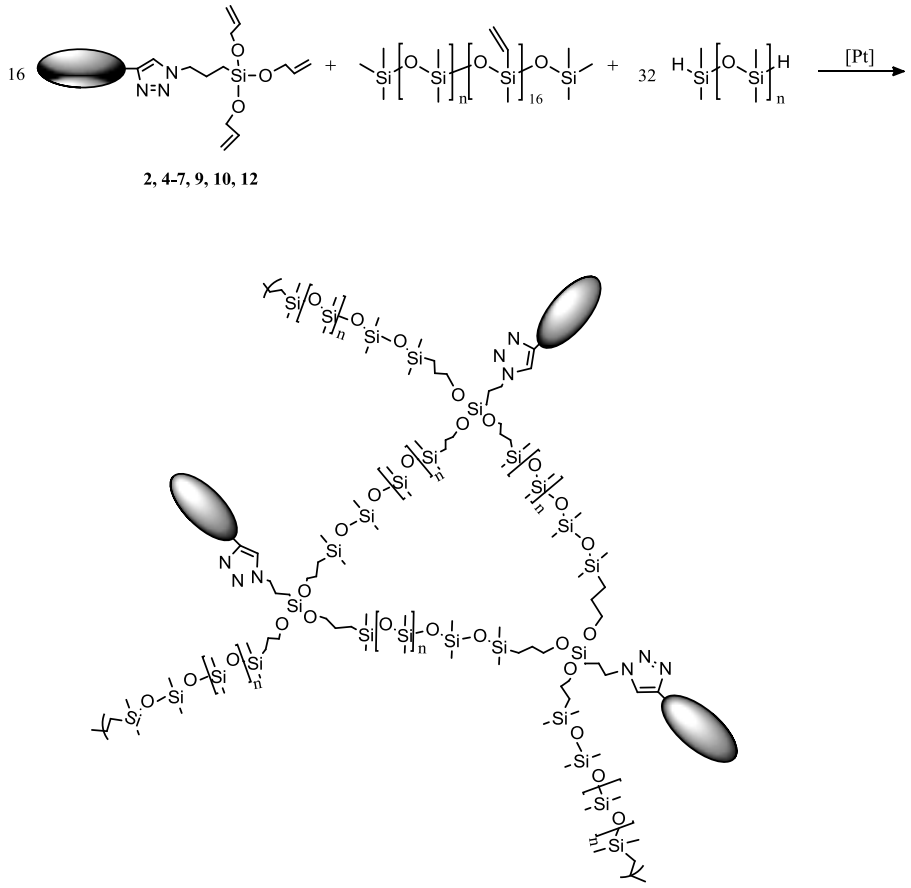

Scheme 8 Cross-linking reaction between **2**, **4**-**7**, **9**, **10** or **12** and hydride-terminated PDMS.

A commercially available 16-functional silicone cross-linker was used to reinforce the network, since networks prepared solely from tri-functional cross-linkers can be very soft and have low mechanical breakdown strength[139]. The molar ratio between the tri-functional synthesised cross-linkers and the 16-functional commercial silicone cross-linker was 16:1, to ensure a high concentration of the functionalised cross-linkers and minimise possible competition from the 16-functional cross-linker. The networks were prepared with equimolar amounts, meaning that the number of functional hydride groups of the polymer corresponded to the total number of reactive groups on the two cross-linkers. The PDMS films ranged from light yellow in colour for films with **10** and **7** to light brown for films with **5** and **6** and darker brown for **9**. The film with **2** was completely transparent, whereas the film with **4** was light grey and opaque. Images of all the films can be seen in Figure 6.

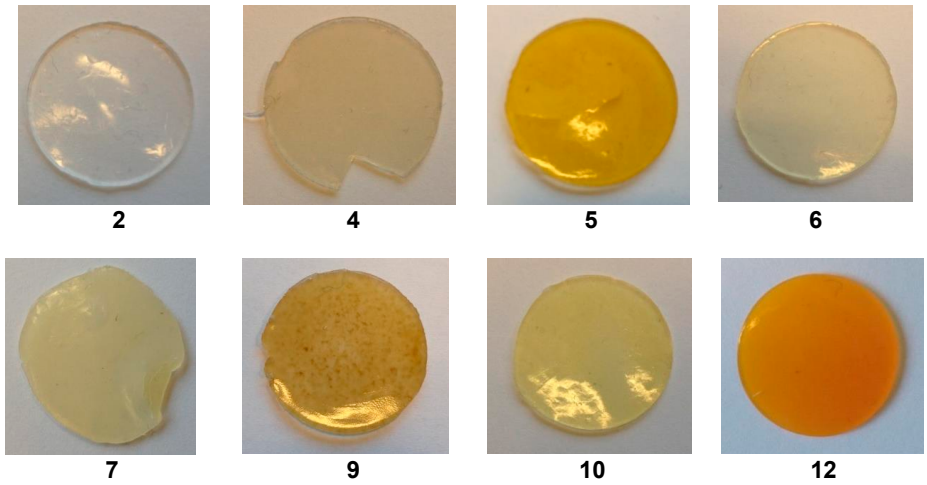

Figure 6 Photos of the films prepared with the synthesised cross-linkers.

All prepared films were characterised by FTIR. There were, however, no differences between the films with different functional cross-linkers, since the concentrations of cross-linkers in the films were found to be too low to be detected by this technique. Solid state ^{13}C-NMR of the elastomer with **4** obtained over 20 hours revealed the dominating Si-CH_3 resonance at ~1 ppm. In addition, three small resonances at ~4, ~8 and ~24 ppm can be assigned to -CH_2 close to Si atoms. Weak signals in the 100-160 ppm range indicate the presence of aromatic carbons. The solid state ^{13}C-NMR analysis thus strongly supports the presence of the silyl-based cross-linker in the network.

Swelling and extraction experiments with chloroform were used to determine the amount of bonded (gel fraction) and non-bonded (sol fraction) species in the films. Gel fractions were calculated as the weight after extraction and drying (m_e) divided by the initial weight of the sample (m_0) as W_{gel}(%) = m_e/m_0 ×100. This was done in order to further elucidate if the synthesised cross-linkers had reacted with the PDMS chains and were incorporated covalently in the network. Possible problems that such modified networks could encounter include poor compatibility with the matrix and steric hindrance of the tri-functional cross-linker, leading to dangling chains and extractable substructures containing primarily triazole cross-linkers. Some of the produced films had indeed large sol fractions, especially from the Soxhlet extraction data (Table 1). Nonetheless, it is not common practice to perform this type of extraction when investigating PDMS network gel fractions, as it is a very aggressive method. The swelling experiments performed are therefore more suitable for comparison with previously performed PDMS swelling experiments[73,140]. Optimised PDMS elastomers usually have gel fractions of 95-97% whereas stoichiometric PDMS networks usually have gel fractions at around 90%. This can be explained by the optimised PDMS elastomers having a stoichiometry of 1.1-1.4, which means that the cross-linker is in excess and that all cross-linker sites do not need to react, thus reducing steric hindrance[30]. The networks prepared in this study are all stoichiometric, such that gel fractions of less than 90% are anticipated.

Table 1 Gel fractions (W_{gel}) of samples as results from Soxhlet extractions and swelling experiments.

Cross-linker	W_{gel} (Soxhlet extraction) [%]	W_{gel} (Swelling) [%]
2	79	84
4	57	92
5	53	83
6	74	90
7	56	59
9	42	69

A visual evaluation of the dry sol and gel fraction revealed that all films (gel fractions) retained their initial colours, due the presence of the functional cross-linkers. Furthermore, all sol fractions bore little or no evidence of colour from cross-linkers. In order to further investigate the nature of the gel and sol fraction, fluorescent intensity was measured for both the dried sol and the gel fraction of the film prepared with the fluorescent cross-linker **4** after the Soxhlet extraction experiment. Fluorescent intensity was also measured for the film with **4**, before the Soxhlet extraction. Results are shown in Figure 7.

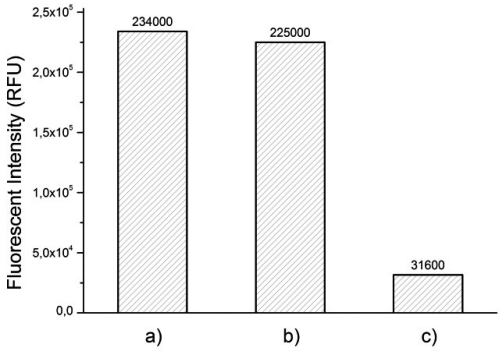

Figure 7 Fluorescent intensity of: a): film with **4** before Soxhlet extraction; b): dried film with **4** after Soxhlet extraction (gel fraction) and c): dried sol fraction of film with **4**.

It was observed that the fluorescent intensity of the film prepared with **4** only decreases by 4% after extraction. This indicates that cross-linker **4** is indeed incorporated into the PDMS network gel fraction and is thus bound covalently to the network. The sol fraction exhibits very low fluorescent intensity and therefore most likely consists of PDMS substructures not connected to the network, such as inert or mono-functional PDMS chains. It can hence be concluded, that the synthesised cross-linkers can be incorporated successfully into PDMS networks.

To investigate the distribution of the grafted functionalities, fluorescent microscopy was performed on the film prepared with cross-linker **4**, which acts as a fluorescent tag in the network, as seen in Figure 8.

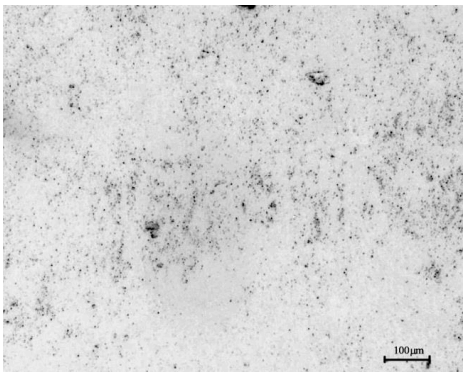

Figure 8 Grayscale fluorescent microscopy image of a film prepared with cross-linker **4**.

It is evident that the film with **4** is indeed fluorescent and that the fluorescent cross-linker is evenly distributed throughout the network. This indicates that the synthesised triazole cross-linkers can be incorporated successfully into PDMS networks in a well-distributed manner.

Mechanical characterisation was performed by determining the storage and loss moduli for the films, as seen in Figure 9.

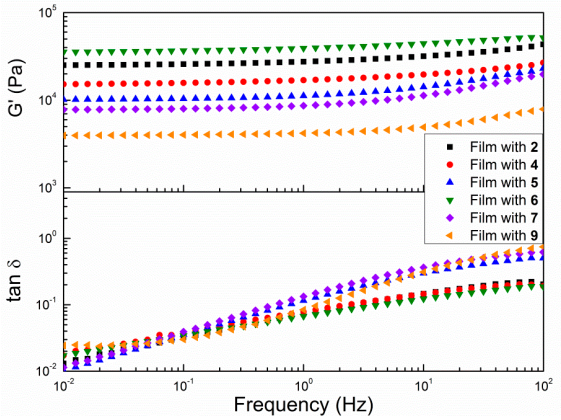

Figure 9 Top: storage moduli (G') and bottom: loss (tan δ) as functions of frequency for films prepared with cross-linkers **2**, **4**-**7** and **9**.

It is evident that the networks are well cross-linked, as the storage moduli are of an order of 10 to 100 times greater than the loss moduli for the investigated frequency regime[30]. Elastomers containing functional groups are all (expect for the film with **6**) seen to have lower moduli than the film prepared with azido-functional cross-linker **2**. This can be explained by the bulky groups attached to the cross-linkers, which thereby create a small diluting effect in the network and thus create softer films.

The elastomer with cross-linker **9** has lower modulus than the other films. This corresponds with the results seen from the extraction experiments, which showed that the film with **9** has a signifi-

cantly smaller gel fraction than the other networks. The large poly(pentafluorostyrene) groups thereby create a soft network with a large portion of extractable substructures. This could be due to incompatibility between the two polymers, leading to phase separation, which is also visually evident from the darker domains formed in the film (see Figure 6).

Thermal gravimetric analysis (TGA) was used to investigate the effects of the different functional cross-linkers on the thermal stability of the PDMS films (Figure 10).

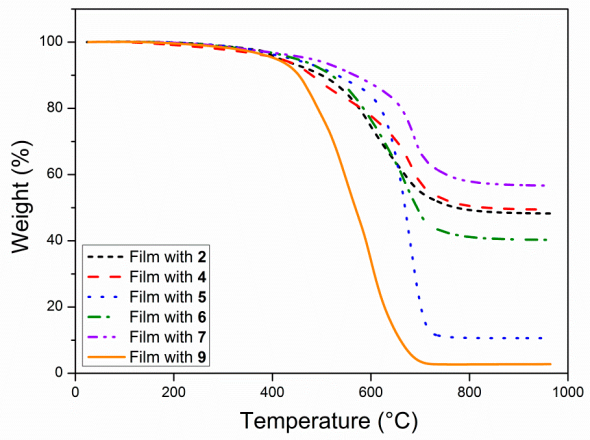

Figure 10 TGA measurements of PDMS films prepared with cross-linkers **2**, **4**-**7** and **9**.

All TGA curves exhibit a two-step mass loss process, and decomposition temperatures are taken as the peak temperature of the first derivate of the temperature with time. The first degradation step occurring from 360°C to 540°C (mass loss of 1.8-12.7 wt%) depending on functionality, corresponds to the cleavage of Si-CH_3 bonds. In the case of **9** it is noted that at 510°C all the poly(pentafluorostyrene) has degraded[141]. The second decomposition step, occurring from 410°C to 570°C (mass loss of 32.5-86.4 wt%), can be attributed to structural rearrangements followed by mineralisation of the materials[142]. The TGA curves show that the PDMS samples have different decomposition temperatures, depending on the incorporated functionality, with **5** providing the highest initial degradation temperature (540°C), due to the higher thermal stability of ferrocene[143], which increases the degradation temperature of the PDMS film. It is hypothesised that the ferrocene cross-linker, however, also catalyses the PDMS degradation to such an extent that significant mineralisation occurs. The effect can also be observed for the film with **9** (poly(pentaflurostyrene)), where the release of fluoride ions degrades the PDMS to a greater extent than the other cross-linkers[144]. It is moreover noted that all films with a functional cross-linker, except for **9**, induced a higher decomposition temperature than the film with a non-functional cross-linker (**2**).

The impact of the fluorine containing cross-linkers (**6** and **9**) on the surface properties of the PDMS films was determined using contact angle measurements with water. The contact angle was found to increase from 108±2.5° for the film with cross-linker **2** to 116±2.5° for the PDMS film with cross-linker **9**. This is due to the hydrophobic nature of the poly(pentafluorostyrene) which

causes the migration of the fluorinated polymer to the PDMS surface, before curing[145], thus increasing the contact angle and thereby also a possible improvement of release properties for PDMS films during processing[33]. The film with **6** showed no increase in contact angle compared to the film with **2**. This is probably due to the low concentration of fluorine on this cross-linker, which allows the cross-linker to be encapsulated within the PDMS network, in which case no migration to the surface will consequently occur.

These promising initial studies show that the synthesised cross-linker can be successfully incorporated into PDMS networks, and therefore it represents a novel method for grafting various functionalities onto silicone networks. The different functionalities that were incorporated all illustrate different approaches to expanding the application area of PDMS elastomers with, for example, higher thermal stability (cross-linker **5**), a higher degree of hydrophobicity (cross-linker **9**), fluorescent activity (cross-linker **4**) and improved biocompatibility (cross-linker **7**).

3 Dielectric properties of PDMS networks prepared with dipolar cross-linkers

The work in this chapter is based on the publication *Dipolar cross-linkers for PDMS networks with enhanced dielectric permittivity and low dielectric loss*, published in *Smart Materials and Structures,* 2013, 22, 104002 and reprinted with the kind permission of IOPscience. The manuscript can be found in Appendix B along with all experimental procedures and associated supporting information.

3.1 Introduction

The purpose of the work in this chapter is to investigate the effect of two different dipolar cross-linkers (nitrobenzene-functional cross-linker **10** and nitroazobenzene-functional cross-linker **12**) on the properties of PDMS elastomers. The study will include the effect on mechanical properties, dielectric permittivity and electrical breakdown strength, using varying contents from the two dipole-functional cross-linkers and two different PDMS chain lengths, thus varying network densities and mechanical properties. Networks prepared with a high molecular weight PDMS create softer, highly stretchable films with potential uses as actuators, where large strains are desired. Low molecular weight PDMS elastomers are stiffer and less stretchable, and therefore they find applications within the area of generators, where resonance frequency can be tuned to optimise performance using the stiffness of the material[18,146].

3.2 Results and discussion

Dipole-functional PDMS networks were created using cross-linkers **10** and **12**, hydride-terminated PDMS of 28,000 g mol^{-1} or 6000 g mol^{-1} and a platinum catalyst, as seen in Scheme 8. The functional PDMS films were reinforced with a 16-functional commercial vinyl cross-linker as well as surface-treated silica particles (10 wt%). The ratio between the tri-functional dipole cross-linkers and the commercial cross-linker was varied to create PDMS films of 0.23 to 3.6 wt% of the dipolar cross-linker, corresponding to concentrations of 0.08-1.20 wt% of pure dipole for **10** and 0.11-1.79 wt% of pure dipole for **12**. Reference films prepared solely with 16-functional commercial cross-linkers were also made. All networks were prepared in stoichiometric cross-linking reactions, meaning that the number of functional hydride groups of the PDMS chains corresponds to the total number of vinyl groups on the cross-linkers. Table 2 provides an overview of the content of cross-linkers **10** and **12**, the content of pure dipole and the molar ratio between dipolar cross-linkers **10** and **12** and the additional 16-functional cross-linker. For all films the functional cross-linker is >50 mol% of the total amount of used cross-linker.

Table 2 Overview of cross-linker content in the prepared elastomer films.

Cross-linker content	Films with cross-linker 10		Films with cross-linker 12	
	Content of pure dipole	Molar ratio 10/additional cross-linker	Content of pure dipole	Molar ratio 12/additional cross-linker
[wt%]	[wt%]		[wt%]	
28,000 g mol^{-1}:				
0.00	0.00	0/100	0.00	0/100
0.23	0.08	66/34	0.11	58/42
0.45	0.15	85/15	0.22	78/22
0.72	0.24	96/4	0.36	90/10
6000 g mol^{-1}:				
0.00	0.00	0/100	0.00	0/100
1.35	0.46	80/20	0.67	73/27
2.25	0.77	91/9	1.12	85/15
3.60	1.20	98/2	1.79	94/6

The gel fractions of the films were determined in swelling experiments with chloroform. As seen in Table 3, gel fractions decrease slightly in line with increasing amounts of dipole-functional cross-linker. This decrease can be explained by the increasing amount of tri-functional cross-linkers, which create an increasingly softer network with resulting larger concentrations of non-bonded species and substructures. Furthermore, as the PDMS networks were prepared in stoichiometric reactions, in order to avoid the non-bonded functional cross-linker, gel fractions around or lower than 90% were thus expected.

Table 3 Gel fractions (W_{gel}) as a result of swelling experiments for both dipole cross-linkers.

Cross-linker content	Films with cross-linker 10	Films with cross-linker 12
	W_{gel}	W_{gel}
[wt%]	[%]	[%]
28,000 g mol^{-1}:		
0.00	92	92
0.23	81	89
0.45	87	89
0.72	64	90
6000 g mol^{-1}:		
0.00	95	95
1.35	95	97
2.25	91	93
3.60	77	93

Through visual comparison of the films, before and after the extraction experiments, it is evident that all films retained their colour after extraction, due to the dipole-functional cross-linker remaining in the network. As determined from the work in Chapter 2, when using a fluorescent functionality attached at the cross-linker, only small amounts of the functional cross-linkers are extracted from the networks, which means that the sol fractions most likely predominantly consist of substructures such as inert or mono-functional PDMSs.

The influence of the concentration and type of dipole-functional cross-linker on mechanical properties was investigated by determining the storage and loss moduli of the prepared films. In Figure 11, the results for films with cross-linker **10** and cross-linker **12**, respectively, are presented. Furthermore, the resulting shear storage moduli (G') and loss (tan δ) at 1 Hz are summarised in Table 4.

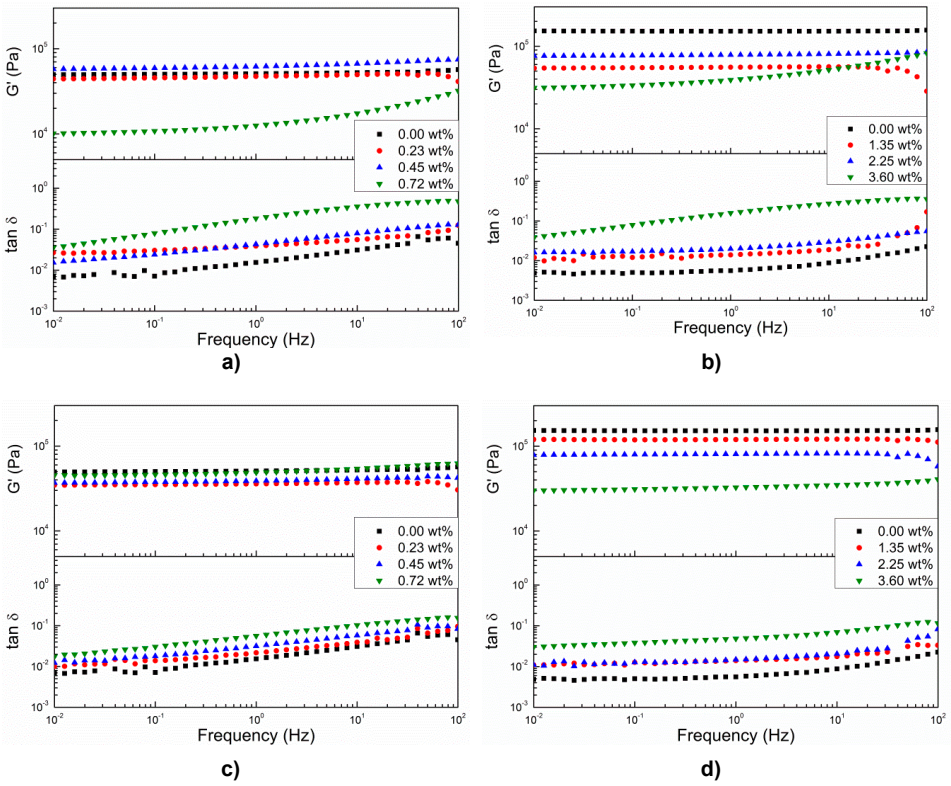

Figure 11 Storage moduli (G') and loss (tan δ) as functions of frequency for films prepared with: a) cross-linker **10** and 28,000 g mol^{-1} PDMS; b) cross-linker **10** and 6000 g mol^{-1} PDMS; c) cross-linker **12** and 28,000 g mol^{-1} PDMS and d) cross-linker **12** and 6000 g mol^{-1} PDMS.

All networks with **10** and **12** for both 28,000 g mol^{-1} and 6000 g mol^{-1} PDMS are very well cross-linked, as the storage moduli (G') are 10 to 100 times larger than the loss moduli (G'') for the investigated frequency regime, with the difference being at its smallest at high frequencies (100 Hz). This means that viscous dissipation at the low-strain low-frequency limit is a few percentage points only. It can also be seen that films prepared with the lower molecular weight PDMS (6000 g mol^{-1}) have higher moduli than films prepared with the higher molecular weight PDMS (28000 g mol^{-1}), due to increased network density, which in turn creates stiffer films. According to fundamental theories on rubber elasticity, elastic moduli are expected to scale linearly with inverse molecular weight, but the systems contain fillers, and the high molecular weight PDMS is furthermore above the entanglement threshold[30], which explains the weaker depend-

ency on molecular weight. For films with cross-linker **10**, elastomers containing large concentrations of the tri-functional cross-linker (0.72 wt% for 28,000 g mol^{-1} and 3.6 wt% for 6000 g mol^{-1}) are seen to have slightly lower moduli than those prepared solely with the 16-functional commercial cross-linker. This can be explained by the cross-linker functionality, *f*, which for $f<4$ is known to have a significant impact on the stiffness of elastomers, since the classical rubber theories predict that the elastic modulus scales with: $1-(2/f)$[139]. For PDMS films prepared with a large amount of the more sterically hindered tri-functional cross-linker, a softer network is created than for films with a 16-functional cross-linker alone.

The prepared networks contain 10 wt% silica particles to reinforce the otherwise fairly weak films (with respect to tearing). The particles limit the mobility of the polymer chains – both the dangling and sol variety in the network and decrease the conversion of the hydrosilylation reaction, due to limitations in the mobility of the reactive groups. The networks are thereby believed to be prone to post-curing. Overall, the elastic properties have not changed extensively following the addition of the two different dipole functional cross-linkers, though viscous loss is increased with increased amounts of cross-linker.

The impact of the type of push-pull dipole cross-linker on dielectric properties was determined through dielectric relaxation spectroscopy on discs of ~1 mm thick films. Dielectric relaxation spectra showing the frequency-dependent dielectric permittivity (ε') and loss tangent ($\tan\delta$) for films with cross-linkers **10** and **12** are presented in Figure 12.

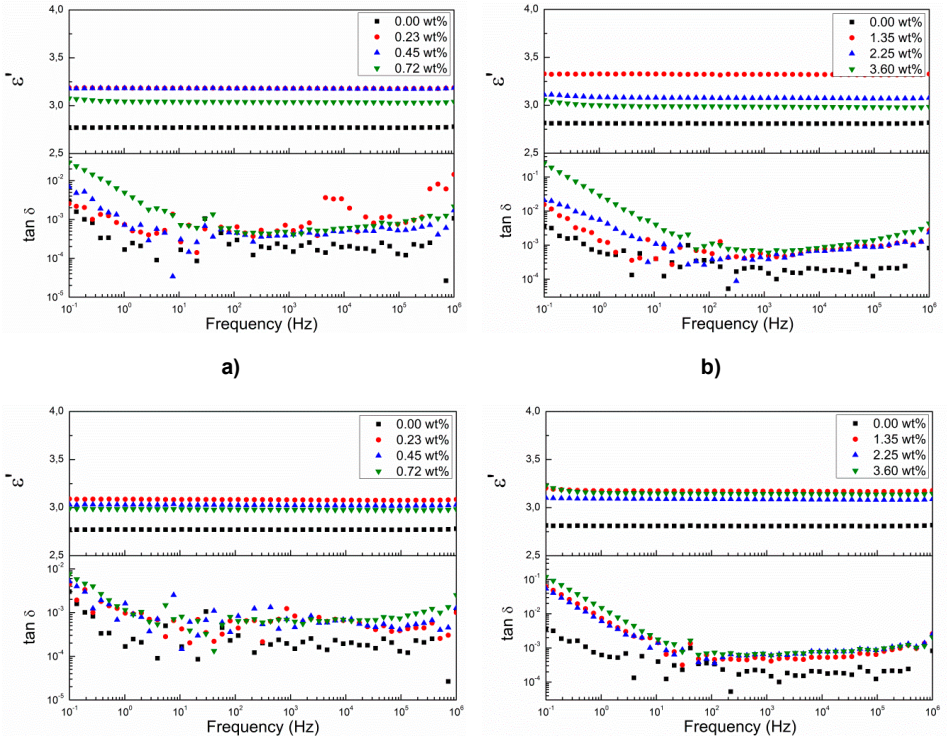

Figure 12 Dielectric permittivity (ε') and loss tangent (tan δ) as functions of frequency for films prepared with: a) cross-linker **10** and 28,000 g mol^{-1} PDMS; b) cross-linker **10** and 6000 g mol^{-1} PDMS; c) cross-linker **12** and 28,000 g mol^{-1} PDMS and d) cross-linker **12** and 6000 g mol^{-1} PDMS.

For both cross-linkers an increase in dielectric permittivity is observed following the addition of the dipole-functional cross-linker. In all cases, the effect is greatest at the lowest amount of added dipole cross-linker. Compared to pure PDMS, with only a commercial cross-linker for which $\varepsilon' = 2.8$ at 100 Hz, the film prepared with 6000 g mol^{-1} PDMS containing 1.35 wt% of cross-linker **10** has $\varepsilon' = 3.3$ at 100 Hz. This corresponds to an increase of 19% at only 0.46 wt% of pure dipole. The reason why permittivity is highest at the lowest cross-linker concentration could be due simply to large uncertainties associated with the measuring method. Furthermore, the concentration of pure dipole does not vary sufficiently to yield differences in permittivity with the given uncertainty of the method. Even though nitroazobenzene has a higher dipole moment than nitrobenzene (μ = 11.2 D for nitroazobenzene[147], μ = 4.22 D for nitrobenzene[148]), cross-linkers **10** and **12** enhance permittivity in the same order of magnitude. Previous reports suggest that this could be due to the *trans-cis* stereochemistry and photo-isomerisation of the nitrogen-nitrogen double bond (N=N) in azobenzene. In visible light the N=N bond adopts a *trans* configuration, which has a much lower dipole moment (close to 0 D) than the UV light-induced *cis* configuration[149,150]. The overall dipole moment of nitroazobenzene is therefore expected to lie within the range of that

of nitrobenzene, thereby yielding the same increases in the dielectric permittivity of the prepared dielectric elastomers. It was unfortunately not possible to irradiate elastomers with cross-linker **12** with UV light and perform subsequent measurements of dielectric permittivity, though this would have been an interesting experiment.

Dielectric permittivity can be observed to remain constant across the entire frequency range; furthermore, dielectric losses – for all films – remain low after the addition of dipole cross-linkers. This means that all films exhibit very low electrical energy dissipation and moreover that the films exhibit very low conductivity, which is also corroborated by conductivity measurements. The measured values of ε' and tan δ at 100 Hz are summarised for all films in Table 4.

Table 4 Dielectric permittivity (ε') and loss tangent (tan δ) at 100 Hz as well as breakdown strength (E_B) and storage moduli (G') and loss (tan δ) for films with different types and weight percentages of cross-linker.

Cross-linker content	Films with cross-linker 10						Films with cross-linker 12					
	Dielectric spectroscopy		Electrical break-down	Rheology		Figure of merit	Dielectric spec-troscopy		Electrical break-down	Rheology		Figure of merit
	ε'	tan δ	E_B	G' @1Hz	tan δ @1Hz	F_{om}/F_{om_ref}	ε'	tan δ	E_B	G' @1Hz	tan δ @1Hz	F_{om}/F_{om_ref}
[wt%]			[V/μm]	[kPa]					[V/μm]	[kPa]		
28,000 g mol^{-1}:												
0.00	2.8	2.69×10^{-4}	91.8	50.8	0.015	1.00	2.8	2.69×10^{-4}	91.8	50.8	0.015	1.00
0.23	3.2	5.78×10^{-4}	88.2	47.3	0.039	1.13	3.1	5.25×10^{-4}	95.0	35.9	0.022	1.68
0.45	3.2	4.54×10^{-4}	49.9	61.8	0.043	0.28	3.0	6.33×10^{-4}	88.9	38.8	0.032	1.32
0.72	3.0	5.24×10^{-4}	39.0	12.5	0.183	0.79	3.0	7.03×10^{-4}	85.9	48.8	0.057	0.98
6000 g mol^{-1}:												
0.00	2.8	3.45×10^{-4}	111.0	151.9	0.006	1.00	2.8	3.45×10^{-4}	111.0	151.9	0.006	1.00
1.35	3.3	6.01×10^{-4}	91.9	55.6	0.014	2.21	3.2	5.21×10^{-4}	124.2	119.7	0.014	1.82
2.25	3.1	3.34×10^{-4}	71.8	78.5	0.020	0.89	3.1	4.04×10^{-4}	68.2	80.8	0.015	0.79
3.60	3.0	10.5×10^{-4}	na[a]	39.9	0.159	-	3.2	7.16×10^{-4}	57.0	32.6	0.048	1.40

[a] Attempts to obtain electrical breakdown strength were unsuccessful, as the prepared 150 μm films were too sticky to be handled.

Electrical breakdown strength, E_B, for films with cross-linkers **10** and **12** are presented in Table 4. For films with cross-linker **12**, an increase in the breakdown field strength was observed following the addition of a low amount of tri-functional cross-linker for both the 28,000 g mol^{-1} and 6000 g mol^{-1} films. In both cases, the measured values of 95.0 V/µm and 124 V/µm, respectively, are remarkably high. Usually, increases in electrical breakdown strengths are the result of an increase in the modulus[151]; however, this is not the case for these samples, and the nitroazobenzene group must therefore contribute to increased breakdown strength. In many other studies, chemical elastomer manipulations, employed to increase permittivity, usually lead to decreasing breakdown strengths[70,71,74,75]. For films with cross-linker **12**, electrical breakdown strengths decrease in line with increasing concentrations of dipole cross-linkers but they remain high at low concentrations. The reduction in breakdown strength at high functional cross-linker concentration could be caused by the reduction in stiffness[151], as seen in Table 4. For all films, breakdown strength stays above ~40 V/µm, which is sufficiently high for most DEAP applications and in the range of commercially available products such as Elastosil RT625 (Wacker Chemie AG), as stated by the manufacturer[152].

Overall, the best properties for DEAP applications are obtained at the lowest functional cross-linker concentrations, where high dielectric permittivities are matched with favourable breakdown strengths. This in turn yields elastomers with enhanced properties for DEAPs compared to the reference materials. At greater cross-linker concentrations, permittivity is still high, but mechanical properties and breakdown strengths are compromised, due to the low functionality of the dipolar cross-linkers which soften the networks and thereby reduce electrical breakdown strengths. Enhanced properties for the dipolar elastomers can be compared with the reference material by calculating the figure of merit $F_{om} = 3\varepsilon' \times E_B^2/3G'$ relative to the figure of merit for the reference films[31,47]. The results for 1.35 wt% of cross-linker **12**, for example, will be: $F_{om}/F_{om\_ref} = (3.2/2.8) \times (124.2/111.0)^2/((3\times119.7)/(3\times151.9)) = 1.82$. All results can be seen in Table 4. The figure of merit is improved for both films with **10** and **12** at low concentrations compared to the reference materials. The best properties are obtained when using cross-linker **12**, as mechanical and breakdown properties are maintained at high concentrations to a greater extent than for cross-linker **10**. This can also be observed from the figure of merit calculations, which could be due to higher compatibility of **12** with the PDMS matrix. However, the synthesis of **12** requires multiple time-consuming steps, whereas **10** is prepared from the commercially available 1-ethynyl-4-nitrobenzene, which also yields a higher figure of merit at low concentrations than the reference material. This factor should also be considered when choosing the best material for DEAP applications.

4 Visualisation and characterisation of heterogeneous bimodal PDMS networks using a fluorescent cross-linker

The work in this chapter is based on the publication *Visualisation and characterisation of heterogeneous bimodal PDMS networks*, published in *RSC Advances*, 2014, 4, 6939-6945 and reprinted with the kind permission of RSC publications. The manuscript can be found in Appendix C along with all experimental procedures and associated supporting information.

4.1 Introduction

In this chapter the objective is to investigate the structure and network density of so-called heterogeneous bimodal networks using a fluorescent cross-linker, in this case **4**. Heterogeneous bimodal networks consist of short polymer chains mixed with chemically identical long polymer chains, and they possess some improved mechanical properties compared to traditional filled elastomers, such as low viscous loss[37]. Heterogeneous bimodal networks, due to their favourable properties, are very promising as next-generation silicone elastomers for DEAP technology; however, not much is yet understood about the structure-property relationship of such networks, so the technology is therefore still very far from being applicable in industry for commercial DEAP products. This chapter presents the first step in tuning and learning more about the properties of heterogeneous bimodal networks, and thereby it paves the way for the implementation of such networks in advanced applications where strong, unfilled and largely extensible networks are required. This is done using a novel method for analysing the size of short-chain domains in heterogeneous bimodal PDMS networks employing a developed fluorescent cross-linker (**4**), which is used to tag short-chain hyperbranched structures at their cross-linking points with fluorescent molecules. The size of the short-chain domains will furthermore be correlated to the mechanical properties of the networks.

4.2 Results and Discussion

Heterogeneous bimodal PDMS networks were prepared in a two-step procedure combining short- and long-chain hyperbranched PDMS structures, as illustrated in Figure 13. First, fluorescent short-chain hyperbranched structures were prepared in a reaction prior to network formation, using the previously prepared fluorescent tri-functional cross-linker (**4**). The cross-linker was used in concentrations below the gelation point, as determined by the Flory-Stockmayer expression: $r_c = 1/(f-1)$, where r_c is the stoichiometry between the reactive groups on the cross-linker and the reactive groups on the polymer required for critical gelation, and f is the functionality of the cross-linker. By using stoichiometry where $r < r_c$, no infinite short-chain network will be created, and the formed hyperbranched structures will still have reactive end groups[73,153].

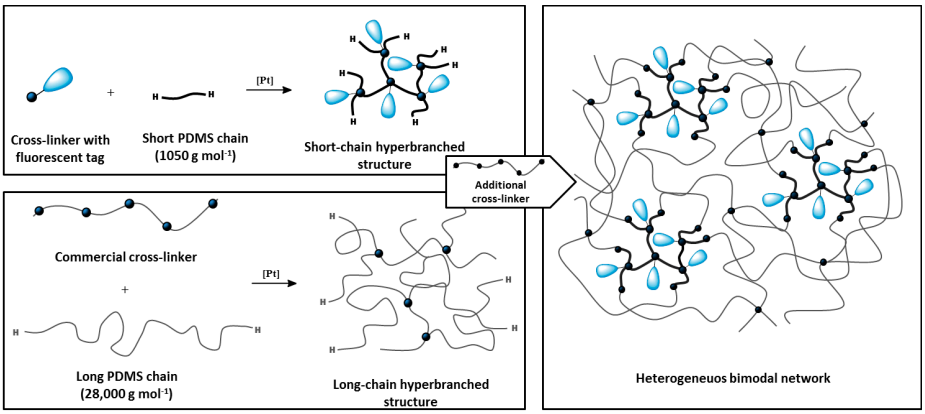

Figure 13 Schematic illustration of the two-step reaction procedure employed to form heterogeneous bimodal networks.

The short-chain hyperbranched structures were characterised by FTIR, ^{1}H-NMR and size-exclusion chromatography (SEC). The reaction between the fluorescent cross-linker (**4**) and the short PDMS chains was followed by FTIR and the decreasing intensity of the cross-linker C=C band at 1610 cm^{-1}. Furthermore, FTIR spectra confirmed the presence of the remaining Si-H end groups (at 2125 cm^{-1}) on the short-chain polymers after the reaction. The reaction employed to form the short-chain hyperbranched structures was also followed with ^{1}H-NMR through the disappearance of -C*H*$_2$=CH resonance at δ_H = 5.26 ppm and -CH$_2$=C*H* resonance at δ_H = 5.12 ppm. The presence of Si-H protons at δ_H = 4.70 ppm after the reaction indicates that reactive polymer end groups were indeed still present on the hyperbranched structures. From the areas under the Si-*H* resonance, before and after the reaction relative to the areas of constant Si-C*H*$_3$ resonances at δ_H = 0.06-0.18 ppm, it can be deduced that ~60% reactive Si-H end groups remained after the reaction. This number is consistent with the stoichiometric ratio of r = 0.4 used in this instance. ^{1}H-NMR spectra can be found as supporting information in Appendix C. SEC was used to confirm the post-reaction increase in the molecular weight of the hyperbranched structures, which appears in the higher molecular weight region compared to the low molecular weight short-chain PDMS (as seen in the SEC traces in Figure 14). In addition, the SEC trace clearly shows that the reaction results in a distribution of hyperbranched structures and not in a mono-modal structure, which is as expected for a hyperbranched structure.

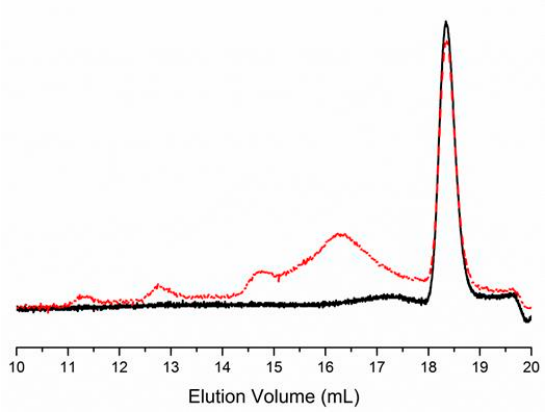

Figure 14 Overlay of the refractive index (RI) SEC detector signals of the short chains before the hyperbranching reaction (black, solid) and the short chains after the hyperbranching reaction with the fluorescent cross-linker (red, dashed).

In a similar manner, the long-chain hyperbranched structures were prepared by using a commercial 16-functional cross-linker and a higher molecular weight PDMS (28,000 g mol^{-1}). The hyperbranched structures, based on the short and long chains, were mixed and cross-linked using surplus commercial cross-linker. The fluorescent short-chain hyperbranched structures thereby became bound covalently to the long-chain hyperbranched structures, thus ensuring sufficient separation of the short-chain structures to maximise their reinforcing effect.

The heterogeneous bimodal networks were prepared with varying short-chain hyperbranched structures, in order to illustrate the effect of the ratio between long- and short-chain hyperbranched structures. The concentration of short-chain structures varied from 0 to 30 wt%, corresponding to 0 to 92 mol% (of the total number of hydride functional polymers). Films based entirely on the short-chain polymer could not be prepared, as the polymer was of too low a molecular weight to form a mechanically stable film.

The prepared heterogeneous bimodal networks were characterised through confocal microscopy, which uses single-point illumination and rejects out-of-focus light. Thus, images with better vertical optical resolution than traditional fluorescence microscopy are obtained. The acquired images had reduced background haze and represent a thin cross-section of the sample, as shown in grayscale in Figure 15. (Original fluorescence confocal microscopy images of all the samples can be found as supporting information in Appendix C).

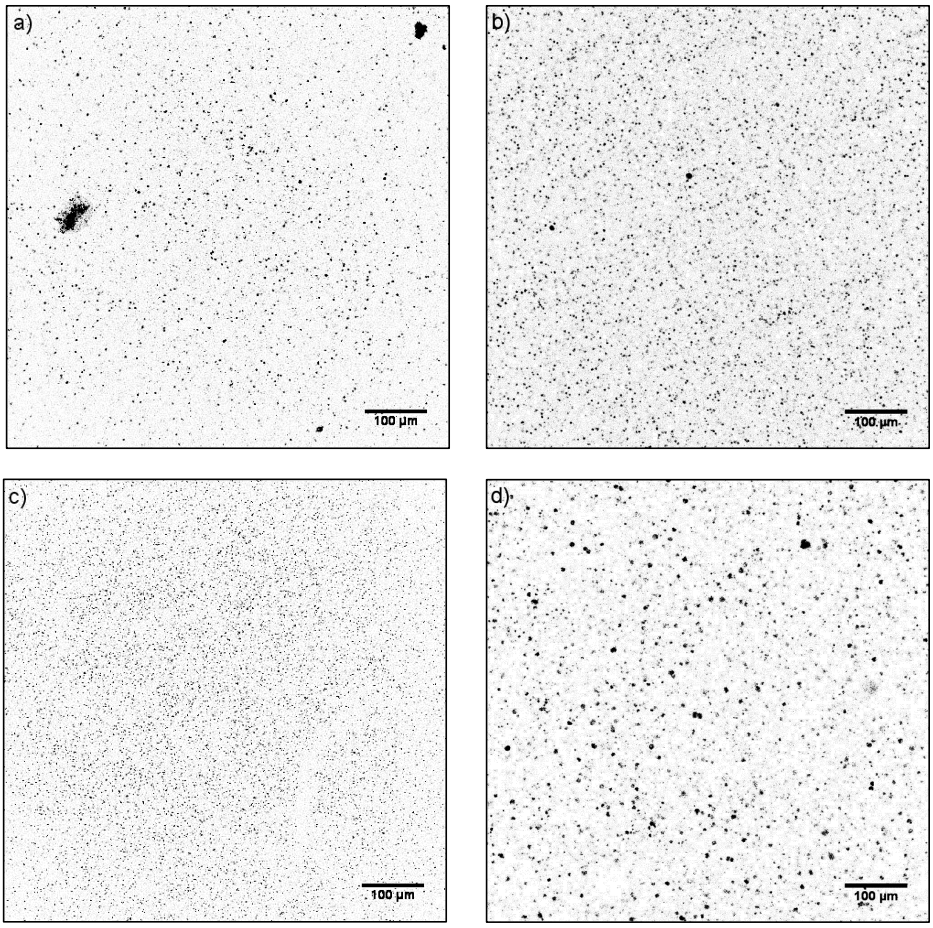

Figure 15 Grayscale confocal fluorescent microscopy images obtained at a wavelength of 400 nm of the prepared heterogeneous bimodal networks with varying concentrations of short-chain hyperbranched structures: a) 3 wt%; b) 10 wt%; c) 20 wt% and d) 30 wt%.

The fluorescent domains are evenly distributed within all networks. Furthermore, it can be seen from Figure 15 that they vary in size and abundance, depending on the ratio between the short- and long-chain hyperbranched structures in the network. The mean diameters of the fluorescent domains were determined as the average of 100 domains, the results for which are summarised in Table 5. The sizes of the fluorescent domains vary only moderately for the concentrations of short-chain hyperbranched structures, from 3 wt% to 20 wt%, whereas substantially larger domains are observed at 30 wt%.

Table 5 Summary of the heterogeneous bimodal networks' properties.

Small chain concentration		Domain diameter (D)[a]	C_N[b]*10^{-9}	Rheology		Swelling
				G' @1Hz	tan δ @1Hz	W_{sol}
[Wt%]	[Mol%]	[µm]	[g^{-1}]	[kPa]		[%]
0	0	-	-	93.4	0.013	5.9±0.5
3	45	2.9±0.9	2.4	11.8	0.027	10.5±0.8
10	75	2.8±0.8	9.0	21.5	0.009	6.0±1.9
20	87	2.1±0.5	43	78.1	0.013	8.5±0.7
30	92	5.7±1.6	3.2	59.5	0.012	4.8±0.1

[a] Mean diameters were determined through the image processing program ImageJ

[b] The number average concentration of short-chain domains is calculated as: $C_N = ((6 \times \text{wt\%})/(\pi D^3))(1/\rho_{PDMS})$, where ρ_{PDMS} is the density of PDMS.

Furthermore, it is clear from Figure 15 that the domains are very well distributed, and the concentration of domains is high for all samples. When the concentration of the short-chain hyperbranched structures is increased to 30 wt%, a substantial increase in the domain's size is evident (Figure 15 d)), due to the short-chain hyperbranched structures becoming so tightly packed that even upon ideal distribution they will interconnect covalently and turn into larger agglomerates. This is also substantiated by the large increase in the standard deviation of the measured average short-chain domain diameter.

The elastic and mechanical properties of the bimodal networks were determined by employing small amplitude rheology. The resulting shear storage moduli (G') and loss (tan δ) are summarised in Table 5. A plot of storage moduli and loss (tan δ) as functions of frequency is shown in Figure 16.

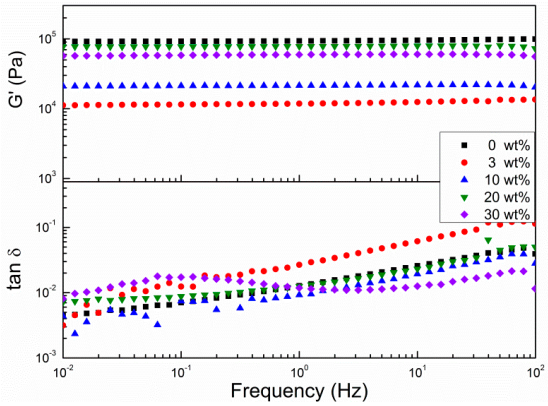

Figure 16 Storage moduli (G') and loss (tan δ) as functions of frequency for PDMS networks prepared with different short-chain concentration.

The mono-modal PDMS reference network, with 0% short chains, has a storage modulus of 93.4 kPa. Upon the addition of the short-chain hyperbranched structures, the modulus decreases significantly to 11.8 kPa. According to fundamental theories on rubber elasticity, elastic moduli are expected to scale linearly with the inverse average molecular weight of the polymer chains in the network[154]. As such, the addition to the system of very short polymer chains would be expected to decrease the average molecular weight of the system and thus increase the elastic modulus significantly. This decrease in the elastic modulus in heterogeneous bimodal networks has been shown previously but not explained with supporting data[37,155]. Based on the unprecedented correlation between the network composition, size and distribution of the fluorescent domains, and the elastic properties of heterogeneous bimodal networks, it is believed that the decrease in the elastic modulus can be explained by a multi-domain theory. When short-chain hyperbranched structures are added, they naturally contain a significant concentration of unreacted hydride groups on the surface. These groups then react with cross-linker molecules, which upon initial reaction are hindered from diffusion by reptation[156]. Consequently, there is a large concentration of cross-linker molecules on the surface of the hyperbranched structures. Small cross-linker molecules, such as those used in a previous study[37], are packed tightly around the surface, whereas the long-chain cross-linker molecules used in this study tend to fold around the short-chain hyperbranched structures. In both cases, this creates areas around the cross-linker molecules where effective cross-linking density is lower than in the bulk long-chain network, as a large number of the cross-linking sites are present around the short-chain domains, as illustrated in Figure 17.

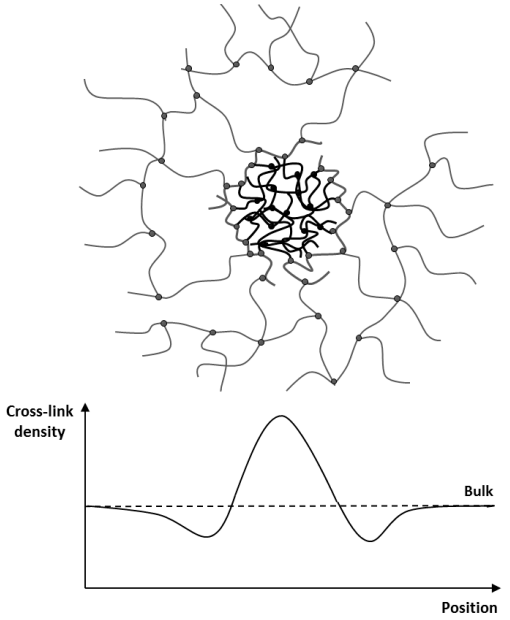

Figure 17 Schematic illustration of the hypothesised efficient cross-linking density.

In this study, with a high molecular weight cross-linker, folding back to the short-chain domains also leads to the formation of loops, which do not contribute to elasticity to the same extent as the true cross-linking sites[30]. Domains with surrounding cross-linker molecules therefore create a local softening effect in the PDMS networks. The heterogeneous bimodal elastomers will consequently be softer and have a lower elastic modulus than the homologous mono-modal networks despite higher average cross-linking density. The reduction in the modulus, from mono-modal to a small amount of short-chain domains, is confirmed experimentally. The elastic modulus is then increased with increasing short-chain concentration. At high concentrations of short chains the elastic modulus drops again, which can be explained by a drop in the number average concentration of short-chain domains C_N = ((6*wt%)/(pD^3))(1/ρ_{PDMS}) (see Table 5). From the calculations it can be seen that for the bimodal networks, the elastic modulus increases with increasing C_N, although not in a trivial way.

Interfaces with a lower cross-linking density are still perfectly cross-linked, due to the high number of functional groups on each hyperbranched structure, and as such they cannot be regarded as network imperfections, since their mechanical properties have not been destroyed.

Very soft silicone elastomer behaviour can also be observed for imperfect networks, which occurs as a result of unreacted groups. This lack of reactivity can be introduced either from stoichiometric imbalanced reactions[73,157] or from incomplete catalyst inhibition reactions[153]. It can also arise naturally from steric hindrance or heterogeneity, thus leading to local cross-linker and polymer excesses, respectively. Therefore, it is important to ensure that heterogeneous bimodal networks do not contain a large fraction of solubles, namely the so-called sol fraction. The sol fractions of heterogeneous bimodal PDMS networks were determined by conducting swelling experiments with toluene and calculated as $W_{sol}(\%) = (1 - m_e/m_0) \times 100$, where m_e is the weight of the dry sample after swelling/extraction and m_0 the initial weight of the (dry) sample before swelling. The results can be found in Table 5. The sol fractions were found to lie in the range of 5-10% and were apparently independent of short-chain concentration. The addition of the short chains as domains therefore does not create additional imperfections in the infinite networks, which means that there is complete compatibility between the short-chain domains and the long-chain matrix.

In general, it is difficult to obtain PDMS elastomers with low elastic moduli, without deteriorating other network properties. Soft PDMS elastomers therefore usually suffer from high viscous losses. Frequency-dependent viscous loss can be determined from the shear loss tangent (tan δ), which is shown in Table 5 and Figure 16. All the prepared bimodal elastomers, except for the film with 3 wt% short-chains, are seen to have lower viscous loss than the mono-modal PDMS network. Furthermore, the heterogeneous bimodal networks are very well cross-linked, as the storage moduli (G') are 10 to 100 times larger than the loss moduli (G'') for the investigated frequency range, with differences being smallest at high frequencies.

Viscous loss at the low strain, low frequency limit is measured as a few percentage points only, which is comparable to previously reported results for heterogeneous bimodal networks[37]. Viscous loss in a polymer network is the result of dangling chains and sol molecules, i.e. incomplete network formation[73]. It is therefore evident from the low viscous losses of the heterogeneous

bimodal networks that the obtained low moduli are not a result of incomplete reactions but rather of network artefacts, as shown in Figure 17. The loops do not contribute significantly to the elastic modulus, but at the same time they do not contribute a loss either, since they cannot relax. Heterogeneous bimodal networks are therefore an effective and simple method of creating soft elastomers with very low viscous losses.

5 Synthesis of well-defined polysiloxanes with high concentration of functional groups

The work in this chapter is based on the manuscript *Synthesis of telechelic vinyl/allyl functional siloxane copolymers with structural control* submitted to Polymer Chemistry, July 2014, which can be found in Appendix D along with all experimental procedures and associated supporting information. Unpublished procedures can be found in Chapter 9.

5.1 Introduction

The work in this chapter focuses on developing siloxane polymers and elastomers with high concentrations of functional groups. The aim is to obtain elastomers with even higher dielectric permittivity than that obtained with the dipolar cross-linkers presented in Chapter 2-4. A higher concentration of functional groups can be obtained through dipolar species attached along the backbone of siloxane polymers, as illustrated in Figure 18.

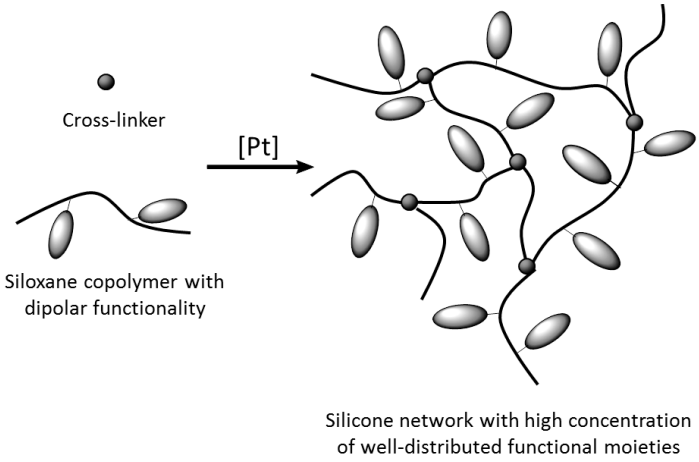

Figure 18 Schematic illustration of functional polysiloxanes used in elastomer synthesis.

The work in this chapter therefore focuses on developing siloxane copolymers with spatially well-distributed functional groups. In order to achieve this goal, two different synthetic strategies were developed. The first strategy was based on the platinum catalysed hydrosilylation polycondensation of a di-functional chain extender, while the second strategy utilised the highly efficient Piers-Rubinsztajn reaction as a polymerisation method.

5.2 Results and discussion

5.2.1 Siloxane chain extender

A di-functional molecule with a similar structure to the cross-linker described in Chapter 2-4 would – rather than cross-linking polymer chains into networks – extend lighter molecular weight hydride-functional polymer chains into longer chains. After proper end-functionalisation, these co-polymers would react thereafter with hydride-functional cross-linkers and form elastomers. Furthermore, this functional chain extender would allow for one-pot film formation, as shown in Figure 19. This means that the chain extender would react with hydride-terminated pre-polymers of low molecular weights to form longer polymer chains. After this initial reaction, commercial cross-linker is added and the mixture is poured into a mould for curing. As a result, there is no need for any purification steps after the polymerisation reaction, and the catalyst is only added once to the mixture.

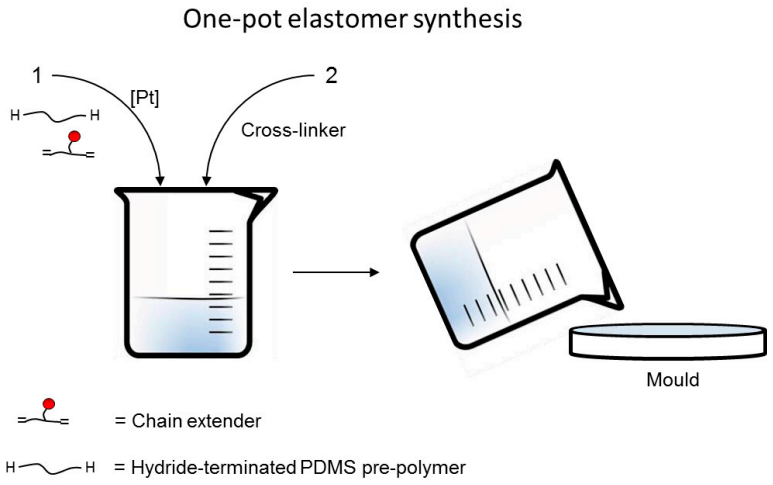

Figure 19 Schematic illustration of a one-pot reaction where the chain extender reacts with short hydride-terminated PDMS pre-polymers to form longer copolymers. Hereafter, a cross-linker is added and the mixture is poured into a mould for curing.

Furthermore, a small hydrosilylation compatible molecule could be added to commercial silicone formulations as an additive with compensating amounts of pre-polymer and cross-linker, as illustrated in Figure 20. Consequently, the improved dielectric permittivity of commercial formulations could be attained, without the need for high dielectric constant filler particles, such as TiO_2. This would be a great advantage – as discussed in Chapter 1.

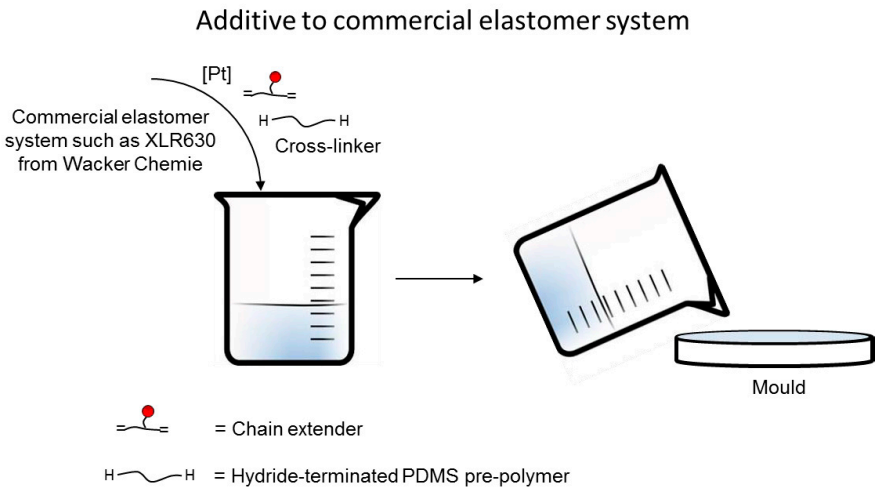

Figure 20 Schematic illustration of the use of the chain extender as an additive to a commercial silicone elastomer system such as XLR630 from Wacker Chemie AG. The chain extender is added with compensating amounts of PDMS pre-polymers, cross-linker and catalyst.

The synthetic route used to create the novel azido-functional chain extender **14** is outlined in Scheme 9. Synthesis was accomplished by the tris(pentafluorophenyl)borane catalysed Piers-Rubinsztajn reaction of 3-chloro(methyl/propyl)methyldimethoxysilane with vinyl- or allyldimethylsilane to form the chloro-functional intermediate **13**. The Piers-Rubinsztajn reaction was chosen for the synthesis of this molecule because it forms hydrolytically-stable Si-O-Si bonds. Furthermore, as this molecule is to be used as a component in polymer backbones, it was determined that more silicon atoms – and thereby a molecule with even more silicone-like properties (than the cross-linker) – would be desirable. The subsequent reaction of **13** with sodium azide in DMF created the azido-functional siloxane chain extenders **14a** and **14b**.

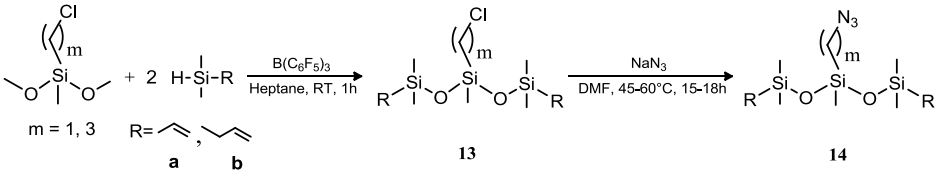

Scheme 9 Synthetic route to azido-functional chain extender **14**.

The synthesis of **14b**, 1,5-di*allyl*-3-(azidomethyl)-1,1,3,5,5-pentamethyltrisiloxane, was straightforward and produced high yields (95%) and high purity. At 45°C ~100% conversion from chloro to azido had taken place after 18 hours, with no detectable (by ^{1}H-NMR) degradation or by-product formation. However, **14a**, 1,5-di*vinyl*-3-(azidopropyl)-1,1,3,5,5-pentamethyltrisiloxane, proved a bigger challenge. At 45°C only 88% conversion of the chloro-group was achieved, even after 48 hours. Furthermore, only 95% of the vinyl groups remained as determined from the inte-

grals in the ^{1}H-NMR spectra of **13a** to **14a**. This indicates that some side-reaction involving the vinyl groups was taking place. Subsequently, various reaction conditions were tested, including temperature, reaction time, solvent and the stoichiometric ratio between **13a** and sodium azide. The conversion of chloro to azido, and the percentage of remaining vinyl groups, was determined by ^{1}H-NMR. These studies proved that it was difficult to obtain high conversion rates from chloro to azido at temperatures lower than 60°C. Kinetic studies of the reaction at 50°C and 55°C ably illustrate this point (see Figure 21).

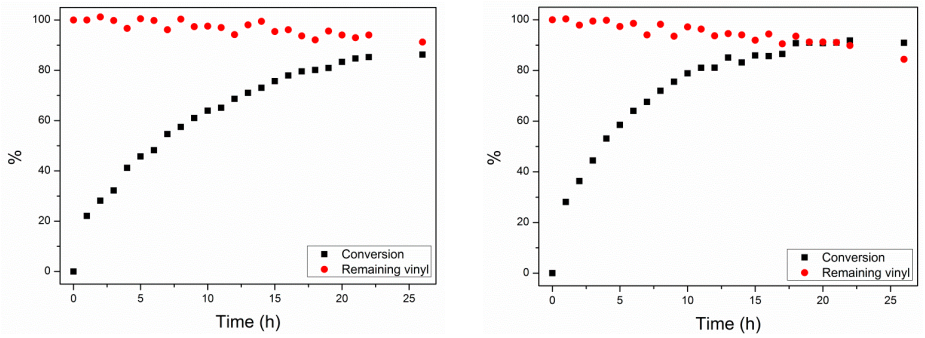

Figure 21 Kinetic studies of the conversion from chloro- to azido-groups and the remaining vinyl groups as a function of time for reactions performed at: left: 50°C and right: 55°C.

Both at 50°C and at 55°C the conversion does not reach higher than 90% after 26 hours. At this stage it is clear that the side-reaction involving the vinyl groups has started, which means that after 26 hours 91% and 84% of the vinyl groups remain at 50°C and 55°C, respectively. Kinetic studies indicate that temperature and time is a significant factor in the degradation of the vinyl groups.

It was furthermore observed that the solvent had an influence on the side-reaction. DMF not freshly distilled is prone to degradation where the base dimethylamine is formed, and this proved to enhance the side-reaction of the vinyl groups. Therefore, dried and distilled DMF was found to be the best choice. Other solvents, such as *N*-methyl-2-pyrrolidone (NMP) and dimethyl sulfoxide (DMSO), also provided outcomes with a higher degree of side-reaction. Stoichiometry was found to be of less importance. Increasing the stoichiometric ratio to ×10 sodium azide to **13a** did not result in a significantly higher conversion rate, though slightly higher side-product formation was observed. At a 1:1 stoichiometric ratio of sodium azide to **13a**, lower conversion was obtained. Temperatures higher than 60°C, i.e. 65°C and 70°C, did not result in a higher conversion, but they did elicit a higher degree of side-reaction.

Optimal reaction conditions were therefore determined to be at 60°C with distilled DMF for 15-16 hours and with a stoichiometric ratio of 1.33:1 of sodium azide to **13a**. This provided a product with ~95% conversion of the chloro-groups and >98% remaining vinyl-groups. This purity was determined to be acceptable.

The nature of the side-reaction involving the vinyl-groups was analysed using SEC and ^{1}H-NMR. SEC showed that a **14a** product with a high degree of side-reaction occurring had signals in the

higher molecular region in the SEC trace. This indicates that the side-reaction forms certain types of high molecular weight structures or polycondensates. In the SEC trace of **14a**, prepared under optimal reaction conditions, the peak in the higher molecular weight region was reduced significantly.

A ^{1}H-NMR spectrum of a **14a** sample with a high degree of side-reaction revealed resonances at δ_H = 3.0 ppm (a), 3.2 ppm (c), 3.4 ppm (d) and 4.1 ppm (b), which may possibly correspond to an azide-alkene 1,3-cycloaddition forming a 1,2,3-triazoline, as shown in Scheme 10. The resonances are corroborated through a calculated theoretical ^{1}H-NMR spectrum of the proposed structure using the ACD/I-lab software.

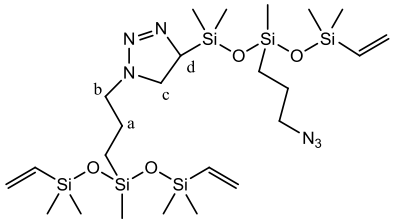

Scheme 10 Proposed structure for the product of a side-reaction through azide-alkene 1,3-cycloaddition.

The proposed cycloaddition is furthermore corroborated by COSY NMR, as clear couplings between protons a-b and c-d can be seen. Azide-alkene cycloadditions have been observed previously[101,158–161] and this reaction could lead to the higher molecular weight structure seen by SEC. The side-reaction becomes more pronounced during shelf-life at RT, which further supports a similar self-condensation reaction to the one proposed in Scheme 10.

5.2.1.1 Chain extension of hydride end-functional PDMS pre-polymers and elastomer synthesis

As a proof-of-concept, **14b** was used in a platinum catalysed polycondensation reaction with a hydride-terminated PDMS pre-polymer, as shown in Scheme 11.

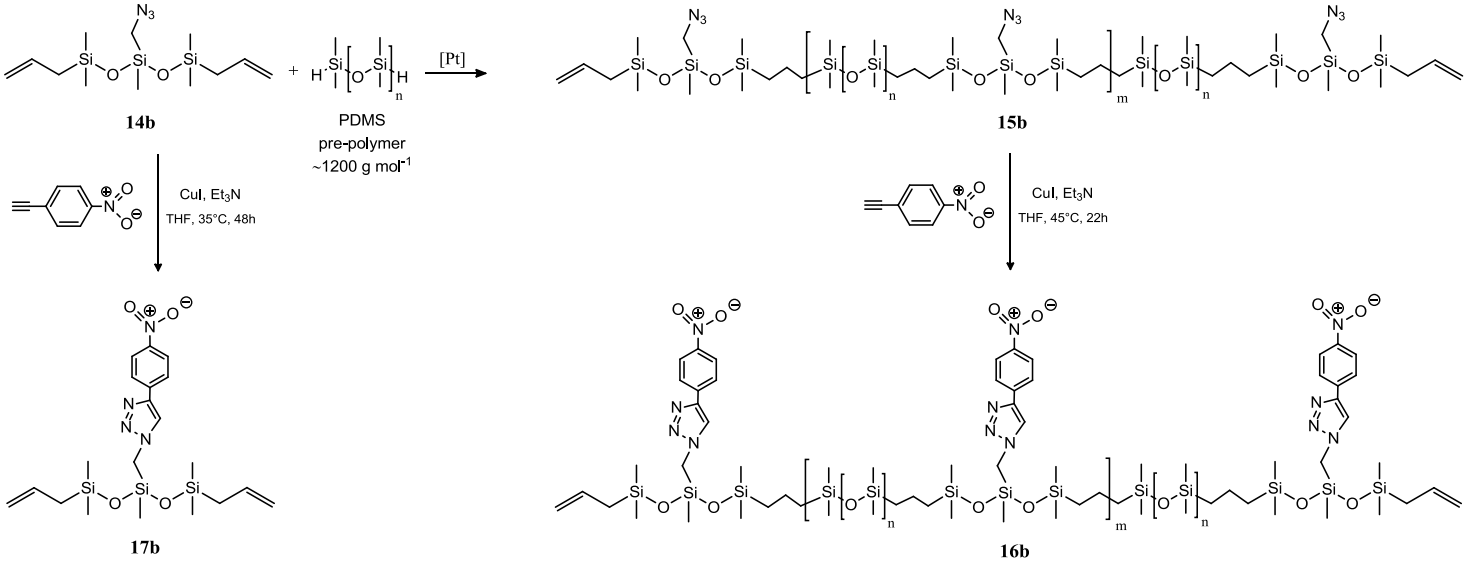

Scheme 11 Synthetic route to chain-extended siloxane copolymer and CuAAC reactions with 1-ethynyl-4-nitrobenzene.

The reaction to form **15b** was carried out for 24 hours at 55°C. At this stage ^{1}H-NMR showed the presence of remaining hydride-groups on the formed copolymers as (small) resonances at δ_H = 4.71 ppm. Therefore, excess **14b** was added to the reaction mixture, which in turn was left stirring for another 24 hours at 55°C. The copolymer was now precipitated in methanol to remove the excess chain extender, and the copolymer was obtained as a clear oil and analysed by FTIR, ^{1}H-NMR and SEC. FTIR confirmed the disappearance of the PDMS hydride groups at 2125 cm^{-1} and the presence of -CH=CH_2 groups at 1630 cm^{-1}. Furthermore, the allyl-groups were detected by ^{1}H-NMR as resonances at δ_H = 1.82 ppm (−C*H*$_2$-CH=CH_2), δ_H = 5.64 ppm (−CH=C*H*$_2$) and δ_H = 6.14 ppm (−C*H*=CH_2). The prepared copolymer, **15b**, was characterised by SEC, and molar mass characteristics were calculated from linear polydimethylsiloxane standards. A molecular weight of $\bar{M}_w$= 33,100 g mol^{-1} was obtained, which is suitable for DEAP elastomers. Furthermore, the polydispersity index ($\bar{M}_w/\bar{M}_n$) was found to be 4.51. A high polydispersity index is expected for a polymer prepared from this type of polycondensation reaction.

Thereafter, **15b** was reacted with 1-ethynyl-4-nitrobenzene through CuAAC, as shown in Scheme 11. The reaction was followed by FTIR and the disappearance of the azide band at approximately ~2095 cm^{-1} and the alkyne band at approximately ~3300 cm^{-1}. ^{1}H-NMR confirmed the formation of the product **16b** through the presence of the triazole proton at δ_H = 7.83 ppm.

Another approach involved clicking 1-ethynyl-4-nitrobenzene directly onto **14b** before the polymerisation reaction, according to Scheme 11. The synthesis of **17b** was successful, with the complete conversion of the azido-groups and the formation of the triazole ring corroborated by the presence of the triazole proton as a resonance at δ_H = 7.84 ppm in the ^{1}H-NMR spectrum. The product was obtained as a red solid powder, which was completely insoluble in all available solvents. This excluded the use of the molecule as a chain extender, since it renders it incompatible with silicone pre-polymers. The reason for the insoluble nature of **17b** could be the complexing of triazole rings to copper ions as shown by Li et al.[162] who formed polymer gels through the complexation of copper ions and triazole rings. Li et al. were able to eliminate the gel-forming effect by removing the copper ions with EDTA solution. A similar attempt with **17b**, however, did not change the insoluble nature of the molecule. This route was therefore not selected for further experiments.

Polymer **16b** was used in a cross-linking reaction with a commercial hydride-functional cross-linker with ~8-functional groups/molecule. This film contained approximately 10 wt% of the nitrobenzene moiety. The curing time was very slow (one week at RT and two weeks at 80°C), and soft and slightly sticky films were obtained.

At this stage dielectric permittivity was tested, in order to establish if the chain-extended polymers had a positive impact on dielectric permittivity. Dielectric relaxation spectra showing frequency-dependent dielectric permittivity (*ε*') and loss (tan δ) are shown in Figure 22.

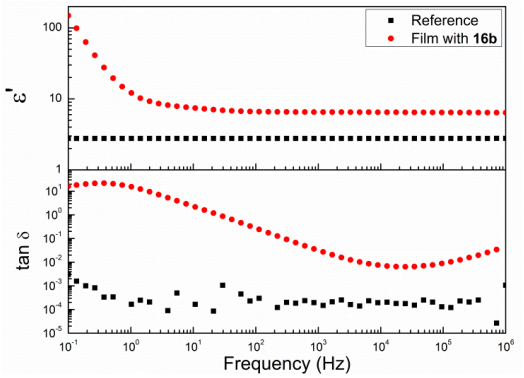

Figure 22 Dielectric permittivity (ε') and loss tangent (tan δ) as functions of frequency for a film prepared with **16b** and a reference prepared with pure PDMS.

As seen from Figure 22, dielectric permittivity, ε', increases from 2.8 for the reference film to 6.6 at 100 Hz for the film prepared with **16b**. This corresponds to an over two-fold increase in the permittivity. It is, however, seen that the loss tangent also increases significantly.

Dielectric permittivity results show, that using the new synthesised chain extender will have a positive impact on dielectric permittivity. There are, however, several time-dependent parameters that need to be optimised. The long reaction times required for copolymer synthesis, end-functionalisation and film formation render this method unattractive before further optimisation of the reaction conditions has been performed. It is furthermore difficult at this stage to tune the obtainable molecular weight of the copolymer, as it depends both on the stoichiometry of the reactants and on the reaction time.

Due to some of the previously mentioned disadvantages with this method and limited available time, another and much more rapid polymerisation method was explored instead, as described in the next section. The chain extender, however, remains a promising method that can be applied to, for example, one-pot reactions with polymerisation and film formation in two consecutive steps. Furthermore, the use of the synthesised chain extender should also have great potential as a low molecular weight additive to commercial formulations. Both of these strategies are part of ongoing projects in our group, and promising preliminary results have been obtained.

5.2.2 Functional siloxane copolymers based on Piers-Rubinsztajn polymerisation

The aim of this work is to prepare spatially well-distributed functional siloxane copolymers, by using a more rapid polymerisation method than that described in the previous section. A possible method for this is the fast and efficient Piers-Rubinsztajn reaction, which moreover uses the less expensive borane catalyst. Furthermore, this much more rapid polymerisation method will allow for more precise control over copolymer molecular weight by varying the stoichiometric ratios of the reactants (since reaction time is not a factor). This is very useful, especially given the application of the copolymers for elastomer synthesis, as quite a narrow molecular weight range is desired ($\bar{M}_w$ ~ 20,000-30,000 g mol^{-1}).

The copolymers should contain vinyl or allyl end groups, which will allow for platinum-catalysed

cross-linking reactions with hydride-functional cross-linker molecules. As mentioned in Chapter 1, Rubinsztajn and Cella[122–124] and others[87,127] have previously used tris(pentafluorophenyl)borane as a catalyst for siloxane homo- and copolymers, obtaining low levels of copolymer structure randomisation. To our knowledge, however, the reaction has never been employed for the synthesis of spatially distributed functional telechelic copolymers, which are useful in hydrosilylation elastomer synthesis.

Siloxane copolymers with spatially well distributed functional groups were prepared as illustrated in Scheme 12**.**

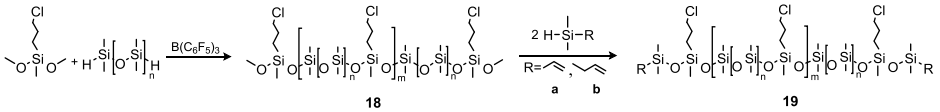

Scheme 12 Synthetic route for telechlic vinyl/allyl siloxane copolymers via borane catalysed polycondensation.

Synthesis was accomplished by the tris(pentafluorophenyl)borane-catalysed Piers-Rubinsztajn reaction of 3-chloropropylmethyldimethoxysilane and hydride-terminated dimethylsiloxane pre-polymers to form the methoxy-terminated copolymers **18**. The borane-catalysed polycondensation of hydrosilanes and methoxysilanes to form **18** involves cleaving C-O and Si-H bonds while forming Si-O and C-H bonds in an exothermic reaction ($\Delta H \approx -250$ kJ/mol)[123]. The reaction is performed at room temperature using low levels of $B(C_6F_5)_3$ catalyst (< 0.5 mol%). At higher catalyst concentrations (~1−5 mol%), hydrosilylation reactions may compete with the Piers-Rubinsztajn polycondensation reaction[86,87]. The reaction is almost instantaneous and is completed within a few minutes, but it was left to stir for 1 hour, in order to ensure the full conversion of reagents. Furthermore, high yields were obtained (> 95%). At this point ^{1}H-NMR and FTIR spectroscopy were used to confirm the completeness of the reaction through assessing the disappearance of the hydride-groups on the hydride-terminated pre-polymers. In ^{1}H-NMR, resonance at $\delta_H = 4.7$ ppm disappeared, which was also corroborated by FTIR, where the distinctive stretch at 2125 cm^{-1} was no longer present. In order to ensure at this stage that all polymers contained methoxy end-groups, significant amount of excess dimethoxydimethylsilane was added to the reaction mixture so that any remaining hydride groups would react. The excess dimethoxydimethylsilane was easily removed *in vacuo*.

.

Poly((cyanopropyl)methylsiloxane-*co*-dimethylsiloxane) synthesis was also attempted, as illustrated in Scheme 13. Cyano-groups have previously been used to increase the dielectric permittivity of silicone elastomers[74,75].

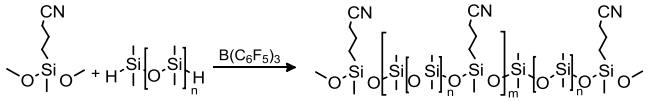

Scheme 13 Hypothesised synthetic route to a cyano-functional siloxane copolymer.

The reaction did, however, not work, which could be the result of the cyano-group supressing the reaction due to complexation with the borane-catalyst. Complexation of boron was also observed by Grande et al.[129] for amino-groups.

The prepared copolymers were characterised by SEC, and molar mass characteristics were calculated from linear polydimethylsiloxane standards. The results are summarised in Table 6.

Table 6 SEC results for prepared functional siloxane copolymers with varying pendant groups as well as varying end groups.

No	Entry	$\bar{M}_w$ pre-polymer [g mol^{-1}]	Stoichiometry hydrosilane/ methoxysilane	Functional group	End group	$\bar{M}_w \cdot 10^{-3}$ [g mol^{-1}]	$\bar{M}_w / \bar{M}_n$
1	**18**	~1200	1/1	Chloro	Methoxy	50.4	2.22
2	**19a-1**	~1200	1/1	Chloro	Vinyl	47.9	2.20
3	**19a-2**	~1200	0.95/1	Chloro	Vinyl	70.3	2.03
4	**19a-3**	~1200	0.95/1	Chloro	Vinyl	69.9	2.25
5	**19a-4**	~1200	1/0.9	Chloro	Vinyl	25.9	3.23
6	**19a-5**	~1200	1/0.8	Chloro	Vinyl	13.2	3.80
7	**19a-6**	~580	1/1	Chloro	Vinyl	37.4	3.17
8	**19a-7**	~580	0.95/1	Chloro	Vinyl	20.6	3.47
9	**19a-8**	~580	0.975/1	Chloro	Vinyl	22.5	2.79
10	**19b-1**	~580	0.95/1	Chloro	Allyl	22.1	3.49
11	**19a-9**	~580	1/0.95	Chloro	Vinyl	56.7	2.84
12	**20**	~580	0.95/1	Azido	Allyl	18.4	3.62
13	**21**	~580	0.95/1	2-Bromoisobutyrate	Allyl	27.5	2.43
14	**22**	~580	0.95/1	4-Nitrobenzene	Allyl	33.3	3.29
15	**23**	~580	0.975/1	1-Ethylimidazolium chloride	Vinyl	32.7	4.30

Two dimethylsiloxane pre-polymers of different molecular weights were used, in order to create copolymers with varying mol% of the (chloropropyl)methylsiloxane unit and with different spacer lengths between the functional groups. The molecular weights of the final copolymers were varied furthermore by changing the stoichiometry between the hydrosilane pre-polymers and the methoxysilane compound. According to standard polycondensation theory, the highest molecular weight would be obtained when using stoichiometries closest to unity[163]. This is not the case in these experiments, solely due to rough estimates of exact pre-polymer molecular weights, in which case the exact stoichiometry cannot be calculated. In the case of the pre-polymer of $\bar{M}_w$ ~ 1200 g mol^{-1} the highest molecular weight is obtained when using a stoichiometry of hydrosilane/methoxysilane of 0.95/1, with a molecular weight of $\bar{M}_w$ = 70,300 g mol^{-1}. For the pre-polymer of $\bar{M}_w$ ~ 580 g mol^{-1} the highest molecular weight was obtained using the stoichiometry of hydrosilane/methoxysilane of 1/0.95, where $\bar{M}_w$ = 56,700 g mol^{-1} was attained.

In order to test the reproducibility of the borane-catalysed polycondensation a reaction with the pre-polymer of $\bar{M}_w$ ~ 1200 g mol^{-1} was repeated. As seen in Table 1 entries **19a-2** and **19a-3** were prepared using similar reaction conditions and SEC provided comparable results for both experiments. This shows that the polycondensation reaction is quite robust when using similar reaction conditions.

No metathesis or consequent scrambling leading to unexpected molecular weights and unalternating polymer structures were detected using the available analysis techniques. For a more detailed analysis of the copolymers' structures, the possibility of running ^{29}Si-NMR was investigated, but it was not possible in the given time frame.

The aim of this study was to create functional copolymers with molecular weights suitable for silicone elastomer synthesis. The best elastomer properties are usually obtained when using polymers with molecular weights of $\bar{M}_w$ ~ 20,000-30,000 g mol^{-1}[88]. Molecular weights in this range were obtained for copolymer **19a-4** with a stoichiometric ratio of hydrosilane/methoxysilane of 1/0.9 using the pre-polymer of $\bar{M}_w$ ~ 1200 g mol^{-1}, where a molecular weight of $\bar{M}_w$= 25,900 g mol^{-1} was reached, and for **19a-7**, **19a-8** and **19b-1** with stoichiometries of hydrosilane/methoxysilane of 0.95/1 and 0.975/1, respectively, using the pre-polymer of $\bar{M}_w$ ~ 580 g mol^{-1}, where molecular weights of $\bar{M}_w$ = 20,600 g mol^{-1}, $\bar{M}_w$ = 22,500 g mol^{-1} and $\bar{M}_w$ = 22,100 g mol^{-1} were achieved. Copolymers prepared with the $\bar{M}_w$ ~ 1200 g mol^{-1} pre-polymer display polydispersity indexes ($\bar{M}_w/\bar{M}_n$) from 2.03 to 3.80, whereas copolymers prepared with the lower molecular weight pre-polymer of $\bar{M}_w$ ~ 580 g mol^{-1} display $\bar{M}_w/\bar{M}_n$ in the range of 2.84 to 3.49.

The molecular weights can be further fine-tuned to any desired molecular weight by using even more specific stoichiometric ratios (see Chapter 6).

5.2.2.1 End-functionalisation reaction

End-functionalisation of **18** with vinyl- or allyldimethylsilane produced copolymers **19a** and **19b**, as seen in Scheme 12. These end groups were chosen because they allow prepared copolymers to be used in the synthesis of silicone elastomers in platinum-catalysed hydrosilylation reactions. It

is also possible to create copolymers with other end groups, as long as the groups are compatible with the borane-catalysed reaction. Such end groups, for example, could be, but are not limited to, silanes with aliphatics such as trimethyl-groups, aromatics and halogen-containing compounds[129]. The prepared telechelic vinyl/allyl copolymers were characterised by FTIR, ^{1}H- and ^{13}C-NMR and SEC. For the telechelic vinyl copolymers (**19a**) ^{1}H- and ^{13}C-NMR confirmed the reaction through the disappearance of the O-CH_3 protons and a carbon atom at δ_H = 3.49 ppm and δ_C = 49.9 ppm, respectively. The presence of −CH=CH_2 protons as three distinctive doublets of doublets at δ_H = 5.74-6.12 ppm in the ^{1}H-NMR spectrum of **19a** points to the successful formation of vinyl end-groups. Furthermore, the presence of −CH=CH_2 groups can be detected in the ^{13}C-NMR spectra of **19a** with resonances at δ_C = 131.86 and 139.10 ppm. For telechelic allyl copolymers (**19b**) the reactions could be followed similarly by ^{1}H- and ^{13}C-NMR through the disappearance of the O-CH_3 protons and a carbon atom at δ_H = 3.49 ppm and δ_C = 49.9 ppm, respectively. The allyl-groups were detected by ^{1}H-NMR as resonances at δ_H = 1.5 ppm (−CH_2-CH=CH_2), δ_H = 4.86-4.92 ppm (−CH=CH_2) and δ_H = 5.79 ppm (-CH=CH_2) and by ^{13}C-NMR as resonances at δ_C = 26.4 ppm (−CH$_2$-CH=CH_2), δ_C = 113.7 ppm (−CH=CH$_2$) and 133.8 ppm (−CH=CH_2).
Converting the methoxy end groups to vinyl/allyl end groups did not alter the molecular weight of the copolymers, as illustrated in the SEC traces presented in Figure 23. This also indicates that no significant unintended hydrosilylation reactions between the end groups and vinyl- or allyldimethylsilane occur.

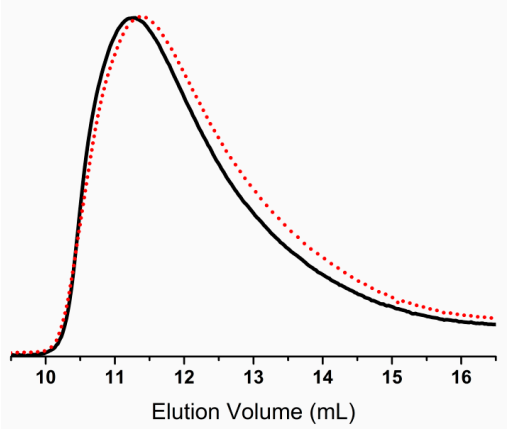

Figure 23 An overlay of the RI SEC traces of methoxy end-functional copolymer **18** (black, −−) and vinyl end-functional copolymer **19a-1** (red, • • •).

In the synthesis of **19b** additional peaks were observed in ^{1}H-NMR as a multiplet at δ_H = 1.36 ppm when using catalyst concentrations around 0.5 mol%. These resonances were assigned to CH_2 groups formed from the hydrosilylation reactions of allyl end groups subsequently reacting with allyldimethylsilane molecules. Previously reported levels for competing hydrosilylation are 1-5 mol%, but in this case even at 0.5 mol% a small degree of hydrosilylation reaction occurred. This side-reaction, however, did not change the obtained molecular weight, meaning that only a

small degree of this reaction took place. Decreasing the catalyst concentration to 0.2 mol% did not alter the reaction time or obtainable molecular weight, either, but at this concentration no peaks emanating from hydrosilylation reactions were observed by ^{1}H-NMR. A further reduction of the catalyst concentration to 0.1 mol% yielded copolymers of slightly lower molecular weights, so 0.2 mol% was therefore determined to be the optimal catalyst concentration for the polymerisation reaction.

5.2.2.2 Functionalisation reactions

The synthesised chloro-functional copolymers were converted to azido-functional (**20**) by nucleophilic substitution in THF using tetrabutylammonium azide as a phase-transfer catalyst by a procedure adapted from Rambarran et al.[98], as shown in Scheme 14.

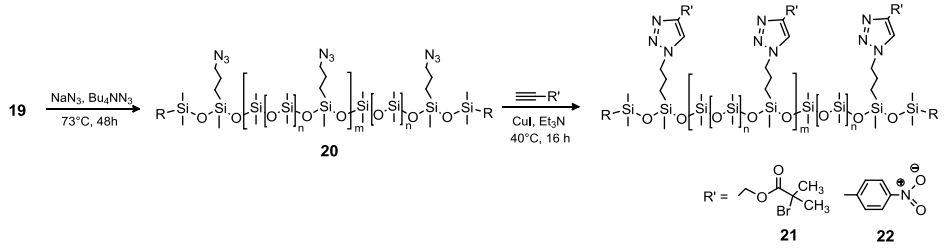

Scheme 14 Synthetic route to azido- and CuAAC-functionalised copolymers.

Entry **19b-1** was selected for this purpose, as the obtained molecular weight of $\bar{M}_w$ = 22,100 g mol^{-1} lies within the desired range for use in elastomer synthesis. The copolymer was successfully converted from chloro- to azido-functional, and this reaction was followed by FTIR through the appearance of the distinctive −N_3 band at 2095 cm^{-1}. Furthermore, ^{1}H- and ^{13}C-NMR corroborated this through a shift in the resonance signals of CH_2-Cl (δ_H = 3.50 ppm, δ_C = 47.6 ppm) to CH_2-N_3 (δ_H = 3.23 ppm, δ_C = 54.1 ppm). The prepared azido-functional copolymer was characterised by SEC, the results for which are shown in Figure 24.

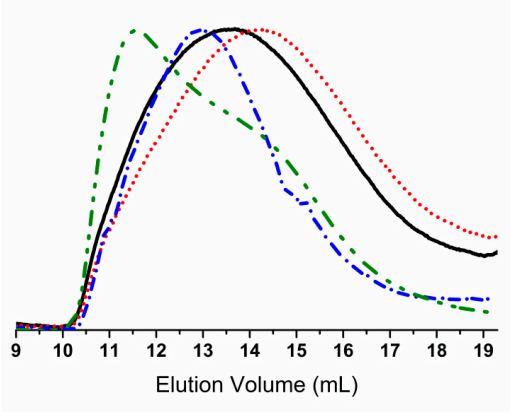

Figure 24 An overlay of the RI SEC traces of chloro-functional copolymer **19-b1** (black, −−), azido-functional copolymer **20** (red, • • •), 2-bromoisobutyrate-functional copolymer **21** (blue, − •) and 4-nitrobenzene-functional copolymer **22** (green, − • •).

It is evident that the molecular weight after the azido-substitution reaction is lower than for the corresponding chloro-functional copolymer, which could indicate that degradation has taken place. However, upon examination of the SEC overlays seen in Figure 24, it is clear that no degradation has taken place, as both chromatograms are broad yet monomodal, with no lower molecular weight fragments appearing at higher elution volumes. The lower obtained $\bar{M}_w$ for the azido-functional copolymer must be ascribed to tailing and a shift in the baseline due to enhanced interactions of the latter with the SEC columns.

Functional dimethylsiloxane copolymers were created through a reaction with alkyne-functional molecules using CuAAC. Two different alkyne-containing molecules were chosen, in order to illustrate the versatility of the reaction. An aliphatic ATRP initiator and an alkyne-functional nitrobenzene were utilised as seen in Scheme 14.

The ATRP initiator can be used to create polysiloxanes with different polymer side-chains whereas the aromatic compound 4-nitrobenzene can be used to increase dielectric permittivity in dielectric elastomers. Functionalised copolymers were prepared under similar reaction conditions by means of a CuI-Et_3N catalytic system. The reaction products were characterised by FTIR, ^{1}H- and ^{13}C-NMR and SEC. FTIR was used to confirm the completion of the CuAAC reaction through the disappearances of the alkyne and azido bands at ~3300 cm^{-1} and ~2095 cm^{-1}, respectively. For the reaction with the ATRP initiator (**21**), which produced a green-brown polymer, a distinct ester C=O band at 1740 cm^{-1} confirmed the presence of the 2-bromoisobutyrate group. In **22** the presence of 4-nitrobenzene was indicated by the red colour of the obtained polymer and confirmed by bands at ~1605 cm^{-1} for the aromatic C=C bonds and at ~1520 cm^{-1} and ~1340 cm^{-1} for the N=O bonds. FTIR spectra of **20**, **21** and **22** can be seen in Figure 25. The formation of the CuAAC-products was furthermore confirmed by the presence of the triazole protons in ^{1}H-NMR, which appear at δ_H = 7.61 ppm and δ_H = 7.90 ppm for **21** and **22**, respectively.

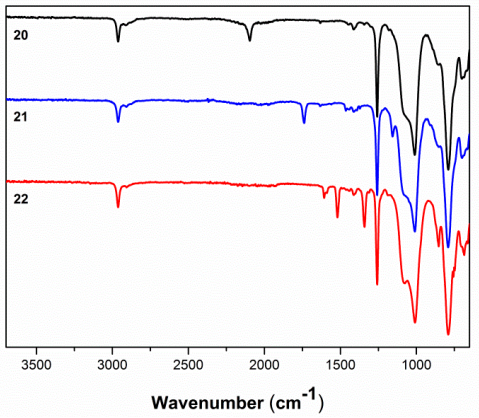

Figure 25 FTIR spectra of azido-functional copolymer **20** (black, top), 2-bromoisobutyrate-functional copolymer **21** (blue, middle curve) and 4-nitrobenzene-functional copolymer **22** (red, bottom curve).

The SEC results for CuAAC-products **21** and **22** can be seen in Table 6 and Figure 24. For both CuAAC-products, higher molecular weights are obtained, and a slight shift towards higher molecular weight regions can be seen in the SEC traces, pointing to the successful attachment of functional groups onto the copolymers. Furthermore, SEC showed that **22** had a strong UV signal, unlike the starting materials **19b-1** and **20**, which points towards the attachment of the 4-nitrobenzene chromophore.

Ionic polymers are a rapidly expanding class of materials with interesting and promising properties[164–166] which have recently been extended to silicone materials[167]. Thus, as an example of another possible post polymerisation modification, the prepared chloro-functional copolymer **19a-8** was used in a substitution reaction with 1-ethylimidazole to form the ionic copolymer seen in Scheme 15. An ionic compound could also potentially enhance the dielectric permittivity of an elastomer.

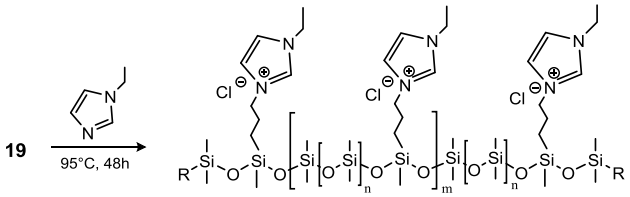

23

Scheme 15 Synthetic route to imidazolium-functional copolymer.

This reaction was followed by ^{1}H-NMR through a shift in the resonance of CH_2-Cl (δ_H = 3.50 ppm) to CH_2-N$^+$ (δ_H = 4.43 ppm). After the reaction, the orange-brown copolymer was less soluble in toluene, thereby demonstrating the increased ionic/polar nature of the copolymer **23**. The SEC results for the chloro-functional copolymer **19a-8** and imidazolium-functional copolymer **23** can be

seen in Table 6 and Figure 26. As observed for the CuAAC-products, a slight shift towards the higher molecular region is seen in the SEC traces for copolymer **23**, which indicates the successful attachment of the functional group.

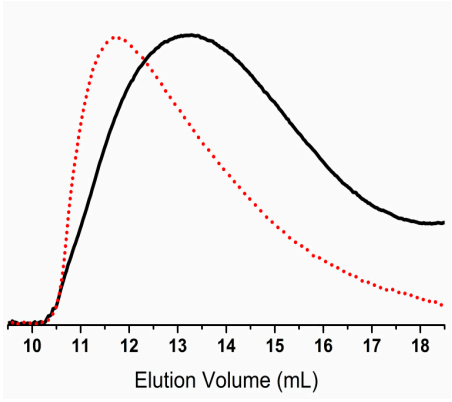

Figure 26 An overlay of the RI SEC traces of chloro-functional copolymer **19a-8** (black, −−) and imidazolium-functional copolymer **23** (red, • • •).

The prepared chloro- and azido-functional siloxane copolymers have great potential in the preparation of functional silicone elastomers where the properties of the elastomers can be altered and improved according to the given application and the type of group attached to the copolymer. The specific functional groups could include many different types as shown in Chapter 2 and are not limited to those used in this study.

6 Dielectric properties of elastomers prepared with dipolar copolymers

The work in this chapter is based on the manuscript *Silicone elastomers with high dielectric permittivity and high dielectric breakdown strength based on dipolar copolymers* submitted to Polymer, August 2014, which can be found in Appendix E along with all experimental procedures and associated supporting information.

6.1 Introduction

The aim of the work in this chapter is to create new and improved silicone elastomer systems with high dielectric permittivity using the dipolar siloxane copolymers prepared in Chapter 5 by Piers-Rubinsztajn polycondensation while maintaining reasonable levels of other favourable properties such as viscous and dielectric losses and electrical breakdown strengths.

Because elastomers prepared from an imidazolium-functional copolymer (**23**) did not cure properly, the study comprises elastomers prepared from azido- and nitrobenzene-functional copolymers. The synthesised copolymers allow for a high degree of chemical freedom, as several parameters can be varied during the preparation phase. Thus, the space between the functional groups can be varied by using different dimethylsiloxane spacer units between the high dielectric permittivity molecules. Furthermore, the degree of functionalisation of the copolymers can be varied accurately by changing the feed of the high dielectric permittivity molecules. As a result, a completely tuneable elastomer system, with respect to functionalisation, is achieved. It is investigated how the different functionalisation variables affect essential DEAP properties, including dielectric permittivity, dielectric loss, elastic modulus and dielectric breakdown strength. The optimal degree of chemical functionalisation, where important properties are not significantly compromised, is also determined.

6.2 Results and discussion

Siloxane copolymers that allow for functionalisation with high dielectric constant molecules were prepared according to the procedure described in Chapter 5. The copolymers were prepared from commercially available starting materials through the tris(pentafluorophenyl)borane-catalysed Piers-Rubinsztajn reaction of 3-chloropropylmethyldimethoxysilane and hydride-terminated dimethylsiloxane pre-polymers. Dimethylsiloxane pre-polymers constitute the spacer unit between the functional groups. The copolymers were then end-functionalised with allyl-groups that allow for hydrosilylation cross-linking reactions with hydride-functional cross-linker molecules to form polymer networks. The chloro-functional copolymers were converted to azido-functional through nucleophilic substitution with sodium azide. Azido groups on the siloxane copolymer allow for Cu-AAC reactions where high dielectric constant alkyne molecules can be attached. The structure of

the formed azido-functional siloxane copolymer, with various spacer units between the azido-groups, is shown in Figure 27.

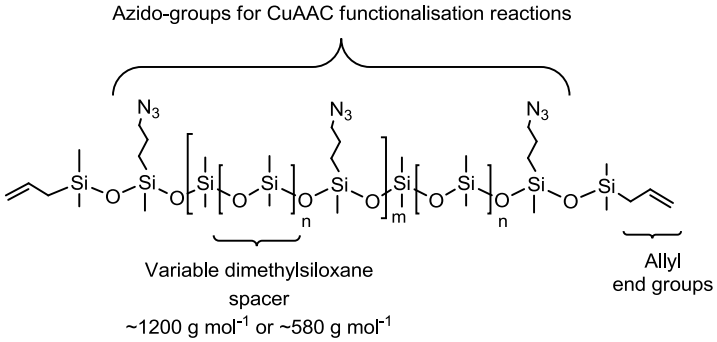

Figure 27 Structure of functionalisable siloxane copolymers with various spacer lengths between the azido-groups and allyl end groups, thereby allowing for hydrosilylation cross-linking reactions.

Copolymers with two different spacer lengths between the azido-group were synthesised. One copolymer contains azido-groups with ~1200 g mol^{-1} dimethylsiloxane spacers between each group and the other copolymer contains azido-groups with ~580 g mol^{-1} dimethylsiloxane spacers between the functional groups. The copolymers with the shorter spacer thus contain approximately double the amount of functional groups than the copolymers with the long spacer at comparable copolymer lengths.

Copolymers were analysed with SEC, and molar mass characteristics were calculated from linear polydimethylsiloxane standards. The molecular weights of the copolymers prepared with different spacers were both found to be $\overline{M}_w$ ≈ 23,000 g mol^{-1}, which is a suitable molecular weight for silicone elastomers. Molecular weights of 23,000 g mol^{-1} signify that each copolymer contains approximately 15 and 30 azido-groups for the copolymers with the ~1200 g mol^{-1} dimethylsiloxane spacer and ~580 g mol^{-1} dimethylsiloxane spacer, respectively.

The azido-copolymers with different spacer lengths between the groups were thereafter functionalised with the high dielectric constant molecule, 1-ethynyl-4-nitrobenzene, through CuAAC, as illustrated in Scheme 16.

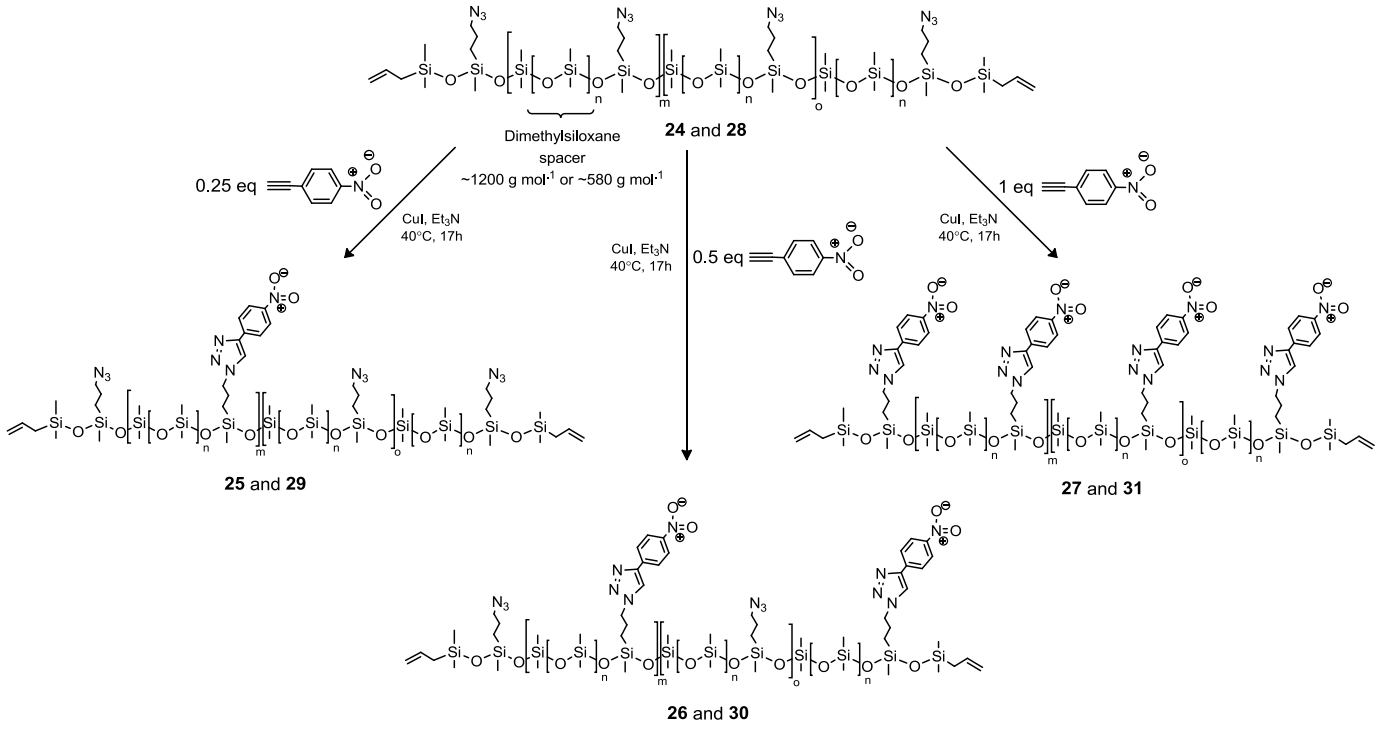

Scheme 16 Synthetic route to nitrobenzene-functionalised copolymers through CuAAC reactions. The azido-functional copolymers are reacted with 0.25, 0.5 or 1 equivalents of 1-ethynyl-4-nitrobenzene to the total number of azido-groups.

The azido-groups on the copolymers were reacted to different extents so that copolymers with different degrees of functionalisation would be obtained. The feed of 1-ethynyl-4-nitrobenzene into the content of azido-groups was varied, and the effectiveness of the CuAAC reaction allowed for direct control over the degree of functionalisation. The feed of 1-ethynyl-4-nitrobenzene to the azido-groups and the resulting obtained degree of functionalisation, as determined by ^{1}H-NMR, are shown in Table 7.

Table 7 Overview of the prepared functionalised dipolar copolymers.

Entry	$\bar{M}_w$ dimethylsiloxane spacer [g mol^{-1}]	Feed of 1-ethynyl-4-nitrobenzene [% of azido-groups]	Degree of functionalisation from ^{1}H-NMR [% of azido-groups]	Content of 4-nitrobenzene [wt%]
24	~1200	0	0	0
25	~1200	25	25	2.75
26	~1200	50	51	5.6
27	~1200	100	100	11
28	~580	0	0	0
29	~580	25	19	3.8
30	~580	50	42	8.4
31	~580	100	100	20

The actual degrees of functionalisation were determined by ^{1}H-NMR through the integration of the CH_2-N$_3$ resonance at δ_H = 3.23 ppm against the CH_2-N$_{triazole}$ resonance at δ_H = 4.41 ppm. For copolymers **25**-**27** and **31** the 1-ethynyl-4-nitrobenzene feed matched almost perfectly the degree of functionalisation determined from ^{1}H-NMR such that, for example, copolymer **25** with 25% substituted azido-groups had an integral of 0.25 for the CH_2-N$_{triazole}$ resonance and an integral of 0.75 for the CH_2-N$_3$ resonance. For copolymers **29** and **30** slightly lower degrees of functionalisation were obtained. As the CuAAC reaction is almost 100% effective, the slightly lower obtained degrees of functionalisation could simply be due to inaccuracies when measuring the feed of 1-ethynyl-4-nitrobenzene during the synthesis of these copolymers. Overall, the degree of functionalisation can be varied accurately by changing the 1-ethynyl-4-nitrobenzene feed. The corresponding actual content of nitrobenzene on the copolymers is shown in Table 7.

The functional copolymers were thereafter used in cross-linking reactions with ~8-functional functional hydride cross-linkers and furthermore reinforced with 20 wt% surface-treated silica particles to create silicone elastomers, as shown in Scheme 17.

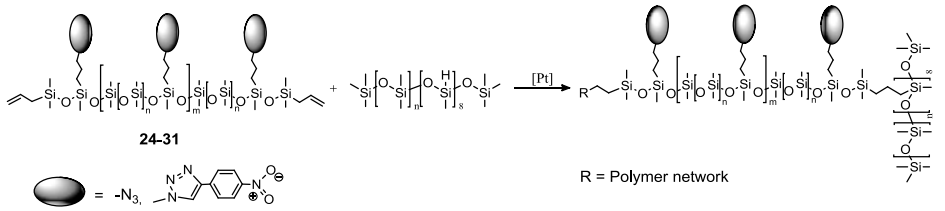

Scheme 17 Cross-linking reaction between copolymers **24**-**31** and a hydride-functional cross-linker.

A reference sample made from PDMS of $\overline{M}_w$ = 25,000 g mol^{-1} using similar reaction conditions (same catalyst, cross-linker and particle concentration) was also produced. The elastomers prepared with different degrees of functional groups showed different curing rates. The azido-functional copolymers (**24** and **28**) cured relatively quickly (<12 hours) at low catalyst levels (20 ppm). For elastomers containing nitrobenzene, higher catalyst concentration was generally needed (100 ppm) and the films cured within 24 hours. At 100% conversion of the azido-groups to nitrobenzene (**27** and **31**), longer reaction times (one week) were needed. This indicates that the presence of larger amounts of nitrobenzene or triazole-groups inhibits, to some extent, the hydrosilylation reaction.

The prepared elastomers were characterised by FTIR. The spectra of azido- and nitrobenzene-functional films are shown in Figure 28.

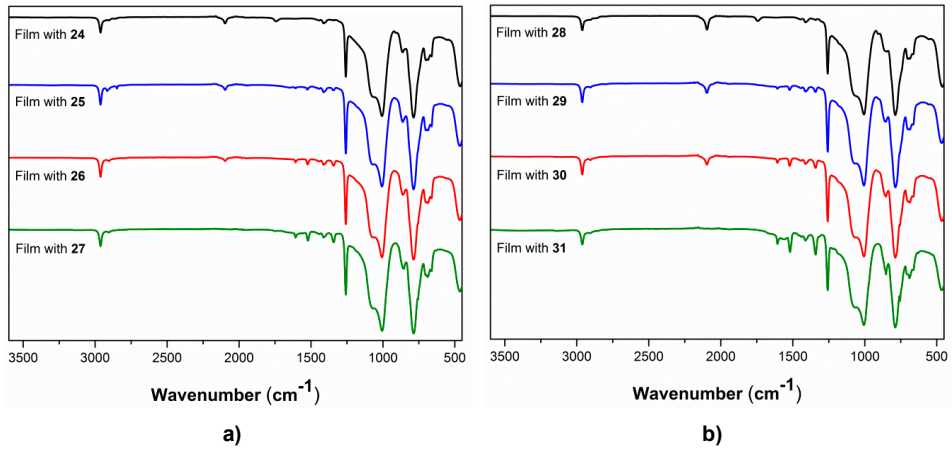

Figure 28 FTIR spectra of elastomer films prepared with the different functionalised copolymers: a): films prepared with copolymers with a ~1200 g mol^{-1} spacer and b): films prepared with copolymers with a ~580 g mol^{-1} spacer.

The films with the two azido-functional copolymers **24** and **28** show distinctive -N_3 bands at approximately 2095 cm^{-1}. The azido-band is sharper for the film with copolymer **28**, confirming the higher content of azido-groups on this copolymer due to the shorter dimethylsiloxane spacer be-

tween the functional groups. The more substituted the azido-group becomes with nitrobenzene, the less intense the -N_3 bands become. For the films with 100% substituted azido-groups, no -N_3 bands are visible (films with **27** and **31**). The films containing nitrobenzene (**25**-**27** and **29**-**31**) all show bands of increasing intensity at ~1605 cm^{-1} for the aromatic C=C bonds and at ~1520 cm^{-1} and ~1340 cm^{-1} for the N=O bonds with increasing nitrobenzene content, which corroborates increasing functionalisation with nitrobenzene in the elastomers.

The gel fractions of the films were determined from swelling experiments with chloroform, in order to elucidate the amount of bonded (gel fraction) and non-bonded (sol fraction) species in the networks.

Table 8 Gel fractions (W_{gel}) as a result of swelling experiments.

Film with entry	W_{gel} [%]
Ref.	97
24	83
25	95
26	84
27	64
28	84
29	97
30	88
31	69

As seen in Table 8 the gel fractions decrease with increasing degrees of functionalization; thus, the lowest gel fractions are obtained for films with copolymers that are fully substituted with nitrobenzene (**27** and **31**). This could be due to the slow curing time of these films, indicating that not all reactive end groups on the copolymers react, which leaves larger fractions of non-bonded substructures in the networks. The gel fractions for the other films are within an acceptable limit, thereby suggesting that these films are better cross-linked.

The effect of the degree of functionalisation on the thermal transition behaviour of the elastomer films was determined by differential scanning calorimetry (DSC). The reference film showed clear melting and crystallisation temperatures at T_m = −42.6°C and T_c = −74.7°C, respectively. For all films prepared with copolymers **24**-**31**, no T_m or T_c were observed, which means that no crystalline regions were present in the films. This points towards the successful formation of the spatially well-distributed azido- and nitrobenzene-functional groups, which prevents crystallisation from taking place. The glass transition temperature (T_g) of the pure PDMS reference sample was determined to be −127°C. For films prepared with the azido-functional copolymers, the glass transition temperatures increased slightly to −120°C and −115°C for **24** and **28**, respectively. The higher the content of nitrobenzene in the films, the higher the measured glass transition temperature. The glass transition temperatures ranged from -118°C for the film prepared with copolymer **25** to −95°C for the film prepared with copolymer **31**.

The effect of the functional copolymers on the thermal stability of the elastomer films was determined by TGA, and the resulting thermograms can be found as supporting information in Appen-

dix E. The thermal degradation temperatures were not significantly altered for the films with the functional copolymers compared to the reference film.

The influence of the concentration and type of copolymer on the mechanical properties was investigated by determining the shear storage and shear loss modulus of the prepared films. In Figure 29 the results for films with different spacers and functional groups are presented. Furthermore, the resulting shear storage moduli (G') and loss (tan δ) at 1 Hz are summarised in Table 9.

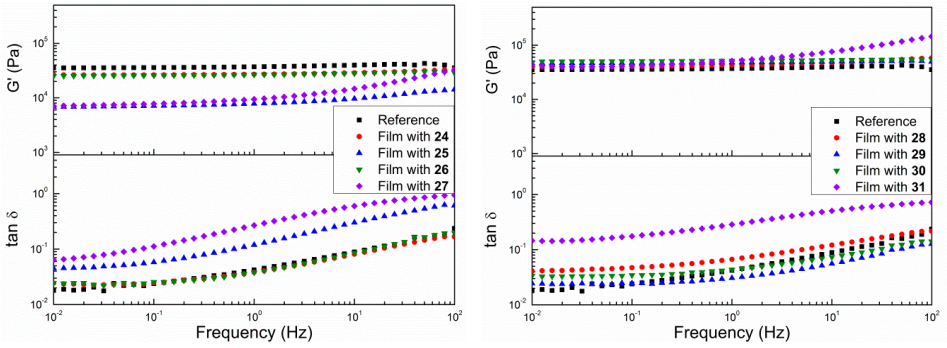

a) **b)**

Figure 29 Storage moduli (G') and loss (tan δ) as functions of frequency for: a): films prepared with a ~1200 g mol^{-1} pre-polymer spacer (**24**-**27**) and b): films prepared with a ~580 g mol^{-1} pre-polymer spacer (**28**-**31**).

It is evident that the films with the ~1200 g mol^{-1} pre-polymer spacer (copolymers **24**-**27**) all have lower moduli than the reference film. The films prepared with the ~580 g mol^{-1} pre-polymers (copolymers **28-31**) have quite similar, but slightly higher, moduli – as for the reference film. Viscous losses and tan δ remain low for all films prepared with the functional copolymers except for the high concentration nitrobenzene films **27** and **31**. For these films the viscous losses increased six-fold, indicating increased damping behaviour, which is partly or fully due to the larger fractions of extractable substructures and the deterioration of network properties[73].

The impact of the type of copolymer on dielectric properties was determined by dielectric relaxation spectroscopy on discs of ~1 mm thick films. Dielectric relaxation spectra showing the frequency-dependent dielectric permittivity (*ε*') and loss tangent (tan δ) for films with copolymers **24**-**31**, as well as the reference film, are presented in Figure 30. Permittivity and loss at 1 Hz and 100 Hz are summarised further in Table 9. Enlarged spectra of dielectric permittivity at the plateau region from 10^2 to 10^5 Hz are also shown in Figure 30.

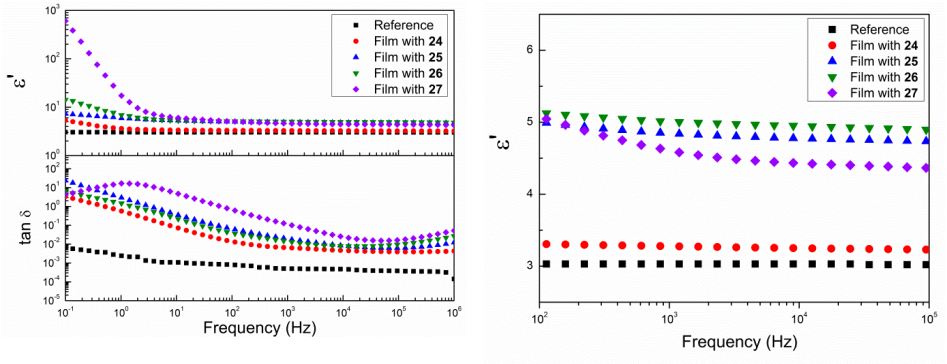

a)

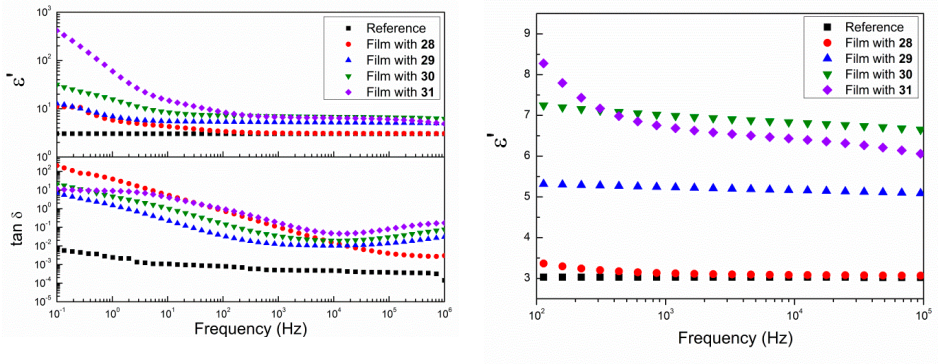

b)

Figure 30 Dielectric permittivity (ε') and loss tangent (tan δ) as functions of frequency for films prepared with: a): a ~1200 g mol^{-1} pre-polymer spacer (**24**-**27**) and b): a ~580 g mol^{-1} pre-polymer spacer (**28**-**31**).

For all films prepared with functional copolymers dielectric permittivity is seen to increase compared to the reference film, for which $\varepsilon' = 3.0$. The films with the two azido-functional copolymers **24** and **28** both show increased dielectric permittivity to $\varepsilon' = 3.3$ and $\varepsilon' = 3.4$ at 100 Hz, respectively. These permittivities correspond to a 10-13% increase. Increasing (doubling) the content of azido-groups thereby does not increase permittivity at medium to higher frequencies. The film with **28**, however, shows elevated permittivity at low frequencies. At 1 Hz, for instance, permittivity increases to $\varepsilon' = 5.8$, thus corresponding to an almost two-fold increase. These results show that the azido-groups alone also yield increased permittivities for the elastomer films. The azido-functional copolymers, however, do exhibit increased dielectric losses, which are especially visible on the film prepared with **28**.

The films prepared with copolymers with the ~1200 g mol^{-1} pre-polymer spacer and different degrees of nitrobenzene (copolymers **25-27**) show increased permittivities in the same order of

magnitude ($\varepsilon' \approx 5.0$) at 100 Hz. This corresponds to an increase in permittivity of ~70 %. At lower frequencies dielectric permittivity increases in line with the increased content of nitrobenzene, reaching $\varepsilon' = 17.3$ at 1 Hz for the film prepared with copolymer **27** containing 11 wt% nitrobenzene. Dielectric losses, tan δ, increase slightly in line with increasing nitrobenzene content.

Films prepared with copolymers with the ~580 g mol^{-1} spacer between the functional groups show largely increased permittivities at 100 Hz, with the highest dielectric permittivity obtained for the film prepared with copolymer **31**, which contains 20 wt% nitrobenzene ($\varepsilon' = 8.5$). This corresponds to an increase of 180%. At frequencies higher than 100 Hz the film prepared with copolymer **30** shows the highest dielectric permittivity of $\varepsilon' \approx 7$. At lower frequencies dielectric permittivity also increases in line with the increased content of nitrobenzene, reaching $\varepsilon' = 59.3$ at 1 Hz for the film prepared with copolymer **31** containing 20 wt% nitrobenzene. Relative dielectric losses (tan δ), furthermore, increase in line with increasing nitrobenzene content but are lower than the film prepared with the corresponding azido-functional copolymer **28**.

It is evident in Figure 30 that in the medium to high frequency region (10^2-10^6 Hz) there are no significant changes in ε' with frequency. In this region dielectric response depends mainly on bulk polarisation processes[168]. Therefore, the most promising increases in permittivity for DEAP applications are observed in this region. Interestingly, the largest increases in permittivity in this frequency region are not necessarily observed for the copolymers with the largest concentration of nitrobenzene, which indicates that there is a maximum concentration of nitrobenzene above which further improvement to dielectric permittivity is not possible. Above this concentration, it is only permittivity at low frequencies (due to Maxwell polarisation[169]) and dielectric losses that increases and thereby there is a higher risk of unwanted conductivity.

The nature of this system makes it possible to tune the concentration and distribution of functional groups, and so it is possible to obtain the most optimal dielectric elastomer with regards to permittivity and dielectric loss.

In order to investigate the nature of the large increases in permittivity and loss at low frequencies for the films prepared with copolymers with high concentrations of nitrobenzene, plots of conductivity as a function of frequency are shown in Figure 31.

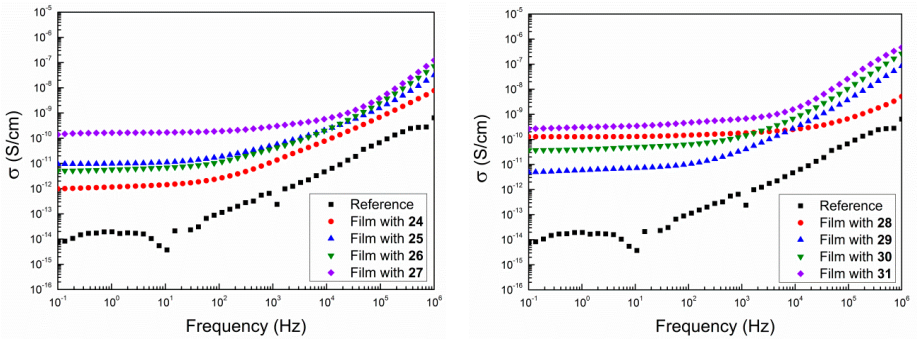

Figure 31 Conductivity as a function of frequency for films prepared with: a): a ~1200 g mol^{-1} pre-polymer spacer (**24**-**27**) and b): a ~580 g mol^{-1} pre-polymer spacer (**28**-**31**).

It can be seen from Figure 31 that some of the films show higher electric conductivity at low frequencies, as conductivity becomes independent of frequency. The observed conductivities, however, remain very low. For the films prepared from the 100% substituted copolymers (**27** and **31**) slightly higher conductivities are observed, which could be the reason for the high dielectric losses of these films at low frequencies.

The electrical breakdown strengths, E_B, for films with copolymers **24**-**31** as well as the reference film are presented in Table 9.

Table 9 Dielectric permittivity (ε') and loss tangent (tan δ) at 1 Hz and 100 Hz as well as the breakdown strength (E_B) and storage moduli (G') and loss (tan δ) for films with copolymers **24**-**31** and the PDMS reference.

	Dielectric spectroscopy				Electrical breakdown	Rheology		Figure of merit
Film with entry	**ε' @1Hz**	**ε' @100Hz**	**tan δ @1Hz**	**tan δ @100Hz**	**E_B**	**G' @1Hz**	**tan δ @1Hz**	**F_{om}/ F_{om_ref}**
					[V/μm]	**[kPa]**		
Ref.	3.0	3.0	0.002	0.0008	55.4	37.0	0.042	1.0
24	3.6	3.3	0.56	0.01	61.4	27.0	0.038	1.9
25	5.9	5.0	2.90	0.06	63.2	7.81	0.119	10.3
26	6.9	5.1	1.47	0.04	69.2	26.5	0.038	3.7
27	17.3	5.0	16.7	0.60	60.5	9.41	0.268	7.8
28	5.8	3.4	38.7	0.70	81.1	43.1	0.067	2.1
29	6.9	5.3	1.51	0.03	66.7	47.9	0.031	1.8
30	15.6	7.3	4.52	0.15	64.1	51.5	0.044	2.3
31	59.3	8.5	9.07	0.90	65.0	51.3	0.286	1.8

For all films, electrical breakdown strength is seen to increase compared to the reference film. This increased breakdown strength, as seen in Table 9, is not solely due to increased elastic moduli, which is often the case[151]. This suggests that the introduction of functional groups does not compromise electrical breakdown strength, which is an essential DEAP property. The high dielectric breakdown strengths of the films could be due to a low degree of chemical and physical impurities, the result of which has a large effect on the dielectric strength of insulating materials[170]. The prepared copolymers are all purified after synthesis, which implies that the prepared films have higher breakdown strengths than the commercial PDMS reference material.

As mentioned in Chapter 1, the enhancement in the properties of the dipolar elastomers can be compared with the reference material by calculating the figure of merit, F_{om}, relative to the figure of merit for the reference films[31,47]. All results can be seen in Table 9. All films prepared with copolymers **24**-**31** show increased F_{om}. The largest increase in the figure of merit is obtained for the film with the nitrobenzene-functional copolymer **25** where the figure of merit is increased 10 times compared to the reference film. The high figure of merit of this film is among other things obtained because of its low modulus. The viscous and dielectric losses, however, are not incorporated into the figure of merit calculations but are important parameters that need to be considered. Therefore, when considering the losses, the best overall properties were obtained for a film prepared with a copolymer with a ~1200 g mol^{-1} dimethylsiloxane spacer and 5.6 wt% nitrobenzene (copolymer **26**), as it has high dielectric permittivity (~70% increase at 100 Hz) and low dielectric loss. Furthermore, the obtained film was soft with low modulus, without compromising the viscous loss and gel fraction. Electrical breakdown strength also increased 25% compared to that of the pure PDMS reference film.

Moreover, the best overall properties were obtained for the films prepared with copolymers with the ~1200 gmol^{-1} pre-polymer spacer, as the films prepared with copolymers with a shorter dimethylsiloxane spacer (~580 g mol^{-1}) and a higher concentration of functional groups were slightly stiffer and therefore less extensible.

7 Dielectric properties of elastomers prepared with chloro-functional copolymers

The work in this chapter is based on so far unpublished results. Experimental procedures can be found in Chapter 9.

7.1 Introduction

The work in this chapter investigates the surprisingly effective dielectric properties of chloro-functional copolymers. The chloro-functional copolymers were prepared as precursors for the azido- and nitrobenzene-functional copolymers, whose dielectric properties were investigated in Chapter 6. Upon measurement of the mechanical and dielectric properties of elastomers prepared from the chloro-functional copolymer precursors, interesting results were obtained, which will be elaborated in this chapter.

7.2 Results and discussion

Chloro-functional copolymers were prepared as described in Chapter 5 through the Piers-Rubinsztajn polycondensation of 3-chloropropylmethyldimethoxysilane and hydride-terminated dimethylsiloxane pre-polymers, according to Scheme 12. The copolymers were prepared with a ~1200 g mol^{-1} dimethylsiloxane pre-polymer and a ~580 g mol^{-1} dimethylsiloxane pre-polymer to form the copolymers **32** and **33**, respectively, both of $\overline{M}_w$ ≈ 23,000 g mol^{-1} as determined by SEC. The chloro-functional copolymers were reacted with ~8-functional functional hydride cross-linkers and furthermore reinforced with 20 wt% surface-treated silica particles to create silicone elastomers, as shown in Scheme 18.

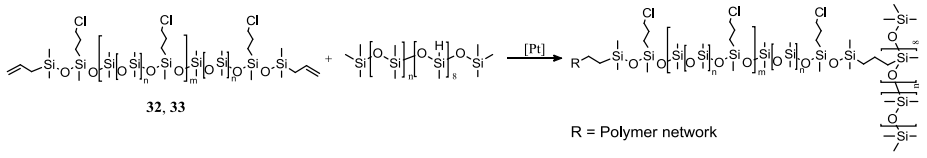

Scheme 18 Cross-linking reaction between chloro-functional copolymers **32** and **33** and a hydride-functional cross-linker.

A reference sample made from pure PDMS of $\overline{M}_w$ = 25,000 g mol^{-1} using similar reaction conditions (cross-linker and particle concentration) was also produced. The films prepared with chloro-functional copolymers cured extremely rapidly at room temperature at very low catalyst concentrations (<1 ppm) and in order to obtain suitable curing times for proper film casting, 1 wt% of inhibitor (Pt88 from Wacker Chemie) was added to the mixture. At this point the films were fully cured after 3 hours at 115°C.

The gel fractions of the films were determined from swelling experiments with chloroform, in order to elucidate the amount of bonded (gel fraction) and non-bonded (sol fraction) species in the networks (see Table 10).

Table 10 Gel fractions (W_{gel}) determined from swelling experiments of films prepared with chloro-functional copolymers with ~1200 g mol^{-1} pre-polymer spacer (**32**) and ~580 g mol^{-1} pre-polymer spacer (**33**).

Films with entry	W_{gel} [%]
Ref.	97
32	80
33	77

The gel fractions for the two films prepared with chloro-functional copolymers are both somewhat low, which could be due to improper curing that leaves larger fractions of non-bonded substructures in the networks. This could potentially be optimised by longer curing times at a lower temperature and this would ensure that the polymer networks will be mechanically stable during long-term usage.

The effect of the degree of the chloro-functional copolymers on the thermal transition behaviour of the elastomer films was determined by DSC. The reference film showed clear melting and crystallisation temperatures at T_m = −42.6°C and T_c = −74.7°C, respectively. For films prepared with the chloro-functional copolymers **32** and **33**, no T_m or T_c was observed, which means that no crystalline regions were present in the films. This is probably due to the alkyl chloride side-chains, which prevent the alignment of linear polymer segments necessary for crystallisation. The glass transition temperature, T_g, of the pure PDMS reference sample was determined to be −127°C. For films prepared with the chloro-functional copolymers, the glass transition temperatures increased slightly to −120°C and −115°C for **32** and **33**, respectively. This indicates that the higher the concentration of alkyl chloride-groups in the films, the higher the T_g, because the alkyl chloride-groups hamper some segmental rotation. The glass transition temperatures, however, remain low.

The effect of the chloro-functional copolymers on the thermal stability of the elastomer films was determined by TGA. The thermal degradation temperatures were not significantly altered for the films with the chloro-functional copolymers compared to the reference film but mineralisation of the films occurred to a greater extent.

The influence of the chloro-functional copolymers on the mechanical properties was investigated by determining the shear storage and shear loss moduli of the prepared films. The results are presented in Figure 32. Furthermore, the resulting shear storage moduli (G') and loss as tan δ at 1 Hz are summarised in Table 11.

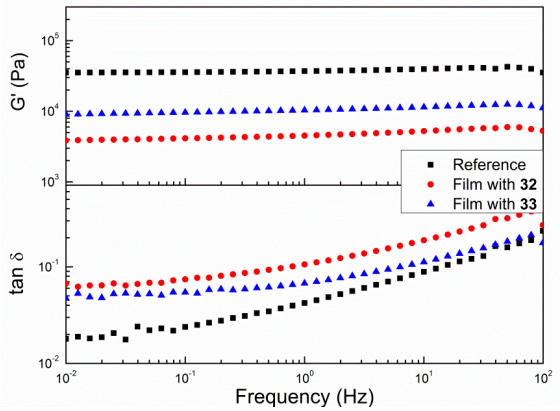

Figure 32 Storage moduli (G') and loss (tan δ) as functions of frequency for films prepared with chloro-functional copolymers with ~1200 g mol^{-1} pre-polymer spacer (**32**) and ~580 g mol^{-1} pre-polymer spacer (**33**).

It is evident from Figure 32 that films prepared with the chloro-functional copolymers have significantly lower moduli than the reference film based on pure PDMS. Furthermore, viscous losses (tan δ) have increased slightly, which could be due to the larger fractions of extractable substructures seen from the swelling experiments. However, when comparing these films with the films prepared with the azido-functional copolymers, **24** and **28** from the previous chapter, which have quite similar gel fractions, this does not fully explain the soft nature of the films with the chloro-functional copolymers, as significantly lower moduli are observed for these films compared with the films prepared with azido-functional copolymers. The soft nature of the films prepared with the chloro-functional copolymers could be an advantage for DEAP applications, if the end result is not only due to lower gel fractions.

The impact of the chloro-functional copolymers on dielectric properties was determined through dielectric relaxation spectroscopy on discs of ~1 mm thick films. Dielectric relaxation spectra showing the frequency-dependent dielectric permittivity (ε') and loss tangent tan δ are presented in Figure 33, while permittivity and loss at 1 Hz and 100 Hz are summarised further in Table 11.

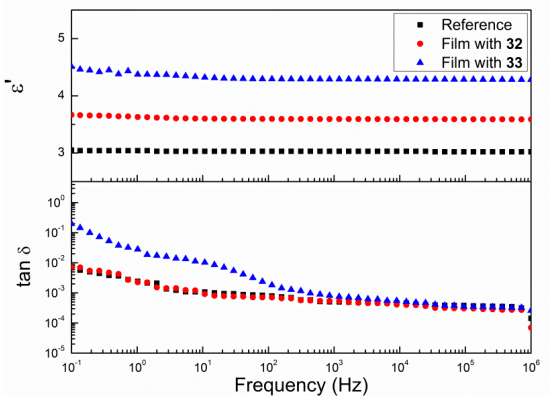

Figure 33 Dielectric permittivity (*ε'*) and loss tangent (tan δ) as functions of frequency for films prepared with chloro-functional copolymers with ~1200 g mol^{-1} pre-polymer spacer (**32**) and ~580 g mol^{-1} pre-polymer spacer (**33**).

For both films prepared with the chloro-functional copolymers dielectric permittivity in Figure 33 is seen to increase compared to the reference film, for which $\varepsilon' = 3.0$. The chloro-functional films **32** and **33** have $\varepsilon' = 3.6$ and $\varepsilon' = 4.3$ at 100 Hz, respectively. This corresponds to 20% and 43% increase in permittivity, respectively. Furthermore, the losses, tan δ, remain as low as for the reference film. These preliminary results indicate that chloro-functional silicones are promising DEAP candidates, as the films are soft and dielectric permittivity is improved significantly, especially for the film with **33**. Furthermore, the films with the chloro-functional copolymers show no increased conductivity, as the conductivity curves follow that of the reference film.

The electrical breakdown strengths, E_B, for films with copolymers **32** and **33** as well as the reference are presented in Table 11. For both films prepared with chloro-functional copolymers the electrical breakdown strength is observed to increase, which could be due to lower degrees of chemical and physical impurities. Overall, it can be seen from the figures of merit calculations in Table 11 that the films with the chloro-functional copolymers show significantly enhanced properties compared to the reference films. This is the result of their very low moduli and improved dielectric permittivity and breakdown strengths. Furthermore, as the viscous and dielectric losses do not increase considerably, the figure of merit, in this case, gives a realistic value for the possible actuation improvement that these films might exhibit.

Table 11 Dielectric permittivity (ε') and loss tangent (tan δ) at 1 Hz and 100 Hz as well as the breakdown strength (E_B) and storage moduli (G') and loss (tan δ) for films with chloro-functional copolymers **32** and **33**.

	Dielectric spectroscopy				Electrical breakdown	Rheology		Figure of merit
Film with entry	**ε' @1Hz**	**ε' @100Hz**	**tan δ @1Hz**	**tan δ @100Hz**	**E_B**	**G' @1Hz**	**tan δ @1Hz**	**F_{om}/ F_{om_ref}**
					[V/μm]	**[kPa]**		
Ref.	3.0	3.0	0.002	0.0008	55.4	37.0	0.042	1.0
32	3.6	3.6	0.002	0.0007	70.0	4.52	0.106	15.7
33	4.4	4.3	0.03	0.002	63.0	10.4	0.068	6.7

8 Conclusions and outlook

8.1 Conclusion

High dielectric permittivity silicone elastomers were prepared through the covalent grafting of functional moieties onto silicone polymer networks. Two different synthetic strategies were followed. The first strategy was based on the development of a new type of silicone-compatible cross-linker. The cross-linker allowed for the attachment of functional moieties at the polymer network cross-linking point through CuAAC reactions, and thus elastomers with well-distributed functionalities were obtained. The attachment of different functional groups led to elastomers with various properties, such as increased thermal stability and increased hydrophobicity. Dipolar groups (nitrobenzene and nitroazobenzene) on the cross-linker resulted in improved dielectric permittivity, which in turn increased ~20% at ~0.5 wt% of the dipolar group. The increase in permittivity is significant in light of the low concentration of dipolar species. This was most likely due to the well-distributed manner in which the dipolar groups were incorporated, meaning that none of the dipolar groups cancelled out the others, and the full effect of the dipolar species on the permittivity was therefore achieved. At the concentration of cross-linker where permittivity was the greatest, electrical breakdown strength, mechanical properties and dielectric loss were not compromised. The cross-linker method has some limitations, since compatibility issues between certain functional groups and the silicone matrix can arise. Furthermore, the tri-functional cross-linker creates increasingly softer networks, when the concentration of functional cross-linker is increased. It is moreover not possible to achieve further increases in permittivity using this method, as there is a limit to how much cross-linker it is possible to add to a polymer network without deteriorating the mechanical properties.

The second synthetic strategy for high dielectric constant silicone elastomers involved the synthesis of functional copolymers, through two different approaches. The first route involved the synthesis of a new type of functionalisable chain extender. Nitrobenzene-functional copolymers were successfully created using the synthesised chain extender and hydride-terminated low molecular weight PDMS through platinum catalysed polycondensation and its subsequent reaction with 1-ethynyl-4-nitrobenzene through CuAAC. The resulting elastomer showed more than a two-fold increase in dielectric permittivity. The chain extender method was promising for one-pot elastomer synthesis and as a high dielectric constant additive for commercial silicone systems. The limitations of this approach, however, were that tuning of the molecular weight was not trivial, because the reaction time, catalyst concentration, end group functionalisation and stoichiometric ratio between the starting materials needed further optimisation. Therefore, another synthetic approach for functional copolymers was followed, by using the highly efficient borane-catalysed Piers-Rubinsztajn reaction. Through this method spatially well-distributed functional copolymers with tailored molecular weights and high end group fidelity were obtained. Functional groups on the copolymers, such as alkyl azide and nitrobenzene, created silicone elastomers with varying increases in dielectric permittivity. High permittivities were obtained for nitrobenzene-functional copoly-

mers (e.g. a 180% increase at 20 wt% of nitrobenzene). This concentration, however, did increase dielectric loss and stiffness, though electrical breakdown strength was not compromised. An optimum loading of functional groups was determined and the best overall properties were thus obtained with an elastomer prepared from a nitrobenzene-functional copolymer containing 5.6 wt% of the nitrobenzene moiety. At this concentration dielectric permittivity was increased by 70%, while breakdown strength and mechanical properties were improved. Dielectric loss remained suitable for DEAP applications.

Interesting results were also obtained from elastomers prepared with alkyl chloride functional copolymers. A total of 43% increased dielectric permittivity was obtained and the prepared elastomers were very soft, though electrical breakdown strengths were not compromised. Furthermore, dielectric losses and conductivities remained as they were for the reference film containing pure PDMS. The gel fractions of these elastomers, however, still need to be improved.

8.2 Future work

The work presented herein could provide the basis for further research or even further investigations into some of the obtained data.

Firstly, the actuation strain should be measured for the most promising synthesised elastomers, in order to determine their actuation response and thereby their potential use as DEAPs.

It would be very interesting to investigate further the properties of elastomers prepared from alkyl chloride functional copolymers, as the obtained increases in dielectric permittivity for these elastomers are achieved without affecting other important DEAP properties. The concentration of alkyl chloride functional groups – and thereby dielectric permittivity – could be increased further, by using an even smaller molecular weight PDMS spacer between the functional groups. Furthermore, the curing procedure, and thereby the gel fractions of these films, should be optimised further.

Moreover, it would be interesting to create composite elastomers using, for example, alkyl chloride-functional or nitrobenzene-functional copolymers and a high dielectric constant filler such as TiO_2. As the base polymers would have higher dielectric permittivity than pure PDMS, it would be possible to obtain elastomers with good DEAP properties using low concentrations of TiO_2.

It would furthermore be interesting to investigate the properties of the heterogeneous bimodal networks as dielectric elastomers both in actuation and in combination with the dipolar cross-linkers and/or dipolar copolymers. The soft nature of the heterogeneous bimodal networks and the high dielectric constant synthesised materials could potentially induce a synergistic effect on the actuation properties.

9 Experimental procedures

All reactions were carried out in a nitrogen atmosphere.

4-(bromomethyl)-2,7-dimethyl-3,6-dioxa-2,7-disilaoctane (0a):

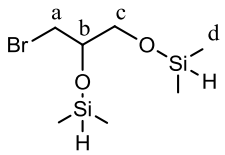

3-bromo-1,2-propanediol (1 g, 6.45 mmol) was dissolved in dry THF (40 mL) and transferred to a 100 mL two-necked round-bottomed flask equipped with magnetic stirring. The mixture was cooled to 0°C in an ice bath and 1,1,3,3-tetramethyldisilazane (1.27 g, 9.49 mmol) was now added drop wise together with 2 drops of chlorodimethylsilane catalyst. The reaction was carried out under reflux for 5 hours. The reaction mixture was then diluted with THF (50 mL), filtered and the solvent was removed *in vacuo*. The product was obtained in the form of a colourless oil in quantitative yield. IR (cm^{-1}): 2960 (C-H stretch); 2120 (Si-H stretch); 1255 (Si-CH_3 stretch); 1110 (C-O stretch); 1055 (Si-O stretch). ^{1}H NMR ($CDCl_3$, δ_H, ppm): 0.07-0.27 (m, 12H, C*H*$_3$-Si), 3.38-3.52 (m, 2H, Br-C*H*$_2$), 3.68 (m, 2H, C*H*$_2$-O), 3.89-4.02 (m, 1H, C*H*-O), 4.63-4.70 (m, 2H, Si-*H*). ^{13}C-NMR ($CDCl_3$, δ_C, ppm): -0.5 (d), 32 (a), 65 (c), 71 (b).

4-(azidomethyl)-2,7-dimethyl-3,6-dioxa-2,7-disilaoctane (0b):

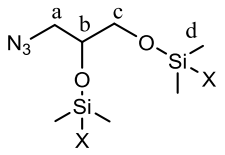

0a (0.5 g, 1.84 mmol) and NaN_3 (0.16 g, 2.46 mmol) were dissolved in DMF (5 mL) and stirred at 45°C for 17 hours. The reaction mixture was now quenched with 30 mL H_2O and the aqueous DMF was extracted with EtOAc (3 x 30 mL). The organic phases were combined and washed with H_2O (5 x 50 mL) and brine (1 x 50 mL), dried with $MgSO_4$, filtered and concentrated *in vacuo* to give the product in the form of a slightly yellowish oil in quantitative yield. IR (cm^{-1}): 2960 (C-H stretch); 2100 (-N_3 stretch); 1258 (Si-CH_3 stretch); 1050 (Si-O stretch). ^{1}H NMR ($CDCl_3$, δ_H, ppm): 0.07-0.22 (m, 12H, C*H*$_3$-Si), 3.29 (m, 2H, N_3-C*H*$_2$), 3.63 (m, 2H, C*H*$_2$-O), 4.04 (m, 1H, C*H*-O). ^{13}C-NMR ($CDCl_3$, δ_C, ppm): -0.5 (d), 52 (a), 63 (c), 72 (b).

3-(3-chloropropyl)-1,1,3,5,5-pentamethyl-1,5-divinyltrisiloxane (13a):

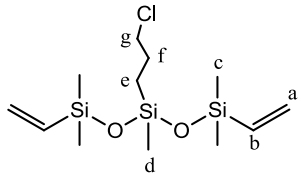

3-Chloropropylmethyldimethoxysilane (6.7 g, 36.7 mmol) was dissolved in dry heptane (70 mL) in a 500 mL two-necked round-bottomed flask. Vinyldimethylsilane (7.7 g, 90.0 mmol) was added and the mixture was stirred for 5 min. Tris(pentafluorophenyl)borane (350 µl, 0.04 M) in dry toluene (2 mL) was added and methane gas was developed. The mixture was stirred at RT for 1 h where after neutral aluminum oxide (3 g) was added to remove the tris(pentafluorophenyl)borane catalyst. The reaction mixture was now filtered and solvent and excess reagents were removed *in vacuo* to give the product as a clear oil (11.5 g, 97 %). IR (cm^{-1}): 2960 (C-H stretch); 1595 (Si-CH=CH_2 stretch); 1405 (Si-CH_2 stretch); 1255 (Si-CH_3 stretch); 1040 (Si-O stretch). ^{1}H NMR ($CDCl_3$, δ_H, ppm): 0.05-0.16 (m, 15H, C*H*$_3$-Si), 0.59 (m, 2H, -Si-C*H*$_2$-CH_2-), 1.79 (m, 2H, -CH_2-C*H*$_2$-CH_2-), 3.49 (t, 2H, ^3J=6.9 Hz, Cl-C*H*$_2$-CH_2), 5.73 (dd, 2H, ^2J=4.2 Hz, ^3J=20 Hz, CH=C*H*$_2$), 5.94 (dd, 2H, ^2J=2.7 Hz, ^3J=14 Hz, CH=C*H*$_2$), 6.12 (dd, 2H, ^3J=15 Hz, ^3J=20 Hz, -C*H*=CH_2). ^{13}C-NMR ($CDCl_3$, δ_C, ppm): -0.31 (d), -0.25 (c), 15.12 (e), 26.78 (f), 47.68 (g), 131.85 (a), 139.09 (b)

1,5-diallyl-3-(chloromethyl)-1,1,3,5,5-pentamethyltrisiloxane (13b):

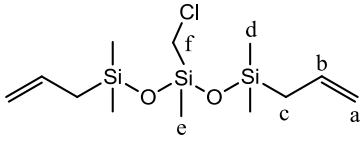

Chloromethyl(methyl)dimethoxysilane (3.00 g, 19.4 mmol) was dissolved in dry heptane (30 mL) in a 250 ml two-necked round-bottomed flask. Allyldimethylsilane (5.83 g, 58.2 mmol) was added and the mixture was stirred for 5 min. Tris(pentafluorophenyl)borane (240 µl, 0.04 M) in dry toluene (2 ml) was added and methane gas was developed. The mixture was stirred at RT for 1 h where after neutral aluminium oxide (3 g) was added to remove the tris(pentafluorophenyl)borane catalyst. The reaction mixture was now filtered and solvent and excess reagents were removed *in vacuo* to give the product as a clear oil (6.46 g, 93.9 %). IR (cm^{-1}): 2960 (C-H stretch); 1630 (C=C stretch); 1255 (Si-CH_3 stretch); 1055 (Si-O stretch). ^{1}H NMR ($CDCl_3$, δ_H, ppm): 0.13-0.17 (m, 15H, C*H*$_3$-Si), 1.60 (d, 4H, ^2J=8 Hz, Si(CH_3)$_2$-C*H*$_2$-CH), 2.62 (s, 2H, Cl-C*H*$_2$-Si), 4.85-4.92 (m, 4H, CH=C*H*$_2$), 5.80 (m, 2H, -C*H*=CH_2). ^{13}C-NMR ($CDCl_3$, δ_C, ppm): -2.26 (e), -0.34 (d), 26.05 (c), 29.49 (f), 113.66 (a), 133.96 (b).

3-(3-azidopropyl)-1,1,3,5,5-pentamethyl-1,5-divinyltrisiloxane (14a):

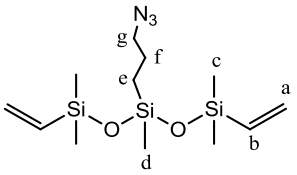

13a (5.0 g, 15.5 mmol) and NaN_3 (1.35 g, 20.6 mmol) were dissolved in DMF (70 mL) in a 250 mL two-necked round-bottomed flask. The reaction mixture was stirred at 60°C for 15 hours. The reaction mixture was quenched with H_2O (70 mL) and extracted with heptane (5 x 70 mL). The organic phases were combined and washed with H_2O (3 x 70 mL) and brine (1 x 70 mL), dried with $MgSO_4$, filtered and concentrated *in vacuo* to give the product in the form of a light yellow oil (4.5 g, 88 %). IR (cm^{-1}): 2960 (C-H stretch); 2095 (-N_3 stretch); 1595 (Si-CH=CH_2 stretch); 1405 (Si-CH_2 stretch); 1255 (Si-CH_3 stretch); 1040 (Si-O stretch). ^{1}H NMR ($CDCl_3$, δ_H, ppm): 0.05-0.16 (m, 15H, C*H*$_3$-Si), 0.59 (m, 2H, -Si-C*H*$_2$-CH_2-), 1.62 (m, 2H, -CH_2-C*H*$_2$-CH_2-), 3.22 (t, 2H, ^3J=7.2 Hz, N_3-C*H*$_2$-CH_2), 5.73 (dd, 2H, ^2J=4.2 Hz, ^3J=20, CH=C*H*$_2$), 5.94 (dd, 2H, ^2J=4.2 Hz, ^3J=15 Hz, CH=C*H*$_2$), 6.12 (dd, 2H, ^3J=15 Hz, ^3J=20 Hz, -C*H*=CH_2). ^{13}C-NMR ($CDCl_3$, δ_C, ppm): -0.33 (d), -0.24 (c), 14.58 (e), 22.79 (f), 54.08 (g), 131.86 (a), 139.09 (b).

1,5-diallyl-3-(azidomethyl)-1,1,3,5,5-pentamethyltrisiloxane (14b):

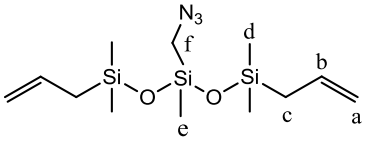

13b (6.3 g, 19.5 mmol) and NaN_3 (1.7 g, 24.0 mmol) were dissolved in DMF (20 mL) in a 50 ml two-necked round-bottomed flask. The reaction mixture was stirred at 45°C for 18 hours. The reaction mixture was quenched with H_2O (40 mL) and extracted with heptane (5 x 40 mL). The organic phases were combined and washed with H_2O (3 x 40 mL) and brine (1 x 40 mL), dried with $MgSO_4$, filtered and concentrated *in vacuo* to give the product in the form of a clear oil (6.1 g, 95 %). IR (cm^{-1}): 2960 (C-H stretch); 2095 (-N_3 stretch); 1630 (C=C stretch); 1255 (Si-CH_3 stretch); 1055 (Si-O stretch). ^{1}H NMR ($CDCl_3$, δ_H, ppm): 0.07-0.14 (m, 15H, C*H*$_3$-Si), 1.60 (d, 4H, ^2J=8 Hz, $Si(CH_3)_2$-C*H*$_2$-CH), 2.63 (s, 2H, N_3-C*H*$_2$-Si), 4.86-4.93 (m, 4H, CH=C*H*$_2$), 5.80 (m, 2H, -C*H*=CH_2). ^{13}C-NMR ($CDCl_3$, δ_C, ppm): -1.11 (e), -0.32 (d), 26.04 (c), 41.15 (f), 113.76 (a), 133.83 (b).

Chain extended copolymer (15b):

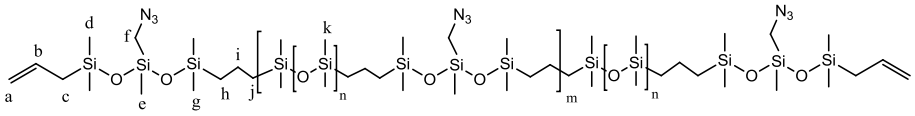

14b (0.89 g, 2.7 mmol) and hydride-terminated PDMS (DMS H-11) (3.1 g, 2.8 mmol) were dissolved in dry THF (5 mL) in a 50 ml two-necked round-bottomed flask. The platinum cyclovinylmethyl siloxane complex catalyst (511) (150 µl of a 0.04 g/ml solution in THF) was added drop-wise. The reaction mixture was stirred overnight at 55°C. After the chain extension reaction, the reaction mixture was diluted with 20 mL dry THF and end-capped with **14b** (0.21 g, 0.64 mmol) overnight at 55°C. The chain extended PDMS with allyl end-groups were now precipitated in dry methanol, which was hereafter decanted. The PDMS was dried overnight at RT to give a transparent oil (3.26 g 81.1 %). IR (cm^{-1}): 2960 (C-H stretch); 2095 (-N_3 stretch); 1630 (C=C stretch); 1255 (Si-CH_3 stretch); 1015 (Si-O stretch). ^{1}H NMR ($CDCl_3$, δ_H, ppm): 0.05-0.12 (m, C*H*$_3$-Si), 0.62 (m, -C*H*$_2$-Si), 1.38 (m, CH_2-C*H*$_2$-CH_2), 1.82 (dd, 4H, ^3J=6 Hz and ^4J=1.5 Hz, $Si(CH_3)_2$-C*H*$_2$-CH), 2.60 (s, N_3-C*H*$_2$-Si), 5.64 (m, 4H, CH=C*H*$_2$), 6.14 (m, 2H, -C*H*=CH_2). ^{13}C-NMR ($CDCl_3$, δ_C, ppm): -1.06-1.17 (d, e, g, k) 17.06 (h, j) 22.65 (i), 41.28 (f) (a, b and c not visible).

Click reaction on 15b (16b):

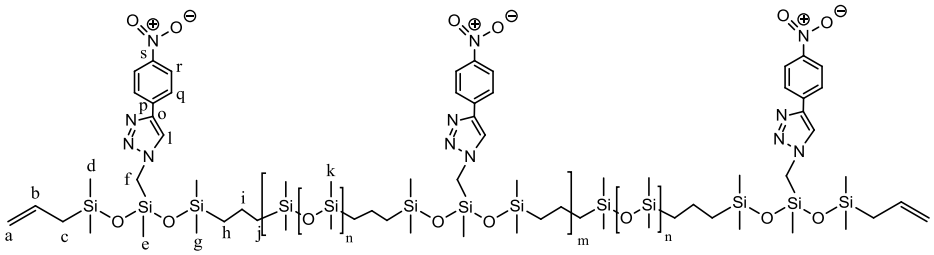

15b (2.74 g, 1.97 mmol) and 1-ethynyl-4-nitrobenzene (0.305 g, 2.1 mmol) were dissolved in dry THF (20 ml) in a 250 mL two-necked round-bottomed flask. The mixture was stirred for 5 min. CuI (0.04 g, 0.21 mmol) was subsequently added, the mixture was stirred again for 5 min and Et_3N (0.31 g, 3.1 mmol) was added drop-wise. The reaction was carried out at 45°C for 22 h. The functionalized chain extended PDMS with allyl end-groups were now precipitated in dry methanol, which was hereafter decanted. The PDMS was dried overnight at RT to give a red oil in quantitative yield. IR (cm^{-1}): 2960 (C-H stretch); 1605 (aromatic C=C stretch); 1520 (N=O asymmetric stretch); 1340 (N=O symmetric stretch); 1255 (Si-CH_3 stretch); 1010 (Si-O stretch). ^{1}H NMR ($CDCl_3$, δ_H, ppm): 0.03-0.21 (m, C*H*$_3$-Si), 0.61 (m, -C*H*$_2$-Si), 1.38 (m, CH_2-C*H*$_2$-CH_2), 1.79 (d, 4H, ^3J=6 Hz, $Si(CH_3)_2$-C*H*$_2$-CH), 3.88 (s, N-C*H*$_2$-Si), 5.60 (m, 4H, CH=C*H*$_2$), 6.12 (m, 2H, -C*H*=CH_2), 7.83 (s, -C=C*H*-N-), 7.98 (d, ^3J=9 Hz, Ar-*H*), 8.27, (d, ^3J=9 Hz, NO_2-Ar-*H*). ^{13}C-NMR ($CDCl_3$, δ_C, ppm): -0.89-1.17 (d, e, g, k) 17.05 (h, j) 22.50 (i), 41.95 (f), 121.66 (l) 124.32 (r), 125.91 (q), 137.20 (p), 145.30 (s), 147.17 (o), (a, b and c not visible).

1-((1,5-diallyl-1,1,3,5,5-pentamethyltrisiloxan-3-yl)methyl-4-(4-nitrophenyl)-1*H*-1,2,3-triazole (17b):

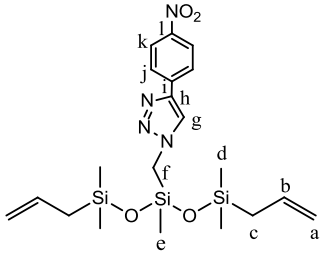

14b (3 g, 9.1 mmol) and 1-ethynyl-4-nitrobenzene (1.4 g, 9.6 mmol) were dissolved in dry THF (150 mL) in a 250 mL two-necked round-bottomed flask. The mixture was stirred for 5 min. CuI (0.18 g, 0.96 mmol) was subsequently added, the mixture was stirred again for 5 min and Et_3N (1.45 g, 14.3 mmol) was added drop-wise. The reaction was carried out at RT for 24 hours then at 40°C for 22 h. The reaction mixture was extracted with heptane and washed with H_2O (3 x 100 mL) and brine (1 x 100 mL), dried with $MgSO_4$, filtered and concentrated *in vacuo.* The product was hereafter washed with diethyl ether and filtered to give a red solid (1.2 g, 28 %). IR (cm^{-1}): 3080 (aromatic =C-H stretch); 2960-2910 (C-H stretch); 1630 (C=C stretch); 1605 (aromatic C=C stretch); 1515 (N=O asymmetric stretch); 1455 (aromatic C=C stretch); 1335 (N=O symmetric stretch); 1255 (Si-CH_3 stretch); 1060 (C-O stretch); 1040 (Si-O stretch). ^{1}H NMR ($CDCl_3$, δ_H, ppm): 0.11-0.12 (m, 12H, C*H*$_3$-Si), 0.24 (s, 3H, C*H*$_3$-Si), 1.57 (d, 4H, ^2J=8 Hz, Si(CH$_3$)$_2$-C*H*$_2$-CH), 3.90 (s, 2H, N-C*H*$_2$-Si), 4.85-4.91 (m, 4H, CH=C*H*$_2$), 5.75 (m, 2H, -C*H*=CH$_2$), 7.84 (s, 1H, -C=C*H*-N-), 7.98 (d, 2H, ^3J=9 Hz, Ar-*H*), 8.39, (d, 2H, ^3J=9 Hz, NO$_2$-Ar-*H*). ^{13}C-NMR ($CDCl_3$, δ_C, ppm): -0.88 (e), -0.32 (d), 25.87 (c), 41.85 (f), 114.08 (a), 121.78 (g), 124.33 (k), 125.91 (j), 133.49 (b) 137.21 (i), 145.31 (l), 147.16 (h).

Preparation of elastomer film of 16b:

16b (2 g, 0.06 mmol) was dissolved in dry THF (1 mL) and mixed with hydride-functional cross-linker (0.04 g, 0.02 mmol, HMS-301, ~8-functional) and 100 ppm Pt catalyst in THF (511, Hanse Chemie). The mixture was mixed on FlackTek Inc. DAC 150.1 FVZK SpeedMixer™, degassed in vacuo and poured into a 1 mm thick steel mould on a fluorinated ethylene propylene (FEP) release liner and cured for 1 week at RT and 2 weeks at 80°C.

Synthesis of 32 and 33:

Copolymer **32** and **33** were prepared according to procedures described in Appendix D using amounts stated in Appendix E.

Preparation of elastomer films with copolymers 32 and 33:

32 or **33** (2.33 g, 10.1 mmol) and an 8-functional cross-linker (HMS-301 (Gelest), 0.066 g, 0.034 mmol) were mixed with treated silica particles (20 wt%) and inhibitor (0.015 g, 1 wt%, Pt88 from

Wacker Chemie AG) and the mixture was treated on a FlackTek Inc. DAC 150.1 FVZ-K Speed-Mixer™. The catalyst (511 from Hanse Chemie) (1 ppm) was added thereafter and the mixture was speed-mixed once more. The mixture was the poured into 1 mm thick steel moulds and furthermore coated as 150 µm films on a glass substrate and cured at 115°C.

Bibliography

[1] Bar-Cohen Y 2004 *Electroactive polymer (EAP) actuators as artificial muscles: reality, potential, and challenges* (Bellingham, Washington USA: SPIE press)

[2] Pelrine R, Kornbluh R, Joseph J, Heydt R, Pei Q and Chiba S 2000 High-field deformation of elastomeric dielectrics for actuators *Mater. Sci. Eng. C* **11** 89–100

[3] Kornbluh R, Pelrine R, Pei Q, Heydt R, Stanford S, Oh S and Eckerle J 2002 Electroelastomers: applications of dielectric elastomer transducers for actuation, generation and smart structures *Proc. SPIE* **4698** 254–70

[4] O'Halloran A, O'Malley F and McHugh P 2008 A review on dielectric elastomer actuators, technology, applications, and challenges *J. Appl. Phys.* **104** 071101

[5] Brochu P and Pei Q 2010 Advances in dielectric elastomers for actuators and artificial muscles. *Macromol. Rapid Commun.* **31** 10–36

[6] Röngten W C 1880 Ueber die durch Elektricität bewirkten Form- und Volume änderungen von elektrischen Körpern *Ann. Phys.* 771 – 786

[7] Bar-Cohen Y 2005 Artificial muscles using electroactive polymers (EAP): capabilities, challenges and potential *http://hdl.handle.net/2014/37602* 1–14

[8] Graz I, Kaltenbrunner M, Keplinger C, Schwödiauer R, Bauer S, Lacour S P and Wagner S 2006 Flexible ferroelectret field-effect transistor for large-area sensor skins and microphones *Appl. Phys. Lett.* **89** 073501

[9] Schwödiauer R, Graz I, Kaltenbrunner M, Keplinger C, Bartu P, Buchberger G, Ortwein C and Bauer S 2008 Cellular ferroelectrets for electroactive polymer hybrid systems: soft matter integrated devices with advanced functionality *Proc. SPIE* **6928** 69270Q–1–69270Q–10

[10] Krause M, Graz I, Bauer-Gogonea S, Bauer S, Ploss B, Zirkl M, Stadlober B and Helbig U 2011 PbTiO3 – P(VD-TrFE) - nanocomposites for pressure and temperature sensitive skin *Ferroelectrics* **419** 23–7

[11] Wang Y, Sun C, Zhou E and Su J 2004 Deformation mechanisms of electrostrictive graft elastomer *Smart Mater. Struct.* **13** 1407–13

[12] Madden J D W 2008 Dielectric elastomers as high-performance electroactive polymers *Dielectric elastomers as electromechanical transducers* ed F Carpi, D De Rossi, R Kornbluh, R Pelrine and P Sommer-Larsen (Amsterdam: Elsevier Science) pp 13–21

[13] Pelrine R, Kornbluh R and Kofod G 2000 High-strain actuator materials based on dielectric elastomers *Adv. Mater.* **12** 1223–5

[14] Graz I M, Cotton D P J and Lacour S P 2009 Extended cyclic uniaxial loading of stretchable gold thin-films on elastomeric substrates *Appl. Phys. Lett.* **94** 071902

[15] Kofod G 2001 *Dielectric elastomer actuators* (Technical University of Denmark, PhD Thesis)

[16] Pelrine R, Kornbluh R, Eckerle J, Jeuck P, Oh S, Pei Q and Stanford S 2001 Dielectric elastomers: generator mode fundamentals and applications *Proc. SPIE* **4329** 148–56

[17] Heydt R, Kornbluh R, Eckerle J and Pelrine R 2006 Sound radiation properties of dielectric elastomer electroactive polymer loudspeakers *Proc. SPIE* **6168** 61681M–1

[18] Sarban R 2011 *Active vibration control using DEAP transducers* (University of Southern Denmark, PhD Thesis)

[19] Pelrine R, Sommer-Larsen P, Kornbuh R, Heydt R, Kofod G and Pei Q 2001 Applications of dielectric elastomer actuators *Proc. SPIE* **4329** 335–49

[20] Pelrine R, Kornbluh R, Pei Q, Stanford S, Oh S, Eckerle J, Full R, Rosenthal M and Meijer K 2002 Dielectric elastomer artificial muscle actuators: toward biomimetic motion *Proc. SPIE* **4695** 126–37

[21] Yu Z, Yuan W, Brochu P, Chen B, Liu Z and Pei Q 2009 Large-strain, rigid-to-rigid deformation of bistable electroactive polymers *Appl. Phys. Lett.* **95** 192904

[22] Ahnert K, Abel M, Kollosche M, Jørgensen P J and Kofod G 2011 Soft capacitors for wave energy harvesting *J. Mater. Chem.* **21** 14492

[23] Sarban R, Jones R W, Rustighi E and Mace B R 2011 Active vibration isolation using a dielectric electro-active polymer actuator *J. Syst. Des. Dyn.* **5** 643–52

[24] Löwe C, Zhang X and Kovacs G 2005 Dielectric elastomers in actuator technology *Adv. Eng. Mater.* **7** 361–7

[25] Tröls A, Kogler A, Baumgartner R, Kaltseis R, Keplinger C, Schwödiauer R, Graz I and Bauer S 2013 Stretch dependence of the electrical breakdown strength and dielectric constant of dielectric elastomers *Smart Mater. Struct.* **22** 104012

[26] Molberg M, Crespy D, Rupper P, Nüesch F, Månson J-A E, Löwe C and Opris D M 2010 High breakdown field dielectric elastomer actuators using encapsulated polyaniline as high dielectric constant filler *Adv. Funct. Mater.* **20** 3280–91

[27] Eissa A M, Khosravi E and Cimecioglu a L 2012 A versatile method for functionalization and grafting of 2-hydroxyethyl cellulose (HEC) via Click chemistry. *Carbohydr. Polym.* **90** 859–69

[28] Gallone G, Galantini F and Carpi F 2010 Perspectives for new dielectric elastomers with improved electromechanical actuation performance: composites versus blends *Polym. Int.* **59** 400–6

[29] Connor M T, Roy S, Ezquerra T A and Baltá Calleja F J 1998 Broadband ac conductivity of conductor-polymer composites *Phys. Rev. B* **57** 2286–94

[30] Larsen A L, Hansen K, Sommer-Larsen P, Hassager O, Bach A, Ndoni S and Jørgensen M 2003 Elastic properties of nonstoichiometric reacted PDMS networks *Macromolecules* **36** 10063–70

[31] Sommer-larsen P and Larsen A L 2004 Materials for dielectric elastomer actuators *Proc. SPIE* **5385** 68–77

[32] Pelrine R, Kornbluh R, Pei Q and Joseph J 2000 High-speed electrically actuated elastomers with strain greater than 100% *Science* **287** 836–9

[33] Vudayagiri S, Junker M D and Skov A L 2013 Factors affecting surface and release properties of thin Polydimethylsiloxane films *Polym. J.* **45** 871–8

[34] Benslimane M Y, Kiil H-E and Tryson M J 2010 Dielectric electro-active polymer push actuators: performance and challenges *Polym. Int.* **59** 415–21

[35] Balakrisnan B and Smela E 2010 Challenges in the microfabrication of dielectric elastomer actuators *Proc. SPIE* **7642** 76420K–1–76420K–10

[36] Larsen A L, Sommer-Larsen P and Hassager O 2004 How to tune rubber elasticity *Proc. SPIE* **5385** 108–17

[37] Bejenariu A G, Yu L and Skov A L 2012 Low moduli elastomers with low viscous dissipation *Soft Matter* **8** 3917–23

[38] Jensen M K, Rasmussen H K, Skov A L and Hassager O 2011 Reversed planar elongation of soft polymeric networks *Rheol. Acta* **50** 729–40

[39] Carpi F and De Rossi D 2005 Improvement of electromechanical actuating performances of a silicone dielectric elastomer by dispersion of titanium dioxide powder *IEEE Trans. Dielectr. Electr. Insul.* **12** 835–43

[40] Ouyang G M, Wang K Y and Chen X Y 2011 Enhanced electro-mechanical performance of TiO2 nano-particle modified polydimethylsiloxane (PDMS) as electroactive polymers *2011 16th Int. Solid-State Sensors, Actuators Microsystems Conf.* 614–7

[41] Ouyang G, Wang K and Chen X Y 2012 TiO2 nanoparticles modified polydimethylsiloxane with fast response time and increased dielectric constant *J. Micromechanics Microengineering* **22** 074002

[42] Zhao H, Wang D-R, Zha J-W, Zhao J and Dang Z-M 2013 Increased electroaction through a molecular flexibility tuning process in TiO2–polydimethylsilicone nanocomposites *J. Mater. Chem. A* **1** 3140

[43] Liu H, Zhang L, Yang D, Yu Y, Yao L and Tian M 2013 Mechanical, dielectric, and actuated strain of silicone elastomer filled with various types of TiO2 *Soft Mater.* **11** 363–70

[44] Cazacu M, Ignat M, Racles C, Cristea M, Musteata V, Ovezea D and Lipcinski D 2014 Well-defined silicone-titania composites with good performances in actuation and energy harvesting *J. Compos. Mater.* **48** 1533–45

[45] Stoyanov H, Brochu P, Niu X, Della Gaspera E and Pei Q 2012 Dielectric elastomer transducers with enhanced force output and work density *Appl. Phys. Lett.* **100** 262902

[46] Razzaghi Kashani M, Javadi S and Gharavi N 2010 Dielectric properties of silicone rubber-titanium dioxide composites prepared by dielectrophoretic assembly of filler particles *Smart Mater. Struct.* **19** 035019

[47] Skov A L, Vudayagiri S and Benslimane M 2013 Novel silicone elastomer formulations for DEAPs *Proc. SPIE* **8687** 86871I–86871I–8

[48] Lotz P, Matysek M, Lechner P, Hamann M and Schlaak H F 2008 Dielectric elastomer actuators using improved thin film processing and nanosized particles *Proc. SPIE* **6927** 692723–1–692723–10

[49] Szabo J P, Hiltz J A, Cameron C G, Underhill R S, Massey J, White B and Leidner J 2003 Elastomeric composites with high dielectric constant for use in Maxwell stress actuators *Proc. SPIE* **5051** 180–90

[50] Zhang Z, Liu L, Fan J, Yu K, Liu Y, Shi L and Leng J 2008 New silicone dielectric elastomer with a high dielectric constant *Proc. SPIE* **6926** 692610–1–692610–8

[51] Khastgir D and Adachi K 1999 Piezoelectric and dielectric properties of siloxane elastomers filled with bariumtitanate *J. Polym. Sci. Part B Polym. Phys.* **37** 3065–70

[52] Liu Y, Liu L, Zhang Z and Leng J 2009 Dielectric elastomer film actuators: characterization, experiment and analysis *Smart Mater. Struct.* **18** 095024

[53] Daugaard A E, Hassouneh S S, Kostrzewska M, Bejenariu A G and Skov A L 2013 High dielectric permittivity elastomers from well-dispersed expanded graphite in low concentrations *Proc. SPIE* **8687** 868729–1–868729–11

[54] Chen L Z, Liu C H, Hu C H and Fan S S 2008 Electrothermal actuation based on carbon nanotube network in silicone elastomer *Appl. Phys. Lett.* **92** 263104

[55] Chen L, Liu C, Liu K, Meng C, Hu C, Wang J and Fan S 2011 High-performance, low-voltage, and easy-operable bending actuator based on aligned carbon nanotube/polymer composites *ACS Nano* **5** 1588–93

[56] Park I-S, Kim K J, Nam J-D, Lee J and Woosoon Y 2007 Mechanical, dielectric, and magnetic properties of the silicone elastomer with multi-walled carbon nanotubes as a nanofiller *Polym. Eng. Sci.* **47** 1396–405

[57] Yadav S K, Kim I J, Kim H J, Kim J, Hong S M and Koo C M 2013 PDMS/MWCNT nanocomposite actuators using silicone functionalized multiwalled carbon nanotubes via nitrene chemistry *J. Mater. Chem. C* **1** 5463–70

[58] Razzaghi-Kashani M, Gharavi N and Javadi S 2008 The effect of organo-clay on the dielectric properties of silicone rubber *Smart Mater. Struct.* **17** 065035
[59] Gharavi N, Razzaghi-Kashani M and Golshan-Ebrahimi N 2010 Effect of organo-clay on the dielectric relaxation response of silicone rubber *Smart Mater. Struct.* **19** 025002
[60] Jia Z, Chen S and Zhang J 2012 RTV silicone rubber filled with surface modified montmorillonite *J. Macromol. Sci. Part B* **51** 2449–61
[61] Gharavi N, Razzaghi Kashani M and Moradi A 2010 Electromechanical properties of Silicone-PZT (Lead-Zirconate Titanate) composite *Proc. SPIE* **7642** 764233–1–764233–7
[62] Zhang X, Wissler M, Jaehne R, Broennimann R and Kovacs G 2004 Effects of crosslinking, prestrain, and dielectric filler on the electromechanical response of a new silicone and comparison with acrylic elastomer *Proc. SPIE* **5385** 78–86
[63] Romasanta L J, Leret P, Casaban L, Hernández M, de la Rubia M A, Fernández J F, Kenny J M, Lopez-Manchado M A and Verdejo R 2012 Towards materials with enhanced electro-mechanical response: CaCu3Ti4O12–polydimethylsiloxane composites *J. Mater. Chem.* **22** 24705–12
[64] Opris D M, Molberg M, Nüesch F, Löwe C, Walder C and Fischer B 2011 Dielectric elastomer materials for actuators and energy harvesting *Proc. SPIE* **7976** 79760G–1–79760G–8
[65] Wichiansee W and Sirivat A 2009 Electrorheological properties of poly(dimethylsiloxane) and poly(3,4-ethylenedioxythiophene)/poly(stylene sulfonic acid)/ethylene glycol blends *Mater. Sci. Eng. C* **29** 78–84
[66] Opris D M, Molberg M, Walder C, Ko Y S, Fischer B and Nüesch F A 2011 New silicone composites for dielectric elastomer actuator applications in competition with acrylic foil *Adv. Funct. Mater.* **21** 3531–9
[67] Carpi F, Gallone G, Galantini F and De Rossi D 2008 Silicone–poly(hexylthiophene) blends as elastomers with enhanced electromechanical transduction properties *Adv. Funct. Mater.* **18** 235–41
[68] Thongbor S and Pattavarakorn D 2011 Electromechanical properties of electroactive polythiophene/elastomer blend *TIChE Int. Conf. 2011* 1–5
[69] Liu H, Zhang L, Yang D, Ning N, Yu Y, Yao L, Yan B and Tian M 2012 A new kind of electro-active polymer composite composed of silicone elastomer and polyethylene glycol *J. Phys. D. Appl. Phys.* **45** 485303
[70] Kussmaul B, Risse S, Kofod G, Waché R, Wegener M, McCarthy D N, Krüger H and Gerhard R 2011 Enhancement of dielectric permittivity and electromechanical response in silicone elastomers: molecular grafting of organic dipoles to the macromolecular network *Adv. Funct. Mater.* **21** 4589–94
[71] Kussmaul B, Risse S, Wegener M, Kofod G and Krüger H 2012 Matrix stiffness dependent electro-mechanical response of dipole grafted silicones *Smart Mater. Struct.* **21** 064005
[72] Risse S, Kussmaul B, Krüger H and Kofod G 2012 A versatile method for enhancement of electromechanical sensitivity of silicone elastomers *RSC Adv.* **2** 9029–35
[73] Frankær S M G, Jensen M K, Bejenariu A G and Skov A L 2012 Investigation of the properties of fully reacted unstoichiometric polydimethylsiloxane networks and their extracted network fractions *Rheol. Acta* **51** 559–67
[74] Risse S, Kussmaul B, Krüger H and Kofod G 2012 Synergistic improvement of actuation properties with compatibilized high permittivity filler *Adv. Funct. Mater.* **22** 3958–62
[75] Racles C, Cazacu M, Fischer B and Opris D M 2013 Synthesis and characterization of silicones containing cyanopropyl groups and their use in dielectric elastomer actuators *Smart Mater. Struct.* **22** 104004

[76] Rochow E G 1990 Preface, acknowledgments, introduction: my favorite element *Silicon-based polymer science - a comprehensive resource* ed J M Zeigler and F W G Fearon (American Chemical Society) pp xiii–xxii
[77] Butts M, Cella J, Wood C D, Gillette G, Kerboua R, Leman L, Lewis L, Rubinsztajn S, Schattenmann F J, Stein J, Wicht D, Rajaraman S and Wengrovius J 2002 Silicones *Kirk-Othmer encyclopedia of chemical technology* (John Wiley & Sons, Inc.) pp 1–89
[78] Mark J E 1990 Silicon-containing polymers *Silicon-based polymer science: a comprehensive resource* ed J M Zeigler and F W G Fearon (American Chemical Society) pp 47–68
[79] Jensen M K, Bach A, Hassager O and Skov A L 2009 Linear rheology of cross-linked polypropylene oxide as a pressure sensitive adhesive *Int. J. Adhes. Adhes.* **29** 687–93
[80] De Jong J, Lammertink R G H and Wessling M 2006 Membranes and microfluidics: a review *Lab Chip* **6** 1125–39
[81] De Buyl F 2001 Silicone sealants and structural adhesives *Int. J. Adhes. Adhes.* **21** 411–22
[82] Flores-Vivian I, Hejazi V, Kozhukhova M I, Nosonovsky M and Sobolev K 2013 Self-assembling particle-siloxane coatings for superhydrophobic concrete *ACS Appl. Mater. Interfaces* **5** 13284–94
[83] Sèbe G and Brook M A 2001 Hydrophobization of wood surfaces: covalent grafting of silicone polymers *Wood Sci. Technol.* **35** 269–82
[84] Xia Y and Whitesides G M 1998 Soft Lithography *Angew. Chemie Int. Ed.* **37** 550–75
[85] Brook M A 2000 Formation of Si-C bonds: the synthesis of functional organosilanes *Silicon in organic, organometallic, and polymer chemistry* (New York: John Wiley & Sons) pp 381–421
[86] Rubin M, Schwier T and Gevorgyan V 2002 Highly efficient B(C6F5)3-catalyzed hydrosilylation of olefins *J. Org. Chem.* **67** 1936–40
[87] Xunjun C, Yingde C, Guoqiang Y and Liewen L 2007 Synthesis of vinyl substitute poly(silphenylene-siloxane) via silyl hydride-dialkoxysilane process *J. Appl. Polym. Sci.* **106** 1007–13
[88] Larsen A L, Sommer-Larsen P and Hassager O 2004 Some experimental results for the end-linked polydimethylsiloxane network system *e-Polymers* **050** 1–18
[89] Mark J E 2003 The rubber elastic state *Physical properties of polymers* ed J Mark, K Ngai, W Graessley, L Mandelkern, E Samulski, J Koenig and G Wignall (Cambridge, United Kingdom: Cambridge University Press) pp 3–71
[90] Dvornic P 2000 Thermal properties of polysiloxanes *Silicon-containing polymers - the science and technology of their synthesis and applications* ed R G Jones, W Ando and J Chojnowski (Dordrecht, The Netherlands: Springer - Verlag) pp 185–212
[91] Li C and Wilkes G L 2001 Silicone/amine resin hybrid materials as abrasion resistant coatings *Chem. Mater.* **13** 3663–8
[92] Mecham S, Sentman A and Sambasivam M 2010 Amphiphilic silicone copolymers for pressure sensitive adhesive applications *J. Appl. Polym. Sci.* **116** 3265–70
[93] Nicolson P C and Vogt J 2001 Soft contact lens polymers: an evolution *Biomaterials* **22** 3273–83
[94] Jonas G and Stadler R 1991 Polysiloxanes with statistically distributed glucose and galactose units, 1. Synthesis and thermal characterization *Die Makromol. Chemie, Rapid Commun.* **12** 625–32
[95] Dodge L, Chen Y and Brook M A 2014 Silicone boronates reversibly crosslink using lewis acid-Lewis base amine complexes *Chem. - A Eur. J.* **20** 9349–56

[96] Mikhail A S, Ranger J J, Liu L, Longenecker R, Thompson D B, Sheardown H D and Brook M A 2010 Rapid and efficient assembly of functional silicone surfaces protected by PEG: cell adhesion to peptide-modified PDMS *J. Biomater. Sci.* **21** 821–42

[97] Pelton R, Cui Y, Zhang D, Chen Y, Thompson K L, Armes S P and Brook M A 2013 Facile phenylboronate modification of silica by a silaneboronate. *Langmuir* **29** 594–8

[98] Rambarran T, Gonzaga F and Brook M A 2012 Generic, metal-free cross-linking and modification of silicone elastomers using click ligation *Macromolecules* **45** 2276–85

[99] Thompson D B, Gonzaga F, Fawcett A S and Brook M A 2008 Hydrolytically stable linkers for silicone carbohydrates derived from hydrodiisopropylsilanes *Silicon Chem.* **3** 327–34

[100] Kolb H C, Finn M G and Sharpless K B 2001 Click chemistry: diverse chemical function from a few good reactions *Angew. Chem. Int. Ed. Engl.* **40** 2004–21

[101] Huisgen R 1963 1,3-Dipolar cycloadditions. Past and future *Angew. Chem. Int. Ed. Engl.* **2** 565–98

[102] Tornøe C W, Christensen C and Meldal M 2002 Peptidotriazoles on solid phase: [1,2,3]-triazoles by regiospecific copper(I)-catalyzed 1,3-dipolar cycloadditions of terminal alkynes to azides. *J. Org. Chem.* **67** 3057–64

[103] Rostovtsev V V, Green L G, Fokin V V and Sharpless K B 2002 A stepwise Huisgen cycloaddition process: copper(I)-catalyzed regioselective "ligation" of azides and terminal alkynes *Angew. Chemie* **114** 2708–11

[104] Binder W H and Sachsenhofer R 2008 "Click" chemistry in polymer and material science: an update *Macromol. Rapid Commun.* **29** 952–81

[105] Iha R K, Wooley K L, Nyström A M, Burke D J, Kade M J and Hawker C J 2009 Applications of orthogonal "click" chemistries in the synthesis of functional soft materials *Chem. Rev.* **109** 5620–86

[106] Opsteen J A and van Hest J C M 2005 Modular synthesis of block copolymers via cycloaddition of terminal azide and alkyne functionalized polymers *Chem. Commun.* 57–9

[107] Daugaard A E, Hvilsted S, Hansen T S and Larsen N B 2008 Conductive polymer functionalization by click chemistry *Macromolecules* **41** 4321–7

[108] Wu P, Feldman A K, Nugent A K, Hawker C J, Scheel A, Voit B, Pyun J, Fréchet J M J, Sharpless K B and Fokin V V 2004 Efficiency and fidelity in a click-chemistry route to triazole dendrimers by the copper(I)-catalyzed ligation of azides and alkynes *Angew. Chem. Int. Ed. Engl.* **43** 3928–32

[109] Joralemon M J, O'Reilly R K, Matson J B, Nugent A K, Hawker C J and Wooley K L 2005 Dendrimers clicked together divergently *Macromolecules* **38** 5436–43

[110] Parrish B, Breitenkamp R B and Emrick T 2005 PEG- and peptide-grafted aliphatic polyesters by click chemistry *J. Am. Chem. Soc.* **127** 7404–10

[111] Daugaard A E and Hvilsted S 2008 The influence of pendant carboxylic acid loading on surfaces of statistical poly[(4-hydroxystyrene)-co-styrene]s *Macromol. Rapid Commun.* **29** 1119–25

[112] Halila S, Manguian M, Fort S, Cottaz S, Hamaide T, Fleury E and Driguez H 2008 Syntheses of well-defined glyco-polyorganosiloxanes by "click" chemistry and their surfactant properties *Macromol. Chem. Phys.* **209** 1282–90

[113] Bretzler V, Grübel M, Meister S and Rieger B 2014 PDMS-containing alternating copolymers obtained by click polymerization *Macromol. Chem. Phys.* 10.1002/macp.201400178

[114] Isaacman M J, Barron K A and Theogarajan L S 2012 Clickable amphiphilic triblock copolymers *J. Polym. Sci. A. Polym. Chem.* **50** 2319–29

[115] Schmidt U, Zehetmaier P C and Rieger B 2010 Direct synthesis of poly(dimethylsiloxane) copolymers with TPE-properties via CuAAC (click chemistry) *Macromol. Rapid Commun.* **31** 545–8
[116] Gonzaga F, Yu G and Brook M A 2009 Versatile, efficient derivatization of polysiloxanes via click technology *Chem. Commun.* 1730–2
[117] Gonzaga F, Grande J B and Brook M A 2012 Morphology-controlled synthesis of poly(oxyethylene)silicone or alkylsilicone surfactants with explicit, atomically defined, branched, hydrophobic tails *Chem. - A Eur. J.* **18** 1536–41
[118] Rambarran T, Gonzaga F and Brook M A 2013 Multifunctional amphiphilic siloxane architectures using sequential, metal-free click ligations *J. Polym. Sci. Part A Polym. Chem.* **51** 855–64
[119] Parks D J and Piers W E 1996 Tris(pentafluorophenyl)boron-catalyzed hydrosilation of aromatic aldehydes, ketone, and esters *J. Am. Chem. Soc.* **118** 9440–1
[120] Blackwell J M, Foster K L, Beck V H and Piers W E 1999 B(C6F5)3-catalyzed silation of alcohols: a mild, general method for synthesis of silyl ethers *J. Org. Chem.* **64** 4887–92
[121] Parks D J, Blackwell J M and Piers W E 2000 Studies on the mechanism of B(C6F5)3-catalyzed hydrosilation of carbonyl functions *J. Org. Chem.* **65** 3090–8
[122] Rubinsztajn S and Cella J A 2004 Formation of siloxane bonds via new condensation process *Polym. Prepr.* **45(1)** 635–6
[123] Rubinsztajn S and Cella J A 2005 A new polycondensation process for the preparation of polysiloxane copolymers *Macromolecules* **38** 1061–3
[124] Cella J and Rubinsztajn S 2008 Preparation of polyaryloxysilanes and polyaryloxysiloxanes by B(C6F5)3 catalyzed polyetherification of dihydrosilanes and bis-phenols *Macromolecules* **41** 6965–71
[125] Brook M A, Grande J B and Ganachaud F 2011 New synthetic strategies for structured silicones using B(C6F5)3 *Adv. Polym. Sci.* **235** 161–83
[126] Zhou D and Kawakami Y 2005 Tris(pentafluorophenyl)borane as a superior catalyst in the synthesis of optically active SiO-containing polymers *Macromolecules* **38** 6902–8
[127] Hoque M A, Kakihana Y, Shinke S and Kawakami Y 2009 Polysiloxanes with periodically distributed isomeric double-decker silsesquioxane in the main chain *Macromolecules* **42** 3309–15
[128] Gretton M J, Kamino B A, Brook M A and Bender T P 2012 The use of Piers−Rubinsztajn conditions for the placement of triarylamines pendant to silicone polymers *Macromolecules* **45** 723–8
[129] Grande J B, Thompson D B, Gonzaga F and Brook M A 2010 Testing the functional tolerance of the Piers-Rubinsztajn reaction: a new strategy for functional silicones. *Chem. Commun.* **46** 4988–90
[130] Amela-Cortés M, Heinrîch B, Donnio B, Evans K E, Smith C W and Bruce D W 2011 Unsymmetric main-chain liquid crystal elastomers with tuneable phase behaviour: synthesis and mesomorphism *J. Mater. Chem.* **21** 8427
[131] Brook M A 2000 Hydrosilanes as reducing agents *Silicon in organic, organometallic, and polymer chemistry* (New York: John Wiley & Sons) pp 171–88
[132] Hudson R D A 2001 Ferrocene polymers: current architectures, syntheses and utility *J. Organomet. Chem.* **637-639** 47–69
[133] Köpf-Maier P, Köpf H and Neuse E W 1984 Ferricenium complexes: a new type of water-soluble antitumor agent *J. Cancer Res. Clin. Oncol.* **108** 336–40
[134] Javakhishvili I and Hvilsted S 2010 Miktoarm core-crosslinked star copolymers with biologically active moieties on peripheries *Polym. Chem.* **1** 1650–61

[135] Coates M, Griveau S, Bedioui F and Nyokong T 2012 Layer by layer electrode surface functionalisation using carbon nanotubes, electrochemical grafting of azide-alkyne functions and click chemistry *Electroanalysis* **24** 1833–8
[136] Dreaden E C, Mwakwari S C, Sodji Q H, Oyelere A K and El-Sayed M A 2009 Tamoxifen-poly(ethylene glycol)-thiol gold nanoparticle conjugates: enhanced potency and selective delivery for breast cancer treatment *Bioconjug. Chem.* **20** 2247–53
[137] Li B, Chen S and Zhang J 2012 Synthesis and characterization of vinyl-terminated copolysiloxanes containing 3,3,3-trifluoropropyl groups *Polym. Chem.* **3** 2366–76
[138] Dimitrov I, Takamuku S, Jankova K, Jannasch P and Hvilsted S 2012 Polysulfone functionalized with phosphonated poly(pentafluorostyrene) grafts for potential fuel cell applications. *Macromol. Rapid Commun.* **33** 1368–74
[139] Bejenariu A G, Rasmussen H K, Skov A L, Hassager O and Frankaer S M 2010 Large amplitude oscillatory extension of soft polymeric networks *Rheol. Acta* **49** 807–14
[140] Lee J N, Park C and Whitesides G M 2003 Solvent compatibility of poly(dimethylsiloxane)-based microfluidic devices. *Anal. Chem.* **75** 6544–54
[141] Jankova K and Hvilsted S 2003 Preparation of poly(2,3,4,5,6-pentafluorostyrene) and block copolymers with styrene by ATRP *Macromolecules* **36** 1753–8
[142] Camino G, Lomakin S M and Lageard M 2002 Thermal polydimethylsiloxane degradation. Part 2. The degradation mechanisms *Polymer* **43** 2011–5
[143] Abd-El-Aziz A S and Todd E K 2003 Organoiron polymers *Coord. Chem. Rev.* **246** 3–52
[144] Brook M A, Zhao S, Liu L and Chen Y 2012 Surface etching of silicone elastomers by depolymerization *Can. J. Chem.* **90** 153–60
[145] Borkar S, Jankova K, Siesler H W and Hvilsted S 2004 New highly fluorinated styrene-based materials with low surface energy prepared by ATRP *Macromolecules* **37** 788–94
[146] Chiba S, Waki M, Kornbluh R and Pelrine R 2008 Innovative power generators for energy harvesting using polymer artificial muscles *Proc. SPIE* **6927** 692715–1–692715–9
[147] Kussmaul B 2013 *Modifizierung von Silikonelastomeren mit organischen Dipolen für Dielektrische Elastomer Aktuatoren* (Universität Potsdam, PhD Thesis)
[148] Haynes W M 2014 Molecular structure and spectroscopy *CRC Handb. Chem. Phys.*
[149] Kumar G S and Neckers D C 1989 Photochemistry of azobenzene-containing polymers *Chem. Rev.* 1915–25
[150] Tong X, Wang G, Soldera A and Zhao Y 2005 How can azobenzene block copolymer vesicles be dissociated and reformed by light? *J. Phys. Chem. B* **109** 20281–7
[151] Kollosche M and Kofod G 2010 Electrical failure in blends of chemically identical, soft thermoplastic elastomers with different elastic stiffness *Appl. Phys. Lett.* **96** 071904
[152] Skov A L, Bejenariu A, Bøgelund J, Benslimane M and Egede A D 2012 Influence of micro- and nanofillers on electro-mechanical performance of silicone EAPs *Proc. SPIE* **8340** 83400M–1–83400M–10
[153] Winter H H and Chambon F 1986 Analysis of linear viscoelasticity of a crosslinking polymer at the gel point *J. Rheol.* **30** 367–82
[154] Doi M and Edwards S F 1999 *The theory of polymer dynamics* (Oxford University Press)
[155] Pan S-J and Mark J E 1982 Model networks of end-linked polydimethylsiloxane chains 15. Spatially heterogeneous networks containing domains of very high crosslink density *Polym. Bull.* **7** 553–9
[156] Kunamaneni S, Buzza D M A, Read D J, Parker D, Kenwright A M, Feast W J and Larsen A L 2006 Entanglement transition of randomly branched polymers in the hyperbranched class *Macromolecules* **39** 6720–36
[157] Urayama K, Miki T, Takigawa T and Kohjiya S 2004 Damping elastomer based on model irregular networks of end-linked poly(dimethylsiloxane) *Chem. Mater.* **16** 173–8

[158] Javakhishvili I 2010 *Nanoscale polymeric amphiphiles by combination of controlled polymerizations and "click" reactions: implications for drug delivery* (Technical University of Denmark, PhD Thesis)
[159] Tiecco M, Testaferri L, Santi C, Tomassini C, Marini F and Bagnoli L 2003 Asymmetric azidoselenenylation of alkenes: a key step for the synthesis of enantiomerically enriched nitrogen-containing compounds *Angew. Chemie* **115** 3239–41
[160] De Miguel I, Herradón B and Mann E 2012 Intramolecular azide-alkene 1,3-dipolar cycloaddition/enamine addition(s) cascade reaction: synthesis of nitrogen-containing heterocycles *Adv. Synth. Catal.* **354** 1731–6
[161] Zhou Y and Murphy P V 2008 New access to 1-deoxynojirimycin derivatives via azide-alkene cycloaddition *Org. Lett.* **10** 3777–80
[162] Li Y, Wan L, Zhou H, Huang F and Du L 2013 A novel polytriazole-based organogel formed by the effects of copper ions *Polym. Chem.* **4** 3444
[163] Flory P J 1953 *Principles of polymer chemistry. Ch. 3, 8 and 9* (Cornell University Press, Ithaca, New York)
[164] Green M D, Cruz D S, Ye Y, Layman J M, Elabd Y A, Winey K I and Long T E 2011 Alkyl-substituted N-vinylimidazolium polymerized ionic liquids: thermal properties and ionic conductivities *Macromol. Chem. Phys.* **212** 2522–8
[165] Dimitrov-Raytchev P, Beghdadi S, Serghei A and Drockenmuller E 2013 Main-chain 1,2,3-triazolium-based poly(ionic liquid)s issued from AB + AB click chemistry polyaddition *J. Polym. Sci. Part A Polym. Chem.* **51** 34–8
[166] Jana S, Vasantha V A, Stubbs L P, Parthiban A and Vancso J G 2013 Vinylimidazole-based asymmetric ion pair comonomers: synthesis, polymerization studies and formation of ionically crosslinked PMMA *J. Polym. Sci. Part A Polym. Chem.* **51** 3260–73
[167] Yu L, Gonzalez L B, Hvilsted S and Skov A L 2014 Soft silicone based interpenetrating networks as materials for actuators *Proc. SPIE* **9056** 90560C
[168] Carpi F, Gallone G, Galantini F and De Rossi D 2008 Enhancing the dielectric permittivity of elastomers *Dielectric elastomers as electromechanical transducers* ed F Carpi, D De Rossi, R Kornbuh, R Pelrine and P Sommer-Larsen (Amsterdam: Elsevier Science) pp 51–68
[169] Goswami K, Galantini F, Mazurek P, Daugaard a E, Gallone G and Skov A L 2013 Reinforced poly(propylene oxide): a very soft and extensible dielectric electroactive polymer *Smart Mater. Struct.* **22** 115011
[170] Bostrom J-O, Marsden E, Hampton R N, Nilsson U and Lennartsson H 2003 Electrical stress enhancement of contaminants in XLPE insulation used for power cables *IEEE Electr. Insul. Mag.* **19** 6–12

Appendices

Appendix A

F. B. Madsen, I. Dimitrov, A. E. Daugaard, S. Hvilsted, A. L. Skov, 2013 Novel cross-linkers for PDMS networks for controlled and well distributed grafting of functionalities by click chemistry, *Polymer Chemistry*, **4**, 1700-1707.

Polymer Chemistry

RSC Publishing

PAPER

View Article Online
View Journal | View Issue

Novel cross-linkers for PDMS networks for controlled and well distributed grafting of functionalities by click chemistry†

Cite this: *Polym. Chem.*, 2013, **4**, 1700

Frederikke Bahrt Madsen, Ivaylo Dimitrov, Anders Egede Daugaard, Søren Hvilsted and Anne Ladegaard Skov*

Received 14th November 2012
Accepted 15th December 2012

DOI: 10.1039/c2py20966g

www.rsc.org/polymers

An azide-containing, trifunctional vinyl cross-linker for silicone networks has been synthesized. The cross-linker has through Cu(I) catalyzed 1,3-cycloaddition been reacted with six different alkyne-containing chemical groups which each possess a particular functionality. The functional cross-linkers have been utilized to prepare novel polydimethylsiloxane (PDMS) networks. All functional cross-linkers were successfully incorporated into the networks and were demonstrated to be well distributed within the PDMS films. This was substantiated by fluorescence microscopy of a film prepared with the 4-methylumbelliferone containing cross-linker. TGA showed that a ferrocene functionality increased the thermal degradation temperature of PDMS. It was furthermore shown that the incorporation of only 0.25 wt% of the push–pull dipole, ethynyl-4-nitrobenzene, increased the dielectric permittivity of PDMS by 35%. The contact angle of PDMS films was increased from 108° to 116° by the introduction of a small poly(pentafluorostyrene) chain. Finally, 17α-ethynyl-1,3,5(10)-estratriene-3,17β-diol and 1-ethynyl-3,5-bis(trifluoromethyl)benzene were incorporated as examples of other functional groups.

Introduction

Polydimethylsiloxane (PDMS) is the most widely used siloxane polymer.[1] PDMS elastomers have numerous and widespread applications such as membranes,[2] adhesives,[3] dielectric elastomers[4] and biomedical applications. PDMS owes its many excellent properties to the presence of methyl groups along the flexible Si–O–Si backbone which gives the polymer high thermal stability, high gas permeability, low surface tension and chemical and biological inertness.[5]

Due to the many excellent properties of PDMS it is of great interest to extend the range of applications even further. The properties of PDMS are usually altered and improved by the application of fillers such as metal oxides or most frequently by silicates. However, such filler materials often agglomerate due to favorable particle–particle interactions and this leads to a deterioration of the properties locally instead of the desired macroscopic improvement. The possibility of incorporating evenly distributed functionalities into the PDMS elastomer networks without risking agglomeration could greatly improve and expand the application area of PDMS.[6] The incorporation is envisioned to be performed by covalent attachment of functional molecules to the network, which would provide a matrix with well distributed modifications that prevent leakage of the functional moieties from the PDMS network during use. Modification of the PDMS network by covalent grafting of functionality will change the properties and improve the applicability of PDMS within many areas such as electrical, optical and biomedical areas. The modification could furthermore improve properties such as oil and solvent resistance[7] and current release problems encountered for thin PDMS films where the release forces between PDMS and the substrate easily exceed the tear strength of the material since the excellent wetting properties of PDMS may lead to strong substrate–PDMS interactions.[8]

The cross-linking of PDMS into an elastomer is frequently achieved by hydrosilylation where vinyl groups of one component react with hydrosilane groups of the other component in a platinum catalyzed reaction. In this work, a novel silicone compatible vinyl cross-linker containing an azide functionality is introduced. The vinyl groups allow for cross-linking reactions with hydride-terminated PDMS molecules whereas the azide group allows for modification of the PDMS network either before or after network cross-linking. The azide moiety opens up for click reactions, in this case the copper-catalyzed cycloaddition of an azide group and an alkyne (CuAAC) forming a 1,4-disubstituted-1,2,3-triazole.[9–12] Click chemistry has previously been demonstrated to be successful for functionalization of polymers in general[13–15] and in combination with

Technical University of Denmark, Department of Chemical and Biochemical Engineering, Danish Polymer Centre, Building 227, DK-2800 Kgs. Lyngby, Denmark. E-mail: al@kt.dtu.dk; Tel: +45 4525 2825

† Electronic supplementary information (ESI) available: Mechanical characterization of all films, solid state ^{13}C-NMR spectrum and images of all prepared films can be found as ESI. See DOI: 10.1039/c2py20966g

polysiloxanes in particular.[16–19] The azide group on the cross-linker therefore enables reactions with various types of alkyne functional molecules and thereby significantly widens the functionality that can be introduced into PDMS elastomers. Therefore a number of different functionalities are elaborated. Introduction of 4-methylumbelliferone will provide the PDMS network with a fluorescent tag at the cross-linking site that can not only be used to visualize the distribution of incorporated functionality but also create luminescent PDMS films. A push–pull dipole that potentially enhances the dielectric permittivity of the silicone elastomer can be inserted from an ethynyl-4-nitrobenzene and thus improve the dielectric elastomer performance.[20] The incorporation of ferrocene will provide PDMS films with potential applications within the optical, magnetic or electronic field[21] and within the area of cancer research as certain ferricenium complexes are known to show anti-tumor activity.[22] Ferrocene has also recently been positioned on surfaces of nanoparticles[23] or single-walled carbon nanotubes[24] by application of click chemistry and ethynylferrocene. Different kinds of drugs or therapeutics for biomedical applications will also be possible by the introduction of an estradiol functionality.[25] Recently, it has been shown that introduction of trifluoromethyl groups improve the oil and solvent resistance of PDMS films.[7] With this in mind bis(trifluoromethyl)phenyl and a short poly(pentafluorostyrene) chain will be inserted into the PDMS network. Also possible improvements of the release properties of such fluorine containing PDMS films during processing will be investigated. An important property of the system is that the alkyne-functional molecule in principle can be clicked onto the azide cross-linker before or after the cross-linking reaction that leads to the PDMS network.

Here we present the preparation and characterization of novel PDMS networks containing the elaborated functionalities using the pre-cross-linking approach with the series of new silicone compatible cross-linkers. The pre-cross-linking procedure avoids the step of swelling the PDMS network for successful click reactions and furthermore allows for comprehensive characterization of the individual functional cross-linkers.

Experimental

Materials and methods

Hydride-terminated PDMS, DMS-H31 ($\bar{M}_n$ = 28 000 g mol^{-1}) and a vinyl functional PDMS cross-linker, VDT-431 ($\bar{M}_n$ = 28 000 g mol^{-1}, 16-functional) were acquired from Gelest Inc. The platinum cyclovinylmethyl siloxane complex catalyst (511) was purchased from Hanse Chemie AG. All other chemicals were acquired from Aldrich and used as received unless otherwise specified.

FTIR was conducted on a PerkinElmer Spectrum One model 2000 Fourier Transform Infrared apparatus equipped with a universal attenuated total reflection accessory on a ZnSe–diamond composite. Spectra were recorded in the range of 4000–650 cm^{-1} with 4 cm^{-1} resolution and 16 scans. ^{1}H- and ^{13}C-NMR experiments were performed on a Bruker 250 MHz spectrometer. Solid state ^{13}C-NMR was recorded on a Bruker Avance 500 MHz spectrometer. Thermogravimetric analysis (TGA) was performed on a Q500 from TA Instruments in a nitrogen atmosphere with a heating rate of 10 °C min^{-1} from RT to 950 °C. Differential scanning calorimetry (DSC) measurements were performed on a DSC Q1000 from TA Instruments. The thermal analyses were performed with a heating and cooling rate of 10 °C min^{-1} from 25–200 °C. Mechanical characterization of the prepared films was performed with a TA Instruments 2000 Rheometer set to a controlled strain mode at 1% strain, which was ensured to be within the linear viscoelastic regime. The measurements were performed at RT with a parallel plate geometry of 25 mm in the frequency range of 100–0.01 Hz. Optical characterization was performed on a Leica DMLB microscope with a Olympus Highlight 2000 light source. Fluorescence intensity measurements were performed on a BMG Labtech POLARstar Omega (excitation 355 nm, emission 460 nm). Size-exclusion chromatography (SEC) was performed on a Viscotek GPCmax VE-2001 instrument equipped with a Viscotek TriSEC Model 302 triple detector using two PLgel mixed-D columns from Polymer Laboratories. Samples were run in THF at 30 °C at a rate of 1 ml min^{-1} and molar mass characteristics were calculated using polystyrene standards. Dielectric relaxation spectroscopy (DRS) was performed on a Novocontrol Alpha-A high performance frequency analyzer. Contact angle measurements with water were conducted on a Dataphysics OCA 20. A drop of 6 μl was placed on the surface of the film with the needle inside the drop. The drop was expanded at a rate of 0.125 ml s^{-1}. All reported contact angles are an average of 3 measurements on 3 drops.

Synthesis

All reactions were carried out under a nitrogen atmosphere.

Tris(allyloxy)(3-bromopropyl)silane (1). Allyl alcohol (4.24 g, 73.11 mmol) was dissolved in dry THF (120 ml) in a 250 ml 2-necked round bottomed flask. The mixture was cooled to 0 °C in an ice bath and triethylamine (9.87 g, 97.5 mmol) was added dropwise. (3-Bromopropyl)trichlorosilane (5 g, 19.5 mmol) was then added dropwise to the reaction mixture. The reaction was carried out for 17 hours at RT. The reaction mixture was filtered and the solvent and excess allyl alcohol and triethylamine were removed *in vacuo*. The product was obtained in the form of a light yellow oil (5.35 g, 86%). IR (cm^{-1}): 2870 (C–H stretch); 1645 (C=C stretch); 1070 (C–O stretch); 1035 (Si–O stretch). ^{1}H NMR ($CDCl_3$, δ_H, ppm): 0.81 (m, 2H, CH_2–Si); 1.98 (m, 2H, CH$_2$–CH_2–CH$_2$), 3.40 (t, ^3J = 5.6 Hz, 2H, Br–CH_2), 4.30 (m, 6H, O–CH_2), 5.12 (dd, ^3J = 8.6 Hz and ^2J = 1.25 Hz, 3H, CH=C), 5.27 (dd, 3H, ^3J = 14.25 Hz and ^2J = 1.5 Hz, CH=C), 5.92 (m, 3H, =CH–CH$_2$). ^{13}C-NMR ($CDCl_3$, δ_C, ppm): 9.55 (d); 26.48 (e); 36.51 (f); 63.60 (c); 114.84 (a); 136.30 (b).

Tris(allyloxy)(3-azidopropyl)silane (2). 1 (5.16 g, 16.06 mmol) and NaN_3 (1.39 g, 21.41 mmol) were dissolved in DMF (50 ml) in a 250 ml 2-necked round bottomed flask. The reaction mixture was stirred at RT for 17 hours. The reaction mixture was then quenched with H_2O (70 ml) and extracted with ethyl acetate (3 × 70 ml). The organic phases were combined and washed with

H_2O (3 × 70 ml) and brine (1 × 70 ml), dried with $MgSO_4$, filtered and concentrated *in vacuo* to give the product in the form of an orange-yellow oil (3.91 g, 86%). IR (cm^{-1}): 2870 (C–H stretch); 2095 (–N_3 stretch); 1640 (C=C stretch); 1070 (C–O stretch); 1035 (Si–O stretch). ^{1}H NMR ($CDCl_3$, δ_H, ppm): 0.74 (m, 2H, CH_2–Si), 1.71 (m, 2H, CH_2–CH_2–CH_2), 3.26 (t, ^3J = 5.75 Hz, 2H, N_3–CH_2), 4.30 (m, 6H, O–CH_2), 5.12 (dd, ^3J = 8.5 Hz and ^2J = 1.25 Hz, 3H, CH=C), 5.27 (dd, ^3J = 14.5 Hz and ^2J = 1.75 Hz, 3H, CH=C), 5.92 (m, 3H, =CH–CH_2). ^{13}C-NMR ($CDCl_3$, δ_C, ppm): 7.60 (d); 27.47 (e); 53.69 (f); 63.58 (c); 114.77 (a); 136.29 (b).

4-Methyl-7-(prop-2-yn-1-yloxy)-2*H*-chromen-2-one (3). 4-Methylumbelliferone (3 g, 17,0 mmol) and K_2CO_3 (2.04 g, 20 mmol) were dissolved in acetone (85 ml). Propargyl bromide (2.43 g, 20 mmol) was added at a rate of 0.06 ml min^{-1}. The reaction was carried out under reflux for 24 hours. The reaction mixture was then quenched with H_2O (80 ml) and subsequently extracted 3 times with ethyl acetate. The organic phases were combined and washed with H_2O (3 × 80 ml) and brine (1 × 80 ml), dried with $MgSO_4$, filtered and concentrated *in vacuo*. The crude was recrystallized in an ethyl acetate–heptane mixture (1 : 0.75) to give the product in the form of a white solid in quantitative yield. IR (cm^{-1}): 3305 (C≡C–H stretch); 1720 (O–C=O stretch); 1605 (C=C stretch). ^{1}H NMR ($CDCl_3$, δ_H, ppm): 2.40 (s, 3H, Ar–CH_3), 2.57 (s, 1H, C≡C–H), 4.76 (d, ^4J = 2 Hz, 2H, O–CH_2–), 6.16 (s, 1H, O=C–CH–), 6.95 (m, 2H, Ar–H), 7.52 (m, 1H, Ar–H). ^{13}C-NMR ($CDCl_3$, δ_C, ppm): 18.58 (s); 56.09 (i); 76.43 (g); 77.34 (h); 102.07 (o); 112.31 (q); 112.59 (k); 114.16 (m); 125.56 (l); 152.56 (n); 154.93 (p); 160.27 (j); 160.99 (r).

General procedure for click reactions, 4-methyl-7-((1-(3-(tris(allyloxy)silyl)propyl)-1*H*-1,2,3-triazol-4-yl)methoxy)-2*H*-chromen-2-one (4). **2** (3.01 g, 10.6 mmol) and **3** (2.17 g, 10.0 mmol) were dissolved in THF (50 ml) in a 250 ml 2-necked round bottomed flask. CuI (0.206 g, 10.6 mmol) was subsequently added and Et_3N (1.61 g, 15.9 mmol) was added dropwise. The reaction was carried out at RT for 17 hours. The reaction mixture was extracted with ethyl acetate and washed with H_2O (3 × 40 ml) and brine (1 × 40 ml), dried with $MgSO_4$, filtered and concentrated *in vacuo* to give the product in the form of a light grey oil (2.66 g, 53%). IR (cm^{-1}): 2935 (C–H stretch); 1715 (O–C=O stretch); 1610 (C=C stretch); 1070 (C–O stretch); 1035 (Si–O stretch). ^{1}H NMR ($CDCl_3$, δ_H, ppm): 0.60 (m, 2H, CH_2–Si), 2.05 (m, 2H, CH_2–CH_2–CH_2), 2.40 (s, 3H, Ar–CH_3), 4.28 (m, 2H, N–CH_2–), 4.37 (m, 6H, O–CH_2–), 5.11 (dd, ^3J = 8.5 Hz and ^2J = 1.25 Hz, 3H, CH_2=C), 5.25 (s, 2H, O–CH_2–C–N), 5.26 (dd, ^3J = 14.25 Hz and ^2J = 1.5 Hz, 3H, CH=C), 5.92 (m, 3H, =CH–CH_2), 6.14 (s, 1H, O=C–CH–), 6.95 (m, 2H, Ar–H), 7.50 (m, 1H, Ar–H), 7.65 (s, 1H, –C=CH–N–). ^{13}C-NMR ($CDCl_3$, δ_C, ppm): 7.39 (d); 18.54 (s); 23.93 (e); 52.39 (f); 62.20 (i); 63.70 (c); 101.98 (o); 112.08 (q); 112.27 (k); 113.89 (l); 114.90 (a); 122.95 (m); 125.60 (g); 136.10 (b), 142.69 (h); 152.39 (n); 154.99 (p); 161.02 (j); 161.07 (r).

4-Ferrocene-1-(3-(tris(allyloxy)silyl)propyl)-1*H*-1,2,3-triazole (5). The product was prepared according to the general click procedure using **2** (0.204 g, 0.71 mmol) and ethynylferrocene (0.145 g, 0.67 mmol), CuI (0.0134 g, 0.071 mmol) and Et_3N (0.107 g, 1.06 mmol) to give a brown oil (0.31 g, 94%). IR (cm^{-1}): 2955–2870 (C–H stretch); 1590 (C=C ring stretch); 1430 (C=C ring stretch); 1070 (C–O stretch); 1035 (Si–O stretch). ^{1}H NMR ($CDCl_3$, δ_H, ppm): 0.68 (m, 2H, CH_2–Si), 2.07 (m, 2H, CH_2–CH_2–CH_2), 4.07 (m, 2H, N–CH_2–), 4.2–4.25 (m, 8H, Ar–H), 4.30 (m, 6H, O–CH_2–), 4.72 (m, 1H, Ar–H), 5.12 (dd, ^3J = 8.75 Hz and ^2J = 1.25 Hz, 3H, CH=C), 5.28 (dd, ^3J = 14.25 Hz and ^2J = 1.25 Hz, 3H, CH=C), 5.92 (m, 3H, =CH–CH_2), 7.46 (s, 1H, –C=CH–N–). ^{13}C-NMR ($CDCl_3$, δ_C, ppm): 7.40 (d); 24.32 (e); 52.21 (f); 63.73 (c); 66.52 (k); 68.51 (j); 69.50 (i); 114.92 (a); 118.83 (g); 136.16 (b); 143.46 (h).

4-(4-Nitrophenyl)-1-(3-(tris(allyloxy)silyl)propyl)-1*H*-1,2,3-triazole (6). The product was prepared according to the general click procedure using **2** (0.203 g, 0.72 mmol), 1-ethynyl-4-nitrobenzene (0.103 g, 0.68 mmol), CuI (0.0137 g, 0.072 mmol) and Et_3N (0.109 g, 1.07 mmol) to give a light yellow oil which crystallized upon cooling (0.156 g, 54%). M_p: 69 °C. IR (cm^{-1}): 2915–2860 (C–H stretch); 1645 (C=C stretch); 1605 (aromatic C=C stretch); 1505 (N=O asymmetric stretch); 1460 (aromatic C=C stretch); 1340 (N=O symmetric stretch); 1075 (C–O stretch); 1035 (Si–O stretch). ^{1}H NMR ($CDCl_3$, δ_H, ppm): 0.71 (m, 2H, CH_2–Si), 2.11 (m, 2H, CH_2–CH_2–CH_2), 4.31 (m, 2H, N–CH_2–), 4.44 (m, 6H, O–CH_2–), 5.13 (dd, ^3J = 8.75 Hz and ^2J = 1.25 Hz, 3H, CH=C), 5.28 (dd, ^3J = 14.25 Hz and ^2J = 1.25 Hz, 3H, CH=C), 5.92 (m, 3H, =CH–CH_2), 7.91–8.00 (m, 2H, Ar–H), 8.95 (m, 2H, NO_2–Ar–H), 8.30 (s, 1H, –C=CH–N–). ^{13}C-NMR ($CDCl_3$, δ_C, ppm): 7.46 (d); 24.04 (e); 52.56 (f); 63.82 (c); 115.03 (a); 121.19 (g); 124.27 (k); 126.04 (j); 136.16 (b); 136.96 (i); 145.39 (l); 147.21 (h).

4-(3,5-Bis(trifluoromethyl)phenyl)-1-(3-(tris(allyloxy)silyl)-propyl)-1*H*-1,2,3-triazole (7). The product was prepared according to the general click procedure using **2** (0.200 g, 0.706 mmol), and 1-ethynyl-3,5-bis(trifluoromethyl)benzene (0.17 g, 0.67 mmol), CuI (0.0138 g, 0.071 mmol) and Et_3N (0.107 g, 1.06 mmol) at 45 °C for 24 hours. Azide functional Merrifield resin (0.150 g, 0.21 mmol)[26] was added towards the end of the click reaction in order to remove excess 1-ethynyl-3,5-bis(trifluoromethyl)benzene. This reaction was carried out at 45 °C for 17 hours. The reaction mixture was thereafter filtered and extracted with ethyl acetate (3 × 60 ml) and washed with H_2O (3 × 60 ml), dried with $MgSO_4$, filtered and concentrated *in vacuo* to give the product in the form of an orange-brown oil (0.28 g, 80%). IR (cm^{-1}): 2930–2870 (C–H stretch); 1615 (aromatic C=C stretch); 1465 (aromatic C=C stretch); 1275 (C–F stretch), 1170 (C–F stretch), 1125 (C–F stretch), 1085 (C–O stretch); 1035 (Si–O stretch). ^{1}H NMR ($CDCl_3$, δ_H, ppm): 0.71 (m, 2H, CH_2–Si), 2.11 (m, 2H, CH_2–CH_2–CH_2), 4.31 (m, 2H, N–CH_2–), 4.45 (m, 6H, O–CH_2–), 5.12 (dd, ^3J = 8.75 Hz and ^2J = 1.25 Hz, 3H, CH=C), 5.27 (dd, ^3J = 14.25 Hz and ^2J = 1.5 Hz, 3H, CH=C), 5.93 (m, 3H, =CH–CH_2), 7.92 (s, 1H, Ar–H), 7.94 (s, 1H, –C=CH–N–), 8.28 (s, 2H, Ar–H). ^{13}C-NMR ($CDCl_3$, δ_C, ppm): 7.45 (d); 24.07 (e); 52.59 (f); 63.74 (c); 114.96 (a); 120.78 (g); 121.55 (l); 125.54 (m); 132.03 (i); 132.47 (j); 132.89 (k); 136.27 (b); 144.93 (h).

4-(1,2,5(10)-Estratriene-1,17β-diol)-1-(3-(tris(allyloxy)silyl)-propyl)-1*H*-1,2,3-triazole (8). The product was prepared according to the general click procedure using **2** (0.197 g, 0.71 mmol), 17α-ethynyl-1,3,5(10)-estratriene-3,17β-diol (0.203 g, 0.67 mmol), CuI (0.0134 g, 0.074 mmol) and Et_3N (0.107 g, 1.06 mmol) at RT for 17 hours then at 45 °C for 24 hours to give a light yellow oil (0.373 g, 96%). IR (cm^{-1}): 3310 (O–H stretch); 2930–2870 (C–H stretch); 1610 (aromatic C=C stretch), 1455

(aromatic C=C stretch), 1055 (C–O stretch); 1035 (Si–O stretch). ^{1}H NMR ($CDCl_3$, δ_H, ppm): 0.68 (m, 2H, CH_2–Si), 1.04 (s, 3H, –CH_3), 1.41–2.82 (m, 15H, Al–*H*), 2.06 (m, 2H, CH_2–CH_2–CH_2), 4.29 (m, 2H, N–CH_2–), 4.39 (m, 6H, O–CH_2–), 5.11 (dd, ^3J = 8.63 Hz and ^2J = 1.38 Hz, 3H, C*H*=C), 5.26 (dd, ^3J = 14.15 Hz and ^2J = 1.5 Hz, 3H, C*H*=C), 5.91 (m, 3H, =C*H*–CH_2), 6.56 (m, 2H, Ar–*H*), 7.04 (m, 1H, Ar–*H*), 7.42 (s, 1H, –C=C*H*–N–). ^{13}C-NMR ($CDCl_3$, δ_C, ppm): 7.41 (d); 14.19 (z); 23.29 (k); 23.97 (e); 26.16 (o); 27.17 (r); 29.58 (s); 32.91 (j); 37.85 (n); 39.35 (q); 43.28 (p); 47.27 (m); 48.47 (l); 52.31 (f); 63.77 (c); 82.29 (i); 112.77 (w); 115.15 (a); 115.30 (y); 121.40 (g); 126.22 (v); 132.00 (u); 136.21 (b); 137.96 (t); 153.39 (x); 153.75 (h).

Alkyne end-functionalized poly(pentafluorostyrene) (9). Alkyne functionalised poly(pentafluorostyrene) was synthesized according to a recently published procedure[27] by atom transfer radical polymerization (ATRP) of 2,3,4,5,6-pentafluorostyrene in bulk initiated with 3-bromo-1-(trimethylsilyl)-1-propyne. T_g = 97 °C. IR (cm^{-1}): 3316 (C≡C–H stretch); 2960 (C–H stretch); 1496 (F-aromatic stretch); 981 (C–F-aromatic bend). ^{1}H NMR ($CDCl_3$, δ_H, ppm): 1.70–3.00 (CH_2–C≡ + CH_2–C*H* + *H*–C≡C), 4.8 (m, 1H, C*H*–Br). ^{13}C-NMR ($CDCl_3$, δ_C, ppm): 16.56 (i); 32.12 (j); 37.13–38.67 (k); 69.24 (g); 81.79 (h); 135.81 (l); 139.18 (n); 143.15 (o); 146.45 (m). SEC (THF): $\bar{M}_n$ = 3300 Da, $\bar{M}_w/\bar{M}_n$ = 1.4.

4-Poly(pentafluorostyrenyl)-1-(3-(tris(allyloxy)silyl)propyl-1*H*-1,2,3-triazole (10). The alkyne end-functional polymer **9** (0.6 g, 0.18 mmol) and CuI (0.031 g, 0.162 mmol) were mixed in THF (4 ml) followed by the addition of **2** (0.062 g, 0.216 mmol) and Et_3N (0.1 ml, 0.72 mmol). The click reaction proceeded at 35 °C for 20 h. The product was precipitated in methanol and dried *in vacuo*. Yield: 0.59 g (89%). T_g = 112 °C. IR (cm^{-1}): 2960–2870 (C–H stretch); 1653 (C=C stretch); 1498 (F-aromatic stretch); 981 (C–F-aromatic bend). ^{1}H NMR ($CDCl_3$, δ_H, ppm): 0.70 (Si–CH_2), 1.70–3.00 (Si–CH_2–CH_2 + CH_2–C*H* + CH=C(N)–CH_2), 4.25 (Si–O–CH_2 + Si–CH_2–CH_2–CH_2–N), 5.15 (CH_2=CH), 5.87 (CH_2=C*H*), 7.60 (N–C*H*=C(N)–CH_2). ^{13}C-NMR ($CDCl_3$, δ_C, ppm): 7.51 (d); 24.07 (e); 25.52 (i); 32.12 (j); 37.05–38.79 (k); 52.85 (f); 63.26 (c); 114.15 (a); 125.27 (g); 135.93 (l); 136.11 (b); 139.32 (n); 143.42 (o); 146.24 (m); 153.16 (h). $\bar{M}_n$ = 3300 Da, $\bar{M}_w/\bar{M}_n$ = 1.4.

Procedure for stability measurements

The hydrolytic stability of the Si–O–C linkage in **2** was determined using a previously described method.[28] 30 mg of sample was dissolved in 0.8 ml $CDCl_3$ in an NMR tube to which 50 µl D_2O was added. The ^{1}H-NMR of the mixture was recorded over time for 72 h. The silyl ether cleavage was evaluated by integration and comparison of the O–CH_2 peak and the CH_2–Si peak.

Preparation of polymer films

Cross-linkers (**2**, **4**–**8** and **10**) (0.043 mmol) were dissolved in dry THF (0.3 ml) and mixed with a 16-functional cross-linker (VDT-431) (0.0027 mmol) and hydride-terminated PDMS (DMS-H31) (0.086 mmol). The platinum cyclovinylmethyl siloxane complex catalyst (511) (10–30 ppm) in dry THF was thereafter added and the mixture was mixed on a vortex mixer for 2 minutes. The mixture was thereafter degassed *in vacuo* to remove solvent and air bubbles. The mixture was poured into 1 mm thick steel molds on a fluorinated ethylene propylene (FEP) release liner and cured at 60 °C for 24 h.

Swelling experiments

The gel fractions were determined using two methods. The first method, Soxhlet extraction with chloroform for 48 hours, was used to pull out all extractables. The samples were thereafter dried for 24 h and the gel fraction was determined as the weight after extraction and drying (m_e) to the initial weight of the sample (m_0) as $W_{gel} = m_e/m_0$.

The second method consisted of swelling experiments used to pull out leachables from the prepared films. Samples were swelled in chloroform for 48 hours at RT. The solvent was replaced after 24 hours. The solvent was then decanted and the films were washed several times with chloroform. The samples were thereafter dried for 24 h. Gel fractions were determined as the weight after extraction and drying (m_e) to the initial weight of the sample (m_0) as $W_{gel} = m_e/m_0$.

Results and discussion

The azide functional, silicone compatible vinyl cross-linker (**2**) was synthesized in two steps *via* the silyl ether reaction between (3-bromopropyl)trichlorosilane and allyl alcohol and subsequent substitution of bromine with azide as illustrated in Scheme 1.

The azide cross-linker was isolated as an orange-yellow oil with a high yield and high purity. The vinyl cross-linker proved to be hydrolytically stable under the utilized synthesis conditions which included several extraction procedures with water. The stability of the formed silyl ether bond was evaluated using ^{1}H-NMR in D_2O. Spectra were recorded over time and integration of the O–CH_2 peak compared to integration of other peaks indicated that no detectable cleavage of the Si–O–C bond had taken place in the stability test during the 72 hours.

The alkyne functional molecules used in the click reactions with **2** are shown in Table 1. A general reaction scheme for the click reaction is illustrated in Scheme 2.

The click reaction was used to prepare a variety of different functional cross-linkers as shown in Table 1. Two of the employed alkynes, **3** and **9**, were not commercially available but prepared for this study. **3** was prepared through a Williamson ether synthesis of 4-methylumbelliferone and propargyl bromide using K_2CO_3 as the base catalyst. **9** was polymerized under controlled ATRP conditions using a previously published procedure[27] yielding an alkyne functional poly(pentafluorostyrene). The functionalized cross-linkers were all prepared under similar click reaction conditions in THF using a CuI–Et_3N catalytic system. In the case

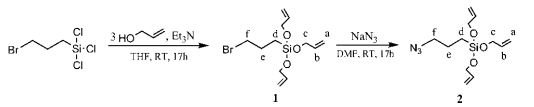

Scheme 1 Preparation of the azide-functional vinyl cross-linker **2**.

Table 1 Alkynes and functional cross-linkers from click reactions. Letters are used in assignment of ^{13}C-NMR spectra

Alkyne	Click-product
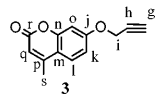 **3**	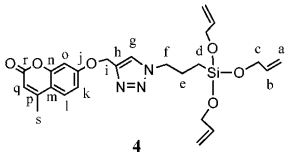 **4**
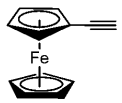	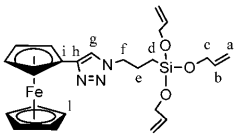 **5**
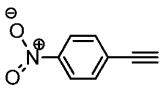	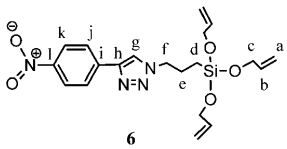 **6**
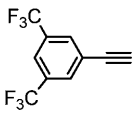	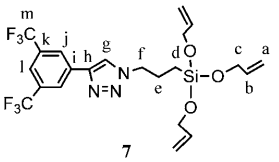 **7**
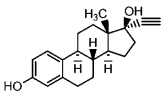	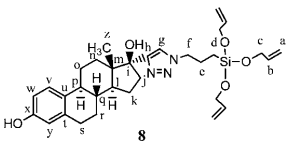 **8**
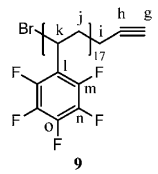 **9**	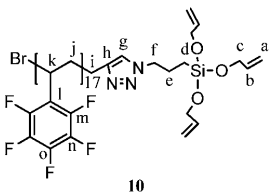 **10**

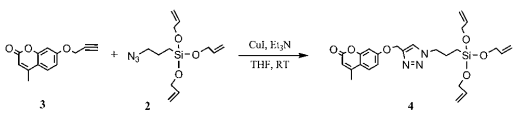

Scheme 2 General reaction scheme for click reaction between the azide cross-linker (**2**) and alkyne exemplified by **3**.

of **5**, **8** and **10** yields were high (~90%) but in the case of **4** and **6** the yields were in the order of 50%. This was assessed to be acceptable and was not attempted optimized.

The synthesized alkynes and all novel vinyl cross-linkers, **4**–**8** and **10**, were thoroughly characterized by FTIR and ^{1}H- and ^{13}C-NMR. FTIR was used to confirm the completion of the click reactions by the disappearances of the alkyne band at approximately 3300 cm^{-1} and the very distinct azide band at approximately 2100 cm^{-1}. The presence of the triazole proton in ^{1}H-NMR points to the successful formation of reaction products. The triazole proton appears from $\delta_H = 7.42$ ppm to $\delta_H = 8.30$ ppm depending on the electron density of the triazole. Representative spectra can be found as ESI.† If small residues of azide/alkyne can be detected, they are easily removed by use of resins which facilitates a simple purification procedure. In connection with the synthesis of **7**, a small alkyne band was detected by FTIR and a peak for the alkyne proton was also detected by ^{1}H-NMR at $\delta_H = 3.26$ ppm. **7** was consequently treated with an azide functional Merrifield resin in order to remove the residual alkyne reactant by additional click reaction and resulting attachment of the alkyne reactant to the resin. The azide resin with the excess alkyne attached could thereafter be removed from the reaction mixture by simple filtration.

The PDMS networks were prepared from cross-linkers **2**, **4**–**8** and **10**, hydride terminated PDMS and a platinum catalyst according to Scheme 3.

A commercially available 16-functional silicone vinyl cross-linker was used to reinforce the network since networks prepared solely from three-functional cross-linkers are known to be very soft and have low mechanical breakdown strength.[29] The molar ratio between the three-functional synthesized cross-linkers and the 16-functional commercial silicone cross-linker were 16 : 1 to ensure a high concentration of the functionalized cross-linkers and minimize possible competition from the 16-functional cross-linker. The networks were prepared with equimolar amounts, meaning that the number of functional hydride groups of the polymer corresponds to the total number

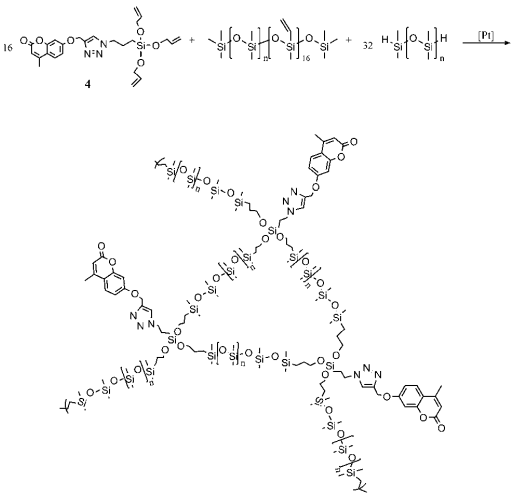

Scheme 3 Cross-linking reaction between **4** and hydride terminated PDMS.

of vinyl groups on the two cross-linkers. The PDMS films ranged from light yellow in color for films with **6** and **8** to light brown for films with **5** and **7** and dark brown for **10**. The film with **2** was completely transparent whereas the film with **4** was light grey and opaque. Images of all films can be found in the ESI.†

All prepared films were characterized by FTIR. There was, however, no differences between the films with different functional cross-linkers since the concentrations of cross-linkers in the films were found to be too low to be detected by this technique. A solid state ^{13}C-NMR spectrum of the elastomer with **4** obtained over 20 h reveals the dominating Si–CH_3 resonance at ~1 ppm. In addition three small resonances at ~4, ~8, ~24 ppm can be assigned to CH_2 close to Si atoms. Weak signals in the 100–160 ppm range indicate the presence of aromatic carbons. The solid state ^{13}C-NMR analysis thus strongly supports the presence of the silyl-based cross-linker in the network.

Swelling and extraction experiments were used to determine the gel fraction of the films. This was done in order to further elucidate if the synthesized cross-linkers had reacted with the PDMS chains and were incorporated covalently in the network. Possible problems that such modified networks could encounter include poor compatibility with the matrix and steric hindrance of the three-functional cross-linker leading to dangling chains and extractable substructures containing primarily the triazole cross-linkers. Some of the produced films had indeed large sol fractions especially from the Soxhlet extraction data (Table 2). It is, however, not common practice to perform this type of extractions when investigating PDMS network gel fractions as it is a very aggressive method. The swelling experiments performed are therefore more suitable for comparison with previously performed PDMS swelling experiments.[30,31] Optimized PDMS elastomers usually have gel fractions of 95–97% whereas stoichiometrical PDMS networks usually have gel fractions around 90%. This can be explained by the optimized PDMS elastomers having a stoichiometry of 1.1–1.4 which means that the cross-linker is in excess and that all cross-linker sites do not need to react thus reducing steric hindrance.[32] The networks prepared in this study are all stoichiometric such that gel fractions of less than 90% are anticipated.

A visual evaluation of the dry sol and gel fraction revealed that all films (gel fractions) retained their initial colors which are due to the presence of the functional cross-linkers. Furthermore all sol fractions bore little or no evidence of color from cross-linkers. In order to further investigate the nature of the gel and sol fraction, the fluorescence intensity was measured of both the dried sol and the gel fraction of the film prepared with the fluorescence cross-linker **4** after the Soxhlet extraction experiment. The fluorescence intensity was also measured for the film with **4** before the Soxhlet extraction. Results are shown in Fig. 1.

It was observed that the fluorescence intensity of the film prepared with **4** only decreases by 4% after extraction. This indicates that cross-linker **4** is indeed incorporated into the PDMS network gel fraction and is thus covalently bound to the network. The sol fraction exhibits very low fluorescence intensity and therefore most likely consists of PDMS substructures not connected to the network such as inert or mono-functional PDMS chains. It can hence be concluded, that the synthesized cross-linkers can be successfully incorporated into PDMS networks.

To investigate the distribution of the grafted functionalities, fluorescence microscopy was performed on the film prepared with cross-linker **4** which acts as a fluorescent tag in the network as seen in Fig. 2.

It is seen that the film with **4** is indeed fluorescent and that the fluorescent cross-linker is evenly distributed throughout the network. This indicates that the synthesized triazole cross-linkers can successfully be incorporated into PDMS networks in a well distributed manner.

Mechanical characterization was performed by determining the storage and loss moduli for all films. In Fig. 3 the results for films prepared with **2** and **4** are presented. A similar plot for films with **5–8** and **10** can be found in the ESI.†

It is seen in Fig. 3 that both networks are well cross-linked as the storage modulus for both networks are of an order of 10 to 100 times that of the loss modulus for the investigated frequency regime.[32] The elastomer containing cross-linker **4** is seen to have slightly lower moduli than the film with cross-linker **2**. This can be explained by the bulkier group attached on **4** which thereby creates a small diluting effect in the network creating a less elastic film. All other films showed similar mechanical behavior. The elastomer with cross-linker **10** has lower moduli than the other films. This corresponds with the results seen from the extraction experiments which showed that the film with **10** has a significantly smaller gel fraction than the other networks. The large poly(pentafluorostyrene) groups thereby creates a soft network with a large portion of extractable

Table 2 Gel contents of samples as results from Soxhlet extractions and swelling experiments (%)

Cross-linker	Gel fraction (Soxhlet extraction)	Gel fraction (swelling)
2	78.5	84.1
4	57.3	92.2
5	52.8	82.7
6	56.8	68.5
7	74.1	90.1
8	55.9	59.3
10	41.5	69.1

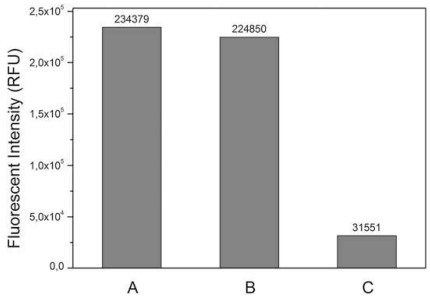

Fig. 1 Fluorescent intensity of A: film with **4** before Soxhlet extraction; B: dried film with **4** after Soxhlet extraction (gel fraction) and C: dried sol fraction of film with **4**.

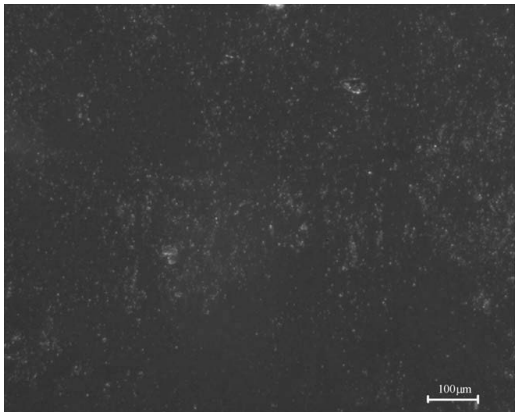

Fig. 2 Fluorescent microscopy image of the film prepared with cross-linker **4**.

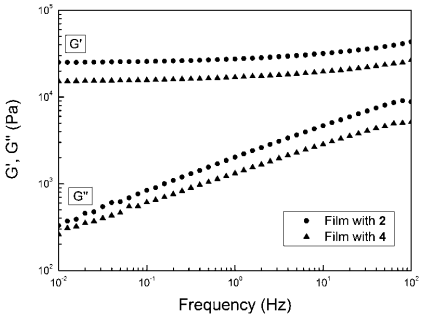

Fig. 3 Storage modulus (*G'*) and loss modulus (*G''*) as functions of frequency for films prepared with **2** and **4**.

substructures. This can be due to incompatibility between the two polymers leading to phase separation which is also visually evident from the darker domains formed in the film.

Thermal gravimetric analysis (TGA) was used to investigate the effects of the different functional cross-linkers on the thermal stability of the PDMS films (Fig. 4).

All TGA curves show a two step mass loss process. The first degradation step occurring from 390 °C to 540 °C (mass loss of 1.8–12.7 wt%) depending on functionality corresponds to the cleavage of Si–CH_3 bonds. In the case of **10** it is noted that at 510 °C all the poly(pentafluorostyrene) has degraded.[33] The second decomposition step occurring from 590 °C to 690 °C (mass loss of 32.5–86.4 wt%) can be attributed to structural rearrangements followed by mineralization of the material.[34] The decomposition temperatures are taken as the peak temperature of the first derivate of the temperature with time. The TGA curves show that the PDMS samples have different decomposition temperatures depending on the incorporated functionality with **5** giving the highest initial degradation temperature (540 °C) due to higher thermal stability of ferrocene[35] which increases the degradation temperature of the PDMS film. It is

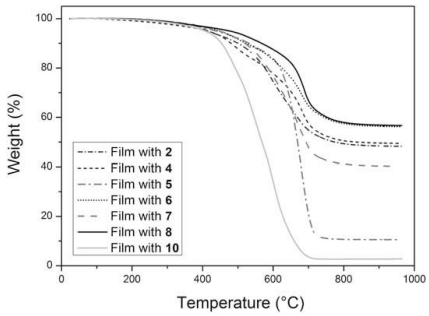

Fig. 4 TGA measurements of PDMS films prepared with cross-linkers **2**, **4**–**8** and **10**.

hypothesized that the ferrocene cross-linker, however, also catalyzes the PDMS degradation such that mineralization occurs to a larger extent. The catalytic effect can also be observed for the film with **10** (poly(pentafluorostyrene)). It is moreover noted that all films with a functional cross-linker except for **10** induced a higher decomposition temperature than films with a non-functional cross-linker (**2**).

The dielectric properties were determined by dielectric relaxation spectroscopy (DRS) for the films prepared with the **2** and **6** cross-linkers, see Fig. 5.

It was found, that the dipolar nature of the **6** cross-linker, due to the nitro group, increases the dielectric properties of the film from 2.3 for films with **2** to 3.1 for films with **6** which corresponds to an increase of 35%. This increase is remarkable since the content of this dipolar cross-linker is only around 0.75 wt% corresponding to 0.25 wt% of the pure dipole molecule. It is therefore likely that by increasing the amount of dipolar cross-linker it would be possible to achieve a large increase in the dielectric permittivity which could improve the performance of dielectric elastomers to a very great extent.

The impact of the fluorine containing cross-linkers on the release properties of the PDMS films was determined using contact angle measurements. The contact angle was found to increase from 108° ± 2.5 for the film with cross-linker **2** to

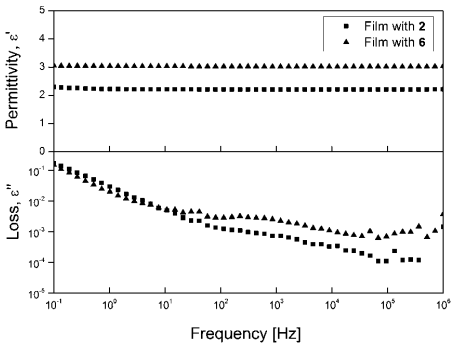

Fig. 5 Permittivity spectra of films prepared with the **2** and **6** cross-linkers showing both the frequency dependence on the permittivity (*ε'*) and the dielectric loss (*ε''*).

116° ± 2.5 for the PDMS film with cross-linker **10**. This is due to the hydrophobic nature of the poly(pentafluorostyrene) which causes a migration of the fluorinated polymer to the PDMS surface[36] and thus increasing the contact angle and thereby also a possible improvement of release properties for PDMS films during processing.[8] The film with **7** showed no increase in contact angle compared to the film with **2**. This is probably due to the low concentration of fluorine on this cross-linker which allows the cross-linker to be encapsulated within the PDMS network and no migration to the surface will consequently occur.

Conclusions

A novel silicone compatible cross-linker that allows for click reactions and thereby grafting of various molecular functionalities into PDMS networks has been developed. The developed system opens up for a wide variety of possible reactions and network functionalizations which can expand the application area of PDMS networks greatly. The functionalization of PDMS networks was demonstrated by the successful synthesis of a number of diverse functional cross-linkers that were used to create PDMS films. It was shown that all functional cross-linkers had been successfully incorporated into the network and that only minute amounts of the functionality could be extracted from the network. It was also demonstrated by fluorescence microscopy that the functional cross-linkers were well distributed within the PDMS network. Thermal gravimetric analysis (TGA) showed that the incorporation of a ferrocene functionality increased the thermal degradation temperature of the PDMS network. Furthermore it was shown that the incorporation of a dipolar cross-linker could improve the dielectric permittivity of PDMS by a factor of 35% at only 0.25 wt% of dipole-functionality and that the contact angle of the PDMS films could be increased from 108° to 116° by the incorporation of a small poly(pentafluorostyrene) chain.

Acknowledgements

The authors wish to express thanks to Morten Bjerring, Aarhus University for help with solid state NMR and acknowledge the Danish National Advanced Technology Foundation for financial support.

Notes and references

1 E. G. Rochow, in *Silicon-Based Polymer Science – A Comprehensive Resource*, ed. J. M. Zeigler and F. W. G. Fearon, American Chemical Society, 1990, pp. xiii–xxii.
2 J. de Jong, R. G. H. Lammertink and M. Wessling, *Lab Chip*, 2006, **6**, 1125–1139.
3 M. K. Jensen, A. Bach, O. Hassager and A. L. Skov, *Int. J. Adhes. Adhes.*, 2009, **29**, 687–693.
4 P. Brochu and Q. Pei, *Macromol. Rapid Commun.*, 2010, **31**, 10–36.
5 J. E. Mark, in *Silicon-based Polymer Science: A Comprehensive Resource*, ed. J. M. Zeigler and F. W. G. Fearon, American Chemical Society, 1990, pp. 47–68.
6 F. Carpi, G. Gallone, F. Galantini and D. De Rossi, *Adv. Funct. Mater.*, 2008, **18**, 235–241.
7 B. Li, S. Chen and J. Zhang, *Polym. Chem.*, 2012, **3**, 2366–2376.
8 S. Vudayagiri, M. D. Junker and A. L. Skov, *Polym. J.*, 2012, DOI: 10.1038/pj.2012.227.
9 H. C. Kolb, M. G. Finn and K. B. Sharpless, *Angew. Chem., Int. Ed.*, 2001, **40**, 2004–2021.
10 P. Wu, A. K. Feldman, A. K. Nugent, C. J. Hawker, A. Scheel, B. Voit, J. Pyun, J. M. J. Fréchet, K. B. Sharpless and V. V. Fokin, *Angew. Chem., Int. Ed.*, 2004, **43**, 3928–3932.
11 M. Meldal, *Macromol. Rapid Commun.*, 2008, **29**, 1016–1051.
12 W. H. Binder and R. Sachsenhofer, *Macromol. Rapid Commun.*, 2008, **29**, 952–981.
13 A. D. Thomsen, E. Malmström and S. Hvilsted, *J. Polym. Sci., Part A: Polym. Chem.*, 2006, **44**, 6360–6377.
14 A. E. Daugaard, S. Hvilsted, T. S. Hansen and N. B. Larsen, *Macromolecules*, 2008, **41**, 4321–4327.
15 S. Hvilsted, *Polym. Int.*, 2012, **61**, 485–494.
16 F. Gonzaga, G. Yu and M. A. Brook, *Macromolecules*, 2009, **42**, 9220–9224.
17 F. Gonzaga, G. Yu and M. A. Brook, *Chem. Commun.*, 2009, 1730–1732.
18 U. Schmidt, P. C. Zehetmaier and B. Rieger, *Macromol. Rapid Commun.*, 2010, **31**, 545–548.
19 S. Halila, M. Manguian, S. Fort, S. Cottaz, T. Hamaide, E. Fleury and H. Driguez, *Macromol. Chem. Phys.*, 2008, **209**, 1282–1290.
20 B. Kussmaul, S. Risse, G. Kofod, R. Waché, M. Wegener, D. N. McCarthy, H. Krüger and R. Gerhard, *Adv. Funct. Mater.*, 2011, **21**, 4589–4594.
21 R. D. A. Hudson, *J. Organomet. Chem.*, 2001, **637–639**, 47–69.
22 P. Köpf-Maier, H. Köpf and E. W. Neuse, *J. Cancer Res. Clin. Oncol.*, 1984, **108**, 336–340.
23 I. Javakhishvili and S. Hvilsted, *Polym. Chem.*, 2010, **1**, 1650–1661.
24 M. Coates, S. Griveau, F. Bedioui and T. Nyokong, *Electroanalysis*, 2012, **24**, 1833–1838.
25 E. C. Dreaden, S. C. Mwakwari, Q. H. Sodji, A. K. Oyelere and M. A. El-Sayed, *BioconjugateChem.*, 2009, **20**, 2247–2253.
26 J. A. Opsteen and J. C. M. van Hest, *Chem. Commun.*, 2005, 57–59.
27 I. Dimitrov, S. Takamuku, K. Jankova, P. Jannasch and S. Hvilsted, *Macromol. Rapid Commun.*, 2012, **33**, 1368–1374.
28 D. B. Thompson, F. Gonzaga, A. S. Fawcett and M. A. Brook, *Silicon Chem.*, 2008, **3**, 327–334.
29 A. G. Bejenariu, H. K. Rasmussen, A. L. Skov, O. Hassager and S. M. Frankaer, *Rheol. Acta*, 2010, **49**, 807–814.
30 S. M. G. Frankær, M. K. Jensen, A. G. Bejenariu and A. L. Skov, *Rheol. Acta*, 2012, **51**, 559–567.
31 J. N. Lee, C. Park and G. M. Whitesides, *Anal. Chem.*, 2003, **75**, 6544–6554.
32 A. L. Larsen, K. Hansen, P. Sommer-Larsen, O. Hassager, A. Bach, S. Ndoni and M. Jørgensen, *Macromolecules*, 2003, **36**, 10063–10070.
33 K. Jankova and S. Hvilsted, *Macromolecules*, 2003, **36**, 1753–1758.
34 G. Camino, S. M. Lomakin and M. Lageard, *Polymer*, 2002, **43**, 2011–2015.
35 A. S. Abd-El-Aziz and E. K. Todd, *Coord. Chem. Rev.*, 2003, **246**, 3–52.
36 S. Borkar, K. Jankova, H. W. Siesler and S. Hvilsted, *Macromolecules*, 2004, **37**, 788–794.

Electronic Supplementary Material (ESI) for Polymer Chemistry

Supporting Information

Novel cross-linkers for PDMS networks for controlled and well distributed grafting of functionalities by click chemistry

Frederikke Bahrt Madsen, Ivaylo Dimitrov, Anders Egede Daugaard, Søren Hvilsted and Anne Ladegaard Skov

Danish Polymer Center, Department of Chemical and Biochemical Engineering, Technical University of Denmark, Building 227, 2800 Kgs. Lyngby, Denmark

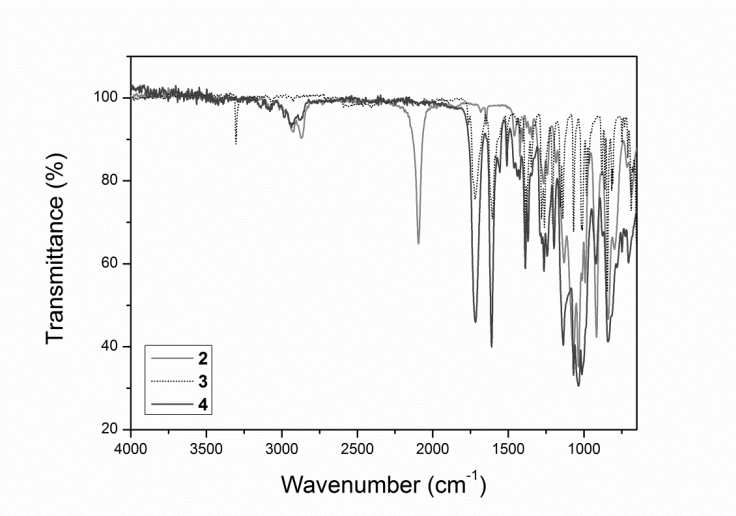

Figure S1: FTIR spectra of azide cross-linker (2), alkyne (3) and click product (4).

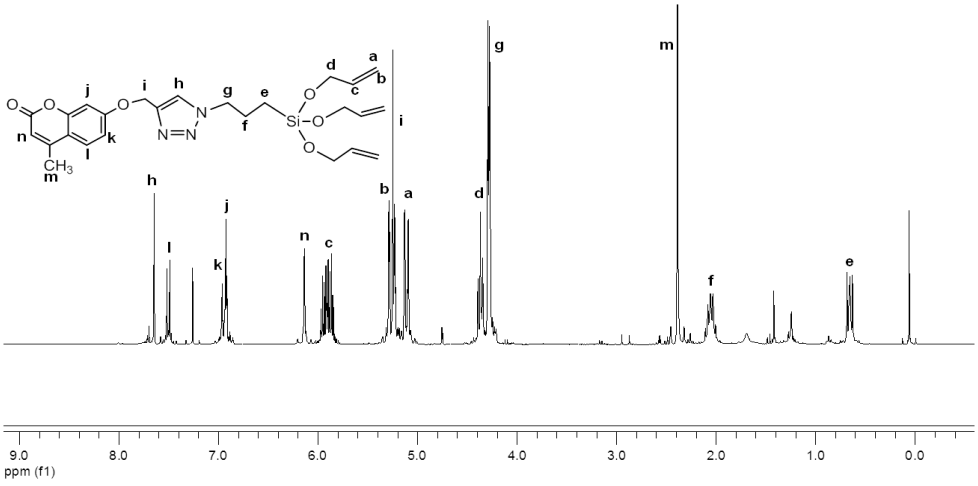

Figure S2: ^{1}H-NMR spectrum of 4 showing the formation of the triazole proton (h).

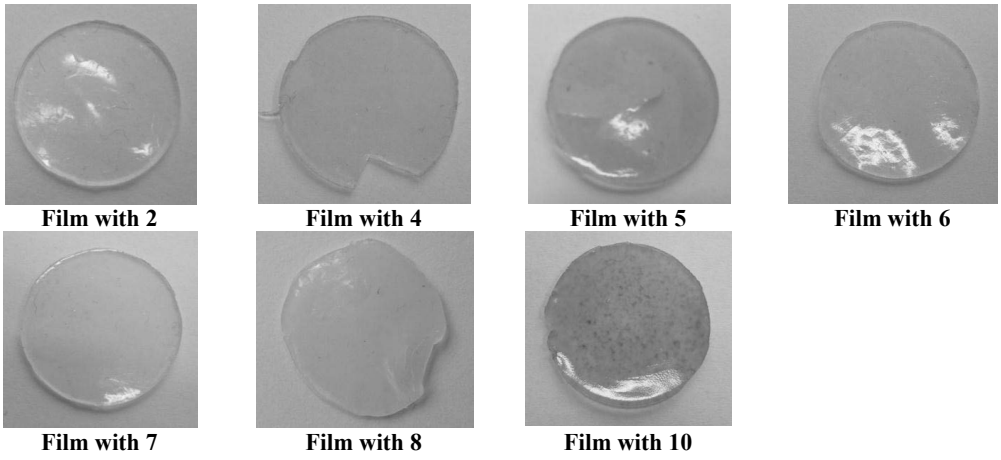

Figure S3: Photos of prepared films.

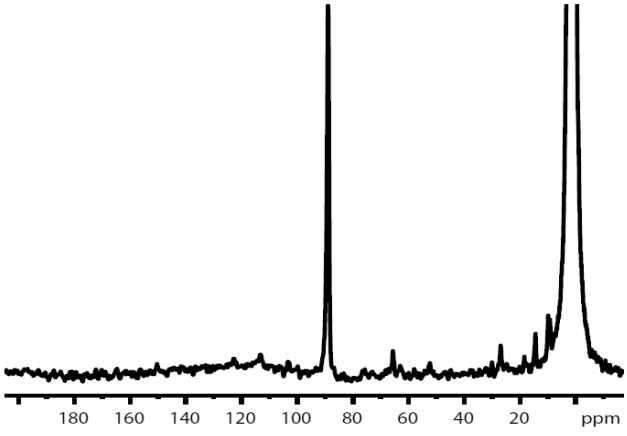

Figure S4: ^{13}C-NMR solid state spectrum of film with 4. A Peak at 89 ppm corresponding to ~2% of the Si-CH_3 signal at 1 ppm could not be assigned and are probably due to some impurity in the network.

Mechanical Characterization

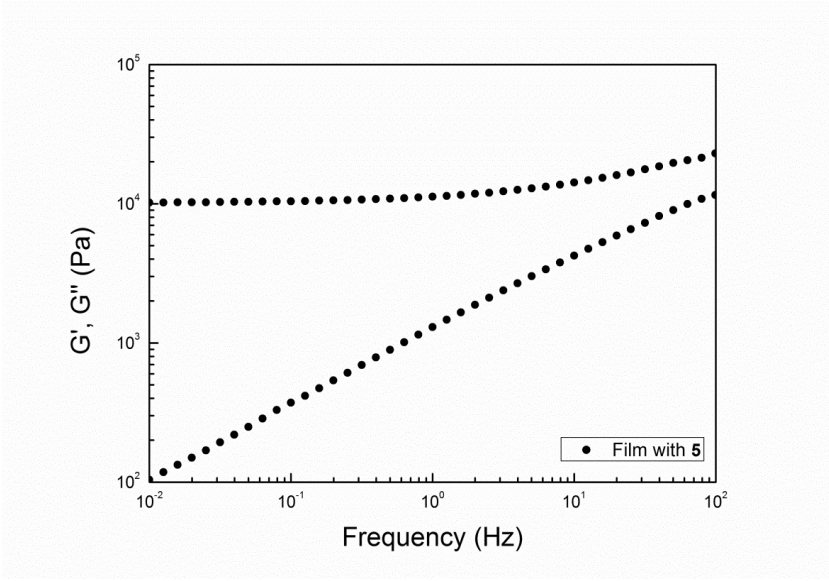

Figure S5: Storage modulus (G') and loss modulus (G'') as functions of frequency for film prepared with 5.

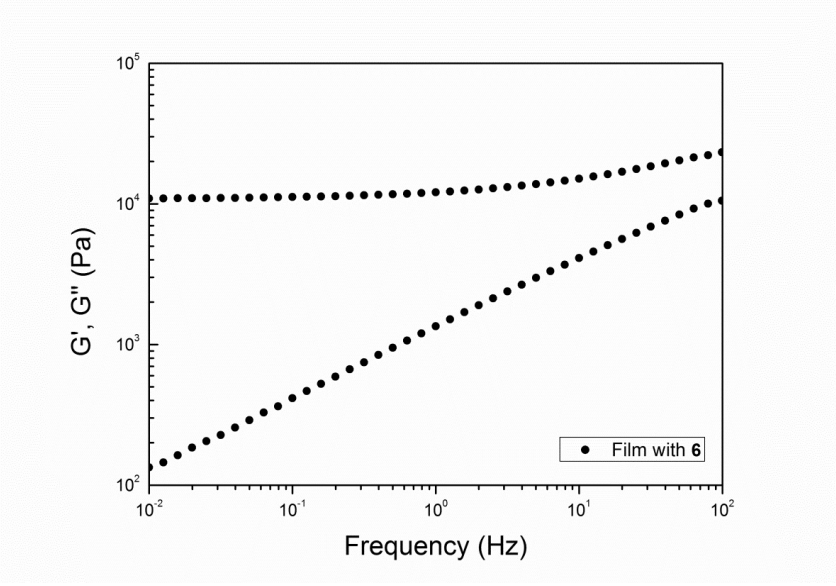

Figure S6: Storage modulus (G') and loss modulus (G'') as functions of frequency for film prepared with 6.

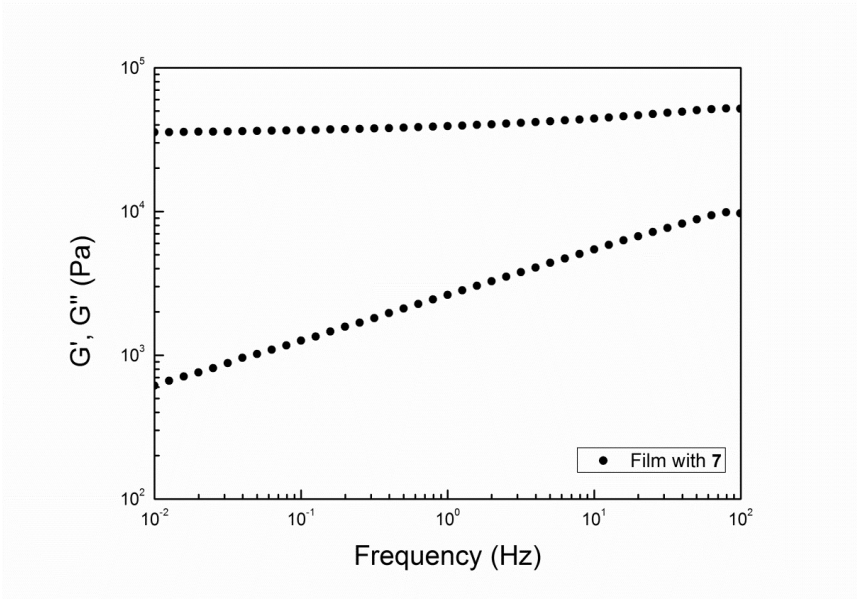

Figure S7: Storage modulus (G') and loss modulus (G'') as functions of frequency for film prepared with 7.

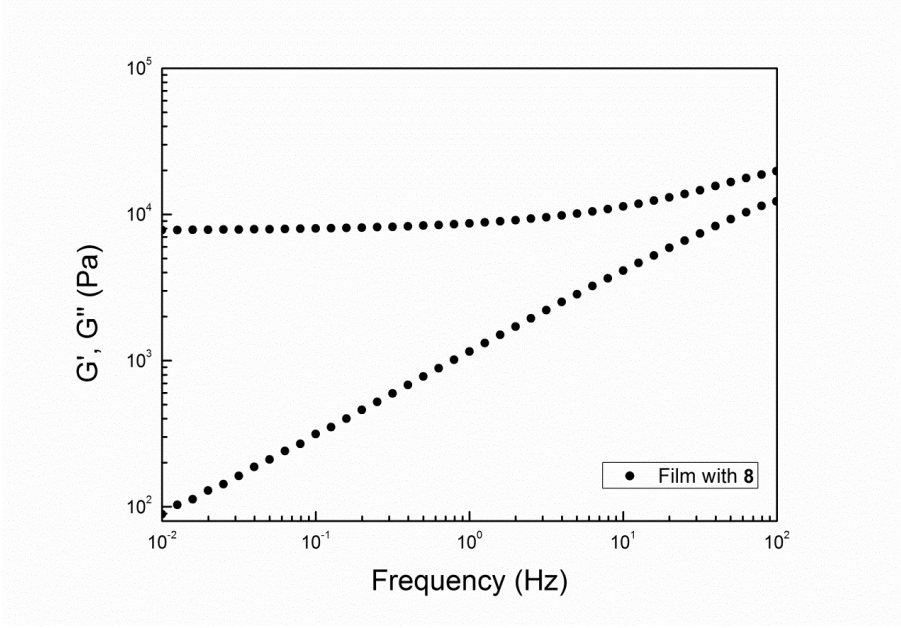

Figure S8: Storage modulus (G') and loss modulus (G'') as functions of frequency for film prepared with 8.

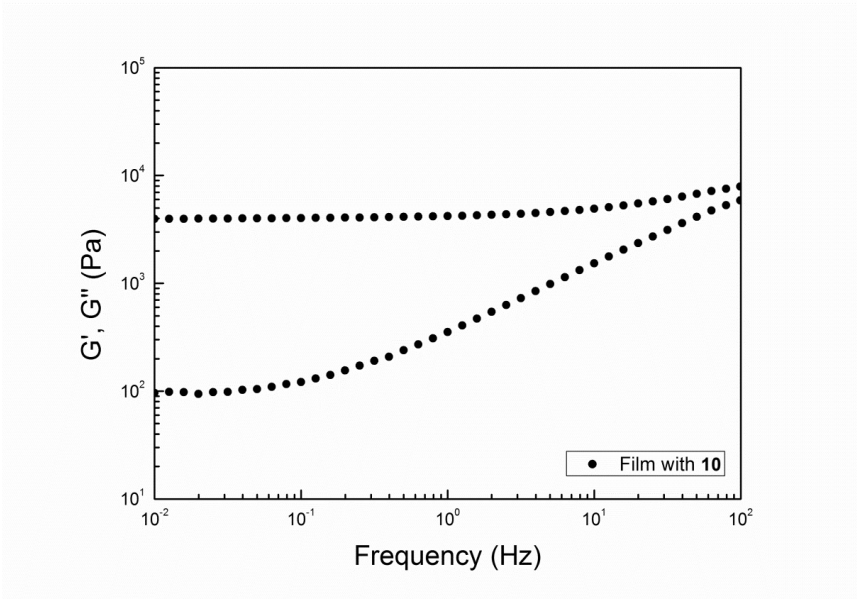

Figure S9: Storage modulus (G') and loss modulus (G'') as functions of frequency for film prepared with 10.

Appendix B

F. B. Madsen, A. E. Daugaard, S. Hvilsted, M. Y. Benslimane, A.L. Skov, 2013 Dipolar cross-linkers for PDMS networks with enhanced dielectric permittivity and low dielectric loss, *Smart Materials and Structures,* **22**, 104002.

Smart Mater. Struct. **22** (2013) 104002 (11pp) doi:10.1088/0964-1726/22/10/104002

Dipolar cross-linkers for PDMS networks with enhanced dielectric permittivity and low dielectric loss

Frederikke Bahrt Madsen[1], **Anders Egede Daugaard**[1], **Søren Hvilsted**[1], **Mohamed Yahia Benslimane**[2] **and Anne Ladegaard Skov**[1]

[1] DTU, The Danish Polymer Centre, Department of Chemical and Biochemical Engineering, DK-2800 Kgs. Lyngby, Denmark
[2] Danfoss PolyPower A/S, Nordborgvej 81, DK-6430 Nordborg, Denmark

E-mail: al@kt.dtu.dk

Received 6 December 2012, in final form 18 February 2013
Published 19 September 2013
Online at stacks.iop.org/SMS/22/104002

Abstract
Dipole grafted cross-linkers were utilized to prepare polydimethylsiloxane (PDMS) elastomers with various chain lengths and with various concentrations of functional cross-linker. The grafted cross-linkers were prepared by reaction of two alkyne-functional dipoles, 1-ethynyl-4-nitrobenzene and 3-(4-((4-nitrophenyl)diazenyl)phenoxy)-prop-1-yn-1-ylium, with a synthesized silicone compatible azide-functional cross-linker by click chemistry. The thermal, mechanical and electromechanical properties were investigated for PDMS films with 0 to 3.6 wt% of dipole-cross-linker. The relative dielectric permittivity was found to increase by ∼20% at only 0.46 wt% of incorporated dipole without significant changes in the mechanical properties. Furthermore, the dielectric losses were proved to be remarkably low while the electrical breakdown strengths were high.

S Online supplementary data available from stacks.iop.org/SMS/22/104002/mmedia

1. Introduction

Dielectric electroactive polymers (DEAPs) are promising materials for advanced electromechanical applications such as actuators, sensors and generators due to their ability to exhibit a change in size and shape when an external voltage is applied as well as to generate electrical energy when a mechanical deformation is induced. Possible applications range from robotics, prosthetics, pumps, valves and optics to wave energy harvesting as they can achieve large strains and have a simple working principle. DEAPs usually consist of a thin filled elastomer film sandwiched between two compliant electrodes [1]. When an external voltage is applied to the electrodes, the electrostatic pressure acting on the film will squeeze the elastomer in thickness and the film is consequently expanded in planar directions. The electrical energy has thus been converted into mechanical energy. When the external voltage is switched off, the elastomer film returns to its original shape.

Polydimethylsiloxane (PDMS) is one of the most utilized polymers for DEAP applications due to its high efficiency and fast response [2, 3]. PDMS owes its excellent properties to the presence of methyl groups along the flexible Si–O–Si backbone which gives the polymer high thermal stability, low surface tension as well as chemical and biological inertness [4]. PDMS, however, suffers from low dielectric permittivity and thus high voltage is required to obtain a large strain. There is, therefore, a need to optimize PDMS materials for DEAPs.

Optimization of elastomers for DEAPs can be carried out on the basis of the equation for actuation strain introduced by Pelrine *et al* [1] which correlates the electrostatic pressure, P_{el}, to the strain, s, and elastic modulus, Y, according to

$$s = \frac{p_{el}}{Y} = \frac{\varepsilon' \varepsilon_0}{Y} \left(\frac{U}{d}\right)^2 \quad (1)$$

where $\varepsilon_0 = 8.854 \times 10^{-12}$ F m^{-1} is the vacuum permittivity, U is the voltage, d is the thickness of the material and

ε' is the relative dielectric permittivity of the elastomer film. As seen from equation (1), the activation voltage can be lowered by reducing the thickness, decreasing the elastic modulus or increasing the dielectric permittivity of the elastomer. A decrease of the thickness has the strongest effect on reducing the operating voltage. A threshold value of 30–40 μm has, however, been identified in the current large scale processing [5]. The mechanical properties of PDMS elastomers are in general favorable for DEAP uses except for the tear strength, which needs to be improved if handling of thin films is required. The tear strength is, however, acceptable for microapplications where the films are spin coated in layers [6]. Most commonly, reinforcing silica particles are added to the elastomer in concentrations of 10–50 wt%. The reinforcing particles do, however, increase the elastic modulus. Various techniques to lower the elastic modulus have been proposed, such as solvent techniques [7] and bimodal networks [8], but silica is still the most used method to reinforce PDMS elastomers, and thus elastic moduli around 0.1–1 MPa are commonly obtained. A few commercial silicone elastomers for optical uses also rely on resins as reinforcing agents. An alteration of the Young's modulus is prone to introduce significant changes in several important properties, such as the viscous dissipation, hysteresis, long-term stability and, as mentioned earlier, tear strength [9, 10]. The processing of DEAPs in large scale also relies heavily on both the Young's modulus and the tear strength [5]. It is, therefore, most desirable and practical to improve DEAPs by developing elastomer materials with higher dielectric permittivities.

The permittivity is generally improved by the use of fillers, resulting in elastomer composites of metal oxides such as TiO_2 and $BaTiO_3$ [11] and conducting fillers such as expanded graphite [12], carbon nanotubes [13] or conducting polymers [14]. These types of composite systems can, however, exhibit drawbacks such as large dielectric losses and reduced electric breakdown strengths due to agglomeration of fillers and consequent significant changes in mechanical properties. Different techniques have been developed in order to avoid agglomeration; these include encapsulated PANI particles [9, 15] and grafting of permanent dipoles to the PDMS elastomer network [16, 17]. Such systems have shown two- to three-fold increase in the dielectric permittivity of PDMS elastomers, but favorable material properties such as tear strength, electrical breakdown strength and dielectric losses are more difficult to achieve and maintain. This is due to the large required concentration of incorporated particles, which is usually around 10–15 wt% to obtain a significant increase in permittivity. A controlled system which allows for an increase in permittivity even at low concentration of added filler materials would make it possible to achieve and maintain good material properties as well as low dielectric losses. We have recently shown that the development of a novel silicone compatible cross-linker allows for controlled and well distributed grafting of different functional groups into PDMS networks without altering the mechanical properties [18]. This silicone compatible cross-linker contains vinyl groups that permit cross-linking of hydride-terminated PDMS through a platinum catalyzed hydrosilylation reaction. Furthermore, an azide-moiety on the cross-linker allows for click reactions, in this case the copper(I)-catalyzed azide-alkyne cycloaddition (CuAAC), where a 1,4-disubstituted-1,2,3-triazole is formed [19–22]. The azide-group therefore facilitates reactions with various alkyne-functional molecules including alkyne-functional push–pull dipoles. It was shown that even at very low concentration ($\sim$0.25 wt%) of incorporated dipole-functionality at the cross-linking point, a large increase of the dielectric permittivity was achieved. This can be related to the controlled nature of the system, since only one functionality is introduced at each cross-linking site. The functionalization is therefore highly controlled and well distributed within the network.

The aim of this work is to investigate the impact of two different alkyne-functional push–pull dipoles at the cross-linking point on the dielectric permittivity of PDMS elastomers. The PDMS networks will be prepared with varying content of the two dipole-functional cross-linkers using two different lengths of PDMS chains, thus varying the network densities and mechanical properties. Networks prepared with high molecular weight PDMS create softer, highly stretchable films with potential uses as actuators where large strains are desired. Low molecular weight PDMS elastomers are stiffer and less stretchable and therefore find applications within the area of generators where the resonance frequency can be tuned to optimize the performance using the stiffness of the material [23, 24].

2. Experimental details

2.1. General methods

FTIR was performed on a PerkinElmer Spectrum One Fourier transform infrared apparatus equipped with a universal attenuated total reflection (ATR) accessory on a ZnSe/diamond composite. Spectra were recorded in the range of 4000–650 cm^{-1} with 4 cm^{-1} resolution and 16 or 32 scans. ^{1}H-NMR and ^{13}C-NMR experiments were performed on a Bruker 300 MHz spectrometer. Differential scanning calorimetry (DSC) measurements were performed on a DSCQ1000 from TA Instruments. Thermo gravimetric analysis (TGA) was performed on a Q500 from TA Instruments in a nitrogen atmosphere with a heating rate of 10 °C min^{-1} from RT to 950 °C. Mechanical characterization of the prepared films was performed with a TA Instruments TA 2000 rheometer set to a controlled strain mode at 1% strain, which was ensured to be within the linear viscoelastic regime. The measurements were performed with a parallel plate geometry of 25 mm in the frequency range of 100–0.01 Hz. The films were approximately 1 mm thick and the films were measured with a small normal force from the upper plate, which ensured that there were no-slip conditions. Dielectric relaxation spectroscopy (DRS) was performed on a Novocontrol Alpha-A high performance frequency analyzer on discs of $\sim$1 mm thin films. Electrical breakdown strengths were measured on an in-house built device based on international standards (IEC 60243-1 (1998) and IEC 60243-2

(2001)). The film thicknesses were measured with microscopy of cross-sectional cuts and the distance between the spherical electrodes was set accordingly with a micrometer stage and gauge. An indent of less than 5% of sample thickness was added to ensure that the spheres were in contact with the sample. The polymer film ($\sim$150 μm) was slid between the two spherical electrodes (radius of 20 mm) and a stepwise increasing voltage was applied (50–100 V/step) at a rate of 100 V s^{-1}. The average breakdown value was found using the Weibull distribution.

2.2. Materials

Hydride-terminated PDMS, DMS-H31 and DMS-H21 ($\bar{M}_n$ = 28 000 g mol^{-1} and $\bar{M}_n$ = 6000 g mol^{-1}), and a vinyl functional PDMS cross-linker, VDT-431 ($\bar{M}_n$ = 28 000 g mol^{-1}, $\sim$16-functional), were acquired from Gelest Inc. The platinum cyclovinylmethyl siloxane complex catalyst (511) was provided by Hanse Chemie. Silicon dioxide amorphous hexamethyldisilazane treated particles (SIS6962.0) were acquired from Fluorochem. All other chemicals were acquired from Sigma-Aldrich and used as received unless otherwise specified.

2.3. Material preparation

All reactions were carried out under a nitrogen atmosphere. Numbered structures for ^{13}C-NMR assignment can be found in the supporting information (available at stacks.iop.org/SMS/22/104002/mmedia).

*2.3.1. Tris(allyloxy)(3-azidopropyl)silane (**1**).* **1** was synthesized according to a recently published procedure [18] by the silyl ether reaction between (3-bromopropyl)trichlorosilane and allyl alcohol and subsequent substitution of bromine with azide to give an orange-yellow oil (3.91 g, 86%). IR (cm^{-1}): 2870 (C–H stretch); 2095 ($-N_3$ stretch); 1640 (C=C stretch); 1070 (C–O stretch); 1035 (Si–O stretch). ^{1}H NMR ($CDCl_3$, δ_H, ppm): 0.74 (m, 2H, CH_2–Si), 1.71 (m, 2H, CH_2–CH_2–CH_2), 3.26 (*t*, ^3J = 6 Hz, 2H, N_3–CH_2), 4.30 (m, 6H, O–CH_2), 5.12 (dd, ^3J = 10 Hz and ^2J = 1.5 Hz, 3H, CH=C), 5.27 (dd, ^3J = 17.5 Hz and ^2J = 2 Hz, 3H, CH=C), 5.92 (m, 3H, =CH–CH_2). ^{13}C-NMR ($CDCl_3$, δ_C, ppm): 7.60 (4); 27.47 (5); 53.69 (6); 63.58 (3); 114.77 (1); 136.29 (2).

*2.3.2. 4-(4-nitrophenyl)-1-(3-(tris(allyloxy)silyl)propyl)-1H-1,2,3-triazole (**2**).* In the typical case, **1** (1 g, 3.53 mmol) and 1-ethynyl-4-nitrobenzene (0.67 g, 4.41 mmol) were dissolved in THF (35 ml) in a 50 ml two-necked round bottomed flask. CuI (0.84 g, 0.441 mmol) was then added. Et_3N (0.67 g, 6.16 mmol) was subsequently added drop wise. The reaction was carried out at RT for 48 h. The excess 1-ethynyl-4-nitrobenzene was thereafter removed with an azide-functional Merrifield resin [25] (0.757 g, 3.41 mmol). The reaction mixture was filtered and extracted with ethyl acetate (5 × 100 ml). The organic phases were combined and washed with water (3 × 100 ml), dried with $MgSO_4$, filtered and concentrated *in vacuo* to give an orange-yellow oil which crystallized upon cooling (1.35 g, 89%). M_p: 69 °C. IR (cm^{-1}): 3120 (aromatic C–H stretch); 2935–2865 (C–H stretch); 1645 (C=C stretch); 1605 (aromatic C=C stretch); 1510 (N=O asymmetric stretch); 1460 (aromatic C=C stretch); 1335 (N=O symmetric stretch); 1075 (C–O stretch); 1035 (Si–O stretch). ^{1}H NMR ($CDCl_3$, δ_H, ppm): 0.70 (m, 2H, CH_2–Si), 2.11 (m, 2H, CH_2–CH_2–CH_2), 4.31 (m, 2H, N–CH_2–), 4.43 (m, 6H, O–CH_2–), 5.13 (dd, ^3J = 10.5 Hz and ^2J = 1.5 Hz, 3H, CH_2 =C), 5.30 (dd, ^3J = 17 Hz and ^2J = 1.5 Hz, 3H, CH_2 =C), 5.92 (m, 3H, =CH–CH_2), 7.91 (s, 1H, –C=CH–N–), 7.98–8.01 (m, 2H, Ar–H), 8.25–8.33 (m, 2H, NO_2–Ar–H). ^{13}C-NMR ($CDCl_3$, δ_C, ppm): 7.46 (4); 24.04 (5); 52.56 (6); 63.82 (3); 115.03 (1); 121.19 (7); 124.27 (11); 126.04 (10); 136.16 (2); 136.96 (9); 145.39 (12); 147.21 (8).

*2.3.3. 4-(4-nitrophenylazo)phenol (**3**).* **3** was synthesized according to a previously published procedure [26] by a diazotization reaction with 4-nitroaniline and phenol. M_p = 210 °C. IR (cm^{-1}): 3340 (–OH stretch); 3115 (aromatic C–H stretch); 1600 (aromatic C=C stretch); 1502 (N=O asymmetric stretch); 1455 (aromatic C=C stretch); 1400 (N=N stretch); 1330 (N=O symmetric stretch). ^{1}H NMR (DMSO-d_6, δ_H, ppm): 6.97 (m, 2H, O–Ar–H), 7.87 (m, 2H, N–Ar–H), 7.97 (m, 2H, N–Ar(NO_2)–H), 8.39 (m, 2H, NO_2–Ar–H), 10.61 (s, 1H, –OH). ^{13}C-NMR (DMSO-d_6, δ_C, ppm): 116.12 (2); 122.88 (6); 124.90 (7); 125.70 (3); 145.29 (4); 147.64 (8); 155.43 (5); 162.24 (1).

*2.3.4. 3-(4-((4-nitrophenyl)diazenyl)phenoxy)-prop-1-yn-1-ylium (**4**).* **3** (3 g, 1.23 mmol) was dissolved in dry acetone (150 ml) in a 250 ml two-necked round bottomed flask. K_2CO_3 (4.26 g, 3.08 mmol) and 18-crown-6 (0.27 g, 0.104 mmol) were then added and the reaction mixture was stirred vigorously for 30 min. Propargylbromide (5.13 g, 4.31 mmol) was subsequently added at a rate of 1.15 ml min^{-1}. The reaction was carried out under reflux for 72 h. The reaction mixture was now quenched with H_2O (150 ml) and was extracted with ethyl acetate (7 × 150 ml). The organic phases were combined and washed with H_2O (3 × 150 ml) and brine (1 × 150 ml), dried with $MgSO_4$, filtered and concentrated *in vacuo*. The crude was recrystallized in an ethyl acetate/heptane mixture (1:0.6) to give the product in the form of a dark orange solid (1.89 g, 55%). M_p: 202 °C. IR (cm^{-1}): 3265 (C≡C–H stretch); 3070 (aromatic C–H stretch); 2130 (C≡C stretch); 1600 (aromatic C=C stretch); 1515 (N=O asymmetric stretch); 1455 (aromatic C=C stretch); 1415 (N=N stretch); 1340 (N=O symmetric stretch). ^{1}H NMR (DMSO-d_6, δ_H, ppm): 2.51 (s, 1H, C≡C–H), 4.96 (d, 2H, ^4J = 2 Hz, O–CH_2–), 7.23 (m, 2H, O–Ar–H), 7.99 (m, 2H, N–Ar–H), 8.03 (m, 2H, N–Ar(NO_2)–H), 8.41 (m, 2H, NO_2–Ar–H). ^{13}C-NMR ($CDCl_3$, δ_C, ppm): 55.90 (3); 78.54 (1); 78.77 (2); 115.63 (5); 123.11 (9); 124.97 (10); 125.19 (6); 146.54 (7); 147.99 (11); 155.23 (8); 160.85 (4).

*2.3.5. 3-((4-((4-nitrophenyl)diazenyl)phenoxy)methyl)-1-(3-(tris(allyloxy)silyl)propyl)-1H-1,2,3-triazole (**5**).* In the typical case, **1** (1.56 g, 5.50 mmol) and **4** (1.55 g, 5.50 mmol) were dissolved in THF (75 ml) in a 100 ml two-necked round bottomed flask. CuI (0.105 g, 0.55 mmol) was then added. Et_3N (0.86 g, 8.53 mmol) was subsequently added drop wise. The reaction was carried out at 45 °C for 48 h. The reaction was now quenched with water (100 ml) and extracted with ethyl acetate (7 × 100 ml). The organic phases were combined and washed with water (3 × 100 ml) and brine (1 × 100 ml), dried with $MgSO_4$, filtered and concentrated *in vacuo*. The product was thereafter recrystallized in 2-propanol to give an orange-red solid (2.00 g, 65%). M_p = 86 °C. IR (cm^{-1}): 2922–2870 (C–H stretch); 1600 (aromatic C=C stretch); 1580 (C=C stretch); 1510 (N=O asymmetric stretch); 1455 (aromatic C=C stretch); 1340 (N=O symmetric stretch); 1070 (C–O stretch); 1035 (Si–O stretch). ^{1}H NMR ($CDCl_3$, δ_H, ppm): 0.65 (m, 2H, CH_2–Si), 2.05 (m, 2H, CH_2–CH_2–CH_2), 4.26 (m, 2H, N–CH_2–), 4.36 (m, 6H, Si–O–CH_2–), 5.10 (dd, ^3J = 10.5 Hz and ^2J = 1.5 Hz, 3H, CH_2 =C), 5.25 (dd, ^3J = 18 Hz and ^2J = 1.8 Hz, 3H, CH_2 =C), 5.29 (s, 2H, Ar–O–CH_2–), 5.89 (m, 3H, = CH–CH_2), 7.12 (m, 2H, O–Ar–H), 7.65 (s, 1H, –C= CH–N–), 7.94 (m, 2H, N–Ar–H), 7.96 (m, 2H, N–Ar(NO_2)-H), 8.32 (m, 2H, NO_2–Ar–H). ^{13}C-NMR ($CDCl_3$, δ_C, ppm): 7.41 (4); 23.96 (5); 52.43 (6); 62.25 (9); 63.74 (3); 114.95 (1); 115.19 (11); 122.87 (7); 123.06 (15); 124.61 (16); 125.51 (12); 136.13 (2); 143.13 (8); 147.08 (13); 148.20 (17); 155.86 (14); 161.75 (10).

2.3.6. Preparation of polymer films. Films with **2**: appropriate amounts of cross-linker **2** (for eight different films) (0, 0.037, 0.073, 0.118 mmol for 28 000 g mol^{-1} PDMS films and 0, 0.219, 0.364, 0.573 mmol for 6000 g mol^{-1} PDMS films) were dissolved in dry THF and mixed with 16-functional cross-linker (VDT-431) (0.024, 0.019, 0.013, 0.005 mmol for 28 000 g mol^{-1} PDMS films and 0.083, 0.055, 0.037, 0.011 mmol for 6000 g mol^{-1} PDMS films) and hydride-terminated PDMS: 28 000 g mol^{-1} (DMS-H31): 0.199, 0.205, 0.211, 0.217 mmol; 6000 g mol^{-1} (DMS-H21): 0.142, 0.165, 0.181, 0.204 mmol. Treated silica particles were added (10 wt%) and the mixture was mixed on a FlackTek Inc. DAC 150.1 FVZ-K SpeedMixer™ to obtain 0, 0.23, 0.45, 0.72, 1.35, 2.25 and 3.6 wt% of functional cross-linker in the PDMS films corresponding to 0, 0.08, 0.15, 0.24, 0.46, 0.77 and 1.20 wt% of pure dipole. The catalyst (511) (5–10) ppm in dry THF was added thereafter and the mixture was once more mixed on the SpeedMixer™. The mixture was poured into 1 mm thick steel molds on a fluorinated ethylene propylene (FEP) release liner and furthermore coated as 150 μm films on a glass substrate and cured at 60 °C.

Films with **5**: films with cross-linker **5** were prepared analogously to films with **2** using 0, 0.028, 0.056, 0.089 mmol for 28 000 g mol^{-1} PDMS films and 0, 0.167, 0.278, 0.446 mmol for 6000 g mol^{-1} PDMS films of **5**, 0.024, 0.020, 0.016, 0.010 mmol for 28 000 g mol^{-1} PDMS films and 0.083, 0.061, 0.048, 0.027 mmol for 6000 g mol^{-1} PDMS films of 16-functional cross-linker (VDT-431) and 0.199, 0.203, 0.208, 0.213 mmol of 28 000 g mol^{-1} PDMS (DMS-H31) and 0.142, 0.159, 0.171, 0.189 mmol of 6000 g mol^{-1} PDMS (DMS-H21) and 10 wt% of surface-treated silica particles to create 0, 0.225, 0.45, 0.72, 1.35, 2.25 and 3.6 wt% of functional cross-linker in the PDMS films, corresponding to 0, 0.11, 0.22, 0.36, 0.67, 1.12 and 1.79 wt% of pure dipole.

2.4. Swelling experiments

The gel fractions were determined using swelling experiments where samples of all the prepared films were swelled in chloroform at RT for 48 h. The chloroform was replaced after 24 h. The solvent was decanted and the films were washed several times. The samples were thereafter dried for 24 h. Gel fractions were calculated as the weight after extraction and drying (m_e) divided by the initial weight of the sample (m_0) as $W_{gel} = m_e/m_0$.

3. Results and discussion

The azide-functional vinyl cross-linker was synthesized using a recently published procedure [18]. The azide cross-linker (**1**) was obtained as an orange-yellow oil in high yield and of high purity. The vinyl cross-linker was thereafter used in a click reaction (the copper(I)-catalyzed azide-alkyne cycloaddition (CuAAC)) with 1-ethynyl-4-nitrobenzene in THF using a CuI/Et_3N catalytic system to give **2** according to scheme 1.

The alkyne-functional nitroazobenzene, **4**, was prepared via a Williamson ether synthesis of 4-(4-nitrophenylazo) phenol (**3**) and propargyl bromide with a K_2CO_3/18-crown-6 catalytic system, as shown in scheme 2.

The nitroazobenzene dipole, **4**, was used in a click reaction with **1** using similar reaction conditions to those in the case of **2** according to scheme 3.

The alkyne-functional nitroazobenzene, **4**, as well as the two click products, **2** and **5**, were characterized using FTIR and ^{1}H- and ^{13}C-NMR. In the case of **4**, FTIR was used to follow the progress of the reaction by the disappearance of the broad –OH band at 3340 cm^{-1} as well as the appearance of the sharp –C≡C–H band at 3265 cm^{-1} and the small –C≡C band at 2130 cm^{-1}. FTIR was furthermore used to verify the completion of the click reactions by following the disappearance of the alkyne (∼3300 cm^{-1}) and azide (∼2100 cm^{-1}) bands. ^{1}H-NMR was used to confirm the formation of the click products **2** and **5** by identification of the triazole proton at δ_H = 7.91 ppm and δ_H = 7.65 ppm, respectively.

Dipole-functional PDMS networks were created using cross-linker **2** or **5**, hydride-terminated PDMS of 28 000 g mol^{-1} or 6000 g mol^{-1} and a platinum catalyst according to scheme 4.

The functional PDMS films were reinforced with a 16-functional commercial vinyl cross-linker (scheme 4) as well as surface-treated silica particles (10 wt%). The 16-functional cross-linker was employed in order to be able to vary the content of dipole-functional cross-linker and furthermore because networks prepared from three-functional cross-linkers alone are known to be very soft and have very

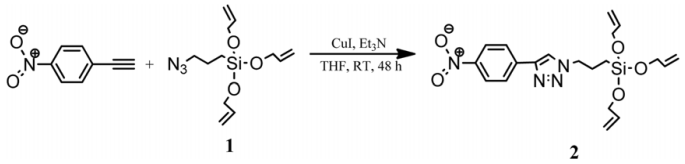

Scheme 1. The click reaction of azide-functional cross-linker (**1**) and 1-ethynyl-4-nitrobenzene.

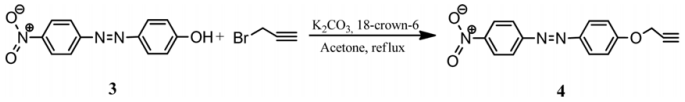

Scheme 2. Williamson ether synthesis giving the alkyne-functional nitroazobenzene **4**.

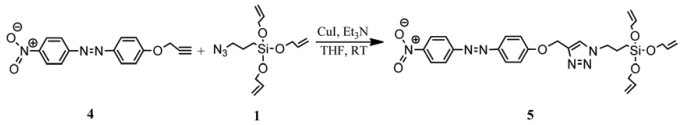

Scheme 3. The click reaction of azide-functional cross-linker (**1**) and **4** yielding the nitroazobenzene cross-linker **5**.

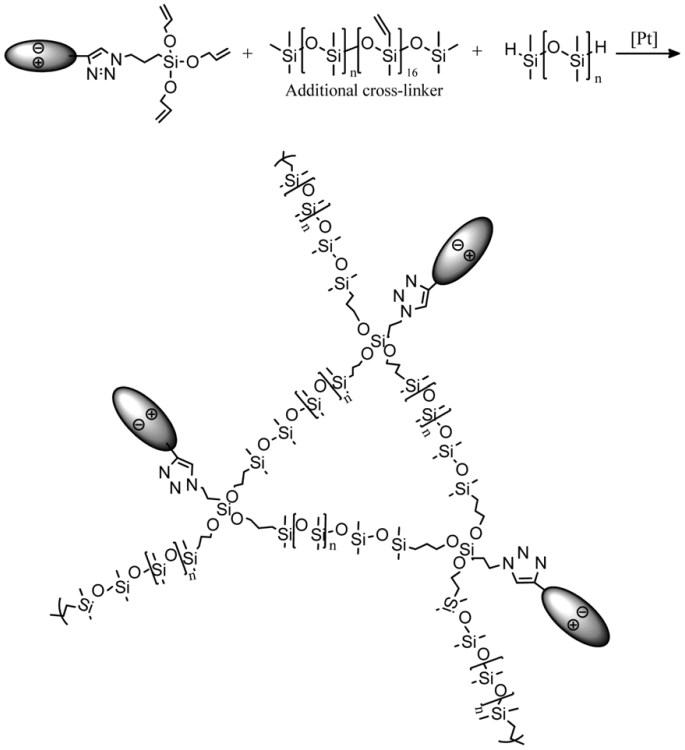

Scheme 4. The PDMS cross-linking reaction between functional dipole cross-linkers and hydride-terminated PDMS.

low mechanical breakdown strength [27]. The ratio between the three-functional dipole cross-linker and the commercial cross-linker was varied to create PDMS films of 0.23–3.6 wt% of dipolar cross-linker, corresponding to concentrations of 0.08–1.20 wt% of pure dipole for **2** and 0.11–1.79 wt% of pure dipole for **5**. Reference films prepared solely

Table 1. Gel fractions (W_{gel}) in % as result of swelling experiments for both dipole cross-linkers.

Cross-linker content (wt%)	Films with cross-linker **2**	Films with cross-linker **5**
28 000 g mol^{-1}		
0.00	92.1	92.1
0.23	80.9	89.4
0.45	86.8	88.9
0.72	64.0	89.9
6000 g mol^{-1}		
0.00	95.0	95.0
1.35	95.3	97.4
2.25	90.6	93.2
3.60	76.9	92.8

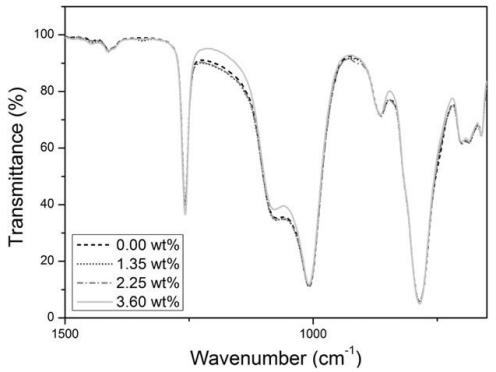

Figure 1. FTIR spectra of 6000 g mol^{-1} PDMS films prepared with cross-linker **2** from 1500–650 cm^{-1}.

with 16-functional commercial cross-linker were also made. All networks were prepared in stoichiometric cross-linking reactions, meaning that the number of functional hydride groups of the PDMS chains corresponded to the total number of vinyl groups on the cross-linkers.

FTIR was used to characterize all the prepared PDMS films. As an example, the enlarged spectra for 6000 g mol^{-1} films with cross-linker **2** are shown in figure 1 (all other spectra are available as supporting information available at stacks.iop.org/SMS/22/104002/mmedia).

At high cross-linker concentration the PDMS bands decrease due to increasing content of dipole-cross-linker. This is especially seen from the 1100–1000 cm^{-1} bands which are due to Si–O stretch.

The gel fractions of the films were determined from swelling experiments with chloroform. The swelling experiments were used to determine the amount of bonded (gel fraction) and non-bonded (sol fraction) species in the network. As seen in table 1, the gel fraction decreases slightly with increasing amount of dipole-functional cross-linker. This decrease can be explained by the increasing amount of three-functional cross-linker which creates an increasingly softer network with a consequent larger concentration of non-bonded species and substructures. In optimized PDMS systems, where the amount of cross-linker is in excess with a stoichiometry of 1.1–1.4, gel fractions are usually of the order of 95–97% as not all cross-linking sites need to react and steric hindrance is thus reduced [28]. Stoichiometric networks usually have lower gel fractions of around 90% but have the advantage that no unbound cross-linker will be present in the system [29]. The PDMS networks prepared in this study were prepared stoichiometrically in order to avoid non-bonded functional cross-linker, and gel fractions around or lower than 90% are thus expected.

By visual comparison of the films before and after the extraction experiments it is evident that all films retained their color after the extraction which is due to the dipole-functional cross-linkers remaining in the networks. We have previously proved, by use of a fluorescent functionality attached at the cross-linker, that small amounts only of the functional cross-linkers are extracted from the networks and that the sol fractions most likely predominantly consist of substructures such as inert or mono-functional PDMS [18].

The influence of the concentration and type of the dipole-functional cross-linkers on the mechanical properties was investigated by determining the shear storage and shear loss modulus of the prepared films. In figure 2 the results for films with cross-linker **2** and cross-linker **5**, respectively, are presented. In the linear regime, which for silicone elastomers is up to approximately 15% strain [28], the elastic and viscous properties are well described by the shear storage modulus (G') and the shear loss modulus (G''). Both are defined from the complex shear modulus as $G^*(\omega) = G'(\omega) + iG''(\omega)$. Due to the incompressibility of silicones (Poisson ratio (ν) close to 0.5) the Young's modulus can be determined as $Y = 2(1 + \nu)G = 3G$ where $G = G'(\omega \to 0)$. For all films in figure 2 it is seen that there is an insignificant dependence only of G' on the applied frequency such that $Y = 3G'$. Thereby we obtain Young's moduli, which describe the frequency-independent elastic moduli up to approximately 15% strain. Furthermore, we can determine the highly frequency dependent viscous loss from G''.

Furthermore, it can be seen from figure 2 that all networks with cross-linkers **2** and **5** for both 28 000 g mol^{-1} and 6000 g mol^{-1} PDMS are well cross-linked as the storage modulus (G') is 10–100 times larger than the loss

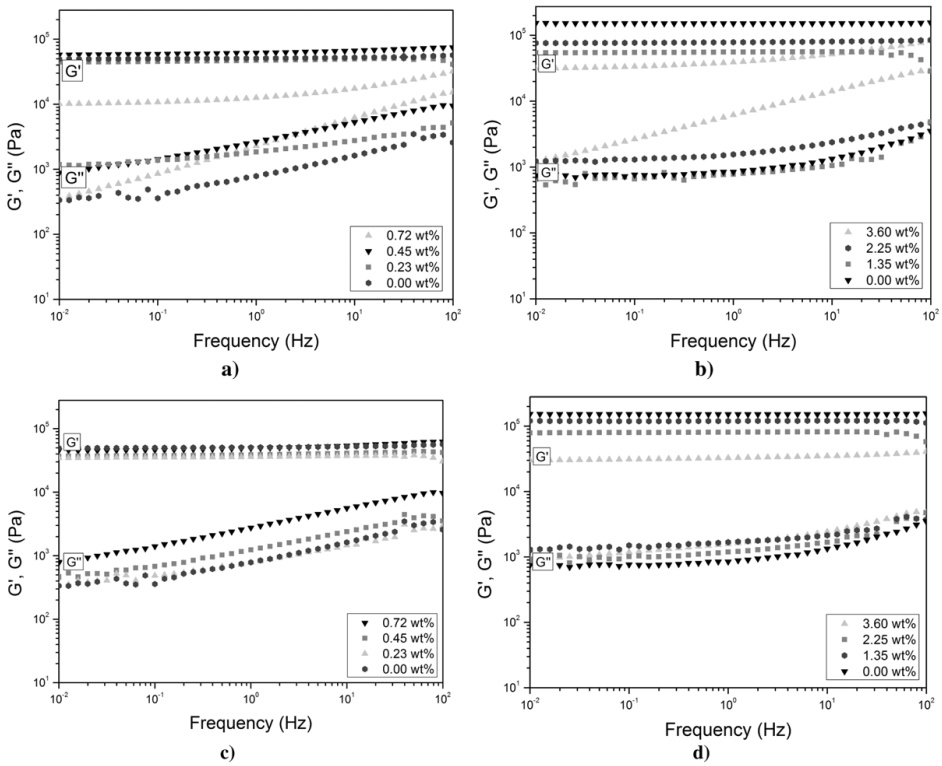

Figure 2. The storage modulus (G') and loss modulus (G'') as functions of frequency for films prepared with (a) cross-linker **2** and 28 000 g mol^{-1} PDMS, (b) cross-linker **2** and 6000 g mol^{-1} PDMS, (c) cross-linker **5** and 28 000 g mol^{-1} PDMS and (d) cross-linker **5** and 6000 g mol^{-1} PDMS.

modulus (G'') for the investigated frequency regime, with the difference being smallest at high frequencies (100 Hz). This means that the viscous dissipation at the low-strain, low-frequency limit is a few per cent only.

It can also be seen that films prepared with the lower molecular weight PDMS (6000 g mol^{-1}) have higher moduli than films prepared with the higher molecular weight PDMS (28 000 g mol^{-1}). This is due to an increased network density which creates stiffer films. From fundamental theories on rubber elasticity the elastic moduli are expected to scale linearly with the inverse molecular weight, but our systems contain fillers and the high molecular weight PDMS is furthermore above the entanglement threshold [28], which explains the weaker dependence on molecular weight. For films with cross-linker **2** the elastomers containing large concentrations of three-functional cross-linker (0.72 wt% for 28 000 g mol^{-1} and 3.6 wt% for 6000 g mol^{-1}) are seen to have slightly lower moduli than the films prepared solely with the 16-functional commercial cross-linker. This can be explained by the cross-linker functionality (f) which is known to have a significant impact on the stiffness of elastomers since classical rubber theories predict that the elastic modulus scales with $1 - 2/f$ [27]. For PDMS films prepared with a large content of three-functional cross-linker a softer network is created than for films with 16-functional cross-linker alone.

The prepared networks contain 10 wt% silica particles to reinforce the otherwise fairly weak films (with respect to tearing). The particles limit the mobility of the polymer chains, both the dangling and the sol ones, in the network and decrease the conversion of the hydrosilylation reaction due to limitations in the mobility of the reactive groups. The networks are thus believed to be prone to post-curing. Overall, the elastic properties have not changed extensively with the addition of the two different dipole-functional cross-linkers but the viscous loss is increased with increased loadings of cross-linker.

For further description of the mechanical properties at larger strains it has previously been shown that the non-linear behavior of a similar elastomer is very well described by the Mooney–Rivlin equations for Hencky strains up to 0.8 in an in-house built filament stretch rheometer [30] with a specialized holder for elastomers to allow for very large elongations [27]. For a filament of this type the elongation in the direction of elongation is given by $\exp(0.8) = 2.23 = 223\%$. Of course, it may not be sufficient to rely on a model for descriptions of the high-strain

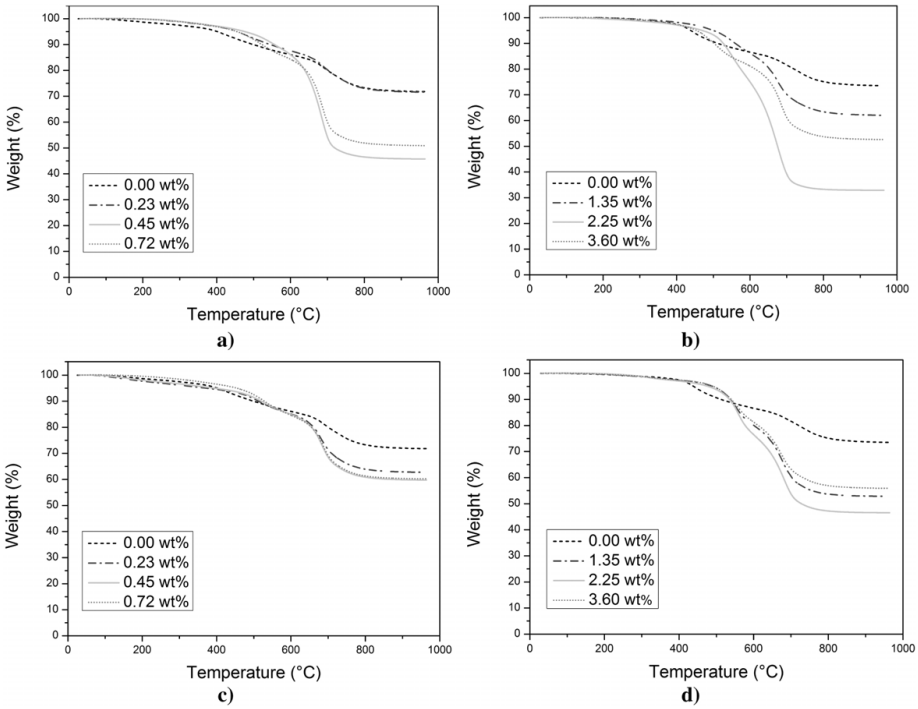

Figure 3. TGA results for films prepared with (a) cross-linker **2** and 28 000 g mol^{-1} PDMS, (b) cross-linker **2** and 6000 g mol^{-1} PDMS, (c) cross-linker **5** and 28 000 g mol^{-1} PDMS and (d) cross-linker **5** and 6000 g mol^{-1} PDMS.

limit due to the very often encountered problems caused by electromechanical instabilities [31–34]. The non-linear rheology can be measured carefully by means of the very precise, but tedious and time-consuming, methods developed by Bejenariu *et al* [27] for uniaxial elongation and by Jensen *et al* [10, 35] for planar elongation. Alternatively, commercial technologies based on the engineering stress nominal strain are readily available.

Furthermore, for a full validation of the applicability of the developed materials as dielectric elastomers, life-time tests would have to be performed. This will be investigated in the future.

The effect of the two dipole-functional cross-linkers on the thermal stability of the PDMS networks was determined by thermal gravimetric analysis (TGA). The results for films with cross-linker **2** and cross-linker **5** are shown in figure 3.

All the prepared films show a two-step mass loss process with all degradation temperatures summarized in table 2.

All degradation temperatures are taken as the peak temperature of the first derivative of the temperature with time. The first degradation step temperature which is due to cleavage of Si–CH_3 bonds is increased with the addition of dipolar cross-linkers compared to the PDMS films made completely with the commercial cross-linker. The second decomposition step temperatures, where mineralization of the material occurs, decrease slightly with the addition of dipole cross-linkers. All films containing a functionalized cross-linker have higher initial decomposition temperatures than films with non-functionalized cross-linker. Both cross-linkers can therefore be said to improve the thermal stability of PDMS networks.

The impact of the type of push–pull dipole-cross-linker on the dielectric properties was determined by dielectric relaxation spectroscopy on discs of ∼1 mm thin films. Dielectric relaxation spectra showing the frequency dependent relative permittivity (ε') and loss tangent ($\tan\delta$) for films with cross-linkers **2** and **5** are presented in figure 4.

For both cross-linkers an increase in dielectric permittivity is observed by the addition of dipole-functional cross-linker. In all cases, the effect is largest at the lowest amount of added dipole cross-linker. Compared to pure PDMS with only commercial cross-linker for which $\varepsilon' = 2.8$ at 100 Hz, the film prepared with 6000 g mol^{-1} PDMS containing 1.35 wt% of cross-linker **2** has $\varepsilon' = 3.3$ at 100 Hz. This corresponds to an increase of ∼20% at only 0.46 wt% of pure dipole. Cross-linkers **2** and **5** induce an enhancement of the permittivity of the same order of magnitude. Furthermore, the dielectric permittivity stays constant in the entire frequency range. For all films, the dielectric loss remains exceptionally low after addition of dipole cross-linkers which means that all films exhibit very low dissipation of energy. The measured values of ε' and $\tan\delta$ at 100 Hz are summarized for all films in table 3.

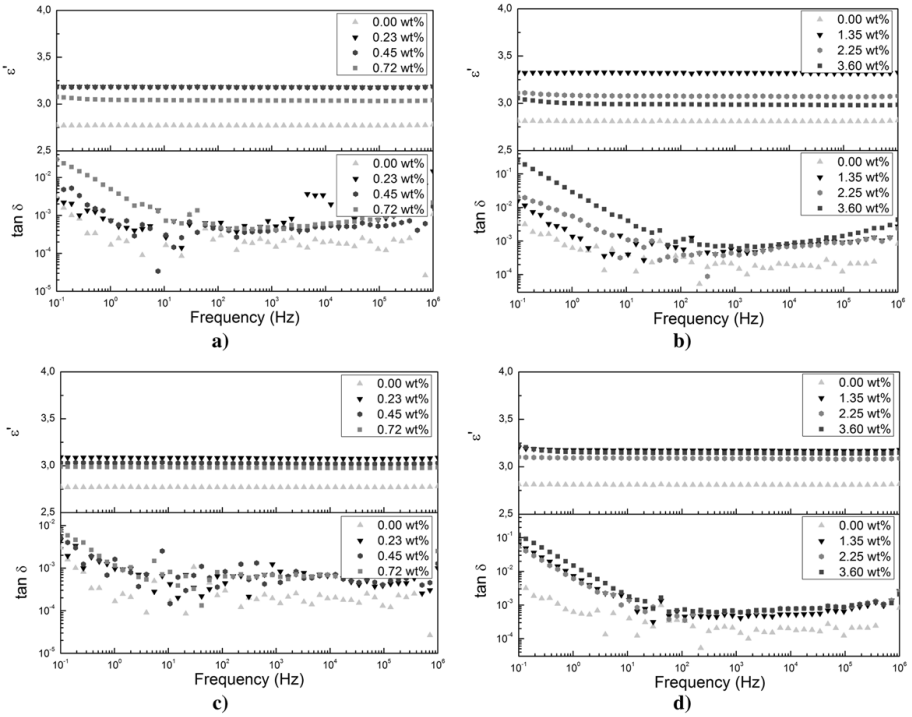

Figure 4. The relative dielectric permittivity (ε') and loss tangent ($\tan\delta$) as functions of frequency for films prepared with (a) cross-linker **2** and 28 000 g mol^{-1} PDMS, (b) cross-linker **2** and 6000 g mol^{-1} PDMS, (c) cross-linker **5** and 28 000 g mol^{-1} PDMS and (d) cross-linker **5** and 6000 g mol^{-1} PDMS.

Table 2. Thermal stability data for films prepared with cross-linkers **2** and **5**.

Cross-linker content (wt%)	Films with cross-linker **2**		Films with cross-linker **5**	
	First degradation step (°C)	Second degradation step (°C)	First degradation step (°C)	Second degradation step (°C)
28 000 g mol^{-1}				
0.00	419	692	419	692
0.23	475	689	513	683
0.45	550	683	523	684
0.72	529	684	531	686
6000 g mol^{-1}				
0.00	444	722	444	722
1.35	555	673	554	682
2.25	550	675	560	683
3.60	508	687	555	674

The electrical breakdown strengths, E_B, for films with cross-linkers **2** and **5** are presented in table 3. For films with cross-linker **5**, an increase in the breakdown field strength was observed with the addition of a low amount of cross-linker for both 28 000 g mol^{-1} and 6000 g mol^{-1} films. In both cases, the measured values of 95.0 V μm^{-1} and 124 V μm^{-1}, respectively, are remarkably high. For cross-linker **2**, the electrical breakdown strengths decrease with increasing concentration of dipolar cross-linker but remain high at low concentrations. The reduction in breakdown strength at high concentration of functional cross-linker could be caused by the reduction in the stiffness [36] which is observed from the mechanical characterization. For all films the breakdown strength stays above ~40 V μm^{-1}, which is high enough for most DEAP applications and in the range of commercially

Table 3. The dielectric permittivity (ε') and loss tangent ($\tan\delta$) at 100 Hz as well as the breakdown strength (E_B) for films with different type and weight per cent of cross-linker.

	Films with cross-linker **2**			Films with cross-linker **5**		
Cross-linker content (wt%)	ε'	$\tan\delta$	E_B (V μm^{-1})	ε'	$\tan\delta$	E_B (V μm^{-1})
28 000 g mol^{-1}						
0.00	2.8	2.69×10^{-4}	91.8	2.8	2.69×10^{-4}	91.8
0.23	3.2	5.78×10^{-4}	88.2	3.1	5.25×10^{-4}	95.0
0.45	3.2	4.54×10^{-4}	49.9	3.0	6.33×10^{-4}	88.9
0.72	3.0	5.24×10^{-4}	39.0	3.0	7.03×10^{-4}	85.9
6000 g mol^{-1}						
0.00	2.8	3.45×10^{-4}	111.0	2.8	3.45×10^{-4}	111.0
1.35	3.3	6.01×10^{-4}	91.9	3.2	5.21×10^{-4}	124.2
2.25	3.1	3.34×10^{-4}	71.8	3.1	4.04×10^{-4}	68.2
3.60	3.0	10.5×10^{-4}	na[a]	3.2	7.16×10^{-4}	57.0

[a] Attempts to obtain the electrical breakdown strength were unsuccessful as the prepared 150 μm film was too sticky to be handled.

available products such as Elastosil RT625 from Wacker Chemie AG, as stated by the manufacturer [11].

4. Conclusion

A novel method of enhancing the electromechanical properties of silicone elastomers by grafting of push–pull dipoles to a synthesized cross-linker was presented. The silicone compatible cross-linker allows for click reactions with various alkyne-functional molecules and thereby creates controlled and well distributed dipole-functionalized PDMS networks. Two different push–pull dipole cross-linkers were prepared with the alkynes 1-ethynyl-4-nitrobenzene and 3-(4-((4-nitrophenyl)diazenyl)phenoxy)-prop-1-yn-1-ylium by click chemistry. The synthesized cross-linkers were used to prepare PDMS films using two different chain lengths with concentrations of 0–3.6 wt% cross-linker, corresponding to 0–1.8 wt% of pure dipole. The thermal, mechanical and electromechanical properties of these dipole-functionalized PDMS networks were investigated by various techniques. Mechanical characterization showed that the mechanical properties did not change significantly by increasing the content of dipole-functional cross-linker. Dielectric permittivity measurements proved an increase in the relative permittivity of ~20% at only 0.46 wt% of incorporated dipole. Furthermore, the dielectric losses were remarkably low while the electrical breakdown strengths were high.

Acknowledgments

The authors wish to express thanks to Mikkel Lotz and Mads Boll for help with the production of the thin films and acknowledge the Danish National Advanced Technology Foundation for financial support.

References

[1] Pelrine R, Kornbluh R, Pei Q and Joseph J 2000 High-speed electrically actuated elastomers with strain greater than 100% *Science* **287** 836–9

[2] Löwe C, Zhang X and Kovacs G 2005 Dielectric elastomers in actuator technology *Adv. Eng. Mater.* **7** 361–7

[3] Brochu P and Pei Q 2010 Advances in dielectric elastomers for actuators and artificial muscles *Macromol. Rapid Commun.* **31** 10–36

[4] Mark J E 1990 Silicon-containing polymers *Silicon-Based Polymer Science: A Comprehensive Resource* ed J M Zeigler and F W G Fearon (Washington, DC: American Chemical Society) pp 47–68

[5] Vudayagiri S, Junker M D and Skov A L 2012 Factors affecting surface and release properties of thin polydimethylsiloxane films *Polym. J.* at press

[6] Balakrisnan B and Smela E 2010 Challanges in the microfabrication of dielectric elastomer actuators *Proc. SPIE* **7642** 76420K

[7] Larsen A L, Sommer-Larsen P and Hassager O 2004 How to tune rubber elasticity *Proc. SPIE* **5385** 108–17

[8] Bejenariu A G, Yu L and Skov A L 2012 Low moduli elastomers with low viscous dissipation *Soft Matter* **8** 3917

[9] Molberg M, Crespy D, Rupper P, Nüesch F, Månson J-A E, Löwe C and Opris D M 2010 High breakdown field dielectric elastomer actuators using encapsulated polyaniline as high dielectric constant filler *Adv. Funct. Mater.* **20** 3280–91

[10] Jensen M K, Rasmussen H K, Skov A L and Hassager O 2011 Reversed planar elongation of soft polymeric networks *Rheol. Acta* **50** 729–40

[11] Skov A L, Bejenariu A, Bøgelund J, Benslimane M and Egede A D 2012 Influence of micro- and nanofillers on electro-mechanical performance of silicone EAPs *Proc. SPIE* **8340** 83400M

[12] Daugaard A E, Hassouneh S S, Kostrzewska M, Bejenariu A G and Skov A L 2013 High dielectric permittivity elastomers from well-dispersed expanded graphite in low concentration *Proc. SPIE* at press

[13] Dang Z-M, Wang L, Yin Y, Zhang Q and Lei Q-Q 2007 Giant dielectric permittivities in functionalized carbon-nanotube/electroactive-polymer nanocomposites *Adv. Mater.* **19** 852–7

[14] Carpi F, Gallone G, Galantini F and De Rossi D 2008 Silicone–poly(hexylthiophene) blends as elastomers with enhanced electromechanical transduction properties *Adv. Funct. Mater.* **18** 235–41

[15] Opris D M, Molberg M, Walder C, Ko Y S, Fischer B and Nüesch F A 2011 New silicone composites for dielectric elastomer actuator applications in competition with acrylic foil *Adv. Funct. Mater.* **21** 3531–9

[16] Kussmaul B, Risse S, Kofod G, Waché R, Wegener M, McCarthy D N, Krüger H and Gerhard R 2011 Enhancement of dielectric permittivity and electromechanical response in silicone elastomers: molecular grafting of organic dipoles to the macromolecular network *Adv. Funct. Mater.* **21** 4589–94

[17] Kussmaul B, Risse S, Wegener M, Kofod G and Krüger H 2012 Matrix stiffness dependent electro-mechanical response of dipole grafted silicones *Smart Mater. Struct.* **21** 064005

[18] Madsen F B, Dimitrov I, Daugaard A E, Hvilsted S and Skov A L 2013 Novel cross-linkers for PDMS networks for controlled and well distributed grafting of functionalities by click chemistry *Polym. Chem.* **4** 1700–7

[19] Kolb H C, Finn M G and Sharpless K B 2001 Click chemistry: diverse chemical function from a few good reactions *Angew. Chem. Int. Edn Engl.* **40** 2004–21

[20] Wu P, Feldman A K, Nugent A K, Hawker C J, Scheel A, Voit B, Pyun J, Fréchet J M J, Sharpless K B and Fokin V V 2004 Efficiency and fidelity in a click-chemistry route to triazole dendrimers by the copper(i)-catalyzed ligation of azides and alkynes *Angew. Chem. Int. Edn Engl.* **43** 3928–32

[21] Meldal M 2008 Polymer clicking by CuAAC reactions *Macromol. Rapid Commun.* **29** 1016–51

[22] Binder W H and Sachsenhofer R 2008 'Click' chemistry in polymer and material science: an update *Macromol. Rapid Commun.* **29** 952–81

[23] Chiba S, Waki M, Kornbluh R and Pelrine R 2008 Innovative power generators for energy harvesting using polymer artificial muscles *Proc. SPIE* **6927** 692715

[24] Sarban R 2011 Active vibration control using DEAP transducers *PhD Thesis* University of Southern Denmark

[25] Opsteen J A and Van Hest J C M 2005 Modular synthesis of block copolymers via cycloaddition of terminal azide and alkyne functionalized polymers *Chem. Commun.* 57–9

[26] Pedersen M 1997 New azobenzene side-chain polyesters for optical information storage *PhD Thesis* Technical University of Denmark

[27] Bejenariu A G, Rasmussen H K, Skov A L, Hassager O and Frankaer S M 2010 Large amplitude oscillatory extension of soft polymeric networks *Rheol. Acta* **49** 807–14

[28] Larsen A L, Hansen K, Sommer-Larsen P, Hassager O, Bach A, Ndoni S and Jørgensen M 2003 Elastic properties of nonstoichiometric reacted PDMS networks *Macromolecules* **36** 10063–70

[29] Frankær S M G, Jensen M K, Bejenariu A G and Skov A L 2012 Investigation of the properties of fully reacted unstoichiometric polydimethylsiloxane networks and their extracted network fractions *Rheol. Acta* **51** 559–67

[30] Bach A, Almdal K, Rasmussen H K and Hassager O 2003 Elongational viscosity of narrow molar mass distribution polystyrene *Macromolecules* **36** 5174–9

[31] Stark K H and Garton C G 1955 Electric strength of irradiated polythene *Nature* **176** 1225–6

[32] Huang J, Li T, Chiang Foo C, Zhu J, Clarke D R and Suo Z 2012 Giant, voltage-actuated deformation of a dielectric elastomer under dead load *Appl. Phys. Lett.* **100** 041911

[33] Zhao X, Hong W and Suo Z 2007 Electromechanical hysteresis and coexistent states in dielectric elastomers *Phys. Rev.* B **76** 134113

[34] De Tommasi D, Puglisi G and Zurlo G 2011 Compression-induced failure of electroactive polymeric thin films *Appl. Phys. Lett.* **98** 123507

[35] Jensen M K, Hassager O, Rasmussen H K, Skov A L, Bach A and Koldbech H 2010 Planar elongation of soft polymeric networks *Rheol. Acta* **49** 1–13

[36] Kollosche M and Kofod G 2010 Electrical failure in blends of chemically identical, soft thermoplastic elastomers with different elastic stiffness *Appl. Phys. Lett.* **96** 071904

Supporting Information

Dipolar cross-linkers for PDMS networks with enhanced dielectric permittivity and low dielectric loss

Frederikke Bahrt Madsen[1], Anders Egede Daugaard[1], Søren Hvilsted[1], Mohamed Yahia Benslimane[2] and Anne Ladegaard Skov[1]*

[1]DTU, The Danish Polymer Centre, Department of Chemical and Biochemical Engineering, DK-2800 Kgs. Lyngby, Denmark

[2]Danfoss PolyPower A/S, Nordborgvej 81, DK-6430 Nordborg

E-mail: al@kt.dtu.dk

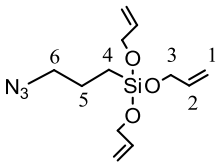

1

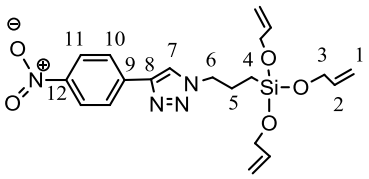

2

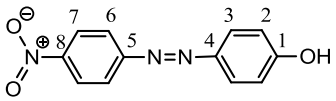

3

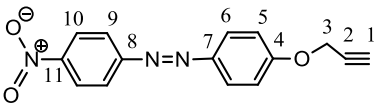

4

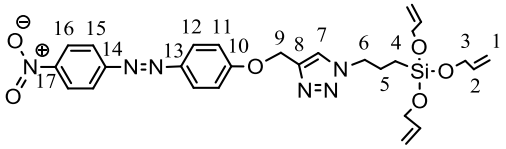

5

Figure S1. Numbered structures for ^{13}C-NMR assignment.

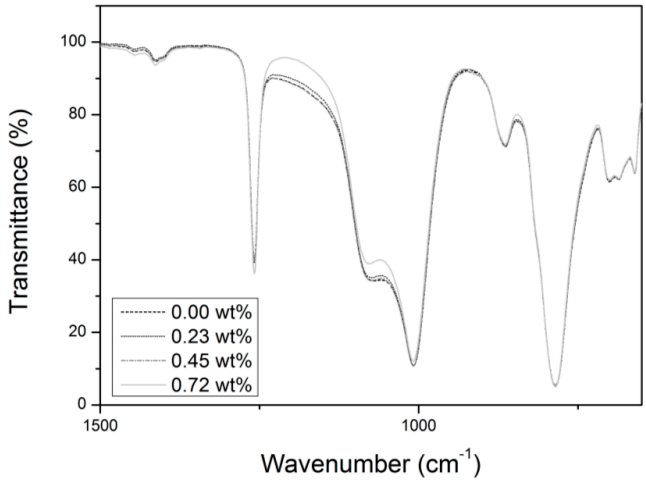

Figure S2. FTIR spectra of 28000 g/mol PDMS films prepared with cross-linker **2** from 1500-650 cm^{-1}.

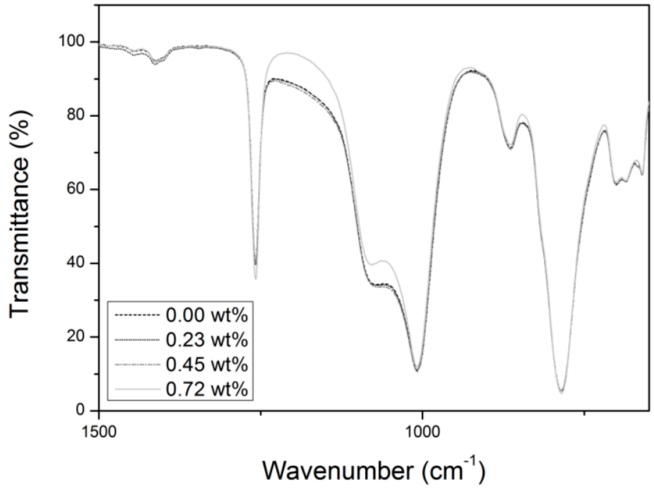

Figure S3. FTIR spectra of 28000 g/mol PDMS films prepared with cross-linker **5** from 1500-650 cm^{-1}.

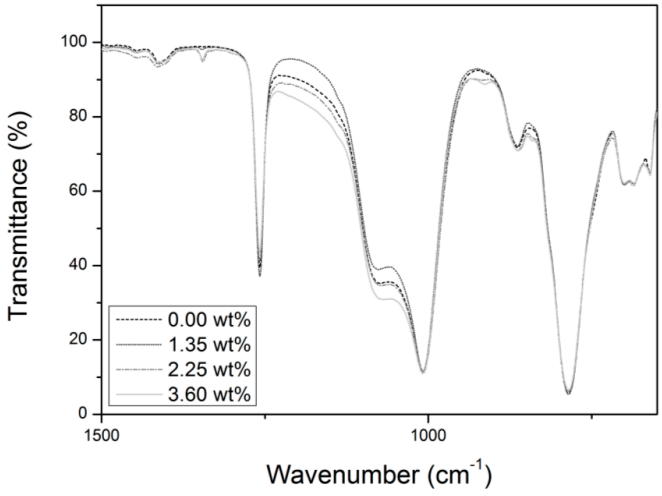

Figure S4. FTIR spectra of 6000 g/mol PDMS films prepared with cross-linker **5** from 1500-650 cm^{-1}.

Appendix C

F. B. Madsen, A. E. Daugaard, C. Fleury, S. Hvilsted, A. L. Skov, 2014 Visualisation and characterisation of heterogeneous bimodal PDMS networks, *RSC Advances*, **4**, 6939-6945.

RSC Advances

PAPER

View Article Online
View Journal | View Issue

Visualisation and characterisation of heterogeneous bimodal PDMS networks†

Cite this: *RSC Adv.*, 2014, **4**, 6939

F. B. Madsen, A. E. Daugaard, C. Fleury, S. Hvilsted and A. L. Skov*

The existence of short-chain domains in heterogeneous bimodal PDMS networks has been confirmed visually, for the first time, through confocal fluorescence microscopy. The networks were prepared using a controlled reaction scheme where short PDMS chains were reacted below the gelation point into hyperbranched structures using a fluorescent silicone compatible cross-linker. The formation of the hyperbranched structures was confirmed by FTIR, ^{1}H-NMR and size exclusion chromatography (SEC). The short-chain hyperbranched structures were thereafter mixed with long-chain hyperbranched structures to form bimodal networks with short-chain domains within a long-chain network. The average sizes of the short-chain domains were found to vary from 2.1 to 5.7 μm depending on the short-chain content. The visualised network structure could be correlated thereafter to the elastic properties, which were determined by rheology. All heterogeneous bimodal networks displayed significantly lower moduli than mono-modal PDMS elastomers prepared from the long polymer chains. Low-loss moduli as well as low-sol fractions indicate that low-elastic moduli can be obtained without compromising the network's structure.

Received 11th December 2013
Accepted 2nd January 2014

DOI: 10.1039/c3ra47522k

www.rsc.org/advances

Introduction

Polydimethylsiloxane (PDMS) elastomers are known for their unique properties, such as high extensibility, high thermal stability, low surface tension and chemical and biochemical inertness.[1] PDMS elastomers consist of a PDMS network, usually resulting from hydrosilylation, radical or condensation reactions, silica particles and other fillers.[2] PDMS networks without fillers suffer from low tear strength and are therefore not easily handled as thin films. The reinforcing silica particles in the elastomer formulations result in a very weak but still not negligible optical distortion, which constitutes a problem in many commercial applications such as adaptable lenses and optical biochips.[3,4]

The mechanical properties of PDMS elastomers, as an alternative, can be improved by creating bimodal networks which are prepared by applying advanced mixing schemes. Bimodal networks consist of very short and relatively long chemically identical polymer chains cross-linked into a network, and their mechanical properties are superior to traditional elastomers.[5,6] Several studies have investigated the unexpected high tear resistance and ultimate strength of bimodal networks.[7–9] The elastic modulus of bimodal networks increases significantly at high elongations, so the ultimate strength of the networks is very high. Improvements in ultimate strength stem from the limited extensibility of the short chains, which gives the networks toughness.[10,11] Furthermore, the relatively long chains retard the rupture process and provide extensibility to the network.[9] Therefore, bimodal networks exhibit both a substantial ultimate stress and ultimate strain.[6] Bimodal networks can be created by the random distribution of short polymer chains within the long chains,[6,12–14] or as heavily cross-linked short-chain domains joined to the long-chain network.[15–17] Bimodal networks with homogenous (random) distributions of short and long chains are prepared in one-step procedures where the chains are mixed and cross-linked simultaneously to form random networks. In contrast, heterogeneous bimodal networks are prepared in two-step procedures. The short-chain domains are prepared in a reaction that happens prior to the cross-linking, where the short chains are reacted below the gelation threshold into hyperbranched structures which are subsequently mixed and cross-linked together with the long chains. Consequently, short-chain domains are created within the long-chain network. Furthermore, the long chains can also be reacted with cross-linker molecules below the gelation threshold – prior to the network formation – in order to obtain even higher control over the network and the distribution of long- and short-chain domains.[17]

Danish Polymer Centre, Department of Chemical and Biochemical Engineering, Technical University of Denmark, DTU, Søltofts Plads, Bldg. 227, 2800 Kgs. Lyngby, Denmark. E-mail: al@kt.dtu.dk

† Electronic supplementary information (ESI) available: ^{1}H-NMR spectra and SEC traces of the short-chain hyperbranched structures before and after the reaction, tabulated data from DSC, TGA and swelling experiments, plot of the elastic moduli ($3G'$) as a function of the degree of equilibrium swelling (Q_v), DSC thermograms, TGA curves, fluorescent confocal microscopy images of all samples and plots of the storage and loss moduli as functions of frequency. See DOI: 10.1039/c3ra47522k

We have previously demonstrated that the advantage of forming heterogeneous bimodal networks with a controlled distribution of short-chains is that the elastic modulus becomes lower compared to both homogenous bimodal networks with similar short chain concentrations and mono-modal PDMS networks.[17] In so doing, softer and more stretchable PDMS elastomers are obtained. The films are at the same time easily handled as thin films, which for the homologues mono-modal PDMS network is difficult without the addition of silica particles. Furthermore, heterogeneous bimodal networks have been shown to exhibit very low viscous losses in combination with low elastic moduli.[17] So they are therefore excellent alternatives to both mono-modal PDMS elastomers, which require fillers to have sufficiently high tear strength to make them manageable as thin films, and to homogenous bimodal networks, which have higher elastic moduli due to the random distribution of short chains.

We herein present a novel method for analysing the size of short-chain domains in heterogeneous bimodal PDMS networks. A recently developed silicone compatible cross-linker allowing for orthogonal chemistry[18] is used to tag the short-chain hyperbranched structures at their cross-linking points with fluorescent molecules. The size of the short-chain domains will furthermore be correlated to the final mechanical properties of the networks. The design scheme offers an unprecedented way of tuning the properties of heterogeneous bimodal networks and thereby paves the way for the implementation of such networks in advanced applications where strong, unfilled and largely extensible networks are needed. The properties of the resulting networks will fulfil the demands of many commercial PDMS elastomer applications, including soft lithography applications where higher fracture energy is needed,[19] optical applications where strong elastomers without optically distorting fillers are desired[3,4] and dielectric elastomers where soft networks with high extensibilities and low viscous losses are essential.[20–25]

Experimental

General methods

FTIR analyses were conducted on a Perkin-Elmer Spectrum One model 2000 Fourier Transform Infrared apparatus equipped with a universal attenuated total reflection accessory on a ZnSe–diamond composite. The spectra were recorded in the range of 4000–650 cm^{-1} with 16 scans using 4 cm^{-1} resolution. ^{1}H-NMR spectra were recorded on a Bruker 300 MHz spectrometer. Size-exclusion chromatography (SEC) was performed on a Viscotek GPCmax VE-2001 instrument, equipped with a Viscotek TriSEC Model 302 triple detector using two PLgel mixed-D columns, provided by Polymer Laboratories. Samples were run in THF at a rate of 1 ml min^{-1}, and molar mass characteristics were calculated using polystyrene standards. Optical characterisations were performed on a Leica TCS SPE high-resolution confocal microscope with a 10× lens at 400 nm in the *z*-direction, equipped with a Leica CTR4000 electronic box. Image analysis was performed with ImageJ, and the domain diameter was taken as an average over 100 domains. Differential scanning calorimetry (DSC) measurements were performed on a DSC Q1000, provided by TA Instruments. The thermal analyses were performed with a heating and cooling rate of 10 °C min^{-1}, from −90 to 150 °C. Thermogravimetric analysis (TGA) was performed on a Q500 (TA Instruments) in a nitrogen atmosphere with a heating rate of 10 °C min^{-1}, from RT to 950 °C. All degradation temperatures were taken as the peak temperature of the first derivative of the temperature with time. Linear rheology of the bimodal films was performed with a TA Instruments TA 2000 Rheometer set to a controlled strain mode of 1%, which was ensured to be within the linear viscoelastic regime. The measurements were performed in the frequency range 100–0.01 Hz with a parallel plate geometry of 25 mm. The films were approximately 1 mm thick and were measured with a small normal force from the upper plate, which ensured that there were no-slip conditions.

Materials

Hydride-terminated PDMS: DMS-H11 ($\bar{M}_n$ = 1050 g mol^{-1}) and DMS-H31 ($\bar{M}_n$ = 28 000 g mol^{-1}) as well as a vinyl functional PDMS cross-linker, VDT-431 ($\bar{M}_n$ = 28 000 g mol^{-1}, ~16 vinyl groups), were acquired from Gelest Inc. The platinum cyclovinylmethyl siloxane complex catalyst (511) was provided by Hanse Chemie. All other chemicals were acquired from Sigma-Aldrich and used as received, unless otherwise specified.

Fluorescent cross-linker: (4-methyl-7-((1-(3-(tris(allyloxy)silyl)-propyl)-1*H*-1,2,3-triazol-4-yl)methoxy)-2*H*-chromen-2-one)

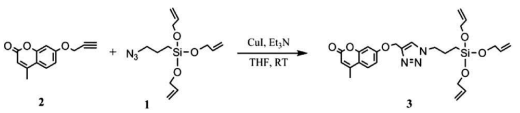

2 1 3

The fluorescent tri-functional cross-linker (**3**) was prepared according to previously described procedures.[18] A silicone compatible tri-functional azide cross-linker (**1**) was synthesised *via* the silyl ether reaction between (3-bromopropyl)trichlorosilane and allyl alcohol and the subsequent substitution of bromine with azide. The azide-functional cross-linker was thereafter used in a click reaction (the copper-catalysed cyclo-addition of an azide and an alkyne (CuAAC) forming a 1,4-disubstituted-1,2,3-triazole) with the alkyne 4-methyl-7-(prop-2-yn-1-yloxy)-2*H*-chromen-2-one (**2**), which was prepared through a Williamson ether synthesis of 4-methylumbelliferone and propargyl bromide.

General procedure for preparing heterogeneous bimodal networks (amounts given for 10 wt% short chains)

The fluorescent tri-functional cross-linker (**3**, 0.027 g, 0.0054 mmol) was dissolved in THF (0.6 ml) and mixed with short PDMS chains (DMS-H11, 1050 g mol^{-1}, 0.212 g, 0.020 mmol). The platinum cyclovinylmethyl siloxane complex catalyst (511) (10 ppm) in dry THF was thereafter added to give a stoichiometry of r = 0.4 and the mixture was mixed in a FlackTek Inc. DAC

150.1 FVZ-K SpeedMixer™ and allowed to react for 1 hour at 60 °C. Next, a 16-functional vinyl cross-linker (VDT-431, 28 000 g mol^{-1}, 0.014 g, 5×10^{-5} mmol) and the long PDMS chains (DMS-H31, 28 000 g mol^{-1}, 1.91 g, 0.0068 mmol) were mixed with platinum cyclovinylmethyl siloxane complex catalyst (511) (10 ppm) in dry THF to give a stoichiometry of $r = 0.06$. The mixture was combined in the SpeedMixer and thereafter allowed to react for 1 hour at 60 °C. After the initial reactions, the short- and long-chain mixtures were combined and additional cross-linker (VDT-431, 28 000 g mol^{-1}, 0.838 g, 0.0030 mmol) and catalyst (10 ppm) were added to give an overall stoichiometry of $r = 1.2$ (20% excess of vinyl groups). The mixture was blended in the SpeedMixer and poured into 1 mm thick steel moulds on an FEP fluorocarbon substrate, degassed *in vacuo* for 1 hour, cured for 24 hours at RT and then post-cured at 60 °C for 1 hour. Short and long chain amounts were varied to create bimodal networks with mass ratios of short : long chains = 0 : 100, 3 : 97, 10 : 90, 20 : 80 and 30 : 70, corresponding to molar ratios of short : long chains = 0 : 100, 45 : 55, 75 : 25, 87 : 13 and 92 : 8.

Swelling experiments

Swelling experiments were performed by placing a pre-weighed sample in a flask containing toluene until the equilibrium swelling state was reached (typically one week). At the end of the swelling period, the samples were removed from the solvent, dried quickly and carefully with lint-free tissue paper and then weighed. The volume degree of equilibrium swelling (Q_v) was then calculated according to: $Q_v = 1 + (Q_w - 1) \times \nu_{toluene}/\nu_{PDMS}$, where $\nu_{toluene}$ is the specific volume of toluene and ν_{PDMS} is the specific volume of PDMS. Q_w is calculated as: $Q_w = m_0/m$, where m_0 is the initial weight of the (dry) sample before swelling and m is the weight of the wet (swollen) sample. After the swelling experiment, the samples were washed several times with toluene and dried for 24 hours. The sol fractions (W_{sol}) were thereafter calculated as: $W_{sol}(\%) = (1 - (m_e/m_0)) \times 100$, where m_e is the weight of the dry sample after the swelling/extraction.

Results and discussion

The heterogeneous bimodal PDMS networks were prepared in a two-step procedure combining short- and long-chain hyperbranched PDMS structures, as illustrated in Fig. 1. First, fluorescent short-chain hyperbranched structures were prepared in a reaction prior to the network formation using a previously prepared fluorescent tri-functional cross-linker.[18] The cross-linker was used in concentrations below the gelation point, as determined by the Flory–Stockmayer expression: $r_c = 1/(f - 1)$ where r_c is the stoichiometry between the reactive groups on the cross-linker and the reactive groups on the polymer required for critical gelation, and f is the functionality of the cross-linker. By using a stoichiometry where $r < r_c$ no infinite short-chain network will be created, and the formed hyperbranched structures still have reactive end groups.[26,27] The short-chain hyperbranched structures were characterised by FTIR, ^{1}H-NMR and size-exclusion chromatography (SEC). The reaction between the fluorescent cross-linker and the short PDMS chains was followed by FTIR and the decreasing intensity of the cross-linker C=C band at 1610 cm^{-1}. Furthermore, FTIR spectra confirmed the presence of the remaining Si–H end groups (at 2125 cm^{-1}) on the short-chain polymers after the reaction. The reaction employed to form the short-chain hyperbranched structures was also followed with ^{1}H-NMR by the disappearance of the $-CH_2{=}CH_2$ resonance at 5.26 ppm and $-CH_2{=}CH$ resonance at 5.12 ppm. The presence of Si–H protons at 4.70 ppm after the reaction indicates that reactive polymer end groups are indeed still present on the hyperbranched structures. From the areas under the Si–*H* resonance before and after the reaction relative to the areas of the constant Si–CH_3 resonances at 0.06–0.18 ppm it can be deduced that ~60% reactive Si–H end groups remain

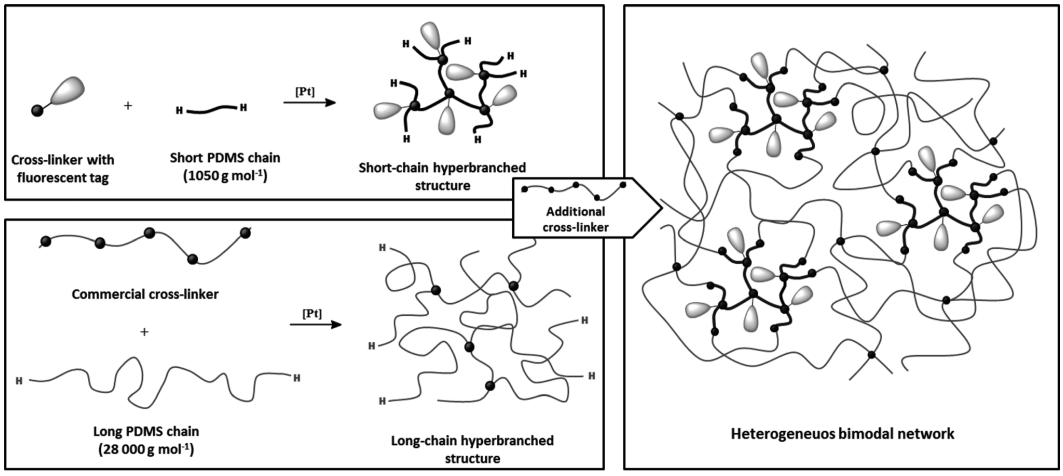

Fig. 1 Schematic illustration of the two-step reaction procedure employed to form heterogeneous bimodal networks.

after the reaction. This number is consistent with the stoichiometric ratio of $r = 0.4$ used in this instance. ^{1}H-NMR spectra can be found as ESI.† SEC was used to confirm the post-reaction increase in molecular weight of the hyperbranched structures, which appear in the higher molecular weight region compared to the low molecular weight short-chain PDMS (as seen in the SEC traces in the ESI†). In addition, the SEC trace clearly shows that the reaction results in a distribution of hyperbranched structures and not in a mono-modal structure, which is as expected for a hyperbranched structure.

In a similar manner, the long-chain hyperbranched structures were prepared by using a commercial cross-linker (28 000 g mol^{-1}, bearing, on average, 16 vinyl groups per chain) and a higher molecular weight PDMS (28 000 g mol^{-1}). The hyperbranched structures, based on the short and long chains, were mixed and cross-linked by using the commercial cross-linker in excess. The fluorescent and reinforcing short-chain hyperbranched structures thereby became covalently bound to the long-chain hyperbranched structures, ensuring sufficient separation of the short-chain structures to maximise the reinforcing effect.

The heterogeneous bimodal networks were prepared with varying contents of short-chain hyperbranched structures, in order to illustrate the effect of the ratio between long- and short-chain hyperbranched structures. The concentration of short-chain structures varied from 0 to 30 wt%, corresponding to 0 to 92 mol% (of the total number of hydride functional polymers). Films based entirely on the short-chain polymer could not be prepared, as the polymer was of a too low molecular weight to form a mechanically stable film.

The prepared heterogeneous bimodal networks were characterised by confocal microscopy, which uses single-point illumination and rejects out-of-focus light. Thus, images with better vertical optical resolution than traditional fluorescence microscopy are obtained. The acquired images had reduced background haze and represent a thin cross-section of the sample, as shown in Fig. 2 (original fluorescence confocal microscopy images of all samples can be found as ESI†).

The fluorescent domains are evenly distributed within all networks. Furthermore, it can be seen from Fig. 2 that the fluorescent domains vary in size and abundance, depending on the ratio between the short- and long-chain hyperbranched structures in the network. The mean diameters of the fluorescent domains were determined as an average of 100 domains, the results for which are summarised in Table 1. As seen in Table 1, the sizes of the fluorescent domains vary only moderately for the concentrations of short-chain hyperbranched structures, from 3 wt% to 20 wt%, whereas substantially larger domains are observed at 30 wt%. Furthermore, it is clear from Fig. 2 that the domains are very well distributed, and the number of domains is high for both samples. When the concentration of the short-chain hyperbranched structures is increased to 30 wt%, a substantial increase in the domain's size is evident (Fig. 2), due to the short-chain hyperbranched structures becoming so tightly packed that even upon ideal distribution they will interconnect covalently and turn into larger agglomerates. This is also substantiated by the large increase in the standard deviation of the measured average short-chain domain diameter.

The influence on the distribution and size of the observed domains on the elastic and mechanical properties of the bimodal networks was determined by employing small amplitude rheology. The resulting shear storage moduli (G') and loss moduli (G'') are summarised in Table 1. The mono-modal

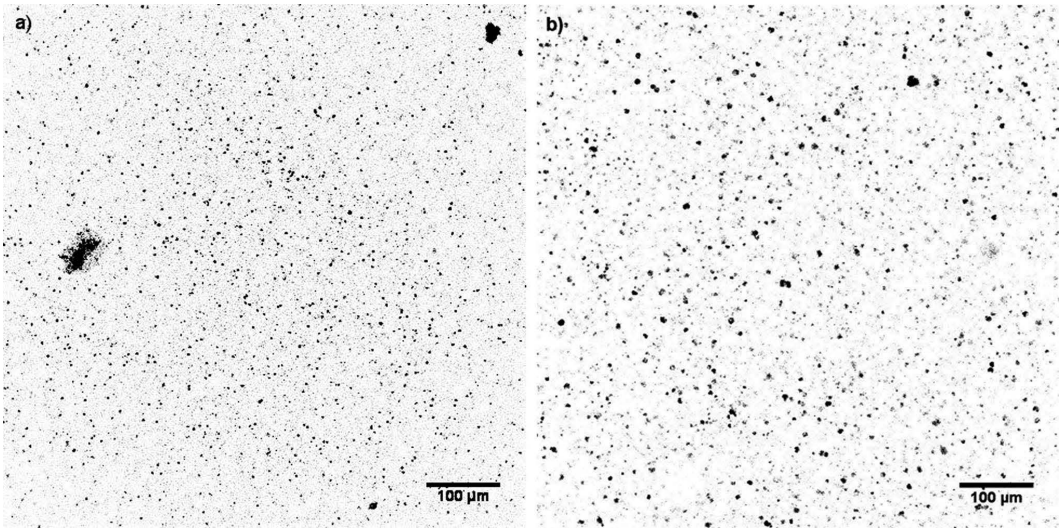

Fig. 2 Grayscale confocal microscopy images obtained at 400 nm of the prepared heterogeneous bimodal networks with varying concentrations of short-chain hyperbranched structures. (a) 3 wt% and (b) 30 wt%.

Table 1 Summary of the heterogeneous bimodal networks' properties

Short-chain concentration		Domain diameter[a] (D)	C_N[b] $\times 10^{-9}$	G′@1 Hz	G″@1 Hz
[Wt%]	[Mol%]	[μm]	[g^{-1}]	[kPa]	[kPa]
0	0	—	—	93.4	1.19
3	45	2.9 ± 0.9	2.4	11.8	0.32
10	75	2.8 ± 0.8	9.0	21.5	0.20
20	87	2.1 ± 0.5	43	78.1	0.98
30	92	5.7 ± 1.6	3.2	59.5	0.70

[a] The mean diameters were determined with the imaging processing program ImageJ. [b] The number average concentration of short-chain domains is calculated as: $C_N = ((6 \times \text{wt\%})/(\pi D^3))(1/\rho_{PDMS})$, where ρ_{PDMS} is the density of PDMS.

PDMS reference network, with 0% of short chains, has a storage modulus of 93.4 kPa. Upon the addition of the short-chain hyperbranched structures, the modulus decreases significantly to 11.8 kPa. From fundamental theories on rubber elasticity the elastic moduli are expected to scale linearly with the inverse average molecular weight of the polymer chains in the network.[28] As such, the addition of very short polymer chains to the system would be expected to decrease the average molecular weight of the system and thus increase the elastic modulus significantly. This decrease in the elastic modulus in heterogeneous bimodal networks has been shown previously but not explained with supporting data.[16,17] Based on the unprecedented correlation between the network composition, size and distribution of the fluorescent domains, and the elastic properties of heterogeneous bimodal networks, we believe that the decrease in the elastic modulus can be explained by a multi-domain theory. When short-chain hyperbranched structures are added, they naturally contain a large concentration of unreacted hydride groups on the surface. These groups react with cross-linker molecules, which upon initial reaction are hindered from diffusion by reptation.[29] Consequently, there is a large concentration of cross-linker molecules on the surface of the hyperbranched structures. Small cross-linker molecules, such as those used in our previous study,[17] are packed tightly around the surface, whereas the long-chain cross-linker molecules used in this study tend to fold around the short-chain hyperbranched structures. In both cases, this creates areas around the cross-linker molecules where the effective cross-linking density is lower than in the bulk long-chain network, as a large number of the cross-linking sites are present around the short-chain domains, as illustrated in Fig. 3. In this study, with a high molecular weight cross-linker, folding back to the short-chain domains also leads to the formation of loops, which do not contribute to elasticity to the same extent as the true cross-linking sites.[30] Domains with surrounding cross-linker molecules therefore create a local softening effect in the PDMS networks. The heterogeneous bimodal elastomers will consequently be softer and have a lower elastic modulus than the homologous mono-modal networks despite higher average cross-linking density. The reduction in the modulus, from mono-modal to a small amount of short-chain domains, is

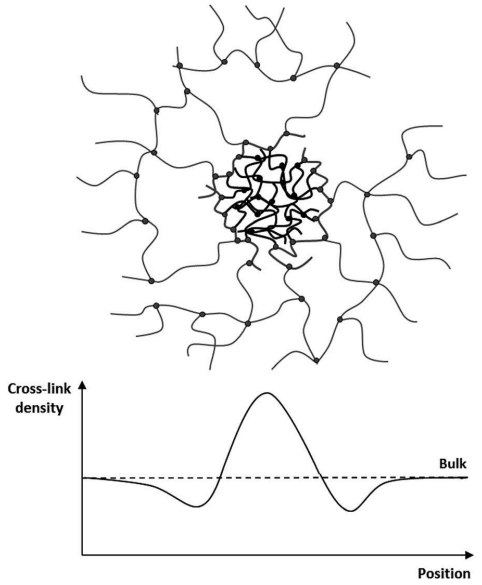

Fig. 3 Schematic illustration of the hypothesised efficient cross-linking density.

confirmed experimentally. The elastic modulus is then increased with increasing short-chain concentration. At high concentrations of short chains the elastic modulus drops again. This can be explained by a drop in the number average concentration of short-chain domains $C_N = ((6 \times \text{wt\%})/(\pi D^3))(1/\rho_{PDMS})$, with the additional increase of short chains (see Table 1). From the calculations it can be seen that for the bimodal networks, the elastic modulus increases with increasing C_N, although, not in a trivial way.

Interfaces with a lower cross-linking density are still perfectly cross-linked due to the high number of functional groups on each hyperbranched structure, and as such they cannot be regarded as network imperfections, since their mechanical properties are not destroyed.

Very soft silicone elastomer behaviour can also be observed for imperfect networks, which occurs as a result of unreacted groups. This lack of reactivity can be introduced either from stoichiometrically imbalanced reactions[27,31] or from incomplete catalyst inhibition reactions.[32] It can also arise naturally from steric hindrance or heterogeneity, thus leading to local cross-linker and polymer excesses, respectively. Therefore it is important to ensure that heterogeneous bimodal networks do not contain a large fraction of solubles, so-called sol fractions. The sol fractions of heterogeneous bimodal PDMS networks were determined by conducting swelling experiments with toluene, the results for which can be found in Table S1 in the ESI.† The sol fractions were found to lie in the range of 5–10% and were apparently independent of short chain concentration. The addition of the short chains as domains therefore does not create additional imperfections in the infinite networks, which

means that there is complete compatibility between the short-chain domains and the long-chain matrix.

Swelling experiments were performed in order to determine the relationship between the volume degree of equilibrium swelling (Q_v) and the mechanical properties. The results can be found in the ESI.† Q_v is found to decrease with increasing short-chain concentration, due to the strong increase in cross-link density. Furthermore, as expected, there is not a linear relationship between the elastic moduli (3G′) and the equilibrium swelling degree (see Fig. S3 in the ESI†), which is observed for traditional mono-modal PDMS elastomers. Heterogeneous bimodal networks therefore behave quite different to mono-modal PDMS networks, since the modulus decreases following the addition of short-chain domains, *i.e.* with increasing cross-link density. This means that swelling capacity is determined from the continuous long-chain part of the network, whereas elasticity is governed by a combination of short- and long-chains properties.

In general, it is difficult to obtain PDMS elastomers with low elastic moduli without deteriorating other network properties. Soft PDMS elastomers therefore usually suffer from high viscous losses. The frequency-dependent viscous loss can be determined from the shear loss modulus G″. All the prepared bimodal elastomers are seen to have lower viscous loss than the mono-modal PDMS network. Furthermore, the heterogeneous bimodal networks are well cross-linked, as the storage moduli (G′) is 10 to 100 times larger than the loss moduli (G″) for the investigated frequency range, with differences being smallest at high frequencies. A plot of the storage and loss moduli as functions of frequency can be found as ESI.† Viscous loss at the low strain low frequency limit is measured as a few percentage points only. This is comparable to our previously reported results for heterogeneous bimodal networks.[17] Viscous loss in a polymer network is due to dangling chains and sol molecules, *i.e.* incomplete network formation.[27] It is therefore evident from the low viscous losses of the heterogeneous bimodal networks that the obtained low moduli are not a result of incomplete reactions but rather of network artefacts, as shown in Fig. 3. The loops do not contribute significantly to the elastic modulus, but at the same time they do not contribute a loss, since they cannot relax. Heterogeneous bimodal networks are therefore an effective and simple method of creating soft elastomers with very low viscous losses.

The thermal transition behaviour of the heterogeneous bimodal networks was determined using differential scanning calorimetry (DSC). The resulting thermograms can be found as ESI,† while the crystallisation and melting temperatures are summarised in Table S1 in the ESI,† too. A large decrease in the area under the crystallization peaks can be seen in the thermograms, along with an increasing concentration of short-chains. This means that there is a smaller degree of crystallinity in the material in line with increasing short-chain content. Consequently, the PDMS elastomers become inherently amorphous at large concentrations of short chains, as almost no crystalline behaviour is observed. This is most likely due to an increased cross-linking density as the short chain domains are highly dense structures in elastomers. This high cross-link density means that the polymer chains are no longer able to arrange into the positions necessary for crystalline regions to form. Melting temperatures are also observed to decrease with higher concentrations of short chains because of the dilution of the crystalline segments. Furthermore, areas under the melting peaks are reduced at higher concentrations, which mean that the energy required for melting is reduced at larger concentrations of short chains.

Moreover, the effect of short-chain domains on the thermal stability of the PDMS networks was investigated by thermal gravimetric analysis (TGA). The determined degradation temperatures for the bimodal PDMS networks with different short-chain concentrations are summarised in Fig. S5 and Table S1 in the ESI.† The first degradation step occurs due to the cleavage of Si–CH_3 bonds. This degradation temperature increases significantly with increasing amounts of short chains (from ~430 °C to ~530 °C), which demonstrates that heterogeneous bimodal networks also have a beneficial influence on the thermal stability of PDMS elastomers.

Conclusions

In summary, a novel method of visualising the size of short-chain domains in heterogeneous bimodal PDMS networks was developed. The method allows for the determination of the size of short-chain domains by confocal fluorescence microscopy. The size of the domains was furthermore correlated to the final elastic properties of the bimodal networks for the first time, which makes it possible to explain the surprisingly low elastic moduli obtained for heterogeneous bimodal networks. The results thereby make it possible to tune the properties of PDMS networks in line with the size and concentrations of short-chain hyperbranched structures. This opens up the possibility of heterogeneous bimodal network implementation in advanced applications where strong, unfilled and largely extensible networks are needed, such as in the field of optics and in the emerging field of dielectric elastomers.

Acknowledgements

The authors would like to acknowledge Lene Feldskov Nielsen, Coloplast A/S, Humlebæk, Denmark for help with the confocal microscopy and the Danish National Advanced Technology Foundation for its financial support.

Notes and references

1 J. E. Mark, in *Silicon-Based Polymer Science: A Comprehensive Resource*, ed. J. M. Zeigler and F. W. G. Fearon, American Chemical Society, 1990, pp. 47–68.
2 C. Ohm, M. Brehmer and R. Zentel, *Adv. Mater.*, 2010, **22**, 3366–3387.
3 A. Werber and H. Zappe, *Appl. Opt.*, 2005, **44**, 3238–3245.
4 J. Ou, T. Glawdel, C. L. Ren and J. Pawliszyn, *Lab Chip*, 2009, **9**, 1926–1932.
5 J. E. Mark, *Br. Polym. J.*, 1985, **17**, 144–148.

6 G. D. Genesky, B. M. Aguilera-Mercado, D. M. Bhawe, F. a. Escobedo and C. Cohen, *Macromolecules*, 2008, **41**, 8231–8241.
7 T. L. Smith, B. Haidar and J. L. Hedrick, *Rubber Chem. Technol.*, 1990, **63**, 256–264.
8 G. B. Shah and R. W. Winter, *Macromol. Chem. Phys.*, 1996, **197**, 2201–2208.
9 J. E. Mark, *Prog. Polym. Sci.*, 2003, **28**, 1205–1221.
10 Z.-M. Zhangt and J. E. Mark, *J. Polym. Sci., Polym. Phys. Ed.*, 1982, **20**, 473–480.
11 P. Xu and J. E. Mark, *Polymer*, 1992, **33**, 1843–1848.
12 M. A. Llorente, A. L. Andrady and J. E. Mark, *J. Polym. Sci., Polym. Phys. Ed.*, 1981, **19**, 621–630.
13 M. Y. Tang and J. E. Mark, *Macromolecules*, 1984, **17**, 2616–2619.
14 B. Viers and J. Mark, *J. Macromol. Sci., Part A: Pure Appl. Chem.*, 2007, **44**, 131–138.
15 J. E. Mark and A. L. Andrady, *Rubber Chem. Technol.*, 1981, **54**, 366–373.
16 S.-J. Pan and J. E. Mark, *Polym. Bull.*, 1982, **7**, 553–559.
17 A. G. Bejenariu, L. Yu and A. L. Skov, *Soft Matter*, 2012, **8**, 3917.
18 F. B. Madsen, I. Dimitrov, A. E. Daugaard, S. Hvilsted and A. L. Skov, *Polym. Chem.*, 2013, **4**, 1700–1707.
19 H. Schmid and B. Michel, *Macromolecules*, 2000, **33**, 3042–3049.
20 R. Pelrine, R. Kornbluh, Q. Pei and J. Joseph, *Science*, 2000, **287**, 836.
21 R. Pelrine, R. Kornbluh and G. Kofod, *Adv. Mater.*, 2000, **12**, 1223–1225.
22 C. Löwe, X. Zhang and G. Kovacs, *Adv. Eng. Mater.*, 2005, **7**, 361–367.
23 R. Shankar, T. K. Ghosh and R. J. Spontak, *Adv. Mater.*, 2007, **19**, 2218–2223.
24 F. B. Madsen, A. E. Daugaard, S. Hvilsted and A. L. Skov, *Proc. SPIE*, 2013, **8687**, 86871H.
25 F. B. Madsen, A. E. Daugaard, M. Y. Benslimane, S. Hvilsted and A. L. Skov, *Smart Mater. Struct.*, 2013, **22**, 104002.
26 F. Chambon and H. H. Winter, *J. Rheol.*, 1987, **31**, 683–697.
27 S. M. G. Frankær, M. K. Jensen, A. G. Bejenariu and A. L. Skov, *Rheol. Acta*, 2012, **51**, 559–567.
28 M. Doi and S. F. Edwards, *The Theory of Polymer Dynamics*, Oxford University Press, 1999.
29 S. Kunamaneni, D. M. A. Buzza, D. J. Read, D. Parker, A. M. Kenwright, W. J. Feast and A. L. Larsen, *Macromolecules*, 2006, **39**, 6720–6736.
30 A. L. Larsen, K. Hansen, P. Sommer-Larsen, O. Hassager, A. Bach, S. Ndoni and M. Jørgensen, *Macromolecules*, 2003, **36**, 10063–10070.
31 K. Urayama, T. Miki, T. Takigawa and S. Kohjiya, *Chem. Mater.*, 2004, **16**, 173–178.
32 H. H. Winter and F. Chambon, *J. Rheol.*, 1986, **30**, 367–382.

Electronic Supplementary Material (ESI) for RSC Advances

Supporting Information

Visualisation and Characterisation of Heterogeneous Bimodal PDMS Networks

Frederikke Bahrt Madsen, Anders Egede Daugaard, Clémence Fleury, Søren Hvilsted and Anne Ladegaard Skov*

*DTU, The Danish Polymer Centre, Department of Chemical and Biochemical Engineering, DK-2800 Kgs. Lyngby, Denmark

^{1}H-NMR spectra

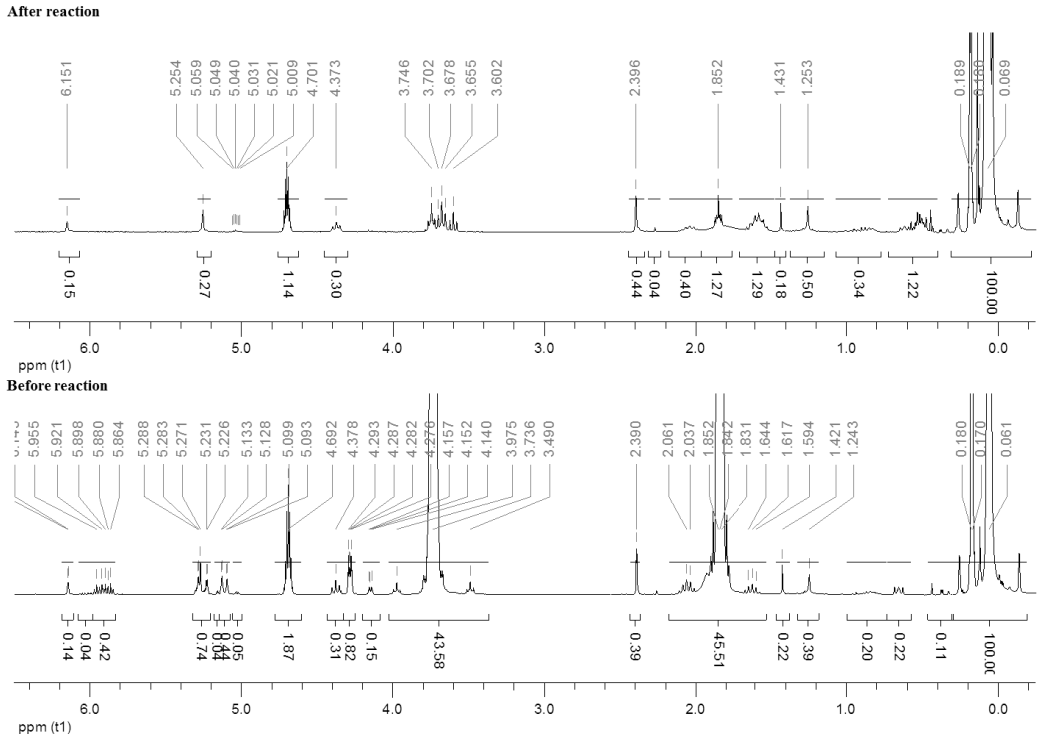

Figure S1. ^{1}H-NMR spectra of the short chains before the hyperbranching reaction (bottom) and the short chains after the hyperbranching reaction with the fluorescent cross-linker (top).

SEC traces

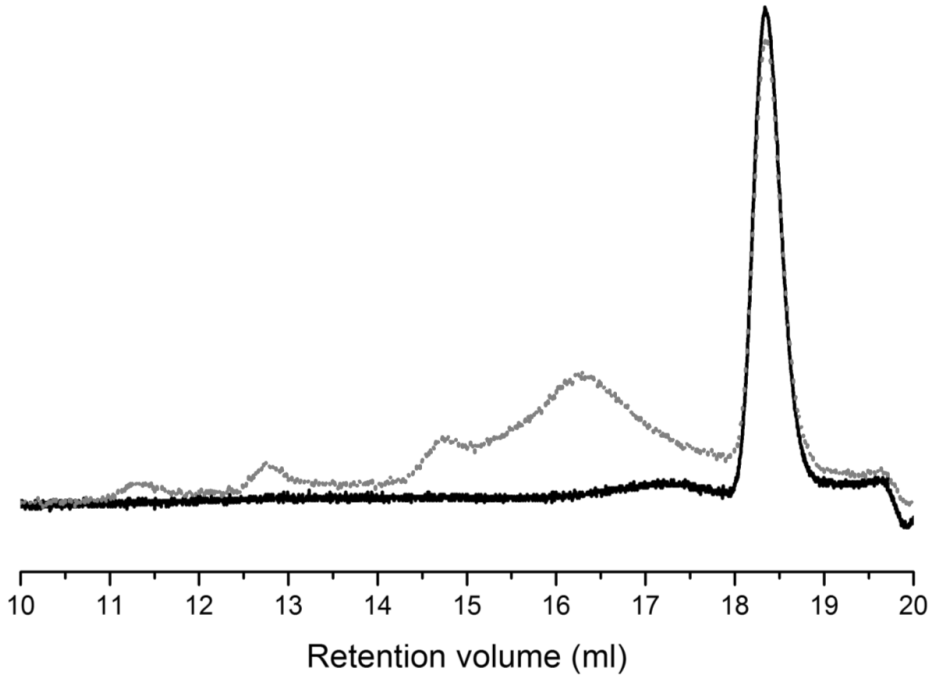

Figure S2. Overlay of the SEC refractive index detector signals of the short chains before the hyperbranching reaction (solid) and the short chains after the hyperbranching reaction with the fluorescent cross-linker (dashed).

Table S1. Summary of the heterogeneous bimodal networks' properties.

Small chain concentration		**Domain diameter**[a)]	**DSC**				**TGA**		**Rheology**		**Swelling**	
			Cooling		**Heating (2nd)**		**1. Degradation step**	**2. Degradation step**	**G´ @1Hz**	**G'' @1Hz**	Q_v	W_{sol}
[Wt%]	**[Mol%]**	**[µm]**	T_c **[°C]**	A_{peak} **[J/g]**	T_m **[°C]**	A_{peak} **[J/g]**	**[°C]**	**[°C]**	**[kPa]**	**[kPa]**		**[%]**
0	0	-	-77.5	20.6	-46.6	24.2	430	678	93.4	1.19	4.2±0.06	5.9±0.5
3	45	2.9±0.9	-75.7	22.7	-46.8	24.0	467	664	11.8	0.32	5.0±0.07	10.5±0.8
10	75	2.8±0.8	-82.5	10.0	-47.3	15.2	470	669	21.5	0.20	3.6±0.11	6.0±1.9
20	87	2.1±0.5	-	-	-49.6	18.1	534	677	78.1	0.98	3.6±0.11	8.5±0.7
30	92	5.7±1.6	-	-	-52.0	6.9	532	678	59.5	0.70	3.1±0.06	4.8±0.1

[a)]The mean diameters were determined with the imaging processing program ImageJ.

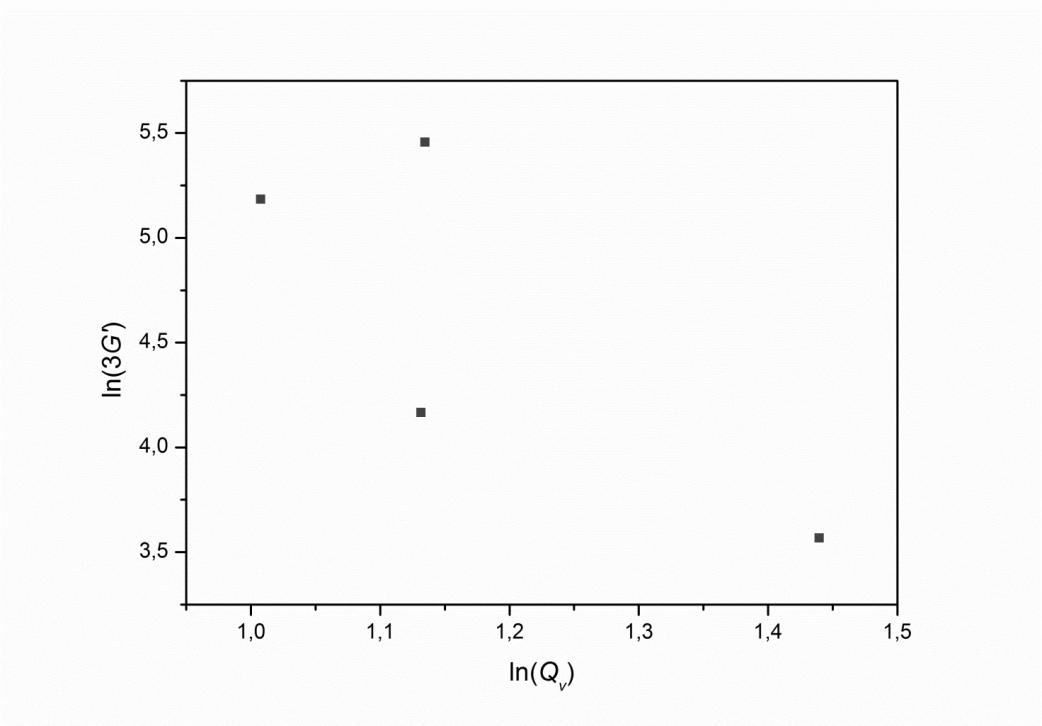

Figure S3. Plot of the elastic moduli ($3G'$) as a function of the degree of equilibrium swelling (Q_v) for heterogeneous bimodal PDMS networks swollen in toluene.

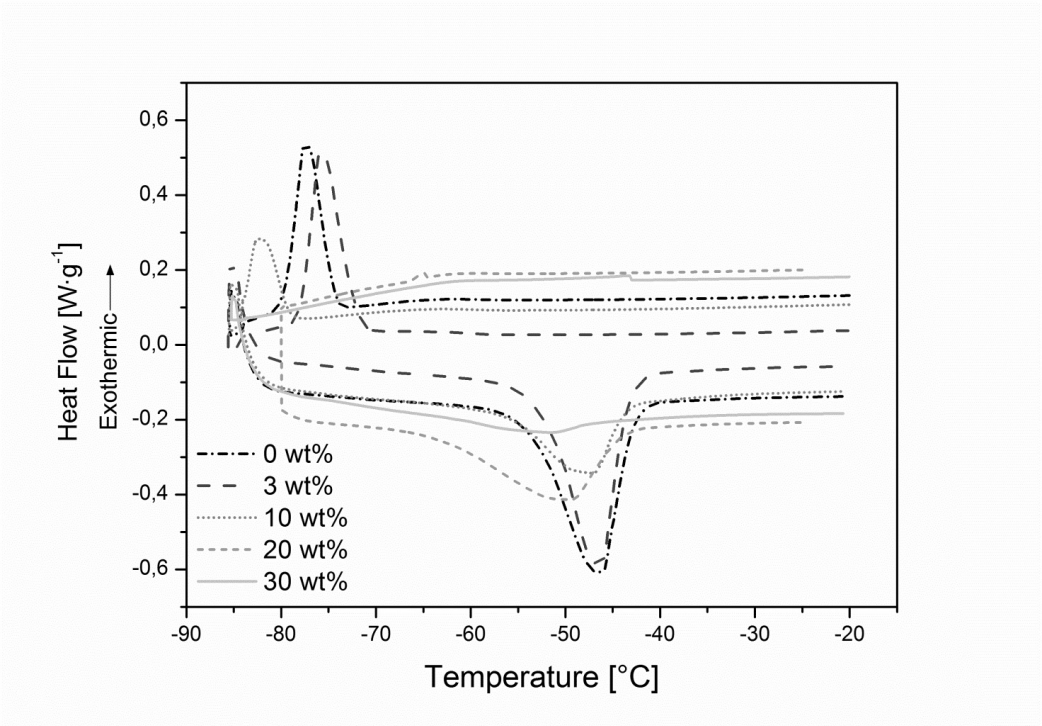

Figure S4. DSC thermograms of the heterogeneous bimodal networks prepared with varying short-chain content.

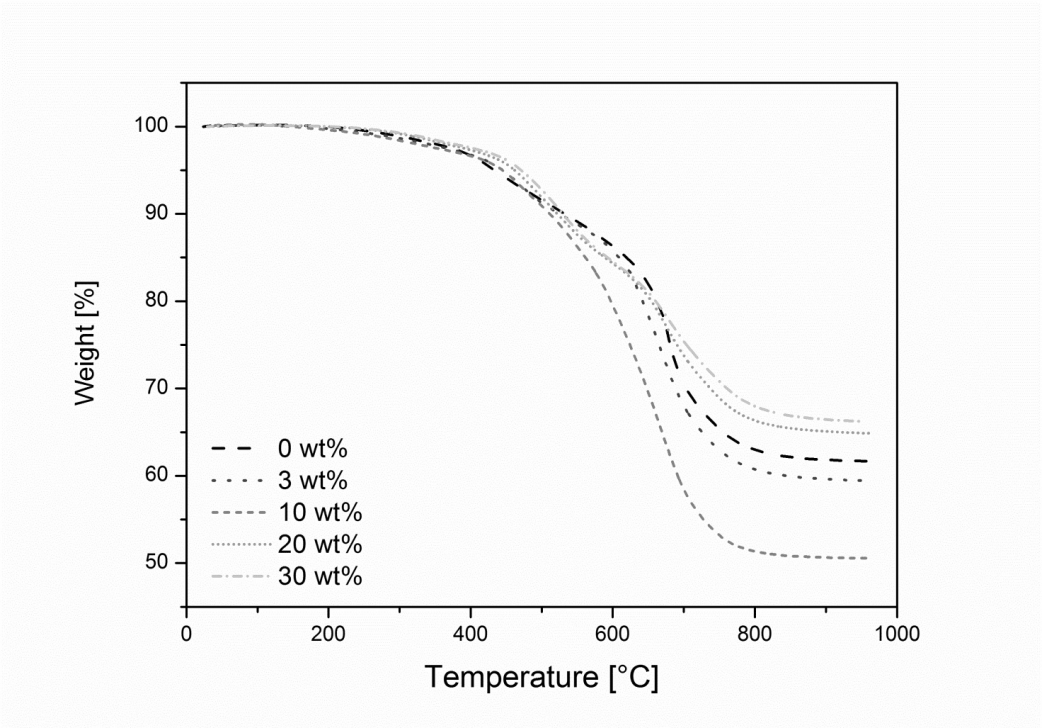

Figure S5. TGA results of the heterogeneous bimodal networks prepared with varying short-chain content.

Confocal Fluorescence Microscopy Images

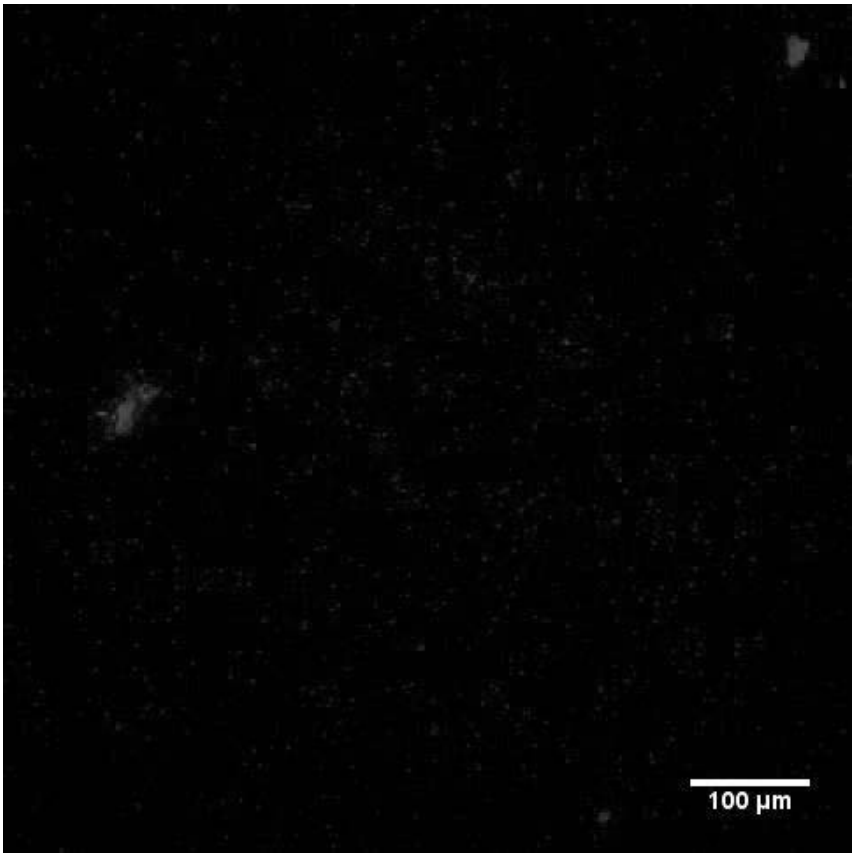

Figure S6. Confocal microscopy image of the prepared heterogeneous bimodal network prepared with 3 wt% short chains.

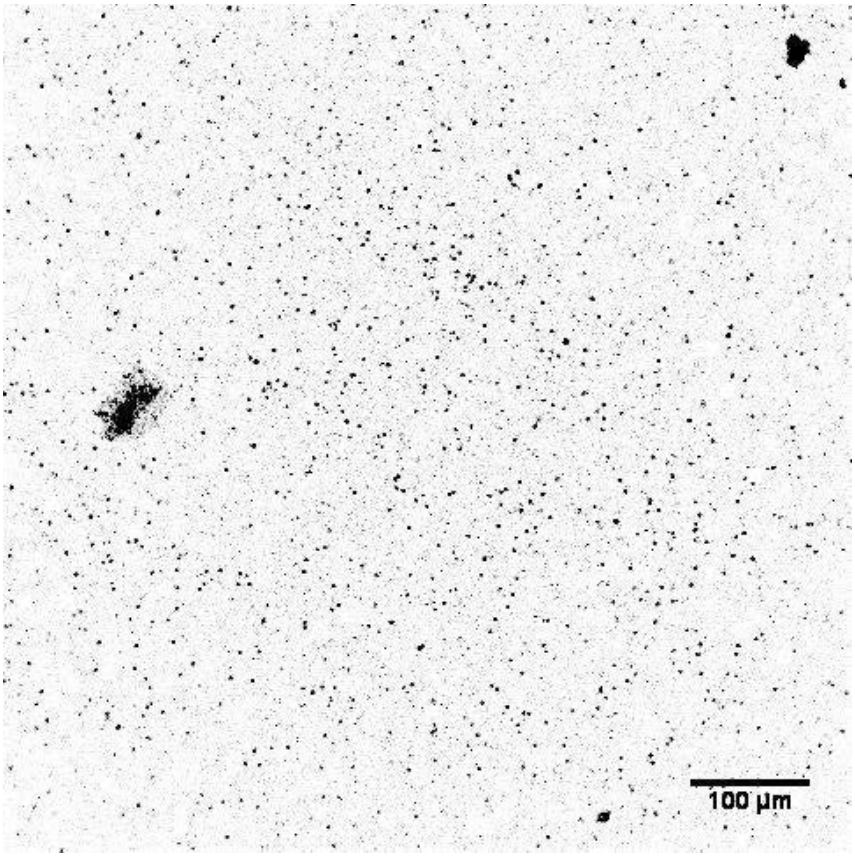

Figure S7. Grayscale confocal microscopy image of the prepared heterogeneous bimodal network prepared with 3 wt% short chains.

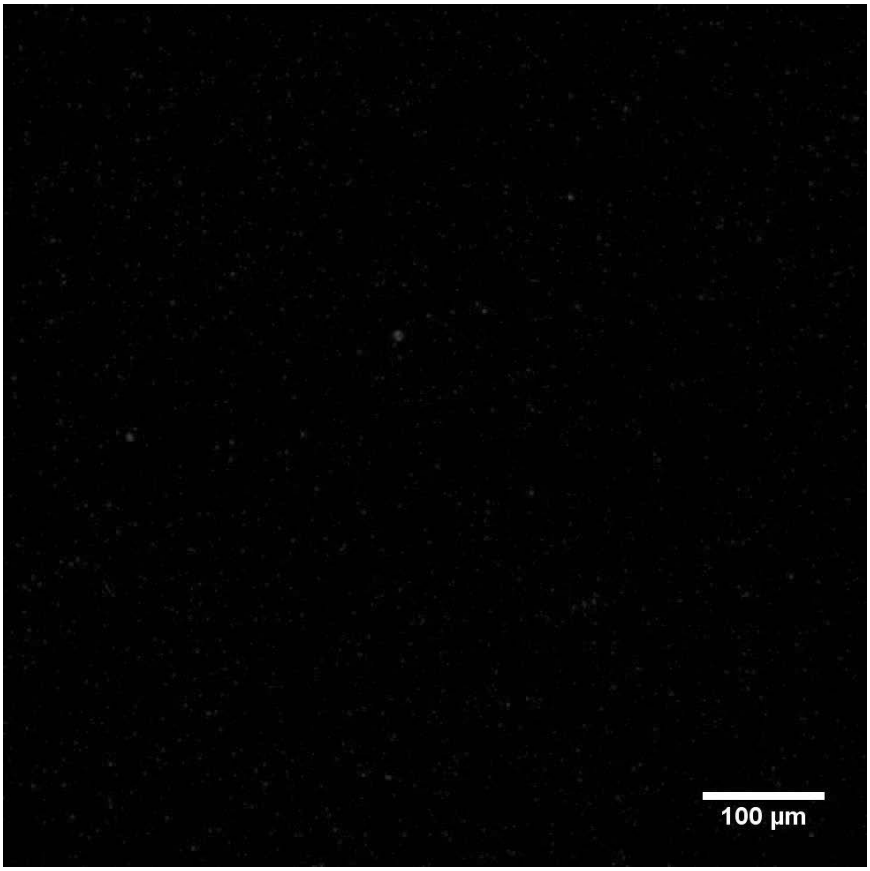

Figure S8. Confocal microscopy image of the prepared heterogeneous bimodal network prepared with 10 wt% short chains.

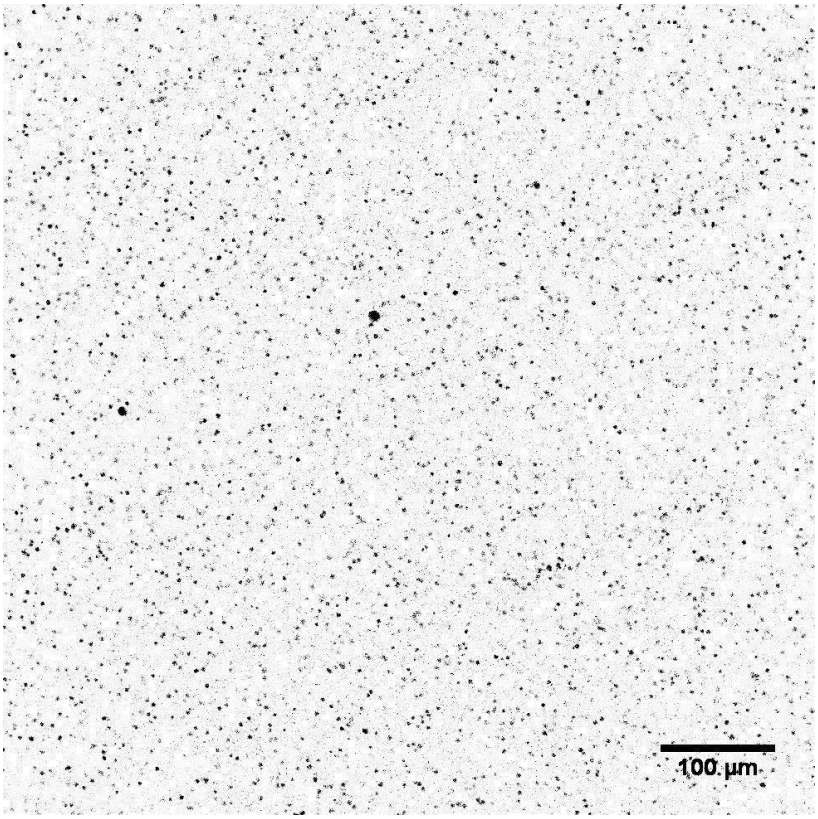

Figure S9. Grayscale confocal microscopy image of the prepared heterogeneous bimodal network prepared with 10 wt% short chains.

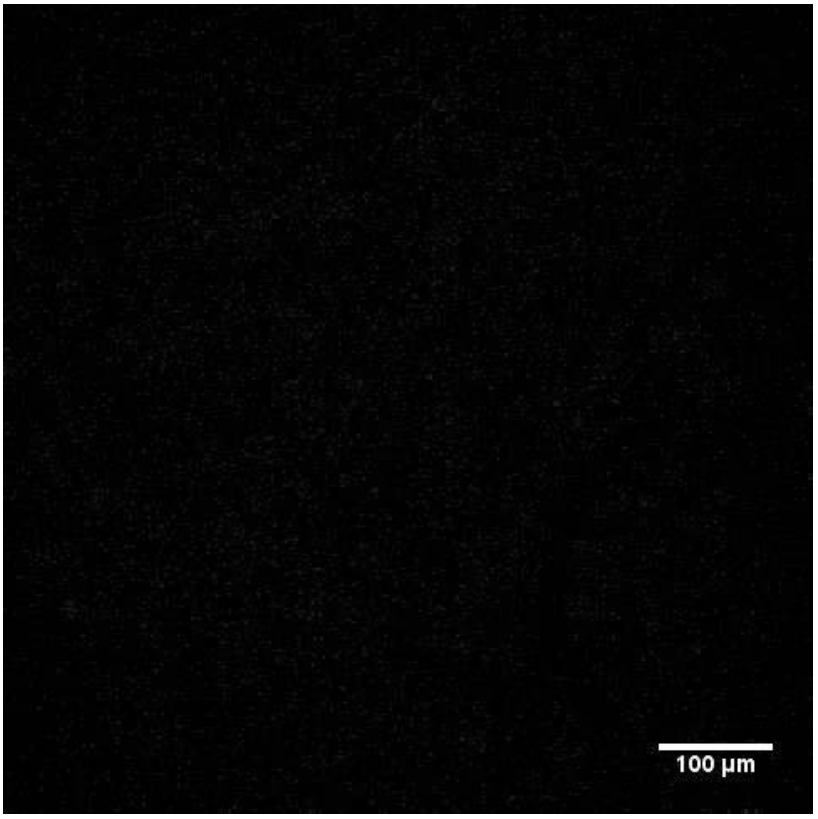

Figure S10. Confocal microscopy image of the prepared heterogeneous bimodal network prepared with 20 wt% short chains.

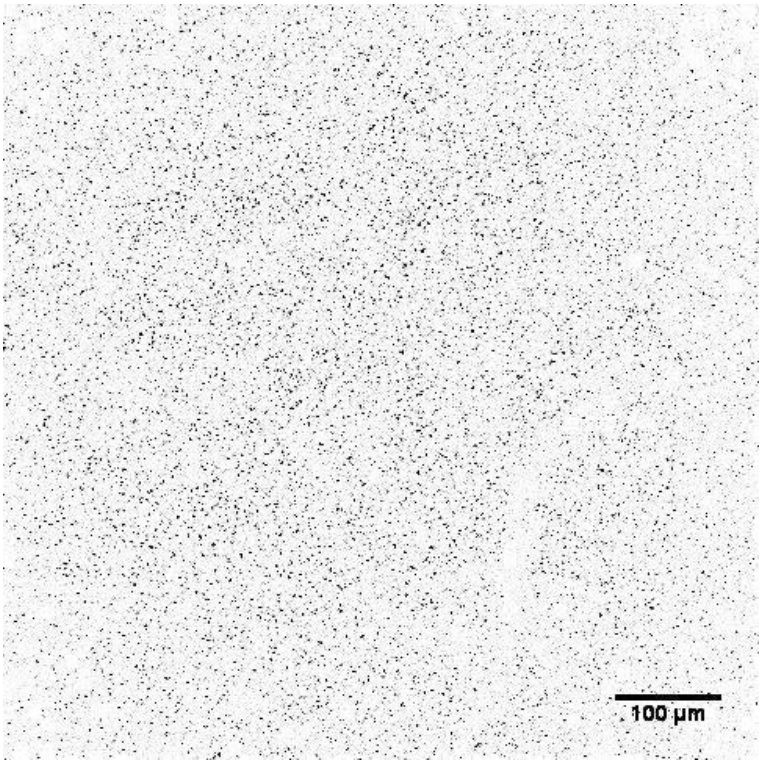

Figure S11. Grayscale confocal microscopy image of the prepared heterogeneous bimodal network prepared with 20 wt% short chains.

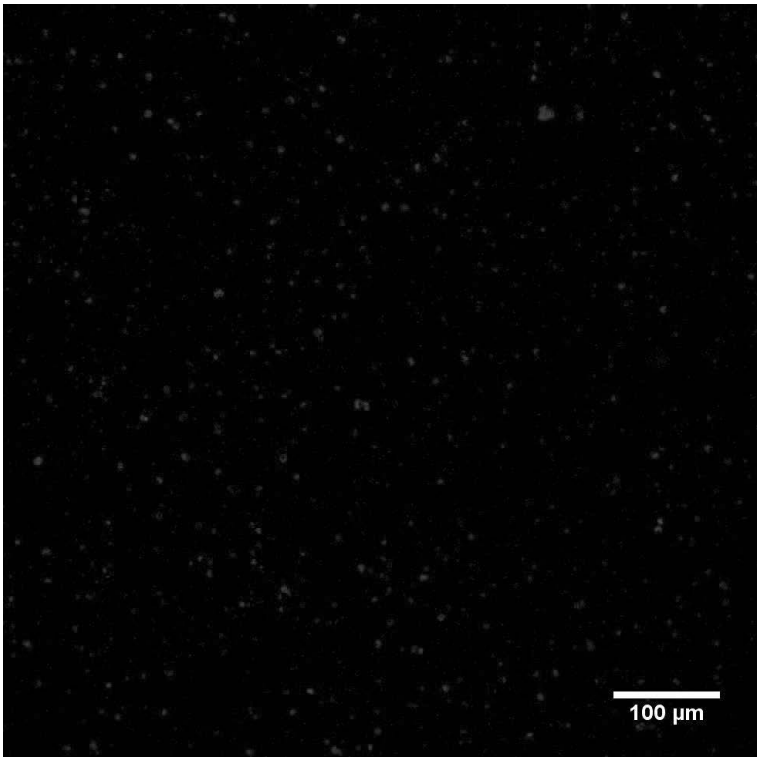

Figure S12. Confocal microscopy image of the prepared heterogeneous bimodal network prepared with 30 wt% short chains.

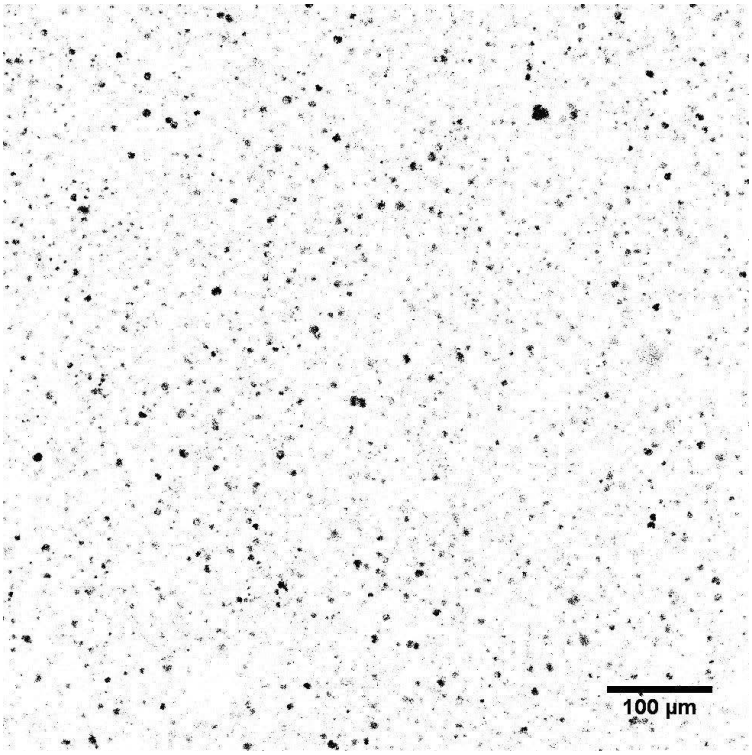

Figure S13. Grayscale confocal microscopy image of the prepared heterogeneous bimodal network prepared with 30 wt% short chains.

Small amplitude rheology

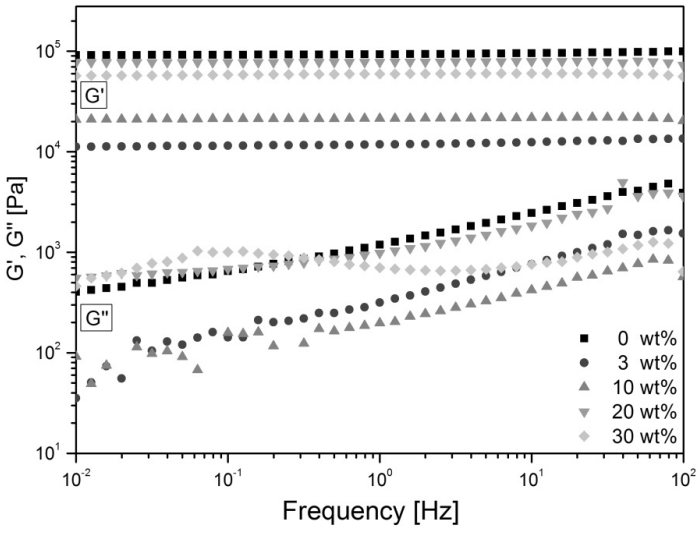

Figure S14. Storage modulus (G') and loss modulus (G'') as functions of frequency for PDMS networks prepared with different concentration of short chains.

[1] Madsen, F. B.; Dimitrov, I.; Daugaard, A. E.; Hvilsted, S.; Skov, A. L. *Polym. Chem.,* 2013, **4**, 1700–1707.

Appendix D

F. B. Madsen, I. Javakhishvili, R. E. Jensen, A. E. Daugaard, S. Hvilsted, A. L. Skov, 2014 Synthesis of telechelic vinyl/allyl functional siloxane copolymers with structural control, *Polymer Chemistry*, **5**, 7054-7061.

Polymer Chemistry

PAPER

View Article Online
View Journal | View Issue

Cite this: *Polym. Chem.*, 2014, **5**, 7054

Synthesis of telechelic vinyl/allyl functional siloxane copolymers with structural control†

F. B. Madsen, I. Javakhishvili, R. E. Jensen, A. E. Daugaard, S. Hvilsted and A. L. Skov*

Received 2nd July 2014,
Accepted 9th September 2014

DOI: 10.1039/c4py00919c

www.rsc.org/polymers

Multifunctional siloxane copolymers with terminal vinyl or allyl functional groups are synthesised through the borane-catalysed polycondensation of hydrosilanes and alkoxysilanes. Copolymers of varying molecular weights ($\bar{M}_w$ = 13 200–70 300 g mol^{-1}), spatially well-distributed functional groups and high end-group fidelity are obtained in a facile and robust synthetic scheme involving polycondensation, end-group transformation and different functionalisation reactions such as Cu(I)-mediated azide–alkyne cycloaddition. Pendant alkyl chloride, alkyl azide, bromoisobutyryl, 4-nitrobenzene and 1-ethyl-imidazolium chloride fragments with programmable spatial distributions are incorporated in the copolymer backbones. NMR and FTIR spectroscopy as well as size exclusion chromatography corroborate the efficacy and versatility of this modular approach.

Introduction

The development of functional polymers is attracting increasing interest, due to a growing number of applications within nanotechnology-, sustainability-, biomedical- and energy-related fields. Functional polymers with specific control over architecture, polarity, functionality, solubility and reactivity are in especially high demand[1] and controlled functionalisation is often used to change bulk and/or surface properties, in order to expand the application range of a given polymer.

Polysiloxanes, *i.e.* polymers containing Si–O–Si repeating units, are a group of polymers with significant industrial importance, since especially polysiloxane elastomers are used widely in advanced applications such as adhesives, membranes, implants and dielectric electro active polymers.[2–6]

The synthesis of polysiloxanes is generally accomplished through the nucleophilic substitution of chlorosilanes with water, to form low molecular weight linear silanols and cyclic siloxanes which are further reacted into high molecular weight polymers catalysed by acids or bases.[7] Ring-opening polymerisation of cyclic siloxanes is very efficient and is extensively used to prepare siloxane homopolymers and random copolymers.[8] A convenient method for more well-defined copolymers is the dehydrogenative coupling of organohydrosilanes with organohydrosilanols, due to the high selectivity and easy removal of the hydrogen by-product. However, this type of reaction requires relatively high concentrations (≥0.1 mol%) of precious metal catalysts such as platinum, palladium, ruthenium or rhodium. Furthermore, only moderate molecular weight copolymers have been achieved, and undesired silanol self-condensation can occur and lead to disruption to a perfectly alternating copolymer structure.[9–13]

The Piers–Rubinsztajn reaction, which uses the tris(pentafluorophenyl)borane catalyst, offers an alternative route to structured siloxane copolymers. Piers *et al.* reported its use as a catalyst for reactions involving organohydrosilanes,[14–16] while Rubinsztajn and Cella used it afterwards as a catalyst for siloxane homo- and copolymers.[8,17,18] The Piers–Rubinsztajn reaction therefore refers to a tris(pentafluorophenyl)borane-catalysed reaction between a hydrosilane and an alkoxysilane, forming siloxanes with concomitant loss of an alkane – as seen in Scheme 1.[19] The reaction is characterised by being exceptionally rapid, mild and efficient, since it can be carried out at ambient temperatures and uses low amounts of borane catalyst.

While functional polysiloxanes with, for example, amino-, chloro- and mercapto-functional groups are commercially available (*e.g.* from Gelest), they do not contain functional end-groups that allow them to be used in the synthesis of silicone elastomers. It is therefore difficult to obtain from commercially available raw materials elastomers with well distribu-

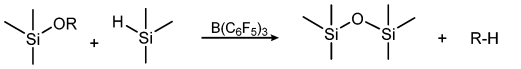

Scheme 1 Condensation reaction between hydrosilanes and alkoxysilanes, forming an inert alkane by-product.

Technical University of Denmark, Department of Chemical and Biochemical Engineering, Danish Polymer Centre, Building 227, DK-2800 Kgs. Lyngby, Denmark. E-mail: al@kt.dtu.dk; Tel: +45 4525 2825

†Electronic supplementary information (ESI) available: Numbered structures for ^{13}C-NMR assignment and ^{1}H-NMR spectrum of **4**. See DOI: 10.1039/c4py00919c

ted functional groups. Silicone elastomers are frequently prepared by platinum-catalysed hydrosilylation reactions, where vinyl end-groups of polysiloxanes react with hydrosilane groups on siloxane cross-linkers. Functional elastomers can hence be prepared by using one of the components in excess and reacting vinyl- or hydride-functional molecules thereon. This approach, however, compromises network formation, meaning that inferior elastomer properties are thus a consequence.[20]

The aim of this work is to prepare spatially distributed and controlled functional siloxane copolymers through borane-catalysed polycondensation, which offers a rapid and efficient reaction method. The copolymers will contain vinyl or allyl end-groups, which will allow for platinum catalysed cross-linking reactions with hydrosilane cross-linkers. Furthermore, various functional groups along the backbone of the copolymers open up, for example, Williamson ether syntheses or copper-catalysed cycloaddition reactions of azides and alkynes (CuAAC) forming 1,4-disubstituted-1,2,3-triazoles, a so-called "click" reaction.[21–24] Click reactions, which previously have been used to functionalise polymers in general[25–28] and polysiloxanes in particular,[29–32] are particularly efficient in the functionalization of polymers, as they do not form any by-products and yields are often high.

The prepared copolymers will vary greatly from the siloxane polymers originally prepared by Rubinsztajn and Cella,[8,17,18] who prepared non-functional alternating aromatic and non-aromatic copolymers, in that the copolymers presented in this study will contain functional end-groups and reactive functional groups, which are spatially well-distributed through the use of dimethylsiloxane pre-polymer spacer units.

Herein we present the synthesis and characterisation of novel functional siloxane copolymers and describe how to tune the obtained molecular weights and the content of the spatially distributed functional units.

Experimental section

Materials and methods

Hydride-terminated PDMS, DMS-H11 ($\bar{M}_w \sim 1200$ g mol^{-1}, as determined by ^{1}H-NMR), 3-(chloropropyl)methyldimethoxysilane, vinyldimethylsilane and allyldimethylsilane were acquired from Gelest Inc. Hydride-terminated PDMS ($\bar{M}_w \sim 580$ g mol^{-1} as stated by supplier) was purchased from Sigma-Aldrich. All other chemicals were acquired from Sigma-Aldrich and used as received unless otherwise stated.

FTIR spectroscopy was conducted on PerkinElmer Spectrum One model 2000 Fourier Transform Infrared apparatus equipped with a universal attenuated total reflection accessory on a ZnSe/diamond composite. Spectra were recorded in the range of 4000–650 cm^{-1}, with 4 cm^{-1} resolution and 16 scans. ^{1}H- and ^{13}C-NMR experiments were performed on a Bruker 300 MHz spectrometer in $CDCl_3$, while size-exclusion chromatography (SEC) was performed on a Tosoh EcoSEC HLC-8320GPC instrument equipped with RI and UV detectors and SDV Linear S columns from PSS, Mainz, Germany. Samples were run in toluene at 35 °C at a rate of 1 mL min^{-1}, and molar mass characteristics were calculated using WinGPC Unity 7.4.0 software and linear polydimethylsiloxane (PDMS) standards acquired from PSS, Mainz, Germany.

Syntheses

All reactions were carried out in a nitrogen atmosphere. Structures for ^{13}C-NMR assignment can be found in the ESI.†

General procedure for Piers–Rubinsztajn polymerisation, α,ω-methoxy-poly((chloropropyl)methylsiloxane-*co*-dimethylsiloxane) (1). 3-Chloropropylmethyldimethoxysilane (2.00 g, 10.9 mmol) was dissolved in dry heptane (20 mL) in a 250 mL two-neck round-bottomed flask. Hydride-terminated dimethylsiloxane (Aldrich, ~580 g mol^{-1}) (6.03 g, 10.4 mmol) was added and the mixture was stirred for 5 minutes. Tris(pentafluorophenyl)borane (0.6 mL, 0.04 M, 0.2 mol%) in dry toluene (2 mL) was added and methane gas developed. The mixture was stirred at RT for 1 hour, where after excess dimethoxydimethylsilane (5.26 g, 43.7 mmol) was added, in order to quench any potentially remaining hydride groups and to ensure that all polymers possessed methoxy end-groups. The reaction mixture was stirred additionally for a couple of hours. The solvent and excess dimethoxydimethylsilane (bp: 82 °C) were removed *in vacuo* at 45 °C with toluene, to give the product as a clear oil (7.42 g, 96.4%). IR (cm^{-1}): 2960 (C–H stretch); 1410 (Si–CH_2 stretch); 1260 (Si–CH_3 stretch); 1010 (Si–O stretch). ^{1}H NMR ($CDCl_3$, δ_H, ppm): 0.08–0.09 (m, CH_3–Si), 0.63 (m, –Si–CH_2–CH_2–), 1.83 (m, –CH_2–CH_2–CH_2), 3.49 (s, 6H, –O–CH_3), 3.50 (t, ^3J = 6.9 Hz, Cl–CH_2–CH_2). ^{13}C-NMR ($CDCl_3$, δ_C, ppm): −0.51 to 1.54 (e + f), 15.06 (b), 26.78 (c), 47.59 (d), 49.90 (a).

General procedure for end-capping, α,ω-vinyl-poly((chloropropyl)methylsiloxane-*co*-dimethylsiloxane) (2a-7). Copolymer **1** (1.5 g, ~0.073 mmol methoxy end-groups) was dissolved in dry heptane (20 mL) in a 250 mL two-neck round-bottomed flask. Vinyldimethylsilane (1.89 g, 21.8 mmol) was added and the mixture was stirred at RT overnight after which ^{1}H-NMR was used in order to confirm the removal of methoxy groups and conversion to vinyl groups. Neutral aluminium oxide (5 g) was added to the reaction mixture to remove the tris(pentafluorophenyl)borane catalyst, and the solution was then filtered through 0.45 μm PFTE filters. The solvent and excess vinyldimethylsilane reagent were removed *in vacuo*, to give the product as a clear oil (1.35 g, 90.3%). IR (cm^{-1}): 2960 (C–H stretch); 1410 (Si–CH_2 stretch); 1260 (Si–CH_3 stretch); 1010 (Si–O stretch). ^{1}H NMR ($CDCl_3$, δ_H, ppm): 0.08–0.09 (m, CH_3–Si), 0.62 (m, –Si–CH_2–CH_2–), 1.82 (m, –CH_2–CH_2–CH_2–), 3.50 (t, ^3J = 6.9 Hz, Cl–CH_2–CH_2), 5.74 (dd, 2H, ^2J = 4.2 Hz, ^3J = 20 Hz, CH═CH_2), 5.94 (dd, 2H, ^2J = 4.2 Hz, ^3J = 15 Hz, CH═CH_2), 6.12 (dd, 2H, ^3J = 16 Hz, ^3J = 21 Hz, –CH═CH_2). ^{13}C-NMR ($CDCl_3$, δ_C, ppm): −0.52 to 1.53 (c + d + h), 15.04 (e), 26.75 (f), 47.61 (g), 131.86 (a), 139.10 (b).

α,ω-Allyl-poly((chloropropyl)methylsiloxane-*co*-dimethylsiloxane) (2b-1). The polymer was prepared according to the general end-capping procedure using **1** (3 g, 0.14 mmol

methoxy end-groups) and allyldimethylsilane (4.38 g, 43.7 mmol) to give a clear oil (2.85 g, 95.1%) IR (cm^{-1}): 2960 (C–H stretch); 1630 (C=C stretch); 1410 (Si–CH_2 stretch); 1260 (Si–CH_3 stretch); 1010 (Si–O stretch). ^{1}H NMR ($CDCl_3$, δ_H, ppm): −0.05 to 0.09 (m, CH_3–Si), 0.62 (m, –Si–CH_2–CH_2–), 1.50 (d, 4H, ^3J = 8.1 Hz, CH_2–CH=CH_2), 1.82 (m, –CH_2–CH_2–CH_2–), 3.50 (t, ^3J = 6.9 Hz, Cl–CH_2–CH_2), 4.83 (m, 4H, CH=CH_2), 5.77 (m, 2H, CH=CH_2). ^{13}C-NMR ($CDCl_3$, δ_C, ppm): −0.53 to 1.54 (d + e + i), 15.04 (f), 23.41 (c), 26.75 (g), 47.61 (h), 112.53 (a), 135.30 (b).

α,ω-Allyl-poly((azidopropyl)methylsiloxane-*co*-dimethylsiloxane) (3). Following a procedure adapted from Rambarran *et al.*[33] copolymer **2b-1** (0.75 g, ~1.02 mmol (chloropropyl) methylsiloxane units), NaN_3 (0.35 g, 5.4 mmol) and tetrabutylammonium azide (0.03 g, 0.11 mmol) were dissolved in dry THF (10 mL) in a 100 mL round-bottomed flask. The reaction mixture was stirred under reflux for 48 hours. THF was removed *in vacuo* and the reaction mixture was re-dissolved in heptane (20 mL), washed with water (3 × 20 mL) and brine (1 × 20 mL), dried with $MgSO_4$ and then filtered and concentrated *in vacuo* to afford a transparent, viscous liquid (0.67 g, 89.5%). IR (cm^{-1}): 2960 (C–H stretch); 2095 (–N_3 stretch); 1630 (C=C stretch); 1410 (Si–CH_2 stretch); 1260 (Si–CH_3 stretch); 1010 (Si–O stretch). ^{1}H NMR ($CDCl_3$, δ_H, ppm): −0.05 to 0.09 (m, CH_3–Si), 0.58 (m, –Si–CH_2–CH_2–), 1.50 (d, 4H, ^3J = 8.1 Hz, CH_2–CH=CH_2), 1.65 (m, –CH_2–CH_2–CH_2–), 3.23 (t, ^3J = 7.1 Hz, N_3–CH_2–CH_2), 4.83 (m, 4H, CH=CH_2), 5.77 (m, 2H, CH=CH_2). ^{13}C-NMR ($CDCl_3$, δ_C, ppm): −0.55 to 1.03 (d + e + i), 14.50 (f), 22.77 (g), 23.40 (c), 54.14 (h), 112.51 (a), 135.32 (b).

General procedure for CuAAC click reactions, synthesis of α,ω-allyl-poly((2-bromo-2-methylpropanoate)-1*H*-1,2,3-triazolepropyl)methylsiloxane-*co*-dimethylsiloxane) (4). 3 (0.2 g, ~0.27 mmol (azidopropyl)methylsiloxane units) and propargyl-2-bromoisobutyrate (0.06 g, 0.28 mmol) were dissolved in dry THF (3.5 mL) in a 25 mL two-neck round-bottomed flask. CuI (0.006 g, 0.03 mmol) was subsequently added and Et_3N (0.04 g, 0.43 mmol) was added drop-wise. The reaction was carried out at RT for 17 hours at which point FTIR confirmed the disappearance of the azide band at 2095 cm^{-1}. THF was evaporated and the reaction mixture was precipitated into cold methanol. The solvent was then decanted and the product was dried *in vacuo*, providing a dark-green viscous oil (0.18 g, 74.0% – after precipitation). IR (cm^{-1}): 2960 (C–H stretch); 1740 (C=O stretch); 1630 (C=C stretch); 1465 (C–H bend); 1370 (C–H bend); 1410 (Si–CH_2 stretch); 1260 (Si–CH_3 stretch); 1155 (C–O stretch); 1010 (Si–O stretch). ^{1}H NMR ($CDCl_3$, δ_H, ppm): −0.06 to 0.13 (m, CH_3–Si), 0.58 (m, –Si–CH_2–CH_2–), 1.54 (d, 4H, ^3J = 7.8 Hz, CH_2–CH=CH_2), 1.82 (m, –CH_2–CH_2–CH_2–), 1.91 (s, Br–C(CH_3)$_2$), 4.33 (t, ^3J = 7.2 Hz, N–CH_2–CH_2), 4.84 (m, 4H, CH=CH_2), 5.33 (s, C–CH–O), 5.76 (m, 2H, CH=CH_2), 7.61 (s, –C=CH–N). ^{13}C-NMR ($CDCl_3$, δ_C, ppm): −0.57 to 1.03 (d + e + q), 14.24 (f), 24.33 (g), 30.62 (p), 52.97 (h), 55.53 (o), 59.22 (k), 123.47 (i), 142.25 (j), 171.46 (l) (a, b and c not visible).

Synthesis of α,ω-allyl-poly((4-(4-nitrophenyl)-1*H*-1,2,3-triazolepropyl)methylsiloxane-*co*-dimethylsiloxane) (5). The polymer was prepared according to the general click reaction procedure using **3** (0.1 g, ~0.14 mmol (azidopropyl)methylsiloxane units), 1-ethynyl-4-nitrobenzene (0.05 g, 0.31 mmol), CuI (0.005 g, 0.02 mmol) and Et_3N (0.03 g, 0.28 mmol) for 24 hours at 45 °C to give a red viscous oil (0.08 g, 69.3% – after precipitation). IR (cm^{-1}): 2960 (C–H stretch); 1605 (aromatic C=C stretch); 1520 (N=O asymmetric stretch); 1410 (Si–CH_2 stretch); 1340 (N=O symmetric stretch); 1260 (Si–CH_3 stretch); 1010 (Si–O stretch). ^{1}H NMR (CDCl3, δ_H, ppm): −0.45 to 0.13 (m, CH_3–Si), 0.55 (m, –Si–CH_2–CH_2–), 1.57 (d, 4H, ^3J = 8.1 Hz, CH_2–CH=CH_2), 2.02 (m, –CH_2–CH_2–CH_2–), 4.41 (t, ^3J = 7.2 Hz, N–CH_2–CH_2), 4.83 (m, 4H, CH=CH_2), 5.77 (m, 2H, CH=CH_2), 7.90 (s, –C=CH–N), 7.99 (m, Ar–H), 8.27 (m, NO_2–Ar–H). ^{13}C-NMR ($CDCl_3$, δ_C, ppm): −0.55 to 1.03 (d + e + q), 14.23 (f), 24.39 (g), 53.09 (h), 120.68 (i), 124.29 (o), 126.05 (l), 137.04 (k), 145.45 (p), 147.26 (j) (a, b and c not visible).

Synthesis of α,ω-vinyl-poly((1-ethyl-1*H*-imidazol-3-ium chloride)-1*H*-1,2,3-triazolepropyl)methylsiloxane-*co*-dimethylsiloxane) (6). 2a-8 (14.0 g, ~19.1 mmol (chloropropyl) methylsiloxane units) and 1-ethylimidazole (9.19 g, 95.6 mmol) were mixed in a 250 mL two-neck round-bottomed flask. The reaction was carried out at 95 °C for 48 hours under reflux. The product was washed four times with toluene to remove excess 1-ethylimidazole and then dried *in vacuo* to give the product as an orange-brown oil (7.3 g, 46.0%). IR (cm^{-1}): 3085 (C=C stretch); 2965 (C–H stretch); 1630 (C=N, C=C stretch); 1565 (C=N ring stretch); 1455 (C–H bend); 1405 (Si–CH_2 stretch); 1260 (Si–CH_3 stretch); 1010 (Si–O stretch). ^{1}H NMR ($CDCl_3$, δ_H, ppm): 0.073–0.16 (m, CH_3–Si), 0.54 (m, –Si–CH_2–CH_2–), 1.60 (m, CH_3–CH_2–N–), 1.94 (m, –CH_2–CH_2–CH_2–), 4.35 (m, CH_3–CH_2–N–), 4.43 (m, –N^+–CH_2–CH_2–CH_2–), 5.73 (dd, 2H, ^2J = 4.2 Hz, ^3J = 20 Hz, CH=CH_2), 5.94 (dd, 2H, ^2J = 4.1 Hz, ^3J = 15 Hz, CH=CH_2), 6.13 (dd, 2H, ^3J = 15 Hz, ^3J = 20 Hz, –CH=CH_2), 7.42 (d, ^3J = 1.5 Hz, N^+–CH=CH–), 7.60 (d, ^3J = 1.5 Hz, N^+–CH=CH–), 10.9 (s, –N–CH=N^+–). ^{13}C-NMR ($CDCl_3$, δ_C, ppm): −0.66 to 1.09 (c + d + m), 13.60 (e), 15.53 (k), 24.24 (f), 45.10 (j), 52.07 (g), 121.34 (i), 122.15 (h), 136.54 (l) (a and b not visible).

Results and discussion

Siloxane copolymers with spatially well-distributed functional groups were prepared as illustrated in Scheme 2. Synthesis was accomplished through the tris(pentafluorophenyl)borane-catalysed Piers–Rubinsztajn reaction of 3-chloropropylmethyldimethoxysilane and hydride-terminated dimethylsiloxane pre-polymers to form methoxy-terminated copolymers **1**. The borane-catalysed polycondensation of hydrosilanes and methoxysilanes to form **1** involves cleaving C–O and Si–H bonds while forming Si–O and C–H bonds in an exothermic reaction ($\Delta H \approx -250$ KJ mol^{-1}).[8] The reaction is performed at room temperature using low levels of $B(C_6F_5)_3$ catalyst (<0.5 mol%). At higher catalyst concentrations (~1–5 mol%), hydrosilylation reactions may compete with the Piers–Rubinsztajn polycondensation reaction.[34,35] The reaction is almost instantaneous and is completed within a few minutes, but it was left to stir

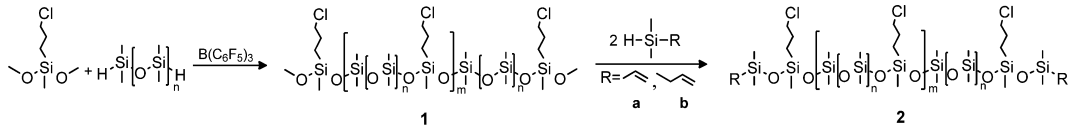

Scheme 2 Synthetic route for telechelic vinyl/allyl siloxane copolymers *via* borane catalysed polycondensation.

for 1 hour, in order to ensure the full conversion of reagents. Furthermore, high yields were obtained (>95%). At this point ^{1}H-NMR and FTIR spectroscopy were used to confirm the completeness of the reaction through assessing the disappearance of the hydride-groups on the hydride-terminated pre-polymers. In ^{1}H-NMR, resonance at δ_H = 4.7 ppm disappeared, which was also corroborated by FTIR, where the distinctive stretch at 2125 cm^{-1} was no longer present. In order to ensure at this stage that all polymers contained methoxy end-groups, significant amount of excess dimethoxydimethylsilane was added to the reaction mixture so that any remaining hydride groups would react. The excess dimethoxydimethylsilane was easily removed *in vacuo*.

The prepared copolymers were characterised by SEC, and molar mass characteristics were calculated from linear polydimethylsiloxane standards. The results are summarised in Table 1. Two dimethylsiloxane pre-polymers of different molecular weights were used, in order to create copolymers with varying mol% of the (chloropropyl)methylsiloxane unit and with different spacer lengths between the functional groups. The molecular weights of the final copolymers were varied furthermore by changing the stoichiometry between the hydrosilane pre-polymers and the methoxysilane compound. According to standard polycondensation theory, the highest molecular weight would be obtained when using stoichiometries closest to unity.[36] This is not the case in these experiments, solely due to rough estimates of exact pre-polymer molecular weights, in which case the exact stoichiometry cannot be calculated. In the case of the pre-polymer of $\bar{M}_w \sim$ 1200 g mol^{-1} the highest molecular weight is obtained when using a stoichiometry of hydrosilane–methoxysilane of 0.95/1, with a molecular weight of $\bar{M}_w$ = 70 300 g mol^{-1}. For the pre-polymer of $\bar{M}_w \sim$ 580 g mol^{-1} the highest molecular weight was obtained using the stoichiometry of hydrosilane–methoxysilane of 1/0.95, where $\bar{M}_w$ = 56 700 g mol^{-1} was attained.

In order to test the reproducibility of the borane-catalysed polycondensations a reaction with the pre-polymer of $\bar{M}_w \sim$ 1200 g mol^{-1} was repeated. As seen in Table 1, entries **2a-2** and **2a-3** were prepared using similar reaction conditions, and SEC provided comparable results for both experiments. This shows that the polycondensation reaction is quite robust when using similar reaction conditions.

The aim of this study was to create functional copolymers with molecular weights suitable for silicone elastomer synthesis. The best elastomer properties are usually obtained when using polymers with molecular weights of $\bar{M}_w \sim$ 20 000–30 000 g mol^{-1}.[37] Molecular weights in this range were obtained for copolymer **2a-4** with a stoichiometric ratio of hydrosilane–methoxysilane of 1/0.9 using the pre-polymer of $\bar{M}_w \sim$ 1200 g mol^{-1}, where a molecular weight of $\bar{M}_w$ = 25 900 g mol^{-1} was reached, and for **2a-7**, **2a-8** and **2b-1** with stoichiometries of hydrosilane–methoxysilane of 0.95/1 and 0.975/1, respectively, using the pre-polymer of $\bar{M}_w \sim$ 580 g mol^{-1}, where molecular weights of $\bar{M}_w$ = 20 600 g mol^{-1}, $\bar{M}_w$ = 22 500 g mol^{-1} and $\bar{M}_w$ = 22 100 g mol^{-1} were achieved. Copolymers prepared with the $\bar{M}_w \sim$ 1200 g mol^{-1} pre-polymer display polydispersity indexes ($\bar{M}_w/\bar{M}_n$) from 2.20 to 3.80, whereas copolymers prepared with the lower molecular weight pre-polymer of $\bar{M}_w \sim$ 580 g mol^{-1} display $\bar{M}_w/\bar{M}_n$ in the range of 2.84 to 3.62.

Table 1 SEC results for prepared functional siloxane copolymers with varying pendant groups as well as varying end-groups

Entry	$\bar{M}_w$ pre-polymer [g mol^{-1}]	Stoichiometry hydrosilane–methoxysilane	Functional group	End-group	$\bar{M}_w \times 10^{-3}$ [g mol^{-1}]	$\bar{M}_w/\bar{M}_n$	Estimated value of n	Estimated value of m
1	~1200	1/1	Chloro	Methoxy	50.4	2.22	15	34
2a-1	~1200	1/1	Chloro	Vinyl	47.9	2.20	15	34
2a-2	~1200	0.95/1	Chloro	Vinyl	70.3	2.03	15	49
2a-3	~1200	0.95/1	Chloro	Vinyl	69.9	2.25	15	49
2a-4	~1200	1/0.9	Chloro	Vinyl	25.9	3.23	15	17
2a-5	~1200	1/0.8	Chloro	Vinyl	13.2	3.80	15	8
2a-6	~580	1/1	Chloro	Vinyl	37.4	3.17	7	46
2a-7	~580	0.95/1	Chloro	Vinyl	20.6	3.47	7	25
2a-8	~580	0.975/1	Chloro	Vinyl	22.5	2.79	7	27
2b-1	~580	0.95/1	Chloro	Allyl	22.1	3.49	7	26
2a-9	~580	1/0.95	Chloro	Vinyl	56.7	2.84	7	71
3	~580	0.95/1	Azido	Allyl	18.4	3.62	7	23
4	~580	0.95/1	2-Bromoisobutyrate	Allyl	27.5	2.43	7	26
5	~580	0.95/1	4-Nitrobenzene	Allyl	33.3	3.29	7	34
6	~580	0.975/1	1-Ethyl-imidazolium chloride	Vinyl	32.7	4.30	7	35

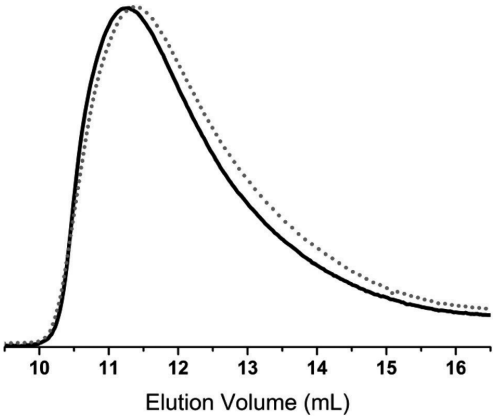

Fig. 1 An overlay of the RI SEC traces of methoxy end-functional copolymer **1** (black, – –) and vinyl end-functional copolymer **2a-1** (red, • • •).

End-functionalisation of **1** with vinyl- or allyldimethylsilane produced copolymers **2a** and **2b**, as seen in Scheme 2. These end-groups were chosen because they allow prepared copolymers to be used in the synthesis of silicone elastomers in platinum-catalysed hydrosilylation reactions. It is also possible to create copolymers with other end-groups, as long as the groups are compatible with the borane-catalysed reaction. Such end-groups, for example, could be, but are not limited to, silanes with aliphatics such as trimethyl-groups, aromatics and halogen-containing compounds.[38] The prepared telechelic vinyl/allyl copolymers were characterised by FTIR spectroscopy, ^{1}H- and ^{13}C-NMR spectroscopy and SEC. The end-group conversion was investigated by NMR using low molecular weight copolymers, *i.e.* **2-a5**, **2a-7** and **2b-1**. In this way it was ensured that the end-groups were clearly visible in the recorded spectra. For the telechelic vinyl copolymers (**2a**) ^{1}H- and ^{13}C-NMR confirmed the reaction through the disappearance of the O–CH_3 protons and a carbon atom at δ_H = 3.49 ppm and δ_C = 49.9 ppm, respectively. The presence of –CH=CH_2 protons as three distinctive doublets of doublets at δ_H = 5.74–6.12 ppm in the ^{1}H-NMR spectrum of **2a** points to the successful formation of vinyl end-groups. Furthermore, the presence of –CH=CH_2 groups can be detected in the ^{13}C-NMR spectra of **2a** with resonances at δ_C = 131.86 and 139.10 ppm. For telechelic allyl copolymers (**2b**) the reactions could be followed similarly by ^{1}H- and ^{13}C-NMR through the disappearance of the O–CH_3 protons and a carbon atom at δ_H = 3.49 ppm and δ_C = 49.9 ppm, respectively. The allyl-groups were detected by ^{1}H-NMR as resonances at δ_H = 1.5 ppm (–CH_2–CH=CH_2), δ_H = 4.86–4.92 ppm (–CH=CH_2) and δ_H = 5.79 ppm (–CH=CH_2) and by ^{13}C-NMR as resonances at δ_C = 26.4 ppm (–CH_2–CH=CH_2), δ_C = 113.7 ppm (–CH=CH_2) and 133.8 ppm (–CH=CH_2).

Converting the methoxy end-groups to vinyl/allyl end-groups did not alter the molecular weight of the copolymers, as illustrated in the SEC traces presented in Fig. 1. This also indicates that no unintended hydrosilylation reactions between the end-groups and vinyl- or allyldimethylsilane occur.

The synthesised chloro-functional copolymers were converted to azido-functional (**3**) through nucleophilic substitution in THF, using tetrabutylammonium azide as a phase-transfer catalyst as seen in Scheme 3. Entry **2b-1** was selected for this purpose, as the obtained molecular weight of $\bar{M}_w$ = 22 100 g mol^{-1} lies within the desired range for use in elastomer synthesis. The copolymer was successfully converted from chloro- to azido-functional, and this reaction was followed by FTIR through the appearance of the distinctive –N_3 band at 2095 cm^{-1}. Furthermore, ^{1}H- and ^{13}C-NMR corroborated this through a shift in the resonance signals of CH_2–Cl (δ_H = 3.50 ppm, δ_C = 47.6 ppm) to CH_2–N_3 (δ_H = 3.23 ppm, δ_C = 54.1 ppm). The prepared azido-functional copolymer was characterised by SEC, the results for which are shown in Fig. 2. It is evident that the molecular weight after the azide-substitution reaction is lower than for the corresponding chloro-functional copolymer, which could indicate that degradation has taken place. However, upon examination of the SEC overlays seen in Fig. 2, it is clear that no degradation has taken place, as both chromatograms are broad yet monomodal, with no lower molecular weight fragments appearing at higher elution volumes.

The lower obtained $\bar{M}_w$ for the azido-functional copolymer must be ascribed to tailing and a shift in the baseline due to enhanced interactions of the latter with the SEC columns.

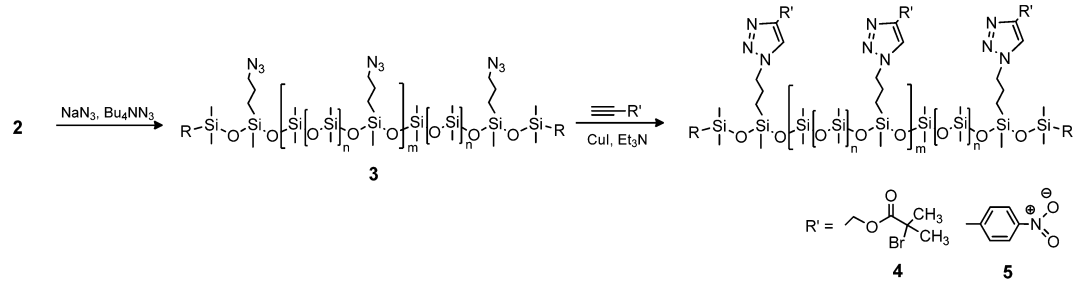

Scheme 3 Synthetic route to azido- and CuAAC-functionalised copolymers.

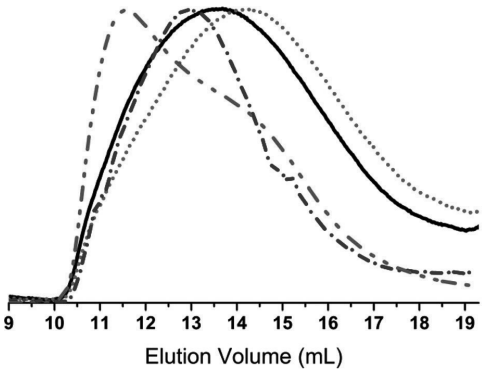

Fig. 2 An overlay of the RI SEC traces of chloro-functional copolymer **2b-1** (black, ––), azido-functional copolymer **3** (red, • • •), 2-bromoisobutyrate-functional copolymer **4** (blue, – •) and nitrobenzene-functional copolymer **5** (green, – • •).

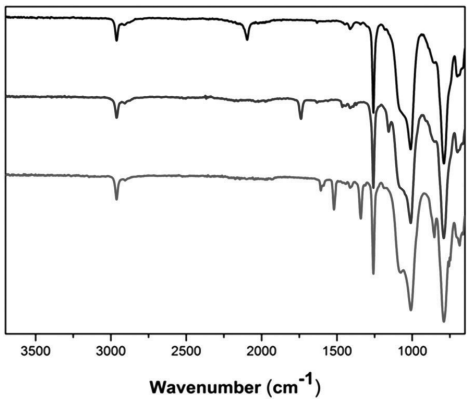

Fig. 3 FTIR spectra of azido-functional copolymer **3** (black, top), 2-bromoisobutyrate-functional copolymer **4** (blue, middle curve) and 4-nitrobenzene-functional copolymer **5** (red, bottom curve).

Functional dimethylsiloxane copolymers were created through a reaction with alkyne-functional molecules using CuAAC. Two different alkyne-containing molecules were chosen, in order to illustrate the versatility of the reaction. An aliphatic ATRP initiator and an alkyne-functional nitrobenzene were utilised as seen in Scheme 3. The ATRP initiator can be used to create polysiloxanes with different polymer side chains, whereas the aromatic compound 4-nitrobenzene can be used to increase dielectric permittivity in dielectric silicone elastomers.[32] Click-functionalised copolymers were prepared under similar reaction conditions by means of a CuI-Et_3N catalytic system. The reaction products were characterised by FTIR spectroscopy, ^{1}H- and ^{13}C-NMR spectroscopy and SEC. FTIR was used to confirm the completion of the click reaction through the disappearances of the alkyne and azide bands at ~3300 cm^{-1} and ~2095 cm^{-1}, respectively. For the reaction with the ATRP initiator (**4**), which produced a green-brown polymer, a distinct ester C=O band at 1740 cm^{-1} confirmed the presence of the 2-bromoisobutyrate group. In **5** the presence of 4-nitrobenzene was indicated by the red colour of the obtained polymer confirmed by bands at ~1605 cm^{-1} for the aromatic C=C bonds and at ~1520 cm^{-1} and ~1340 cm^{-1} for the N=O bonds. FTIR spectra of **3**, **4** and **5** can be seen in Fig. 3. The formation of the click products was furthermore confirmed by the presence of the triazole protons in ^{1}H-NMR, which appear at δ_H = 7.61 ppm and δ_H = 7.90 ppm for **4** and **5**, respectively. An assigned representative ^{1}H-NMR spectrum of **4** can be found in the ESI.†

The SEC results for click-products **4** and **5** can be seen in Table 1 and Fig. 2. For both click-products higher molecular weights are obtained, and a slight shift towards higher molecular weight regions can be seen in the SEC traces, pointing to the successful attachment of functional groups onto the copolymers. Furthermore, SEC showed that **5** had a strong UV signal, unlike the starting materials **2b-1** and **3**, which proves the attachment of the 4-nitrobenzene chromophore.

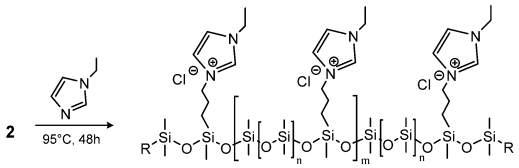

Scheme 4 Synthetic route to imidazole-functional copolymer.

Ionic polymers are a rapidly expanding class of materials with interesting and promising properties[39–41] which have recently been extended to silicone materials.[42] Thus, as an example of another possible post polymerisation modification, the prepared chloro-functional copolymer **2a-8** was used in a substitution reaction with 1-ethylimidazole to form the ionic copolymer seen in Scheme 4. This reaction was followed by ^{1}H-NMR through a shift in the resonance of CH_2–Cl (δ_H = 3.50 ppm) to CH_2–N^+ (δ_H = 4.43 ppm). After the reaction, the orange-brown copolymer was less soluble in toluene, thereby demonstrating the increased ionic/polar nature of the copolymer **6**. The SEC results for the chloro-functional copolymer **2a-8** and imidazolium-functional copolymer **6** can be seen in Table 1 and Fig. 4. As observed for the click-products, a slight shift towards the higher molecular region is seen in the SEC traces for copolymer **6**, which indicates the successful attachment of the functional group.

The prepared chloro- and azido-functional siloxane copolymers have great potential in the preparation of functional silicone elastomers where the properties of the elastomers can be altered and improved according to the given application and the type of group attached to the copolymer. The specific functional groups could include many different types[32] and are not limited to those used in this study. We are currently investi-

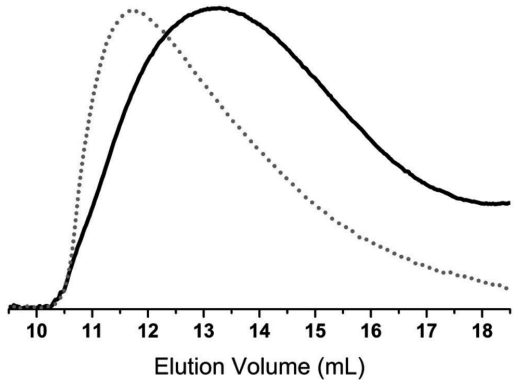

Fig. 4 An overlay of the RI SEC traces of chloro-functional copolymer **2a-8** (black, ––) and imidazole-functional copolymer **6** (red, • • •).

gating the use of synthesised functional copolymers for the preparation of functional elastomers, thus elucidating their properties.

Conclusions

In conclusion, we have successfully synthesised telechelic vinyl/allyl chloro-, azido- and CuAAC-functionalised siloxane copolymers and ensured spatial control over the functional groups. The polycondensation reaction proved to be rapid and very robust, with high yields obtained. The method therefore offers a fast and reliable technique for the synthesis of structured functional polysiloxanes. The content of functional groups in the copolymers could be varied by changing the molecular weight of the hydride-terminated dimethylsiloxane pre-polymers used in the polycondensation reactions. Furthermore, the molecular weights of the copolymers could be tuned by varying the stoichiometry of the hydrosilane and methoxysilane starting materials. Polymers with any conceivable concentration of functionality and molecular weight can thereby be obtained.

Acknowledgements

The authors wish to acknowledge InnovationsFonden for its financial support.

Notes and references

1 R. K. Iha, K. L. Wooley, A. M. Nyström, D. J. Burke, M. J. Kade and C. J. Hawker, *Chem. Rev.*, 2009, **109**, 5620–5686.
2 J. de Jong, R. G. H. Lammertink and M. Wessling, *Lab Chip*, 2006, **6**, 1125–1139.
3 M. A. Brook, *Biomaterials*, 2006, **27**, 3274–3286.
4 C. Löwe, X. Zhang and G. Kovacs, *Adv. Eng. Mater.*, 2005, **7**, 361–367.
5 P. Brochu and Q. Pei, *Macromol. Rapid Commun.*, 2010, **31**, 10–36.
6 F. B. Madsen, A. E. Daugaard, S. Hvilsted, M. Y. Benslimane and A. L. Skov, *Smart Mater. Struct.*, 2013, **22**, 104002.
7 M. A. Brook, *Silicon in organic, organometallic, and polymer chemistry*, John Wiley & Sons, New York, 2000.
8 S. Rubinsztajn and J. A. Cella, *Macromolecules*, 2005, **38**, 1061–1063.
9 Y. Li and Y. Kawakami, *Macromolecules*, 1999, **32**, 6871–6873.
10 Y. Li and Y. Kawakami, *Macromolecules*, 1999, **32**, 8768–8773.
11 C. L. Homrighausen and T. M. Keller, *J. Polym. Sci., Part A: Polym. Chem.*, 2002, **40**, 1334–1341.
12 Y. Li, M. Seino and Y. Kawakami, *Macromolecules*, 2000, **33**, 1–4.
13 R. Zhang, J. E. Mark and A. R. Pinhas, *Macromolecules*, 2000, **33**, 3508–3510.
14 D. J. Parks and W. E. Piers, *J. Am. Chem. Soc.*, 1996, **118**, 9440–9441.
15 J. M. Blackwell, K. L. Foster, V. H. Beck and W. E. Piers, *J. Org. Chem.*, 1999, **64**, 4887–4892.
16 D. Parks, J. Blackwell and W. Piers, *J. Org. Chem.*, 2000, **65**, 3090–3098.
17 S. Rubinsztajn and J. A. Cella, *Polym. Prepr.*, 2004, **45**(1), 635–636.
18 J. Cella and S. Rubinsztajn, *Macromolecules*, 2008, **41**, 6965–6971.
19 M. A. Brook, J. B. Grande and F. Ganachaud, *Adv. Polym. Sci.*, 2011, **235**, 161–183.
20 A. L. Larsen, K. Hansen, P. Sommer-Larsen, O. Hassager, A. Bach, S. Ndoni and M. Jørgensen, *Macromolecules*, 2003, **36**, 10063–10070.
21 H. C. Kolb, M. G. Finn and K. B. Sharpless, *Angew. Chem., Int. Ed.*, 2001, **40**, 2004–2021.
22 P. Wu, A. K. Feldman, A. K. Nugent, C. J. Hawker, A. Scheel, B. Voit, J. Pyun, J. M. J. Fréchet, K. B. Sharpless and V. V. Fokin, *Angew. Chem., Int. Ed.*, 2004, **43**, 3928–3932.
23 M. Meldal, *Macromol. Rapid Commun.*, 2008, **29**, 1016–1051.
24 W. H. Binder and R. Sachsenhofer, *Macromol. Rapid Commun.*, 2008, **29**, 952–981.
25 A. D. Thomsen, E. Malmström and S. Hvilsted, *J. Polym. Sci., Part A: Polym. Chem.*, 2006, **44**, 6360–6377.
26 A. E. Daugaard, S. Hvilsted, T. S. Hansen and N. B. Larsen, *Macromolecules*, 2008, **41**, 4321–4327.
27 S. Hvilsted, *Polym. Int.*, 2012, **61**, 485–494.
28 A. E. Daugaard and S. Hvilsted, *Macromol. Rapid Commun.*, 2008, **29**, 1119–1125.
29 F. Gonzaga, G. Yu and M. A. Brook, *Macromolecules*, 2009, **42**, 9220–9224.
30 F. Gonzaga, G. Yu and M. A. Brook, *Chem. Commun.*, 2009, 1730–1732.

31 U. Schmidt, P. C. Zehetmaier and B. Rieger, *Macromol. Rapid Commun.*, 2010, **31**, 545–548.
32 F. B. Madsen, I. Dimitrov, A. E. Daugaard, S. Hvilsted and A. L. Skov, *Polym. Chem.*, 2013, **4**, 1700–1707.
33 T. Rambarran, F. Gonzaga and M. A. Brook, *Macromolecules*, 2012, **45**, 2276–2285.
34 M. Rubin, T. Schwier and V. Gevorgyan, *J. Org. Chem.*, 2002, **67**, 1936–1940.
35 C. Xunjun, C. Yingde, Y. Guoqiang and L. Liewen, *J. Appl. Polym. Sci.*, 2007, **106**, 1007–1013.
36 P. J. Flory, *Principles of Polymer Chemistry*, Cornell University Press, Ithaca, New York, 1953, ch. 3, 8 and 9.
37 A. L. Larsen, P. Sommer-Larsen and O. Hassager, *e-Polymers*, 2004, **50**, 1–18.
38 J. B. Grande, D. B. Thompson, F. Gonzaga and M. A. Brook, *Chem. Commun.*, 2010, **46**, 4988–4990.
39 M. D. Green, D. S. Cruz, Y. Ye, J. M. Layman, Y. A. Elabd, K. I. Winey and T. E. Long, *Macromol. Chem. Phys.*, 2011, **212**, 2522–2528.
40 P. Dimitrov-Raytchev, S. Beghdadi, A. Serghei and E. Drockenmuller, *J. Polym. Sci., Part A: Polym. Chem.*, 2013, **51**, 34–38.
41 S. Jana, V. A. Vasantha, L. P. Stubbs, A. Parthiban and J. G. Vancso, *J. Polym. Sci., Part A: Polym. Chem.*, 2013, **51**, 3260–3273.
42 L. Yu, L. B. Gonzalez, S. Hvilsted and A. L. Skov, *Proc. SPIE-Int. Soc. Opt. Eng.*, 2014, **9056**, 90560C.

Supporting Information

Synthesis of telechelic vinyl/allyl functional siloxane copolymers with structural control

F. B. Madsen, I. Javakhishvili, R. E. Jensen, A. E. Daugaard, S. Hvilsted and A. L. Skov*,

Danish Polymer Center, Department of Chemical and Biochemical Engineering, Technical University of Denmark, Building 227, 2800 Kgs. Lyngby, Denmark

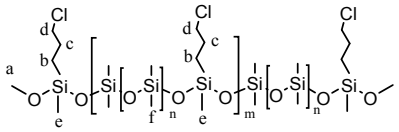

1

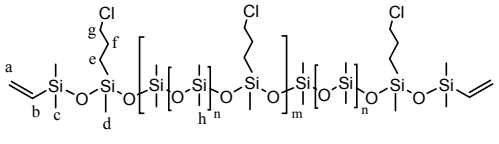

2a-7

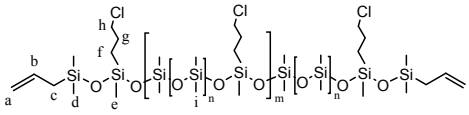

2b-1

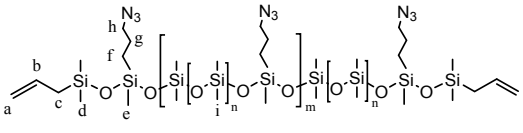

3

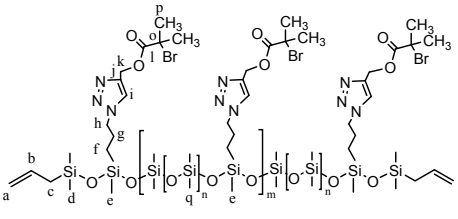

4

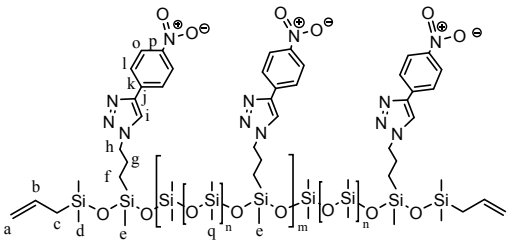

5

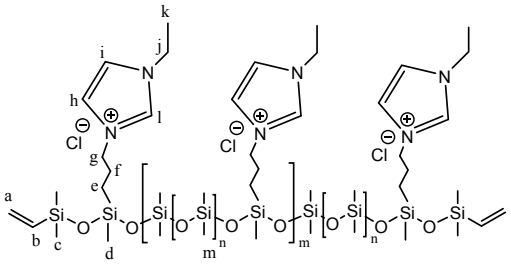

6

Figure S1: Structures for ^{13}C-NMR assignment.

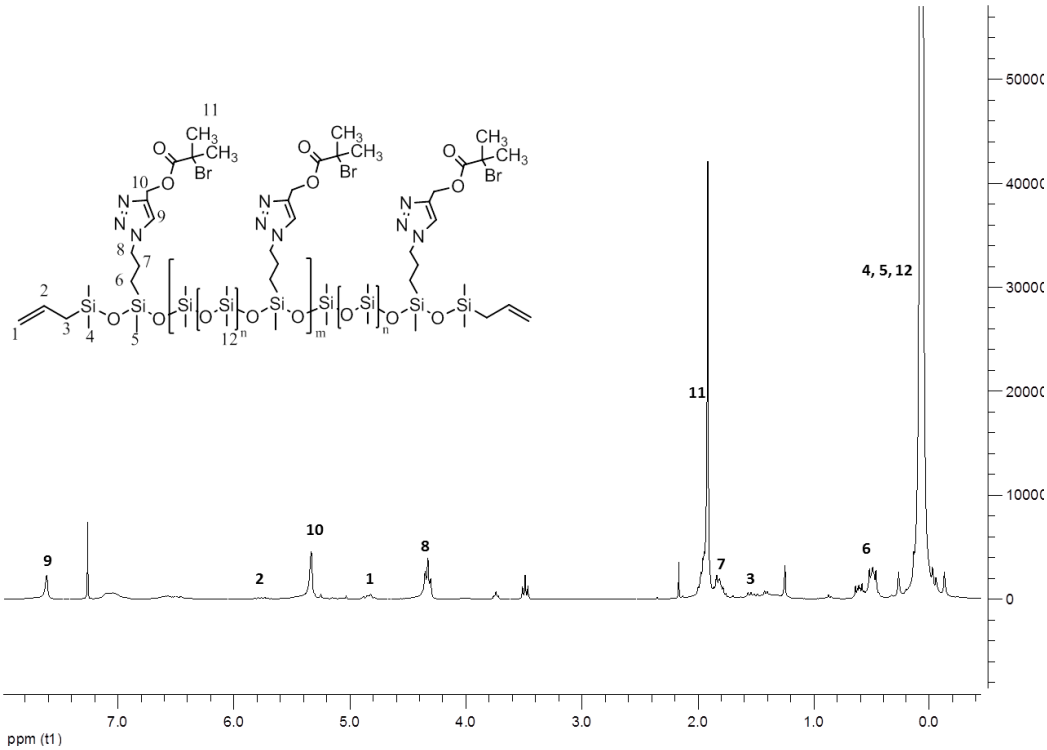

Figure S2: 1H-NMR spectrum of 4.

Appendix E

F. B. Madsen, L. Yu, A. E. Daugaard, S. Hvilsted, A. L. Skov, 2014 Silicone elastomers with high dielectric permittivity and high dielectric breakdown strength based on dipolar copolymers, *Polymer*, **55**, 6212-6219.

Polymer 55 (2014) 6212–6219

Contents lists available at ScienceDirect

Polymer

journal homepage: www.elsevier.com/locate/polymer

Silicone elastomers with high dielectric permittivity and high dielectric breakdown strength based on dipolar copolymers

Frederikke Bahrt Madsen, Liyun Yu, Anders Egede Daugaard, Søren Hvilsted, Anne Ladegaard Skov*

Danish Polymer Center, Department of Chemical and Biochemical Engineering, Technical University of Denmark, Building 227, 2800 Kgs. Lyngby, Denmark

ARTICLE INFO

Article history:
Received 11 August 2014
Received in revised form
22 September 2014
Accepted 23 September 2014
Available online 8 October 2014

Keywords:
Dielectric elastomers
Silicone
CuAAC

ABSTRACT

Dielectric elastomers (DEs) are a promising new transducer technology, but high driving voltages limit their current commercial potential. One method used to lower driving voltage is to increase dielectric permittivity of the elastomer. A novel silicone elastomer system with high dielectric permittivity was prepared through the synthesis of siloxane copolymers, thereby allowing for the attachment of high dielectric permittivity molecules through copper-catalysed azide-alkyne 1,3-dipolar cycloaddition (CuAAC). The copolymers have a high degree of chemical freedom, as the dimethylsiloxane spacer units between the functional groups, as well as the degree of functionalisation, can be varied. Thus, the best overall properties were obtained for an elastomer prepared with a copolymer with a 1200 g mol^{-1} dimethylsiloxane spacer unit and 5.6 wt% of the high dielectric permittivity molecule 1-ethynyl-4-nitrobenzene. Here, a high increase in dielectric permittivity (~70%) was obtained without compromising other favourable DE properties such as elastic modulus, gel fraction, dielectric loss and electrical breakdown strength.

1. Introduction

Dielectric elastomers (DEs) are a new and promising transducer technology and are often referred to as 'artificial muscles', due to their ability to undergo large deformations when stimulated by electric fields. DEs consist of a soft and thin elastomeric film sandwiched between compliant electrodes, thereby forming a capacitor [1]. There are, however, certain issues that currently limit the commercial potential of the technology, including high driving voltages (several kVs) and short device lifetime. Consequently, there is a need to optimise DE materials, in order to overcome the current shortcomings of the technology. One of the most important components of a DE is the elastomer, as it governs dielectric permittivity and the breakdown strength of the DE. Polydimethylsiloxane (PDMS) elastomers are one of the most used materials for DEs, due to their high efficiency, fast response and low viscous losses, which means that the material can be operated at higher frequencies but with lower losses [2,3]. Furthermore, silicone elastomers can be operated across a broad temperature range [3]. The major disadvantage of silicone elastomers is that they possess relatively low dielectric permittivity, which means that a high electrical field is necessary to actuate the DE. The necessary electrical field can be lowered by increasing the energy density of the elastomer, which can be done by creating elastomers with higher dielectric permittivity, i.e. with a higher ability to store electrical energy.

Dielectric permittivity of silicone elastomers has been improved by various techniques, most commonly through metal oxide fillers such as TiO_2 [4–9], $BaTiO_3$ [9–11], and Al_2O_3 [9]. A number of conducting fillers have also been employed, such as expanded graphite [12], carbon nanotubes [13,14], a copper-phthalocyanine oligomer [15,16], and calcium copper titanate ($CaCuTi_4O_{12}$) [17]. These composite-type systems, despite higher dielectric permittivity, exhibit major drawbacks such as large dielectric losses and reduced breakdown strengths, as increases in dielectric permittivity are achieved at loadings near the percolation threshold; thus, the systems are prone to filler agglomeration and consequent significant changes in mechanical properties. Furthermore, the Young's modulus usually also rises significantly, which consequently reduces achievable strain. Various techniques have been developed in order to avoid agglomeration and increasing stiffness when raising dielectric permittivity, including the preparation of encapsulated polyaniline (PANI) particles with insulating polymeric shells that prevent the agglomeration of the PANI particles [18].

* Corresponding author. Tel.: +45 45 25 28 25; fax: +45 45 88 22 58.
E-mail address: al@kt.dtu.dk (A.L. Skov).

http://dx.doi.org/10.1016/j.polymer.2014.09.056
0032-3861/

Furthermore, blends of PDMS/poly(hexylthiophene) [19] and PDMS/polyethylene glycol [20] have been developed to increase homogeneity between the matrix (PDMS) and filler (high dielectric permittivity polymer) and to maintain suitable elastic moduli.

Another approach is to graft organic dipoles chemically to the PDMS elastomer network. This approach potentially leads to a more controlled network structure, as it does not rely on the efficient and perfect mixing of particles or blends. Furthermore, such covalently grafted systems should provide a more stable elastomer system upon continued activation of the material [21]. Several interesting systems have been developed. Kussmaul et al. [22] and Risse et al. [23] added the synthesised dipolar molecule *N*-allyl-*N*-methyl-*p*-nitroaniline, together with compensating amounts of a hydride-functional cross-linker, to a PDMS matrix and a commercial silicone elastomer system, respectively, in one-step processes. Madsen el al. [24,25] developed a new silicone-compatible cross-linker that allowed for specific functionalisation with high dielectric molecules at the cross-linking point of polymer networks. This was done using a copper-catalysed azide-alkyne 1,3-dipolar cycloaddition (CuAAC) reaction, which is orthogonal, so that functionality could be added without compromising the network-forming reaction. Racles et al. [26] developed another approach where cyanopropyl-groups were distributed along the backbone of PDMS chains. Good overall results were obtained for blends of the cyanopropyl-functional PDMS and PDMS. High permittivities have been obtained by these methods, as two-fold increases of permittivity were usually achieved. When increasing dielectric permittivity, however, it is important to keep in mind other essential properties that govern the lifetime of the DE, such as elastic modulus, dielectric loss and electrical breakdown strength. Upon chemical manipulation of the polymer network these properties are also easily compromised.

The aim of this work is to create new and improved silicone elastomer systems with high dielectric permittivity while maintaining reasonable levels of other favourable properties such as viscous and dielectric losses and electrical breakdown strengths. We report herein on a new and controlled silicone elastomer system based on functionalisable siloxane copolymers that allow for the attachment of high dielectric permittivity molecules through CuAAC reactions. The synthesised copolymers allow for a high degree of chemical freedom, as several parameters can be varied during the preparation phase. Thus, the space between the functional groups can be varied, by using different dimethylsiloxane spacer units between the high dielectric permittivity molecules. Furthermore, the degree of functionalisation of the copolymers can be varied accurately by changing the feed of the high dielectric permittivity molecules. As a result, a completely tuneable elastomer system, with respect to functionalisation, is achieved. We have investigated how the different functionalisation variables affect essential DE properties, including dielectric permittivity, dielectric loss, elastic modulus and dielectric breakdown strength, and we have also determined the optimal degree of chemical functionalisation where important properties are not significantly compromised.

2. Experimental

2.1. Materials and methods

Hydride-terminated PDMS, DMS-H11 ($\overline{M}_w \approx 1200$ g mol^{-1} as determined by ^{1}H NMR), 3-(chloropropyl)methyldimethoxysilane, allyldimethylsilane and a hydride-functional cross-linker, HMS-301, were acquired from Gelest Inc. The platinum cyclovinylmethyl siloxane complex catalyst (511) was purchased from Hanse Chemie. Hydride-terminated PDMS ($\overline{M}_w \approx 580$ g mol^{-1} as stated by supplier) and vinyl-terminated PDMS ($\overline{M}_w \approx 25{,}000$ g mol^{-1} as stated by supplier) were purchased from Sigma–Aldrich. Silicon dioxide amorphous hexamethyldisilazane-treated particles (SIS6962.0) were purchased from Fluorochem. All other chemicals were acquired from Sigma–Aldrich and used as received, unless otherwise stated.

FTIR was conducted on a PerkinElmer Spectrum One model 2000 Fourier Transform Infrared apparatus equipped with a universal attenuated total reflection accessory on a ZnSe/diamond composite. Spectra were recorded in the range of 4000–650 cm^{-1} with 4 cm^{-1} resolution and 16 scans. ^{1}H and ^{13}C NMR experiments were performed on a Bruker 300 MHz spectrometer in $CDCl_3$. Size-exclusion chromatography (SEC) was performed on a Tosoh EcoSEC HLC-8320GPC instrument equipped with RI and UV detectors and SDV Linear S columns from PSS. Samples were run in toluene at 35 °C at a rate of 1 mL min^{-1}, and molar mass characteristics were calculated using WinGPC Unity 7.4.0 software and linear polydimethylsiloxane (PDMS) standards acquired from PSS. Differential scanning calorimetry (DSC) measurements were performed on a DSCQ1000 from TA Instruments. Mechanical characterisation of the prepared films was performed with a TA Instruments TA 2000 Rheometer set to a 1% controlled strain mode, which was ensured to be within the linear viscoelastic regime. The measurements were performed with a parallel plate geometry of 25 mm in the frequency range of 100–0.01 Hz. Dielectric relaxation spectroscopy (DRS) was performed on a Novocontrol Alpha-A high performance frequency analyser (Novocontrol Technologies GmbH & Co.) operating in the frequency range 10^{-1}–10^6 Hz at room temperature. The diameter of the tested 1 mm thick samples was 25 mm. Electrical breakdown strengths were measured on an in-house built device based on international standards. The polymer film (~150 μm) was slid between two spherical electrodes, and a stepwise increasing voltage was applied (50–100 V/step).

2.2. Syntheses

All reactions were carried out in a nitrogen atmosphere. Structures for ^{13}C NMR assignment can be found in the Supporting Information.

2.2.1. α,ω-Allyl-poly((azidopropyl)methylsiloxane-co-dimethylsiloxane) with a 1200 g mol^{-1} pre-polymer **1**

1 was synthesised according to a recently published procedure [27] using 3-chloropropylmethyldimethoxysilane (7.23 g, 39.6 mmol), hydride-terminated dimethylsiloxane (1200 g mol^{-1}) (50 g, 41.7 mmol), tris(pentafluorophenyl)borane (2 mL, 0.04 M, 0.2 mol%), dimethoxydimethylsilane (19.4 g, 163 mmol), allyldimethylsilane (9.76 g, 97.4 mmol), NaN_3 (12.4 g, 191 mmol) and tetrabutylammonium azide (1.09 g, 3.82 mmol) to produce a slightly yellowish oil (50.0 g, 96.6%). IR (cm^{-1}): 2960 (C–H stretch); 2095 (-N_3 stretch); 1630 (C=C stretch); 1410 (Si–CH_2 stretch); 1260 (Si–CH_3 stretch); 1010 (Si–O stretch). ^{1}H NMR ($CDCl_3$, δ_H, ppm): −0.05–0.09 (m, CH_3–Si), 0.58 (m, −Si–CH_2–CH_2–), 1.50 (d, 4H, $^3J = 8.1$ Hz, CH_2–CH=CH_2), 1.65 (m, −CH_2–CH_2–CH_2–), 3.23 (t, $^3J = 7.1$ Hz, N_3–CH_2–CH_2), 4.83 (m, 4H, CH=CH_2), 5.77 (m, 2H, CH=CH_2). ^{13}C NMR ($CDCl_3$, δ_C, ppm): −0.55–1.03 ($d + e + i$), 14.50 (f), 22.77 (g), 23.40 (c), 54.14 (h), 112.51 (a), 135.32 (b). SEC (toluene): $\overline{M}_w = 23{,}000$ g mol^{-1}.

2.2.2. α,ω-Allyl-poly((azidopropyl)methylsiloxane-co-dimethylsiloxane) with a 580 g mol^{-1} pre-polymer **5**

5 was synthesised according to a recently published procedure [27] using 3-chloropropylmethyldimethoxysilane (15 g, 82.1 mmol), hydride-terminated dimethylsiloxane (580 g mol^{-1}) (45.7 g, 78.8 mmol), tris(pentafluorophenyl)borane (4.2 mL, 0.04 M, 0.2 mol%), dimethoxydimethylsilane (39.6 g, 329.4 mmol),

allyldimethylsilane (10.0 g, 100 mmol), NaN_3 (19.9 g, 306 mmol) and tetrabutylammonium azide (2.17 g, 7.64 mmol) to produce a slightly yellowish oil (51.0 g, 91.1%). IR (cm^{-1}): 2960 (C–H stretch); 2095 (-N_3 stretch); 1630 (C=C stretch); 1410 (Si–CH_2 stretch); 1260 (Si–CH_3 stretch); 1010 (Si–O stretch). ^{1}H NMR ($CDCl_3$, δ_H, ppm): −0.05–0.09 (m, CH_3–Si), 0.56 (m, −Si–CH_2–CH_2–), 1.50 (d, 4H, ^3J = 8.4 Hz, CH_2–CH=CH_2), 1.65 (m, −CH_2–CH_2–CH_2–), 3.23 (t, ^3J = 7.2 Hz, N_3–CH_2–CH_2), 4.83 (m, 4H, CH=CH_2), 5.77 (m, 2H, CH=CH_2). ^{13}C NMR ($CDCl_3$, δ_C, ppm): −0.55–1.03 ($d + e + i$), 14.51 (f), 22.79 (g), 23.40 (c), 54.14 (h), 112.56 (a), 135.27 (b). SEC (toluene): $\overline{M}_w$ = 23,000 g mol^{-1}.

2.2.3. General procedure for CuAAC, synthesis of α,ω-allyl-poly((4-(4-nitrophenyl)-1H-1,2,3-triazolepropyl)methylsiloxane-co-dimethylsiloxane) with a 1200 g mol^{-1} pre-polymer spacer: (**4**)

1 (20 g, ~15.3 mmol (azidopropyl)methylsiloxane units) and 1-ethynyl-4-nitrobenzene (4.52 g, 30.7 mmol) were dissolved in dry THF (100 mL) in a 250 mL two-neck round bottom flask. CuI (0.29 g, 1.50 mmol) was subsequently added and Et_3N (2.33 g, 23.0 mmol) was added drop-wise. The reaction was carried out at 40 °C for 17 h at which point FTIR confirmed the disappearance of the azide band at 2095 cm^{-1}. THF was evaporated and the reaction mixture was precipitated into methanol. The solvent was decanted and the product was dried *in vacuo* giving a red viscous oil in quantitative yield. IR (cm^{-1}): 2960 (C–H stretch); 1605 (aromatic C=C stretch); 1520 (N=O asymmetric stretch); 1410 (Si–CH_2 stretch); 1340 (N=O symmetric stretch); 1260 (Si–CH_3 stretch); 1010 (Si–O stretch). ^{1}H NMR (CDCl3, δ_H, ppm): −0.45–0.13 (m, CH_3–Si), 0.55 (m, −Si–CH_2–CH_2–), 1.57 (d, 4H, ^3J = 8.1 Hz, CH_2–CH=CH_2), 2.02 (m, −CH_2–CH_2–CH_2–), 4.41 (t, ^3J = 7.2 Hz, N–CH_2–CH_2), 4.83 (m, 4H, CH=CH_2), 5.77 (m, 2H, CH=CH_2), 7.90 (s, −C=CH–N), 7.99 (m, Ar–H), 8.27 (m, NO_2-Ar-H). ^{13}C NMR ($CDCl_3$, δ_C, ppm): −0.55–1.03 ($d + e + q$), 14.23 (f), 24.39 (g), 53.09 (h), 120.68 (i), 124.29 (o), 126.05 (l), 137.04 (k), 145.45 (p), 147.26 (j) (a, b and c not visible).

2.2.4. Example of a partially functionalised copolymer: α,ω-allyl-poly((4-(4-nitrophenyl)-1H-1,2,3-triazolepropyl)methylsiloxane-co-(azidopropyl)methylsiloxane-co -dimethylsiloxane) with a 580 g mol^{-1} pre-polymer spacer (**6**)

The copolymer was prepared according to the general click reaction procedure using **5** (10 g, ~13.7 mmol (azidopropyl)methylsiloxane units), 1-ethynyl-4-nitrobenzene (0.50 g, 3.4 mmol), CuI (0.07 g, 0.34 mmol) and Et_3N (0.52 g, 5.0 mmol) to produce a brown viscous oil in quantitative yield. IR (cm^{-1}): 2960 (C–H stretch); 2095 (-N_3 stretch); 1605 (aromatic C=C stretch); 1525 (N=O asymmetric stretch); 1410 (Si–CH_2 stretch); 1345 (N=O symmetric stretch); 1255 (Si–CH_3 stretch); 1005 (Si–O stretch). ^{1}H NMR (CDCl3, δ_H, ppm): −0.054–0.14 (m, CH_3–Si), 0.56 (m, −Si–CH_2–CH_2–), 1.49 (d, 4H, ^3J = 8.1 Hz, CH_2–CH=CH_2), 1.65 (m, N_3–CH_2–CH_2–CH_2) 2.03 (m, N–CH_2–CH_2–CH_2), 3.23 (t, ^3J = 7.2 Hz, N_3–CH_2–CH_2), 4.41 (t, ^3J = 7.2 Hz, N–CH_2–CH_2), 4.84 (m, 4H, CH=CH_2), 5.79 (m, 2H, CH=CH_2), 7.89 (s, −C=CH–N), 7.99 (m, Ar–H), 8.29 (m, NO_2-Ar-H). ^{13}C NMR ($CDCl_3$, δ_C, ppm): −0.56–1.02 ($d + e + t$), 14.23 (i), 14.49 (f), 22.77 (g) 24.40 (j), 53.09 (k), 54.13 (h), 120.88 (l), 124.29 (r), 126.06 (q), 137.04 (p), 145.46 (s), 147.28 (o) (a, b and c not visible).

2.2.5. General procedure for elastomer synthesis

1–**8** or vinyl-terminated PDMS ($\overline{M}_w$ = 25,000 g mol^{-1}, Sigma–Aldrich) (2.33 g, 10.1 mmol) and an 8-functional cross-linker (HMS-301, 0.066 g, 0.034 mmol) were mixed with treated silica particles (20 wt%) and the mixture was treated on a FlackTek Inc. DAC 150.1 FVZ-K SpeedMixer™. The catalyst (511) (20–100 ppm) was added thereafter and the mixture was speed-mixed once more. The mixture was the poured into 1 mm thick steel moulds and furthermore coated as 150 μm films on a glass substrate and cured at 115 °C.

2.2.6. Swelling experiments

The gel fractions were determined using swelling experiments, where samples of all prepared films were swelled in chloroform at RT for 48 h. The chloroform was replaced after 24 h. The solvent was decanted and the films were washed several times. The samples were thereafter dried for 48 h to a constant weight in an ambient atmosphere. Gel fractions were calculated as the weight after extraction and drying (m_e) against the initial weight of the sample (m_0) as $W_{gel} = m_e/m_0$.

3. Results and discussion

Siloxane copolymers that allow for functionalisation with high dielectric constant molecules were prepared according to a previously described procedure [27]. The copolymers were prepared from commercially available starting materials through the tris(pentafluorophenyl)borane-catalysed Piers–Rubinsztajn reaction of 3-chloropropylmethyldimethoxysilane and hydride-terminated dimethylsiloxane pre-polymers. Dimethylsiloxane pre-polymers constitute the spacer unit between the functional groups. The copolymers were then end-functionalised with allyl-groups that allow for hydrosilylation cross-linking reactions with hydride-functional cross-linker molecules to form polymer networks. The chloro-functional copolymers were converted to azido-functional through nucleophilic substitution with sodium azide. Azido groups on the siloxane copolymer allow for CuAAC click reactions where high dielectric constant alkyne molecules can be attached. The structure of the formed azido-functional siloxane copolymer, with various spacer units between the azido-groups, is shown in Fig. 1.

Copolymers with two different spacer lengths between the azido-group were synthesised. One copolymer contains azido-groups with 1200 g mol^{-1} dimethylsiloxane spacers between each group and the other copolymer contains azido-groups with 580 g mol^{-1} dimethylsiloxane spacers between the functional groups. The copolymers with the shorter spacer thus contain approximately double the amount of functional groups than the copolymers with the long spacer at comparable copolymer lengths.

Copolymers were analysed with size exclusion chromatography (SEC), and molar mass characteristics were calculated from linear polydimethylsiloxane standards. The molecular weights of the copolymers prepared with different spacers were both found to be $\overline{M}_w \approx$ 23,000 g mol^{-1}, which is a suitable molecular weight for silicone elastomers, as good mechanical properties are obtained for polymers of 20,000 to 30,000 g mol^{-1} [28]. Molecular weights of 23,000 g mol^{-1} signify that each copolymer contains approximately 15 and 30 azido-groups for the copolymers with the

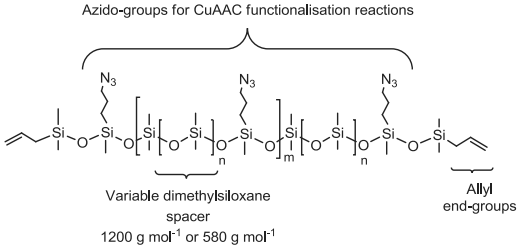

Fig. 1. Structure of functionalisable siloxane copolymers with various spacer lengths between the azido-groups and allyl end groups, thereby allowing for hydrosilylation cross-linking reactions.

1200 g mol^{-1} dimethylsiloxane spacer and 580 g mol^{-1} dimethylsiloxane spacer, respectively.

The azido-copolymers with different spacer lengths between the groups were thereafter functionalised with the high dielectric constant molecule, 1-ethynyl-4-nitrobenzene, through CuAAC, as illustrated in Scheme 1.

The azido-groups on the copolymers were reacted to different extents so that copolymers with different degrees of functionalisation would be obtained. The feed of 1-ethynyl-4-nitrobenzene into the content of azido-groups was varied, and the effectiveness of the CuAAC reactions allowed for direct control over the degree of functionalisation. The feed of 1-ethynyl-4-nitrobenzene to the azido-groups and the resulting obtained degree of functionalisation, as determined by ^{1}H NMR, are shown in Table 1.

The actual degrees of functionalisation were determined by ^{1}H NMR through the integration of the CH_2–N_3 resonance at $\delta_H = 3.23$ ppm against the CH_2–$N_{triazole}$ resonance at $\delta_H = 4.41$ ppm. For copolymers **2**–**4** and **8** the 1-ethynyl-4-nitrobenzene feed matched almost perfectly the degree of functionalisation determined from ^{1}H NMR such that, for example, copolymer **2** with 25% substituted azido-groups had an integral of 0.25 for the CH_2–$N_{triazole}$ resonance and an integral of 0.75 for the CH_2–N_3 resonance. For copolymers **6** and **7** slightly lower degrees of functionalisation were obtained. As the CuAAC reaction is almost 100% effective, the slightly lower obtained degrees of functionalisation could simply be due to inaccuracies when measuring the feed of 1-ethynyl-4-nitrobenzene during the synthesis of these copolymers. Overall, the degree of functionalisation can be varied accurately by changing the 1-ethynyl-4-nitrobenzene feed. The corresponding actual content of nitrobenzene on the copolymers is shown in Table 1.

The functional copolymers were thereafter used in cross-linking reactions with 8-functional functional hydride cross-linkers and furthermore reinforced with 20 wt% surface-treated silica particles to create silicone elastomers, as shown in Scheme 2.

Table 1
Overview of the prepared functionalised dipolar copolymers.

Entry	$\overline{M}_w$ dimethyl siloxane spacer	Feed of 1-ethynyl-4-nitrobenzene	Degree of functionalisation from ^{1}H NMR	Content of nitrobenzene
	[g mol^{-1}]	[% of azido-groups]	[% of azido-groups]	[wt%]
1	1200	0	0	0
2	1200	25	25	2.75
3	1200	50	51	5.6
4	1200	100	100	11
5	580	0	0	0
6	580	25	19	3.8
7	580	50	42	8.4
8	580	100	100	20

A reference sample made from PDMS of $\overline{M}_w = 25{,}000$ g mol^{-1} using similar reaction conditions (same catalyst, cross-linker and particle concentration) was also produced. The elastomers prepared with different degrees of functional groups showed different curing rates. The azido-functional copolymers (**1** and **5**) cured relatively quickly (<12 h) at low catalyst levels (20 ppm). For elastomers containing nitrobenzene, higher catalyst concentration was generally needed (100 ppm) and the films cured within <24 h. At 100% conversion of the azido-groups to nitrobenzene (**4** and **8**) longer reaction times (one week) were needed. This indicates that the presence of larger amounts of nitrobenzene or triazole-groups inhibits, to some extent, the hydrosilylation reaction.

The prepared elastomers were characterised by FTIR. The spectra of azido- and nitrobenzene-functional films are shown in Fig. 2.

The films with the two azido-functional copolymers **1** and **5** show distinctive $-N_3$ bands at approximately 2095 cm^{-1}. The azido-band is sharper for the film with copolymer **5**, confirming the higher content of azido-groups on this copolymer due to the shorter dimethylsiloxane spacer between the functional groups.

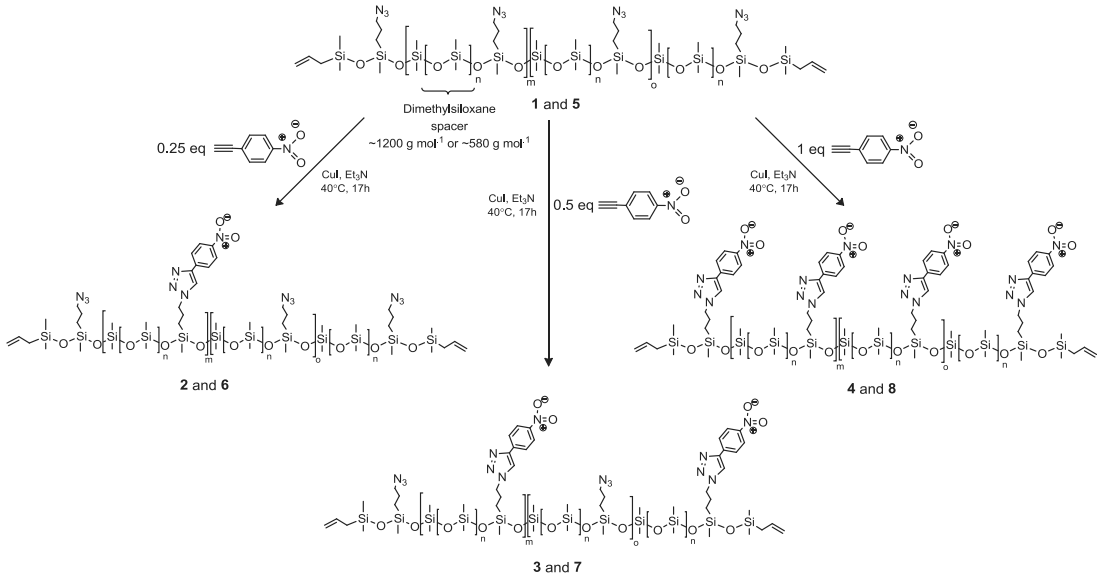

Scheme 1. Synthetic route to nitrobenzene-functionalised copolymers through CuAAC click reaction. The azido-functional copolymers are reacted with 0.25, 0.5 or 1 equivalents of 1-ethynyl-4-nitrobenzene to the total number of azido-groups.

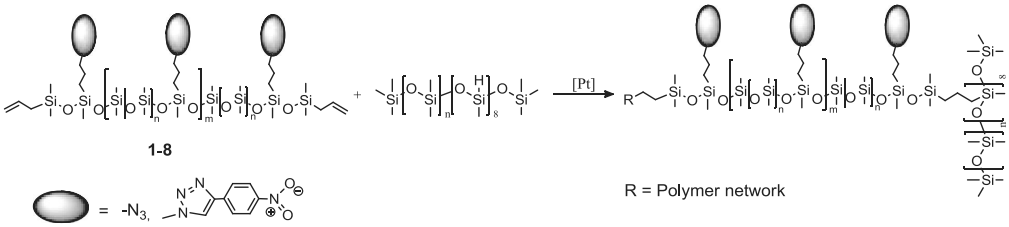

Scheme 2. Cross-linking reaction between copolymer **1**–**8** and a hydride-functional cross-linker.

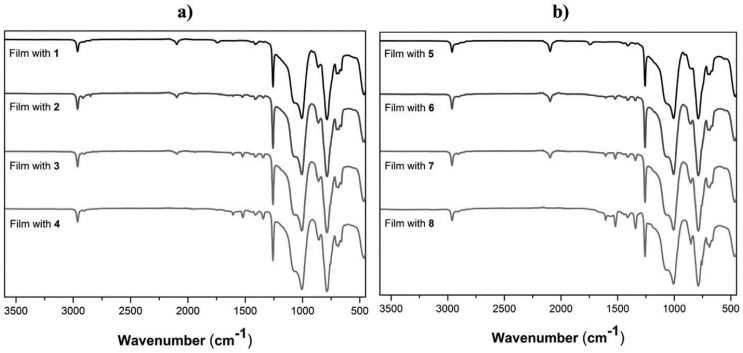

Fig. 2. FTIR spectra of elastomer films prepared with the different functionalised copolymers: a): films prepared with copolymers with a 1200 g mol^{-1} spacer and b): films prepared with copolymers with a 580 g mol^{-1} spacer.

The more substituted the azido-group becomes with nitrobenzene, the less intense the $-N_3$ bands become. For the films with 100% substituted azido-groups no $-N_3$ bands are visible (films with **4** and **8**). The films containing nitrobenzene (**2**–**4** and **6**–**8**) all show bands of increasing intensity at ~1605 cm^{-1} for the aromatic C=C bonds and at ~1520 cm^{-1} and ~1340 cm^{-1} for the N=O bonds with increasing nitrobenzene content, which corroborates increasing functionalisation with nitrobenzene in the elastomers.

The gel fractions of the films were determined from swelling experiments with chloroform, in order to elucidate the amount of bonded (gel fraction) and non-bonded (sol fraction) species in the networks. As seen in Table 2 the gel fractions decrease with increasing degrees of functionalization; thus, the lowest gel fractions are obtained for films with copolymers that are fully substituted with nitrobenzene (**4** and **8**). This could be due to the slow curing time of these films, indicating that not all reactive end groups on the copolymers react, which leaves larger fractions of non-bonded substructures in the networks. The gel fractions for the other films are within an acceptable limit, thereby suggesting that these films are better cross-linked.

Table 2
Gel fractions (W_{gel}) as a result of swelling experiments.

Film with entry	W_{gel} (%)
Ref.	97
1	83
2	95
3	84
4	64
5	84
6	97
7	88
8	69

The effect of the degree of functionalisation on the thermal transition behaviour of the elastomer films was determined by differential scanning calorimetry (DSC). The reference film showed clear melting and crystallisation temperatures at $T_m = -42.6$ °C and $T_c = -74.7$ °C, respectively. For all films prepared with copolymers **1**–**8**, no T_m or T_c were observed, which means that no crystalline regions were present in the films. This points towards the successful formation of the spatially well-distributed azido- and nitrobenzene-functional groups, which prevents crystallisation from taking place. The glass transition temperature (T_g) of the pure PDMS reference sample was determined to be −127 °C. For films prepared with the azido-functional copolymers the glass transition temperatures increased slightly to −120 °C and −115 °C for **1** and **5**, respectively. The higher the content of nitrobenzene in the films, the higher the measured glass transition temperature. The glass transition temperatures ranged from −118 °C for the film prepared with copolymer **2** to −95 °C for the film prepared with copolymer **8**.

The effect of the functional copolymers on the thermal stability of the elastomer films was determined by thermal gravimetric analysis (TGA), and the resulting thermograms can be found as Supporting Information. The thermal degradation temperatures were not significantly altered for the films with the functional copolymers compared to the reference film.

The influence of the concentration and type of copolymer on the mechanical properties was investigated by determining the shear storage and shear loss modulus of the prepared films. In Fig. 3 the results for films with different spacers and functional groups are presented. Furthermore, the resulting shear storage moduli (G′) and loss (tan δ) at 1 Hz are summarised in Table 3.

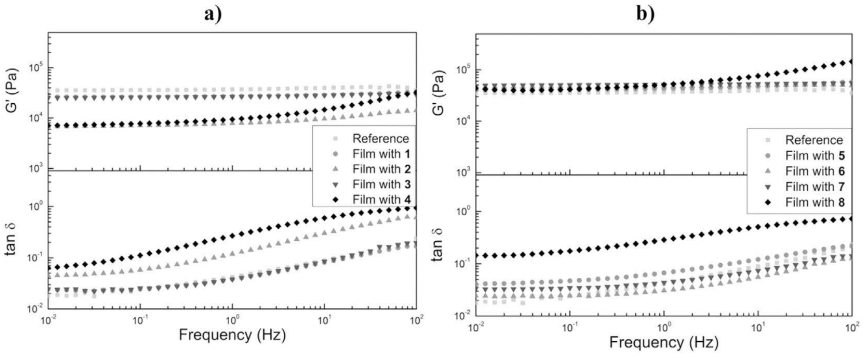

Fig. 3. Storage modulus (G′) and loss (tan δ) as functions of frequency for: a): films prepared with a 1200 g mol^{-1} pre-polymer spacer (**1**–**4**) and b): films prepared with a 580 g mol^{-1} pre-polymer spacer (**5**–**8**).

It is evident that the films with the 1200 g mol^{-1} pre-polymer spacer (copolymers **1**–**4**) all have lower moduli than the reference film. The films prepared with the 580 g mol^{-1} pre-polymers (copolymers **5**–**8**) have quite similar, but slightly higher, moduli – as for the reference film. Viscous losses and tan δ remain low for all films prepared with the functional copolymers except for the high concentration nitrobenzene films **4** and **8**. For these films the viscous losses increased six-fold, indicating increased damping behaviour, which is partly or fully due to the larger fractions of extractable substructures and the deterioration of network properties [29].

The impact of the type of copolymer on dielectric properties was determined by dielectric relaxation spectroscopy on discs of approximately 1 mm thick films. Dielectric relaxation spectra showing the frequency-dependent dielectric permittivity (ε') and loss tangent (tan δ) for films with copolymers **1**–**8**, as well as the reference film, are presented in Fig. 4. Permittivity and loss at 1 Hz and 100 Hz are summarised further in Table 3. Enlarged spectra of dielectric permittivity at the plateau region from 10^2 to 10^5 Hz are also shown in Fig. 4.

For all films prepared with functional copolymers dielectric permittivity is seen to increase compared to the reference film, for which $\varepsilon' = 3.0$. The films with the two azido-functional copolymers **1** and **5** both show increased dielectric permittivity to $\varepsilon' = 3.3$ and $\varepsilon' = 3.4$ at 100 Hz, respectively. These permittivities correspond to a 10–13% increase. Increasing (doubling) the content of azido-groups thereby does not increase permittivity at medium to higher frequencies. The film with **5**, however, shows elevated permittivity at low frequencies. At 1 Hz, for instance, permittivity increases to $\varepsilon' = 5.8$, thus corresponding to an almost two-fold increase. These results show that the azido-groups alone also yield increased permittivities for the elastomer films. The azido-functional copolymers, however, do exhibit increased dielectric losses, which are especially visible on the film prepared with **5**.

Table 3
Dielectric permittivity (ε') and loss tangent (tan δ) at 1 Hz and 100 Hz as well as the breakdown strength (E_B) and storage (G′) and loss (tan δ) moduli for films with copolymers **1**–**8** and the PDMS reference.

Film with entry	Dielectric spectroscopy				Electrical breakdown	Rheology	
	ε' @1 Hz	ε' @100 Hz	tan δ @1 Hz	tan δ @100 Hz	E_B [V/μm]	G′ @1 Hz [kPa]	tan δ @1 Hz
Ref.	3.0	3.0	0.002	0.0008	55.4	37.0	0.042
1	3.6	3.3	0.56	0.01	61.4	27.0	0.038
2	5.9	5.0	2.90	0.06	63.2	7.81	0.119
3	6.9	5.1	1.47	0.04	69.2	26.5	0.038
4	17.3	5.0	16.7	0.60	60.5	9.41	0.268
5	5.8	3.4	38.7	0.70	81.1	43.1	0.067
6	6.9	5.3	1.51	0.03	66.7	47.9	0.031
7	15.6	7.3	4.52	0.15	64.1	51.5	0.044
8	59.3	8.5	9.07	0.90	65.0	51.3	0.286

The films prepared with copolymers with the 1200 g mol^{-1} pre-polymer spacer and different degrees of nitrobenzene (copolymers **2**–**4**) show increased permittivities in the same order of magnitude ($\varepsilon' \approx 5.0$) at 100 Hz. This corresponds to an increase in permittivity of approximately 70%. At lower frequencies dielectric permittivity increases in line with the increased content of nitrobenzene, reaching $\varepsilon' = 17.3$ at 1 Hz for the film prepared with copolymer **4** containing 11 wt% nitrobenzene. Dielectric losses, tan δ, increase slightly in line with increasing nitrobenzene content.

Films prepared with copolymers with the 580 g mol^{-1} spacer between the functional groups show largely increased permittivities at 100 Hz, with the highest dielectric permittivity obtained for the film prepared with copolymer **8**, which contains 20 wt% nitrobenzene ($\varepsilon' = 8.5$). This corresponds to an increase of 180%. At frequencies higher than 100 Hz the film prepared with copolymer **7** shows the highest dielectric permittivity of $\varepsilon' \approx 7$. At lower frequencies dielectric permittivity also increases in line with the increased content of nitrobenzene, reaching $\varepsilon' = 59.3$ at 1 Hz for the film prepared with copolymer **8** containing 20 wt% nitrobenzene. Relative dielectric losses (tan δ), furthermore, increase in line with increasing nitrobenzene content but are lower than the film prepared with the corresponding azido-functional copolymer **5**.

It is evident in Fig. 4 that in the medium to high frequency region (10^2–10^6 Hz) there are no significant changes in ε' with frequency. In this region dielectric response depends mainly on bulk polarisation processes [30]. Therefore, the most promising increases in permittivity for DE applications are observed in this region. Interestingly, the largest increases in permittivity in this frequency region are not necessarily observed for the copolymers with the largest concentration of nitrobenzene, which indicates that there is a maximum concentration of nitrobenzene above which further improvement to dielectric permittivity is not possible. Above this concentration, it is only permittivity at low frequencies (due to Maxwell polarisation [31]) and dielectric losses that increases and thereby there is a higher risk of unwanted conductivity.

The nature of this system makes it possible to tune the concentration and distribution of functional groups, and so it is

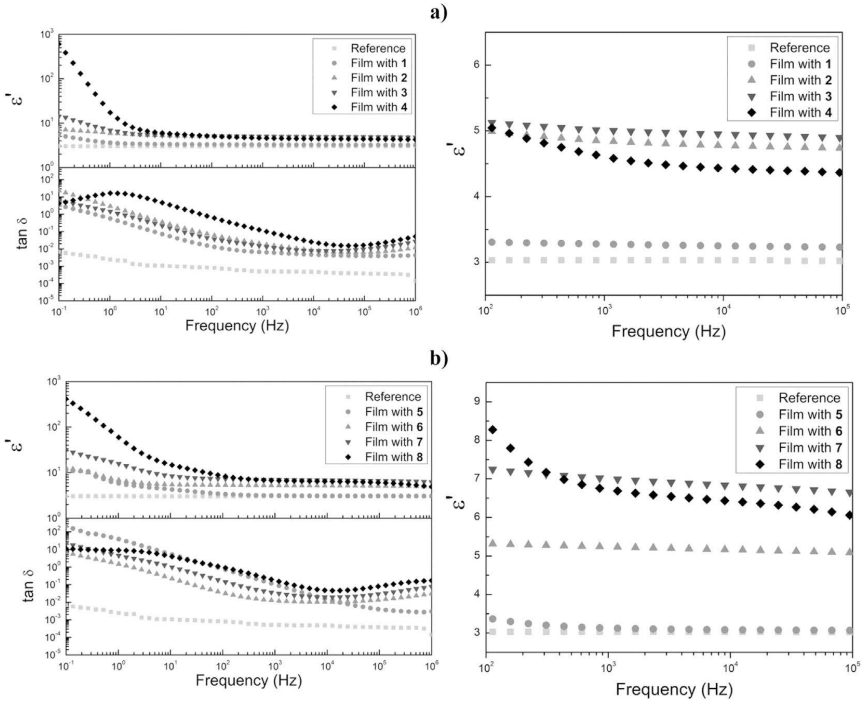

Fig. 4. Dielectric permittivity (ε') and loss tangent ($\tan\delta$) as functions of frequency for films prepared with: a): a 1200 g mol^{-1} pre-polymer spacer (**1**–**4**) and b): a 580 g mol^{-1} pre-polymer spacer (**5**–**8**).

possible to obtain the most optimal DE with regards to permittivity and dielectric loss.

In order to investigate the nature of the large increases in permittivity and loss at low frequencies for the films prepared with copolymers with high concentrations of nitrobenzene, plots of conductivity as a function of frequency are shown in Fig. 5.

It can be seen from Fig. 5 that some of the films show higher electric conductivity at low frequencies, as conductivity becomes independent of frequency. The observed conductivities, however, remain very low. For the films prepared from the 100% substituted copolymers (**4** and **8**) slightly higher conductivities are observed, which could be the reason for the high dielectric losses of these films at low frequencies.

The electrical breakdown strengths, E_B, for films with co-polymers **1**–**8** as well as the reference film are presented in Table 3.

For all films, electrical breakdown field strength is seen to increase compared to the reference film. This increased breakdown strength, as seen in Table 3, is not due to increased elastic moduli, which is often the case [32]. This suggests that the introduction of functional groups does not compromise electrical breakdown strength, which is an essential DE property. The high dielectric breakdown strengths of the films could be due to a low degree of

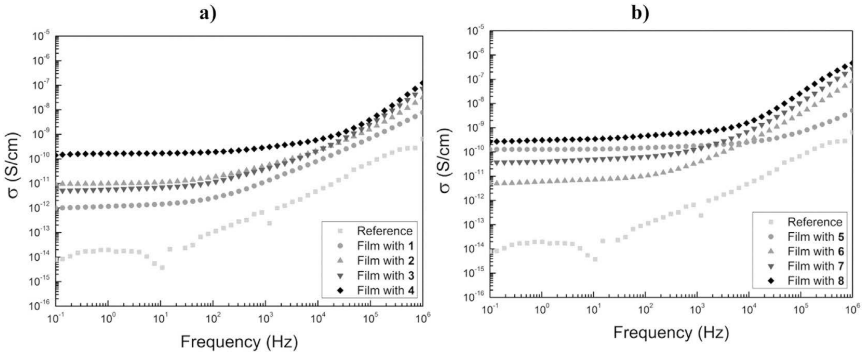

Fig. 5. Conductivity as a function of frequency for films prepared with: a): a 1200 g mol^{-1} pre-polymer spacer (**1**–**4**) and b): a 580 g mol^{-1} pre-polymer spacer (**5**–**8**).

chemical and physical impurities, the result of which has a large effect on the dielectric strength of insulating materials [33]. The prepared copolymers are all purified after synthesis, which implies that the prepared films have higher breakdown strengths than the commercial PDMS reference material.

4. Conclusion

A new high dielectric permittivity elastomer system was prepared through the use of dipolar siloxane copolymers. The copolymers were prepared with two different dimethylsiloxane spacer units between alkyl azide-groups. The azido-groups were functionalised to different extents with the high dielectric permittivity molecule 1-ethynyl-4-nitrobenzene through CuAAC reactions. ^{1}H NMR corroborated the highly efficient functionalisation reactions, and the degree of functionalisation could thus be controlled directly from the 1-ethynyl-4-nitrobenzene feed. High dielectric permittivities were obtained for the nitrobenzene-functional copolymers (e.g. a 180% increase at 20 wt% of nitrobenzene), and this concentration resulted in an increase in dielectric loss and stiffness, though electrical breakdown strength was not compromised. The best overall properties were obtained for a film prepared with a copolymer with a 1200 g mol^{-1} dimethylsiloxane spacer and 5.6 wt% nitrobenzene, as it has high dielectric permittivity (~70% increase at 100 Hz) and low dielectric loss. Furthermore, the obtained film was soft with low modulus, without compromising the viscous loss and gel fraction. Electrical breakdown strength also increased 25% compared to that of the pure PDMS reference film. Moreover, the best overall properties were obtained for the films prepared with copolymers with the 1200 g mol^{-1} pre-polymer spacer, as the films prepared with copolymers with a shorter dimethylsiloxane spacer (580 g mol^{-1}) and a higher concentration of functional groups were slightly stiffer and therefore less extensible.

Acknowledgements

The authors wish to acknowledge Irakli Javakhishvili for his help with SEC measurements and InnovationsFonden (grant number 009-2011-2) for financial support.

Appendix A. Supplementary data

Supplementary data related to this article can be found at http://dx.doi.org/10.1016/j.polymer.2014.09.056.

References

[1] Pelrine R, Kornbluh R, Pei Q, Joseph J. High-speed electrically actuated elastomers with strain greater than 100%. Science 2000;287:836–9.
[2] Löwe C, Zhang X, Kovacs G. Dielectric elastomers in actuator technology. Adv Eng Mater 2005;7:361–7.
[3] Brochu P, Pei Q. Advances in dielectric elastomers for actuators and artificial muscles. Macromol Rapid Commun 2010;31:10–36.
[4] Carpi F, De Rossi D. Improvement of electromechanical actuating performances of a silicone dielectric elastomer by dispersion of titanium dioxide powder. IEEE Trans Dielectr Electr Insul 2005;12:835–43.
[5] Ouyang G, Wang K, Chen XY. TiO_2 nanoparticles modified polydimethylsiloxane with fast response time and increased dielectric constant. J Micromech Microeng 2012;22(07):4002.
[6] Liu H, Zhang L, Yang D, Yu Y, Yao L, Tian M. Mechanical, dielectric, and actuated strain of silicone elastomer filled with various types of TiO_2. Soft Mater 2013;11:363–70.
[7] Stoyanov H, Brochu P, Niu X, Della Gaspera E, Pei Q. Dielectric elastomer transducers with enhanced force output and work density. Appl Phys Lett 2012;100:262902.
[8] Vudayagiri S, Zakaria S, Yu L, Hassouneh SS, Benslimane M, Skov AL. High breakdown-strength composites from liquid silicone rubbers. Smart Mater Struct 2014;23:105017.
[9] Lotz P, Matysek M, Lechner P, Hamann M, Schlaak HF. Dielectric elastomer actuators using improved thin film processing and nanosized particles. Proc SPIE 2008;6927. 692723–692731–692723–10.
[10] Liu Y, Liu L, Zhang Z, Leng J. Dielectric elastomer film actuators: characterization, experiment and analysis. Smart Mater Struct 2009;18(09):5024.
[11] Gallone G, Galantini F, Carpi F. Perspectives for new dielectric elastomers with improved electromechanical actuation performance: composites versus blends. Polym Int 2010;59:400–6.
[12] Daugaard AE, Hassouneh SS, Kostrzewska M, Bejenariu AG, Skov AL. High dielectric permittivity elastomers from well-dispersed expanded graphite in low concentrations. Proc SPIE 2013;8687. 868729–868731–868729–11.
[13] Park I-S, Kim KJ, Nam J-D, Lee J, Woosoon Y. Mechanical, dielectric, and magnetic properties of the silicone elastomer with multi-walled carbon nanotubes as a nanofiller. Polym Eng Sci 2007;47:1396–405.
[14] Yadav SK, Kim IJ, Kim HJ, Kim J, Hong SM, Koo CM. PDMS/MWCNT nanocomposite actuators using silicone functionalized multiwalled carbon nanotubes via nitrene chemistry. J Mater Chem C 2013;1:5463–70.
[15] Szabo JP, Hiltz JA, Cameron CG, Underhill RS, Massey J, White B, et al. Elastomeric composites with high dielectric constant for use in Maxwell stress actuators. Proc SPIE 2003;5051:180–90.
[16] Zhang X, Wissler M, Jaehne R, Broennimann R, Kovacs G. Effects of crosslinking, prestrain, and dielectric filler on the electromechanical response of a new silicone and comparison with acrylic elastomer. Proc SPIE 2004;5385:78–86.
[17] Romasanta LJ, Leret P, Casaban L, Hernández M, de la Rubia MA, Fernández JF, et al. Towards materials with enhanced electro-mechanical response: CaCu3Ti4O12–polydimethylsiloxane composites. J Mater Chem 2012;22:24705–12.
[18] Molberg M, Crespy D, Rupper P, Nüesch F, Månson J-AE, Löwe C, et al. High breakdown field dielectric elastomer actuators using encapsulated polyaniline as high dielectric constant filler. Adv Funct Mater 2010;20:3280–91.
[19] Carpi F, Gallone G, Galantini F, De Rossi D. Silicone–poly(hexylthiophene) blends as elastomers with enhanced electromechanical transduction properties. Adv Funct Mater 2008;18:235–41.
[20] Liu H, Zhang L, Yang D, Ning N, Yu Y, Yao L, et al. A new kind of electro-active polymer composite composed of silicone elastomer and polyethylene glycol. J Phys D Appl Phys 2012;45:485303.
[21] Skov AL, Vudayagiri S, Benslimane M. Novel silicone elastomer formulations for DEAPs. Proc SPIE 2013;8687. 86871I–86871I–8.
[22] Kussmaul B, Risse S, Kofod G, Waché R, Wegener M, McCarthy DN, et al. Enhancement of dielectric permittivity and electromechanical response in silicone elastomers: molecular grafting of organic dipoles to the macromolecular network. Adv Funct Mater 2011;21:4589–94.
[23] Risse S, Kussmaul B, Krüger H, Kofod G. A versatile method for enhancement of electromechanical sensitivity of silicone elastomers. RSC Adv 2012;2:9029–35.
[24] Madsen FB, Dimitrov I, Daugaard AE, Hvilsted S, Skov AL. Novel cross-linkers for PDMS networks for controlled and well distributed grafting of functionalities by click chemistry. Polym Chem 2013;4:1700–7.
[25] Madsen FB, Daugaard AE, Hvilsted S, Benslimane MY, Skov AL. Dipolar cross-linkers for PDMS networks with enhanced dielectric permittivity and low dielectric loss. Smart Mater Struct 2013;22:104002.
[26] Racles C, Cazacu M, Fischer B, Opris DM. Synthesis and characterization of silicones containing cyanopropyl groups and their use in dielectric elastomer actuators. Smart Mater Struct 2013;22:104004.
[27] Madsen FB, Javakhishvili I, Jensen RE, Daugaard AE, Hvilsted S, Skov AL. Synthesis of telechelic vinyl/allyl functional siloxane copolymers with structural control. Polym Chem 2014. http://dx.doi.org/10.1039/C4PY00919C.
[28] Larsen AL, Sommer-Larsen P, Hassager O. Some experimental results for the end-linked polydimethylsiloxane network system. e-Polymers 2004;050:1–18.
[29] Frankær SMG, Jensen MK, Bejenariu AG, Skov AL. Investigation of the properties of fully reacted unstoichiometric polydimethylsiloxane networks and their extracted network fractions. Rheol Acta 2012;51:559–67.
[30] Carpi F, Gallone G, Galantini F, De Rossi D. Enhancing the dielectric permittivity of elastomers. In: Carpi F, De Rossi D, Kornbuh R, Pelrine R, Sommer-Larsen P, editors. Dielectric elastomers as electromechanical transducers. Amsterdam: Elsevier Science; 2008. p. 51–68.
[31] Goswami K, Galantini F, Mazurek P, Daugaard AE, Gallone G, Skov AL. Reinforced poly(propylene oxide): a very soft and extensible dielectric electroactive polymer. Smart Mater Struct 2013;22:115011.
[32] Kollosche M, Kofod G. Electrical failure in blends of chemically identical, soft thermoplastic elastomers with different elastic stiffness. Appl Phys Lett 2010;96(07):1904.
[33] Bostrom J-O, Marsden E, Hampton RN, Nilsson U, Lennartsson H. Electrical stress enhancement of contaminants in XLPE insulation used for power cables. IEEE Electr Insul Mag 2003;19:6–12.

Supporting Information

Silicone elastomers with high dielectric permittivity and high dielectric breakdown strength based on dipolar copolymers

F. B. Madsen, L. Yu, A. E. Daugaard, S. Hvilsted and A. L. Skov*,

Danish Polymer Center, Department of Chemical and Biochemical Engineering, Technical University of Denmark, Building 227, 2800 Kgs. Lyngby, Denmark

^{13}C-NMR:

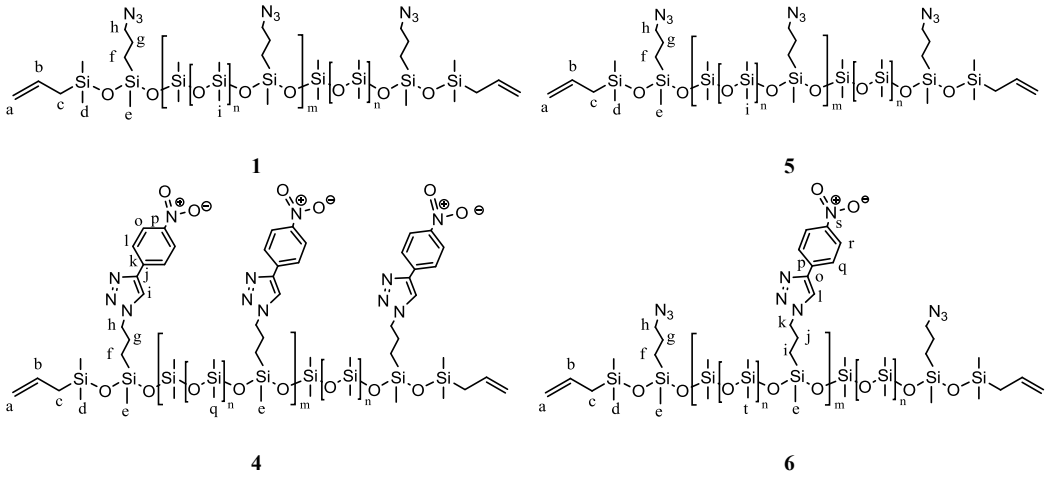

Figure S1: Structures for ^{13}C-NMR assignment.

Thermal gravimetric analysis (TGA):

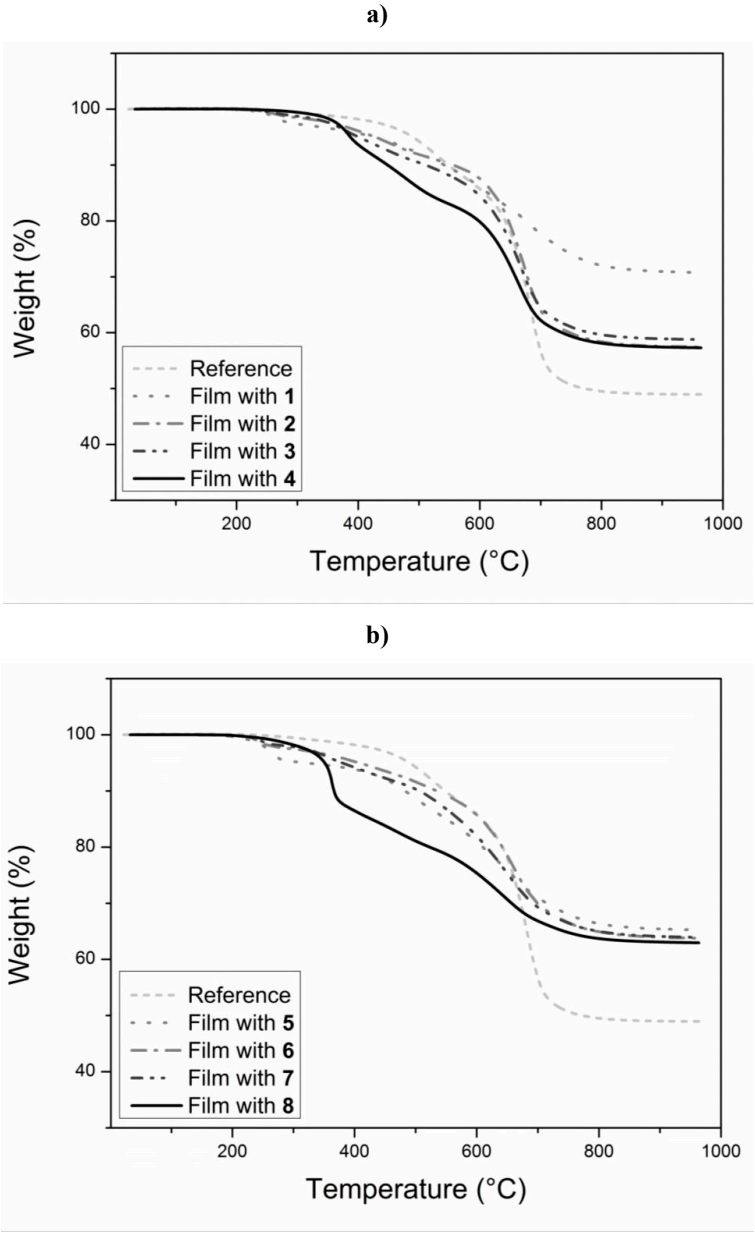

Figure S2: TGA measurements of: a): films prepared with a ~1200 g mol^{-1} pre-polymer spacer (1-4) and b): films prepared with a ~580 g mol^{-1} pre-polymer spacer (5-8).

The Danish Polymer Centre
Department of Chemical and Biochemical Engineering
Technical University of Denmark
Søltofts Plads, Building 227
DK-2800 Kgs. Lyngby
Denmark

Phone: +45 4525 6801
Web: www.dpc.kt.dtu.dk

ISBN : 978-87-93054-56-1